

# PYROLYSIS AND OXIDATION OF SUFLUR MUSTARD SIMULANTS

A Dissertation

Presented to the Faculty of the Graduate School

of Cornell University

In Partial Fulfillment of the Requirements for the Degree of

Doctor of Philosophy

by

Xin Zheng

January 2011

© 2011 Xin Zheng

## PYROLYSIS AND OXIDATION OF SULFUR MUSTARD SIMULANTS

Xin Zheng, Ph. D.

Cornell University 2011

The reaction kinetics of diethyl sulfide ( $\text{C}_2\text{H}_5\text{-S-C}_2\text{H}_5$ ) and ethyl methyl sulfide ( $\text{C}_2\text{H}_5\text{-S-CH}_3$ ), simulants for the chemical warfare agent, sulfur mustard ( $\text{ClC}_2\text{H}_4\text{-S-C}_2\text{H}_4\text{Cl}$ ), was studied at high temperatures under highly diluted conditions. This work has been undertaken with the goals to understand the destruction of sulfur mustard simulants at early stages and explore routes relevant to emissions under off-design incineration modes, such as fuel rich conditions due to inhomogeneous mixing. The studies were conducted in an atmospheric pressure, turbulent flow reactor with a Reynolds number of approximately 5000, at four different operating temperatures between 630 °C and 740 °C. These experiments, with an initial loading of the simulants of 150/100 ppm, involved either a nitrogen carrier gas for pyrolysis experiments or a nitrogen–oxygen carrier gas (including approximately stoichiometric conditions and fuel-lean conditions with an equivalence ratio of approximately 0.1) for oxidation experiments. On-line, extractive sampling in conjunction with analysis by fourier transform infra-red (FT-IR) spectrometry and gas chromatography/mass spectrometry (GC/MS) was performed to quantify species composition at four specific locations along the centerline of the turbulent flow reactor. Species concentrations were represented as a function of residence time in the reactor.

For the pyrolysis of diethyl sulfide, a destruction efficiency of 70% was observed for the 740 °C operating condition at a residence time of 0.06 second. Ethylene, ethane, and methane were detected at significant levels. In the oxidation experiments,

the destruction of diethyl sulfide was significantly enhanced. Complete destruction was observed in the 740 °C operating condition at a residence time of 0.06 second with low O<sub>2</sub> loading and in the 740 °C operating condition at a residence time of 0.03 second with high O<sub>2</sub> loading. Carbon monoxide, carbon dioxide, formaldehyde as well as the pyrolysis product species, were detected in the oxidation experiments.

The experimental investigations of diethyl sulfide were complemented by mechanism development along with thermochemical properties. The present model of H-C-S-O system consists of approximately 1000 elementary reactions among 300 species. Mechanism predictions reproduced the experimental results satisfactorily. Rate of production analysis under several conditions in the present work showed that the initiation of diethyl sulfide destruction is through unimolecular dissociation via C-S bond cleavage. Once the radical pool is established, hydrogen abstraction becomes primary destruction routes.  $\beta$ -scission of the derived radicals forms thioaldehydes and subsequent multi-hydrogen abstractions and  $\beta$ -scissions convert thioaldehydes to sulfur dioxide. Sensitivity analysis indicated that the reactions, having important effects on radical pools, to which mechanism predictions are the most sensitive.

Destruction of ethyl methyl sulfide was observed to be significantly slower than that of diethyl sulfide under the same conditions as those for diethyl sulfide and similar products were experimentally observed as those from diethyl sulfide. The kinetic mechanism is still under development. The formation of the products was explained by a scheme by analogy to that of diethyl sulfide. Significantly slower rates of pyrolysis of ethyl methyl sulfide were explained by the different destruction efficiencies including lower hydrogen abstraction rates, and lower hydrogen atom production as a result of thermal decomposition pathways.

## **BIOGRAPHICAL SKETCH**

Xin Zheng was born on April 13, 1979, in Shaowu, a small town surrounded by forests and mountains on the east coast of China (Fujian province). He was growing there, where he began his education at the Tongtai elementary school in 1985 and then attended No.1 middle school in 1991 and No. 1 high school in 1994. In the summer of 1997, He advanced to the University of Science and Technology of China in Hefei, the capital of Anhui province on the central-east part of China. In June of 2001, He graduated with dual bachelor degrees in Mechanical Engineering and Electronic Engineering. That fall, he entered the Fire Science Laboratory from which he obtained a Master of Science degree in Fire Protection Engineering in June of 2004. He moved to Ithaca, New York, USA, in August of 2004, where he has been studying at Cornell University, in the Sibley School of Mechanical and Aerospace, to complete a doctoral degree.

## ACKNOWLEDGMENTS

I would like to begin by acknowledging the Army Research Office's funding of the work present in the dissertation, under contract W911NF0410120 and through instrument grant DURIP W911NF0610142.

I owe the most to my joint advisors, Professor Elizabeth Mills Fisher and Professor Frederick Caskey Gouldin, who were always to provide insightful suggestions and directions to the work, and in particular in the first couple years when I had numerous troubles with the ventilation system to get the study proceed, their encouragement made today's achievement come true.

I thank Professor Harry Floyd Davis for serving on my committee and thank Professor Paul Houston for giving advices on choosing courses in the field of chemistry.

I thank my collaborators, Professor Joseph W. Bozzelli and his coworkers, Li Zhu and Rubik Asatryan, at New Jersey Institute of Technology, for their great contributions to the mechanism development.

I would also like to thank the Sibley school people, in particular, Richard Schmidt and Matthew Ulinski, who always offered their hands when I needed help in the laboratory.

Many people have supported me throughout my stay at Cornell and I owe a lot to all of them. I especially thank my wife, Hui Zhang, for staying in cold Ithaca with me for the Ph.D. life. I thank my great parents, Guirong Zheng and Yune Pan, and parents in law, Qinhe Zhang and Peihong Fang.

## TABLE OF CONTENTS

<b>BIOGRAPHICAL SKETCH</b>	<b>III</b>
<b>ACENOWLEDGEMENTS</b>	<b>IV</b>
<b>TABLE OF CONTENTS</b>	<b>V</b>
<b>LIST OF FIGURES</b>	<b>VIII</b>
<b>LIST OF TABLES</b>	<b>XII</b>

## CHAPTER 1 INTRODUCTION

1.1 Overview of chemical warfare agents	1
1.2 Disposal past and present: motivation for present research	5
1.3 Overview of combustion chemistry of sulfur compounds	7
1.3.1 Hydrogen sulfide oxidation and pyrolysis	8
1.3.2 Inhibition and sensitization of hydrocarbon combustion by sulfur species	10
1.3.3 Pyrolysis of sulfide and mercaptan	14
1.4 Sulfur mustard simulants	16
1.5 Dissertation overview	19
References	21

## CHAPTER 2 EXPERIMENTAL AND COMPUTATIONAL STUDY OF DIETHYL SULFIDE PYROLYSIS AND MECHANISM

2.1 Introduction	26
2.2 Experimental apparatus and methodology	27
2.2.1 Materials	27
2.2.2 Flow reactor	27
2.2.3 Sampling&Analysis	29
2.3 Mechanism and model calculation	31

2.4 Results and discussion	33
2.5 Summary and conclusions	43
2.6 Acknowledgements	43
References	44
 <b>CHAPTER 3 EXPERIMENTAL AND COMPUTATIONAL STUDY OF OXIDATION OF DIEHTYL SULFIDE IN A FLOW REACTOR</b>	
3.1 Introduction	48
3.2 Experimental apparatus and methodology	49
3.3 Mechanism construction and computational method	50
3.4 Results and discussion	60
3.5 Summary and conclusions	74
3.6 Acknowledgements	75
References	76
 <b>CHAPTER 4 PYROLYSIS AND OXIDATION OF ETHYL METHYL SULFIDE IN A FLOW REACTOR</b>	
4.1 Introduction	80
4.2 Experimental apparatus and methodology	81
4.3 Results	84
4.4 Discussion	97
4.4.1 Mechanism of pyrolysis of ethyl methyl sulfide	97
4.4.2 Destruction efficiency	100
4.4.3 Mechanism of oxidation of ethyl methyl sulfide	102
4.5 Conclusions	107
4.6 Acknowledgements	107
References	108



## **APPENDIX A EXPERIMENTAL APPARATUS AND METHODOLOGY**

A.1 Overview	110
A.2 Flow reactor	110
A.2.1 Flow feed system	111
A.2.1.1 Main flow	112
A.2.1.2 Secondary flow	113
A.2.1.3 Reaction section	115
A.2.2 Sampling system	123
A.3 Flow conditions in the reaction section	129
A.3.1 Gas temperatures	129
A.3.2 Mixing conditions	130
A.3.3 Leak test on the flow reactor	131
A.4 Analysis methods	139
A.4.1 Fourier-transform infrared spectroscopy	139
A.4.2 Gas chromatography-Mass spectrometry	141
References	156

## **KINETIC MECHANISM OF PYROLYSIS OF DIETHYL SULFIDE**

B.1 Kinetic mechanism used for calculations performed in Chapter 2	157
B.2 Thermochemical properties for diethyl sulfide pyrolysis (Chapter 2)	163

## **KINETIC MECHANISM OF OXIDATION OF DIETHYL SULFIDE**

C.1 Kinetic mechanism used for calculations performed in Chapter 3	168
C.2 Thermochemical properties for diethyl sulfide oxidation (Chapter 3)	199

## LIST OF FIGURES

1.1 Molecular structures of blister agents	4
1.2 Molecular structures of mustard simulants	18
2.1A Pyrolysis of diethyl sulfide at 630 °C	37
2.1B Pyrolysis of diethyl sulfide at 670 °C	37
2.1C Pyrolysis of diethyl sulfide at 700 °C	38
2.1D Pyrolysis of diethyl sulfide at 740 °C	38
2.2 Element balances, defined as the mass percent of a given element that is detected in the form of quantified species shown in Figure 2.1 A-D.	39
2.3 Comparison of experimental elemental loss with predicted contribution of major undetectable species, H <sub>2</sub> , CH <sub>3</sub> CH*S and CH <sub>2</sub> *S (regions between lines)	40
2.4 Major reaction pathways	41
3.1A Pyrolysis of CCSCC at 630 °C	58
3.1B Pyrolysis of CCSCC at 670 °C	58
3.1C Pyrolysis of CCSCC at 700 °C	59
3.1D Pyrolysis of CCSCC at 740 °C	59
3.2A Oxidation of CCSCC (Φ~1) at 630 °C	66
3.2B Oxidation of CCSCC (Φ~1) at 670 °C	66
3.2C Oxidation of CCSCC (Φ~1) at 700 °C	67
3.2D Oxidation of CCSCC (Φ~1) at 740 °C	67
3.3A Oxidation of CCSCC (Φ~0.1) at 630 °C	68
3.3B Oxidation of CCSCC (Φ~0.1) at 670 °C	68
3.3C Oxidation of CCSCC (Φ~0.1) at 700 °C	69
3.3D Oxidation of CCSCC (Φ~0.1) at 740 °C	69

3.4 Element balances of CCSCC oxidation ( $\Phi \sim 1$ ), defined as the mass percent of a given element that is detected in form of quantified species shown in Figure 3.3	70
3.5 Element balances of CCSCC oxidation ( $\Phi \sim 0.1$ ), defined as the mass percent of a given element that is detected in form of quantified species shown in Figure 3.4.	70
3.6 Oxidation pathways of 100 ppm diethyl sulfide at the 740 °C with approximately 9000 ppm O <sub>2</sub> loading and with a residence time of 0.06 second	71
4.1 Destruction efficiencies of ethyl methyl sulfide by pyrolysis and oxidation, and destruction efficiencies of diethyl sulfide by pyrolysis, measured at the last sampling port of the flow reactor.	86
4.2 Mole fraction of ethyl methyl sulfide in the pyrolysis and oxidation experiments	87
4.3 Mole fraction of ethylene in the pyrolysis and oxidation experiments	88
4.4 Mole fraction of ethane in the pyrolysis and oxidation experiments	89
4.5 Mole fraction of methane in the pyrolysis and oxidation experiments	90
4.6 Mole fraction of carbon monoxide in the oxidation experiments	91
4.7 Mole fraction of carbon dioxide in the oxidation experiments	92
4.8 Mole fraction of sulfur dioxide in the oxidation experiments.	93
4.9 Mole fraction of formaldehyde in the oxidation experiments	94
4.10 Element balances of CCSC pyrolysis, defined as the mass percent of a given element that is detected in the form of quantified species shown in Figures 4.2-4.5	95
4.11 Element balances of CCSC oxidation, defined as the mass percent of a given element that is detected in the form of quantified species shown in	96

Figures 4.2-4.9

4.12 Bond dissociation energies (BDEs) (cal/mole) of C-S and C-C bonds in ethyl methyl sulfide and diethyl sulfide.	106
A.1 Flow reactor, flow feed system and main flow	117
A.2 Injectors	120
A.3 Secondary flow	121
A.4 Reaction section	122
A.5 Sampling probe	126
A.6 Sampling system for FT-IR	127
A.7 Sampling system for GC/MS	128
A.8 Axial alignment device	133
A.9 Gas temperatures on the centerline of the reaction section	134
A.10 Gas temperatures at the position of the second sampling port in the reaction section at the 700 °C operating temperature	135
A.11 Normalized CO concentrations with or without presence of CCSCC/CCSC	136
A.12 Normalized CO concentrations	137
A.13 Reactor pressure in the leak test	138
A.14 Carbon monoxide calibration data and curve (FT-IR)	145
A.15 Ethylene calibration data and curve (FT-IR)	146
A.16 Carbon dioxide calibration data and curve (FT-IR)	147
A.17 Methane calibration data and curve (FT-IR)	148
A.18 Ethane calibration data and curve (FT-IR)	149
A.19 Sulfur dioxide calibration data and curve (FT-IR)	150
A.20 Diethyl sulfide calibration data and curve (FT-IR)	151
A.21 Ethyl methyl sulfide calibration data and curve (FT-IR)	152

A.22 Formaldehyde calibration data and curve (FT-IR)	153
A.23 Diethyl sulfide calibration data and curve (GC/MS)	154
A.24 Ethyl methyl sulfide calibration data and curve (GC/MS)	155

## LIST OF TABLES

1.1 Common chemical warfare agents	3
2.1 Reactions with the highest sensitivity coefficient affecting the concentrations of major species at the 740 °C	42
3.1 Modifications of kinetic parameters of the pyrolysis mechanism	56
3.2 Modifications of kinetic parameters of Leeds sulfur mechanism	57
3.3 Modifications of kinetic parameters of Hydrocarbon mechanism	57
3.4 Reactions with the highest sensitivity coefficient affecting the concentrations of major species at the 740 °C with approximately 9000 ppm O <sub>2</sub> loading	72
A.1 Flow parameters of pyrolysis experiments of diethyl sulfide	118
A.2 Flow parameters of pyrolysis experiments of ethyl methyl sulfide	118
A.3 Flow parameters of oxidation experiments of diethyl sulfide	119
A.4 Flow parameters of oxidation experiments of ethyl methyl sulfide	119
A.5 Chemicals for calibration data collection	144

# **CHAPTER 1**

## **INTRODUCTION**

### **1.1 OVERVIEW OF CHEMICAL WARFARE AGENTS**

Chemical agents have been utilized for military purposes since ancient times [1]. They were used to pollute water or generate poisonous or irritative smoke on battle fields. Such crude chemical warfare agents were not artificially synthesized, but usually extracted from plants and animals.

Modern development and production of chemical warfare agents started in late 19<sup>th</sup> century. The first large scale employment was of sulfur mustard, a blister agent, by German Army in World War I [2]. After that, development and accumulation of chemical warfare agents continued and became a part of arms race between the Warsaw Pact and NATO countries, during the Cold War.

The United States has been developing and stockpiling chemical warfare agents for 40 years even though it never used any agent in combats. The stockpile inventory of the United States includes some of the most deadly chemical warfare agents such as sarin (GB) and sulfur mustard (H/HD). These lethal agents, as listed in Table 1.1 [3], can be classified into nerve agents and blister agents in terms of their clinical effects.

As shown in Table 1.1, the nerve agents, including GA (tabun), GB (sarin), GD (soman), GF and VX, belong to a class of phosphorus-containing organic compounds that disturb the mechanism by which nerves transfer messages to organs [4]. The nerve agents are the most toxic chemical warfare agents. Inhalation is the primary entry to bodies for nerve agents, while they can also be absorbed through the skin.

Compared to the nerve agents, the vesicant or blister agents are less toxic but disperse more quickly to large areas, because of their higher volatility. The blister agents consist of H/HD (mustard), L (lewisite), Q (sesquimustard), T (bis[2-(2-

chloroethylthio)ethyl] ether) and HN-3 (nitrogen mustard), with molecular structures in Figure 1.1. H/HD, also known as sulfur mustard, probably is the best known chemical warfare agent. Pure sulfur mustard is colorless oily liquid at room temperature and smells like mustard, garlic or onion, while in impure forms, it is usually yellow-brown in color. Some impure forms of mustard are blends between different vesicant agents, such as HL, HT and HQ. In addition to causing blisters, mustard and other blister agents can also damage eyes, respiratory tracts and other organs [4].

In a broad sense, choking agents, vomiting agents, tearing agents and incapacitating agents are also included in chemical warfare agents. But those agents are not lethal (a large overdose does not cause death), and they have common uses outside of military purposes.



Table 1.1 Common chemical warfare agents [3].

CW agent	IUPAC name	Alternative name
GA	O-Ethyl N,N-dimethyl phosphoramidocyanidate	Tabun
GB	O-Isopropyl methylphosphonofluoridate	Sarin
GD	O-Pinacolyl methylphosphonofluoridate	Soman
VX	O-Ethyl S-2-diisopropyl aminoethyl methyl phosphonothiolate	
GF	Cyclohexyl methylphosphonofluoridate	Cyclosarin
H/HD	Bis(2-chloroethyl) sulfide	Mustard
HN-3	Tris(2-chloroethyl) amine	Nitrogen sulfide
L	2-Chlorovinylchloroarsine	Lewisite
Q	1,2-Bis(2-chloroethylthio) ethane	Sesquimustard
T	Bis[2-(2-chloroethylthio)ethyl] ether	O Mustard

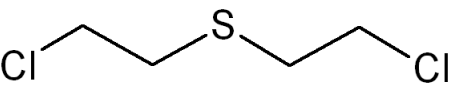
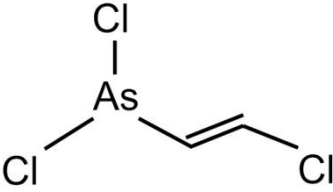
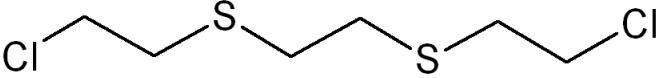
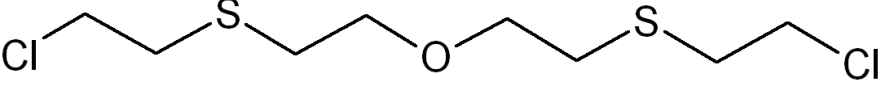
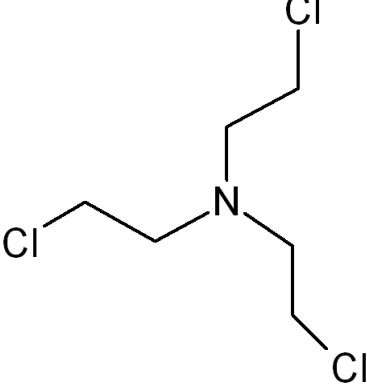
Nerve agents	Molecular structures
H/HD (Mustard)	
L (Lewisite)	
Q (Sesquimustard)	
T (O Mustard)	
HN-3 (Nitrogen mustard)	

Figure 1.1 Molecular structures of blister agents [3].

## **1.2 DISPOSAL PAST AND PRESENT: MOTIVATION FOR PRESENT**

### **RESEARCH**

In the United States, stockpiles of chemical warfare agents were distributed at eight sites throughout the continent (Edgewood, MD; Anniston, AL; Blue Grass, KY; Newport, IN; Pine Bluff, AR; Pueblo, CO; Deseret, UT; Umatilla, OR) and at one site on Johnston island, located southwest of Hawaii. Originally approximate 30000 tonnes of chemical warfare agents, mainly consisting of nerve agents GB, VX and blisters H, HT and HD, were stored at these nine sites [5]. In general, about 60% of the stockpile was in bulk containers, and 40% was stored in munitions including rockets, projectiles and mines. Of these nine sites, the Deseret (Tooele) site was the largest one, storing more than 40% of the original stockpiles.

Before 1972, the US army disposed of the sealed containers of chemical warfare agents in the ocean, e.g. in the Baltic Sea and the Sea of Japan [6]. At that time, it was believed that the huge amount of ocean water could dilute chemical agents that might leak from the containers to non-toxic levels. However, public concerns about environmental risks led to abandoning the dumping of chemical warfare agents offshore.

The Army started developing environmentally acceptable disposal methods in the 1970s. A pilot scale incineration facility was constructed at the Deseret site in 1979. Approximately 100 tonnes of GB were safely destroyed in a demonstration operation [7]. During the same period, binary chemical weapons, designed to mix two non-toxic ingredients to form nerve agents [7], were developed and produced in the United States. The binary chemical weapon program coincided with the start of chemical weapon elimination talks between the United States and the Soviet Union later in the 1980s. In 1989, the two countries signed an agreement to destroy their chemical weapon stockpiles. This agreement sparked international discussions resulting in the

international treaty known as the Chemical Weapons Convention (CWC) [8], which entered into force on April 29, 1997. According to the CWC, the nerve and blister agents are classified in Schedule One as chemicals having few or no use outside of chemical weapons and are mandated to be fully destroyed before April 2007, and no extensions permitted past April 2012.

The US Army's first full scale disposal facility was based on incineration technology and was built at Johnston Atoll site. The facility began processing the stockpiles stored on site in 1990. Following the successful operation of incinerators at Johnston site, similar disposal facilities were constructed at some other sites. Each facility included four incinerators, each for a different waste stream. Each incinerator was equipped with afterburners and pollution abatement systems to treat the exhaust. The incineration process employed in these disposal facilities is a multistage process using extreme temperatures to destroy chemical warfare agents and clean and/or destroy metal parts, explosives and containers [9].

In addition to incineration, alternative technologies are also employed. For instance, a chemical neutralization method is utilized at the Edgewood and Newport sites [7]. However, as the baseline technology for disposal of chemical warfare agents, the incineration is a very mature method with high destruction efficiencies, applicability to a wide range of chemicals, and good cost effectiveness. In the United States, the disposal of chemical warfare agents was, is and probably will be mainly reliant on the incineration technology.

In the past decade, there have been strong public oppositions to chemical weapons incineration [10]. The critics claim that even though the pollution is at trace levels and not lethal, where the incineration is operated properly, the effect may be chronic and difficult to investigate. In addition, of particular concern is emission from the off-design operation, which did occur a few times at both the Johnston and Deseret sites.

After the incidents, chemical release outside of the disposal facilities was detected [11]. Public opposition has been such that the Army slowed down the operation schedule on the existing incineration facilities as well as the construction of additional incinerators. The slowdown has in turn delayed the expected end of disposal operation beyond the 2012 international treaty deadline and beyond the 2017 deadline set by the US Congress.

Responding to the demand of the Army and public concerns, great efforts have been put to investigate the destruction of chemical warfare agents in incineration-relevant conditions [12-15]. Now that 60% of chemical stockpiles in the United States have been destroyed [7], including the complete elimination of GB and VX stockpiles, sulfur mustard is the dominant component of the chemical weapon stockpiles still awaiting destruction. The conditions lead to a particular interest in sulfur mustard chemistry for the development of efficient and clean incineration technologies.

### **1.3 OVERVIEW OF COMBUSTION CHEMISTRY OF SULFUR COMPOUNDS**

In last decades, the increasing concern over environmental pollution from global industrialization, especially acid rain, has led to great efforts to investigate sulfur chemistry. The resulting progress is significant in the development of sulfur chemistry in the troposphere and stratosphere. In contrast, rather less improvement has been achieved in understanding the kinetics by which anthropogenic sulfur species are produced, predominantly from combustion of fossil fuels and in petroleum refining. The quantity of the kinetic data is limited and the quality is generally low.

Early studies (before the 1970s) were reviewed by Cullis et al. [16], who compiled about 20 elementary reactions. Although this list may be outdated, it provided a basis for the subsequent development of combustion chemistry of sulfur containing species.

Numerous studies have transformed our view of the detailed combustion kinetics of sulfur containing species since the review [16]. In the following sections, a few studies of particular interest for the present work, focusing on gas phase combustion kinetics involving volatile small sulfur containing species, are briefly reviewed.

### 1.3.1 HYDROGEN SULFIDE OXIDATION AND PYROLYSIS

Understanding the combustion kinetics of hydrogen sulfide ( $\text{H}_2\text{S}$ ), a naturally occurring compound in fossil fuels, has been driven by the desire to develop emission control technologies. For the oxidation of hydrogen sulfide (H-S-O system), a pioneering work by Frenklach et al. [17] reported a kinetic model, consisting of 57 reactions among 17 species, which made use of some earlier works. The modeling produces generally satisfactory agreement with experimental measurements on the ignition delay behind reflected shock waves with 4-22% hydrogen sulfide in air with or without  $\text{H}_2\text{O}$  addition at pressures of 3-45 atm and temperatures of 900-1200 K. Due to the lack of measured kinetic data for many reactions, a major part of the model was based on generic estimation. In addition, many important species, for instance HOSO and HOSO<sub>2</sub>, are not included in the model.

Years later, Tsuchiya et al. [18] added valuable kinetic data on three key elementary reactions, including  $\text{HS} + \text{O}_2 \leftrightarrow \text{products}$ ,  $\text{S} + \text{O}_2 \leftrightarrow \text{SO} + \text{O}$ , and  $\text{SO} + \text{O}_2 \leftrightarrow \text{SO}_2 + \text{O}$ . They conducted laser photolysis experiments, where H, O and S atom concentrations were measured behind shock waves by applying the atomic resonance absorption spectrometry. A simple kinetic model was presented by combining their data with other experimental works on the kinetics of H-S-O system. The model predictions agree well with the experimental results on the  $\text{SO}_2$  formation delay time by Bradley et al. [19]. However, as admitted by the authors, assuming  $\text{H}_2\text{S} (+\text{M}) \leftrightarrow \text{H}_2 + \text{S} (+\text{M})$  as the primary dissociation route instead of H-S scission reaction  $\text{H}_2\text{S} \leftrightarrow$

HS + H for H<sub>2</sub>S is subject to debate. Direct measurements on these two reactions at high temperatures would be desirable.

More recently, a detailed kinetic model for the pyrolysis of hydrogen sulfide (H-S system) was constructed by Sendt et al. [20] under the conditions relevant to combustion as well as the use of H<sub>2</sub>S as a hydrogen carrier or as a feedstock for elemental sulfur. The model was built by analogy to the well established H-O system with 21 elementary reactions among 8 species. Kinetic parameters, when literature data were not available, were obtained by computational methods including transition state theory, master equation as well as Quantum-Rice-Ramsperger-Kassel (QRRK) [21]. The model was validated against various conditions, for temperatures from 873 to 1423 K, pressures from 0.04 to 3 bar and H<sub>2</sub>S mole fractions between 0.02 and 1. Model predictions are highly sensitive to the kinetic rates of a few radical branching and termination steps involving HSS and HSSH, similar to the results which are found for the H-O system. Such comprehensive modeling work indicates that even for the simple H-S system, the kinetics is complicated and the experimental observations cannot be explained by a global step or a few steps.

Compared to hydrogen sulfide, less attention has been paid to other small sulfur containing species. Chernysheva et al. [22] summarized high temperature kinetic data of the C-S-O system available in literatures and proposed a kinetic mechanism, including 70 elementary reactions, for the gas-phase oxidation of carbon disulfide (CS<sub>2</sub>). They calculated product concentrations under various conditions (temperatures from 300 to 2000 K, pressures from 1 to 2000 torr and CS<sub>2</sub> mole fractions between 0.005% and 50%). Comparison of the results obtained with the available experimental data show fair agreement. However, as it was purely constructed on available literature data without supplementary kinetic-oriented analysis, the mechanism is not

sufficient and considered to be the first approximation for C-S-O system, in need of completion and improvement.

### **1.3.2 INHIBITION AND SENSITIZATION OF HYDROCARBON**

#### **COMBUSTION BY SULFUR SPECIES**

In recent times, with the development of sulfur pre-abatement technologies and the enforced use of fossil fuels with low sulfur content, efforts have been shifted to investigate the effect of the sulfur containing species, even at trace levels, on hydrocarbon combustion instead of the combustion of the sulfur containing species themselves.

Pauwels et al. studied [23][24] low pressure methanol-air flames doped with variant levels of  $\text{H}_2\text{S}$  by using probe sampling in conjunction with electron spin resonance (ESR) detection. They observed depressed radical levels and elevated levels of  $\text{H}_2$  and  $\text{SO}_2$  compared to the undoped flames and hypothesized that the difference is mainly due to the reaction  $\text{H} + \text{H}_2\text{S} \leftrightarrow \text{H}_2 + \text{HS}$ .

Taniguchi et al. [25] reported a similar study on an atmospheric methanol-air flame doped with  $\text{CS}_2$ . Decreased radical levels and elevated hydrogen concentration were also observed. Their conclusions are consistent with those of Pauwels et al [23][24].

Kramlich et al. [26] investigated the combustion of various hydrocarbons doped with  $\text{H}_2\text{S}$ ,  $\text{SO}_2$  and thiophene at temperatures of 1600-1800 K with an equivalence ratio from 0.7 to 1.7 by using a jet-stirred reactor coupled with absorption spectroscopy and gas chromatography. They observed fast oxidation of reduced sulfur species to  $\text{SO}_2$  at all equivalence ratios studied. It was concluded that the effect of the reduced sulfur species on the hydrocarbon combustion is minor and is only present at



very early stages, while the primary effect is through the coupling of SO<sub>2</sub> with hydrocarbon combustion.

Glarborg and his co-workers [27-29] systematically studied the effect of SO<sub>2</sub> on CO oxidation under flow reactor conditions. Their initial work [27] combined experimental measurements and theoretical analysis on reactions of SO<sub>2</sub> in moist CO. The experiments were conducted in an isothermal flow reactor at atmospheric pressure and at temperatures 800-1300 K under fuel lean conditions with various levels of SO<sub>2</sub>, NO and moisture. The onset of CO consumption was experimentally observed to shift toward higher temperatures with the presence of 1500 ppm SO<sub>2</sub> compared to that of the conditions without SO<sub>2</sub> addition. And the temperature shift (20-40 K) was more pronounced at leaner conditions with lower H<sub>2</sub>O levels. Complementary mechanism development on the H-S-O system included estimation of thermodynamic properties of sulfur species as well as QRRK analysis for reactions involving HSO<sub>2</sub>, H<sub>2</sub>SO and HOSO<sub>2</sub>. The model predictions are in reasonable agreement with the experimental results. Based on the kinetic analysis, the inhibition effect of SO<sub>2</sub> on CO oxidation was found to be through catalytic recombination cycles on radical pools as follows: (a) for H atom, SO<sub>2</sub> + H (+M) ↔ HSO<sub>2</sub> (+M), HSO<sub>2</sub> + O<sub>2</sub> ↔ SO<sub>2</sub> + HO<sub>2</sub>; (b) for OH radical, SO<sub>2</sub> + OH (+M) ↔ HOSO<sub>2</sub> (+M), HOSO<sub>2</sub> + O<sub>2</sub> ↔ SO<sub>3</sub> + HO<sub>2</sub>, SO<sub>3</sub> + O ↔ SO<sub>2</sub> + O<sub>2</sub>; (c) for O atom, SO<sub>2</sub> + O (+M) ↔ SO<sub>3</sub> (+M), SO<sub>3</sub> + O ↔ SO<sub>2</sub> + O<sub>2</sub>. The cycle with O is the primary radical sink under the fuel-lean conditions. In this study, additional tests on the effect of NO addition were also conducted under similar conditions. Both promotion and inhibition effects on CO oxidation were observed with the presence of NO. The promotion effect was explained by reaction: NO + HO<sub>2</sub> ↔ NO<sub>2</sub> + OH which converts HO<sub>2</sub> to more reactive OH radical, while the inhibition follows the similar routes to SO<sub>2</sub> inhibition. And direct interactions between NO and SO<sub>2</sub> were estimated to be minor when compared to their reactions with radical pools.

Later in [28], oxidation experiments on moist CO doped with SO<sub>2</sub> are extended from fuel-lean to fuel-rich conditions. The observation on the temperature shift of the CO consumption onset showed that oxidation is promoted by SO<sub>2</sub> in a narrow range of conditions close to stoichiometric, while inhibited when the condition gets richer or leaner. The promotion near stoichiometric was explained through a two-step branching sequence: SO<sub>2</sub> + H ↔ SO + OH, SO + O<sub>2</sub> ↔ SO<sub>2</sub> + O. And the radical recombination mechanisms described in the preceding paragraph were assumed for the inhibition. In addition, the kinetic model was evaluated against literature data [29] from a H<sub>2</sub>/O<sub>2</sub>/N<sub>2</sub> flame doped with SO<sub>2</sub>. The comparison showed a large discrepancy for major sulfur containing species. Two new routes: (a) S<sub>2</sub> + H (+M) ↔ HS<sub>2</sub> (+M), HS<sub>2</sub> + H (+M) ↔ H<sub>2</sub>S<sub>2</sub> (+M), HS<sub>2</sub> + H ↔ S<sub>2</sub> + H<sub>2</sub>, H<sub>2</sub>S<sub>2</sub> + H ↔ HS<sub>2</sub> + H<sub>2</sub>; (b) SO + H (+M) ↔ HSO (+M), HSO + H ↔ SH + OH, SH + H<sub>2</sub> ↔ H<sub>2</sub>S + H, were proposed to explain the enhanced inhibition effect under the conditions of the literature flame[29].

A recent study [30] investigated the effects (1) of NO and SO<sub>2</sub> on the oxidation of a CO/H<sub>2</sub> mixture in a jet-stirred reactor at one atmosphere and temperatures of 800-1400 K with the equivalence ratio ranging from 0.1 to 2 and (2) of SO<sub>2</sub> under similar conditions in a laminar flow reactor. It was demonstrated that the NO and SO<sub>2</sub> effects depend on the operating temperature as well as the equivalence ratio. At fuel-lean conditions below 1000 K, NO addition promoted oxidation of CO/H<sub>2</sub> mixture, whereas the SO<sub>2</sub> effect is insignificant. As the equivalence ratio or the temperature increased, both species inhibited the oxidation of CO/H<sub>2</sub> mixture. The experimental observations were interpreted through kinetic modeling, which was based on previous studies [26][27] and other works [31][32]. As the inhibition effect was more pronounced under the conditions studied, a higher rate for the key reaction: H + SO<sub>2</sub> (+M) ↔ HSO<sub>2</sub> (+M) was suggested.

At Leeds University, Blitz et al. [33] measured kinetic rates for the reaction  $\text{OH} + \text{SO}$  at temperatures 295-703 K by using flash photolysis coupled with laser induced fluorescence. Strong negative temperature dependence was observed and interpreted to be due to the competition between isomerization of the adduct  $\text{HOSO}$  to  $\text{HSO}_2$ , followed by decomposition to  $\text{H} + \text{SO}_2$ , and the reverse step to reproduce  $\text{OH} + \text{SO}$ , [34]. Later, in the study of Hughes et al. [35], the influence of  $\text{SO}_2$  on  $\text{NO}$  under post-combustion conditions was investigated by using laser-induced fluorescence measurements on  $\text{NS}$  and  $\text{NO}$  concentrations in burnt gas region in methane/oxygen/argon flames with a range of equivalence ratios. Experimental observations showed that the influence of  $\text{SO}_2$  varies with  $\text{SO}_2$  concentration, equivalence ratio and dilution level. The experimental data was used to evaluate the kinetic mechanism under the development for modeling the interactions of sulfur and nitrogen containing species under combustion-relevant conditions. A recent ab initio calculation [36] determined kinetic rates for reactions:  $\text{H} + \text{SO}_2 \leftrightarrow \text{HSO}_2$ ,  $\text{H} + \text{SO}_2 \leftrightarrow \text{HOSO}$ ,  $\text{H} + \text{SO}_2 \leftrightarrow \text{OH} + \text{SO}$ , and  $\text{HOSO} \leftrightarrow \text{HO} + \text{SO}$ , between 300-2000 K and  $10^{-3}$ - $10^6$  atm by applying a master equation model.

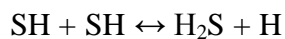
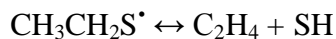
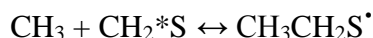
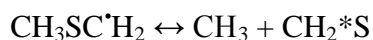
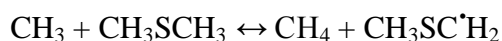
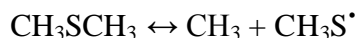
The kinetic data from these studies were compiled in the updated sulfur mechanism extension (V 5.2, 2005) [37], consisting of 117 elementary reactions among 41 species for modeling the kinetics of sulfur containing species ( $\text{CS}_2$ ,  $\text{H}_2\text{S}$  and  $\text{SO}_2$ ) and  $\text{NO}_x$  in methane combustion. As only a few investigations of combustion chemistry of sulfur have appeared since its release, the mechanism [37] may still be the best established sulfur kinetic model for combustion relevant high temperature conditions to date and is usually the first step for the further construction of sulfur kinetic model.

### 1.3.3 PYROLYSIS OF SULFIDE AND MERCAPTAN

Given that the combustion chemistry of the simple sulfur containing species is not quite complete, it is not surprising that the kinetics of more complicated sulfur containing species at high temperatures are even less well studied and less well understood. For methyl mercaptan ( $\text{CH}_3\text{SH}$ ), dimethyl sulfide ( $\text{CH}_3\text{SCH}_3$ ) and dimethyl disulfide ( $\text{CH}_3\text{SSCH}_3$ ), which are important sulfur components of biogenic emission, extensive investigations have been conducted on atmospheric conditions. However, only a few early investigations studied the high-temperature pyrolysis of mercaptans and sulfides. Sehon and co-workers [37,38] studied pyrolysis of benzyl mercaptan ( $\text{C}_6\text{H}_5\text{CH}_2\text{SH}$ ) and methyl benzyl sulfide ( $\text{C}_6\text{H}_5\text{CH}_2\text{SCH}_3$ ), in a quartz flow reactor (20.5 cm long and 3.8 cm ID) with toluene as a carrier gas and a free radical trap at temperatures of 700-1100 K and pressures of 4-20 torr. Concentrations of products as well as undecomposed mercaptan and sulfide were measured. They observed that the decomposition of benzyl sulfide and benzyl methyl sulfide proceeds through a first order process with the activation energy estimated to be similar to the respective C-S bond dissociation energy. Thus they concluded that the destruction of these two species is primarily via C-S bond cleavage. The formation of products including hydrogen sulfide, bibenzyl ( $\text{C}_5\text{H}_6\text{CH}_2\text{CH}_2\text{C}_5\text{H}_6$ ), ethylene ( $\text{C}_2\text{H}_4$ ), methyl mercaptan, methane and hydrogen were explained by using a reaction scheme but no estimation on kinetic parameters for the elementary reactions included. In [37][38], a few tests were also conducted for methyl mercaptan, ethyl mercaptan ( $\text{C}_2\text{H}_5\text{SH}$ ), dimethyl sulfide and dimethyl disulfide in the same flow reactor under more limited conditions. The formation of products including hydrogen sulfide, ethylene, methane and hydrogen were explained by using a reaction scheme. But reaction order and activation energy were not estimated for these species due to insufficient measurements. Thompson et al. [40][41] investigated the pyrolysis of 2-methyl-2-

propanethiol and 1-pentanethiol in similar flow reactor experiments. The reported observation and conclusion are consistent with those of Sehon et al. [38][39].

More recently, Shum et al. [42] studied the pyrolysis of dimethyl sulfide in a static system at temperatures of 681-723 K. The global reaction order was derived to be about 3/2 with respect to the concentration of dimethyl sulfide based on the pressure-time change. The major products were identified to be methane, ethylene, hydrogen sulfide and carbon disulfide by gas chromatogram/mass spectrometry (GC/MS) analysis. Formation of these species was described by a reaction scheme involving the following elementary reactions:



For the reactions above (where ‘\*’ represents a double bond and ‘•’ represents a radical site), kinetic parameters were estimated if literature data was not available. While, since the measurement on the product composition was only qualitative, no kinetic calculations were made to compare with the experimental results.

These preliminary studies provide experimental and kinetic information for the development of sulfur mechanism, but the studied operating temperatures are significantly lower than those of combustion systems.

The present review briefly describes our current kinetic knowledge about oxidation of sulfur containing species and their influences on hydrocarbon combustions. A more complete feeling of our understanding in this area can be obtained from the reviews of Hynes et al. [43] and Cerru et al. [44][45]. In general,

kinetics of sulfur containing species at high temperatures is less understood compared to that of hydrocarbons. Investigations of complicated sulfur components existing in hazardous wastes and biomass, at combustion relevant temperatures, would be very valuable to improve our understanding of combustion chemistry of sulfur.

The objectives of the present research have been to develop and validate a kinetic mechanism for model compounds of mustard chemical warfare agents such as HD. Such a kinetic model could be used to develop a model for the mustard agents themselves, which will be used to assess the impact of incinerator design and off-design operation on destruction efficiency as well as predicting the emissions of products of incomplete combustion.

#### **1.4 SULFUR MUSTARD SIMULANTS**

Experiments with actual sulfur mustard would have been the most direct way to gain maximum insight into the thermochemical process of sulfur mustard incineration. However, university laboratories are not equipped with the facilities needed to safely handle such a toxic chemical. For this reason, chemical simulants are commonly used. Simulants are compounds with physical and/or chemical properties similar to those of the chemical of interest, but with much lower toxicities. In selection of simulants for kinetic studies, similarity in molecular structures is the primary criterion. For sulfur mustard, 2-chloroethyl ethyl sulfide, diethyl sulfide, ethyl methyl sulfide and dimethyl sulfide are possible simulant options as shown in Figure 1.2.

2-chloroethyl ethyl sulfide would have been the best simulant for sulfur mustard as its molecular structure is very similar to that of sulfur mustard, with only one chlorine substitution by hydrogen. However, this compound is unacceptably toxic, and thus was not used. Diethyl sulfide is one simulant which has been chosen for the present research. As shown in Figure 1.2, the molecular structure of diethyl sulfide is similar

to that of sulfur mustard but with ethyl group instead of a chloroethyl group bonded to the sulfur atom. Limited photolytic experiments on 2-chloroethyl ethyl sulfide and diethyl sulfide [46-47] showed that the group substitution between two chemicals does not change major reaction pathways for photolysis.

Another simulant having been used in this project is ethyl methyl sulfide which resembles diethyl sulfide but with one ethyl group substituted by methyl group. Studying ethyl methyl sulfide allows us to compare the effect of methyl group on the destruction efficiency and product distribution with those of ethyl group from the studies on diethyl sulfide. And the study on ethyl methyl sulfide can provide a good data set for the validation of methyl sulfur reactions under development.

Dimethyl sulfide is not used in the present research. Its molecular structure resembles that of sulfur mustard, but with methyl groups attached to sulfur atom instead of 2-chloroethyl groups. As the primary biogenic sulfur emission, dimethyl sulfide may be one of the most extensively studied organosulfur compounds. Detailed reaction schemes for atmospheric oxidation of dimethyl sulfide are reported in [48] [49]. However, extrapolations of the reported kinetic rates to combustion temperatures may not be appropriate and need to be validated with proper experimental combustion data. Studies on dimethyl sulfide would also help us understand methyl subset reactions as with ethyl methyl sulfide.

The experiments on these sulfur mustard simulants are a substantial part of the present work in the following chapters. These experiments were conducted under the conditions, as reported in Appendix A, which were with lower temperatures as well as smaller quantities of oxidizer, compared to the actual incineration conditions. The intent of choosing such experimental conditions was twofold, (1) understanding the initiation of the destruction of sulfur mustard simulants and (2) exploring routes relevant to emissions under off-design incineration modes, such as fuel rich conditions

due to inhomogeneous mixing. The experimental data has been used to validate and further develop the kinetic mechanism.

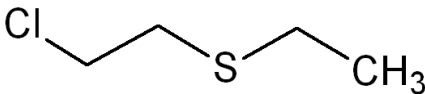
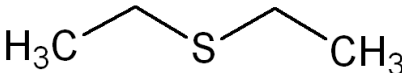
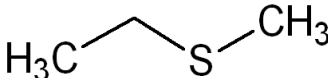
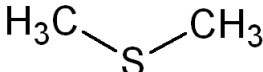
Simulants	Molecular structures
2-chloroethyl ethyl sulfide	
Diethyl sulfide	
Ethyl methyl sulfide	
Dimethyl sulfide	

Figure 1.2 Molecular structures of mustard simulants.



## 1.5 DISSERTATION OVERVIEW

The previous sections of this chapter have reviewed the development and the disposal of chemical warfare agents, and described the motivation for and the objectives of the present research. In the forthcoming dissertation, each chapter is a complete paper, which has been either published or accepted.

The first paper “Experimental and Computational Study of Diethyl Sulfide Pyrolysis and Mechanism”, which has been published in the 32<sup>nd</sup> Proceedings of Combustion Institute, is reported in Chapter 2. The paper focuses on initiation steps, such as unimolecular decomposition, of diethyl sulfide at very early stages of destruction. Those initiation steps are also the primary pathways for the destruction of diethyl sulfide under fuel rich conditions, e.g. the area surrounding the chemical injectors or off-design modes where the desired mixing levels are not accomplished. Flow reactor experiments and mechanism development for pyrolysis conditions are reported. Species profiles are compared to mechanism predictions for validation. Important reactions were determined through rate of production and sensitivity analyses.

Chapter 3 presents the second paper “Experimental and Computational Study of Oxidation of Diethyl Sulfide in A Flow Reactor”, published in the 33<sup>rd</sup> Proceedings of Combustion Institute. This paper continues the investigation reported on Chapter 2. The flow reactor experiments were conducted in the identical conditions as the pyrolysis experiments but with oxygen, either in stoichiometric quantities or in excess of stoichiometric quantities. Chapter 3 mainly deals with additional destruction steps for diethyl sulfide with the presence of oxygen, and secondary reactions of the resulting intermediate products. The mechanism is validated and further refined through comparison with experimental data. Rate of production and sensitivity analyses were performed to determine reactions of great interest.

Chapter 4 is purely an experimental report on pyrolysis and oxidation of ethyl methyl sulfide in a flow reactor. This paper has been accepted by the journal Combustion and Flame. Experiments were conducted in the same flow reactor and the same operating conditions as those for diethyl sulfide. Detected species profiles are reported. The destruction efficiency of ethyl methyl sulfide is compared to that of diethyl sulfide. Initial reactions and main production routes for important species in the pyrolysis and oxidation experiments are discussed by analogy to those of diethyl sulfide. This data set will be used to test a kinetic mechanism of ethyl methyl sulfide currently under development.

After the main body of the dissertation, details on the experimental apparatus and methodology are appended. This appendix is a supplement to the papers in Chapters 2-4, in which experiments are only briefly reviewed due to limited space. In this appendix, flow reactor, flow feeding, gas sampling, and analysis techniques are described in great detail. Schematics of the important reactor parts are provided to help with the description. Calibration curves for species detected at levels of 1 ppm or higher are also included.

At the end of the dissertation, two different versions of the kinetic mechanism for diethyl sulfide are attached, along with associated thermodynamic data files. Appendix B lists the pyrolysis mechanism, developed as described in Chapter 2. Appendix C contains an updated mechanism that also includes oxidation reactions, developed as described in Chapter 3. This version of the mechanism consists of three reaction subsets:  $C_1$ - $C_3$  hydrocarbon reactions, reactions of small sulfur containing compounds, and reactions of diethyl sulfide and resulting intermediate products as well as interactions between the subsets. In all, more than 1000 elementary reactions and 300 species are included in the mechanism. The files are in Chemkin [50] format and thus can be readily implemented for kinetic calculation.

## REFERENCES

- [1] G.G. Harigel, Seventh ISODARCO-Beijing Seminar on Arms Control, Xi'an, Oct. 8-13 (2000).
- [2] L. Szinicz, *Toxicology*, 214-3 (2005) 167-181.
- [3] P.A. D'Agostino, C.L. Chenier, *Analysis of Chemical Warfare Agents*, Report No. 0704-0188, Defence Research and Development Canada, 2006.
- [4] F.R. Sidell, *Military Preventive medicine: Mobilization and Deployment*, Vol. 1, Borden Institute (2003) 611-625.
- [5] S.A. Carnes, A.P. Watson, *the Journal of the American Medical Association*, 262-5 (1989) 653-659.
- [6] G.P. Glasby, *the Science of the Total Environment*, 206 (1997) 267-273.
- [7] *Milestones in U.S. Chemical Weapons Storage and Destruction*, U.S. Army Chemical Materials Agency, 2008.
- [8] *Chemical Weapons Convention*, 2009, <http://www.cwc.gov>.
- [9] G.S Pearson, R.S. Magee, *Pure Appl. Chem.*, 74-2 (2002) 187-316.
- [10] M.R. Green, *American Journal of Public Health*, 93-8 (2003) 1222-1226.
- [11] *Chemical Weapons Working Group (CWWG webpage 1998)*.
- [12] P.A. Glaude, C. Melius, W.J. Pitz, C.K. Westbrook, *Proceedings of the Combustion institute*, 29 (2002) 2469-2476.
- [13] J.H. Werner, T.A. Cool, *Combustion and Flame*, 117 (1999) 78-98.
- [14] P.H. Taylor, B. Dellinger, C.C. Lee, *Environ. Sci. Technol.*, 24 (1990) 316-328.
- [15] E.J. Zegers, *Flow Reactor Pyrolysis of Alkyl Phosphates and Phosphonates*, Ph.D. thesis, Cornell University, Ithaca, NY 14853, USA 1997.
- [16] C.F. Cullis, M.F.R. Mulcahy, *Combustion and Flame*, 18 (1972) 225.
- [17] M. Frenklach, J.H. Lee, J.N. White, W.C. Gardiner, *Combustion and Flame*, 41 (1981) 1-16.

- [18] Tsuchiya, K. Kamiya, H. Matsu, International Journal of Chemical Kinetics, 29 (2003) 57-66.
- [19] J.N. Bradley, D.C. Dobson, J. Chem. Phys., 46 (1967) 2865.
- [20] K. Sendt, M. Jazbec, B.S. Haynes, Proceedings of Combustion Institute, 29 (2002) 2439-2446.
- [21] A.Y. Yang, J.W. Bozzelli, A.M. Dean, International Journal of Research in Physical Chemistry and Chemical Physics, 214 (2000) 1533.
- [22] A.V. Chernysheva, V.Ya. Basevich, V.I. Vedeneev, V.S. Arutyunov, Russian Chemical Bulletin, 41-4(1992) 629-637.
- [23] J.F. Pauwels, M. Carlier, P. Devolder, L.R. Sochet, J. Phys. Chem., 90 (1986) 4377-4381.
- [24] J.F. Pauwels, M. Carlier, P. Devolder, L.R. Sochet, Combust. Sci. Tech., 90 (1990) 4377.
- [25] M. Taniguchi, N. Hirasawa, H. Yoshida, Bull. Chem. Soc. Jpn., 60 (1987) 2349.
- [26] J.C. Kramlich, P.C. Malte, W. Grosshandler, Proc. Combust. Inst., 18 (1981) 151-159.
- [27] P. Glarborg, D. Kubel, K. Dam-Johansen, H.-M. Chiang, J.W. Bozzelli, Int. J. Chem. Kinet., 28 (1996), 773–790.
- [28] M.U. Alzueta, R. Bilbao, P. Glarborg, Combustion and Flame, 127 (2001) 2234–2251.
- [29] A.S. Kallend, Combustion and Flame, 19 (1972) 227-236.
- [30] P. Dagaut, F. Lecomte, J. Mieritz, P. Glarborg, Int. J. Chem. Kinet., 35 (2003) 564-575.
- [31] P. Dagaut, F. Lecomte, S. Chevailler, M. Cathonnet, Combustion Sci. Technol., 139 (1998) 329.

- [32] A. Goumri, J.D.R. Rocha, D. Laakso, C.E. Smith, P. Marshall, *J. Phys. Chem. A*, 103 (1999) 11328.
- [33] M.A. Blitz, K.W. McKee, M.J. Pilling, *Proc. Combust. Inst.*, 28 (2000) 2491–2497.
- [34] A.J. Frank, M. Sadilek, J.G. Ferrier, F. Turecek, *J. Am. Chem. Soc.*, 119 (1997) 12343-12347.
- [35] K.J. Hughes, A.S. Tomlin, V.A. Dupont, M. Pourkashanian, *Faraday Discuss.*, 119 (2001) 337-352.
- [36] K.J. Hughes, M.A. Blitz, M.J. Pilling, S.H. Robertson, *Proc. Combust. Inst.*, 29 (2002), 2431–2437.
- [37] Sulfur Mechanism Extension to the Leeds Methane Mechanism (V5.2, August 2005), Available at: <http://www.chem.leeds.ac.uk/Combustion/sox.html>.
- [38] A.H. Schon, B.D. Darwent, *J. Am. Chem. Soc.*, 76 (1954) 4806-4810.
- [39] E.H. Braye, A.H. Schon, B. D. Darwent, *J. Am. Chem. Soc.*, 77 (1955) 5282-5285.
- [40] C.J. Thompson, R.A. Meyer, J.S. Ball, *J. Am. Chem. Soc.*, 74 (1951) 3284-3287.
- [41] C.J. Thompson, R.A. Meyer, J.S. Ball, *J. Am. Chem. Soc.*, 74 (1951) 3287-3289.
- [42] L.G.S. Shum, S.W. Benson, *International Journal of Chemical Kinetics*, 17 (1985) 749-761.
- [43] A.J. Hynes, P.H. Wine, in: *Gas Phase Combustion Chemistry*, W.C. Gardiner (Jr. Editor), Kinetics and Mechanism of the Oxidation of Gaseous Sulfur Compounds, New York, Springer 2000, 343-387.
- [44] F.G. Cerru, A. Kronenburg, R.P. Lindstedt, *Proceedings of Combustion Institute*, 30 (2005) 1227-1235.
- [45] G. Cerru, A. Kronenburg, R.P. Lindstedt, *Combustion and Flame*, 146 (2006) 437-455.

- [46] A.V. Vorontsov, C. Lion, E.N. Savinov, P.G. Smirniotis, *Journal of Catalysis*, 220-2 (2003) 414-423.
- [47] D.V. Kozlov, A.V. Vorontsov, P.G. Smirniotis, E.N. Savinov, *Applied Catalysis B: Environmental*, 42-1 (2003) 77-87.
- [48] F. Yin, D. Grosjean, J.H. Seinfeld, *Journal of Atmospheric Chemistry*, 11 (1990) 309-364.
- [49] F. Yin, D. Grosjean, J.H. Seinfeld, *Journal of Atmospheric Chemistry*, 11 (1990) 365-399.
- [50] Reaction Design, 2004, Chemkin User Interface 4.0, available at <http://www.reactiondesign.com>.

## CHAPTER 2

### EXPERIMENTAL AND COMPUTATIONAL STUDY OF DIETHYL SULFIDE PYROLYSIS AND MECHANISM

Xin Zheng<sup>1</sup>, E.M. Fisher<sup>1</sup>, F.C. Gouldin<sup>1</sup>, Li Zhu<sup>2</sup> and J.W. Bozzelli<sup>2</sup>

<sup>1</sup>Sibley School of Mechanical and Aerospace Engineering, Cornell University, Ithaca,  
New York 14853, USA

<sup>2</sup>Department of Chemistry and Environmental Science, New Jersey Institute of  
Technology, Newark, New Jersey 07101, USA

#### ABSTRACT

The pyrolysis of diethyl sulfide ( $\text{CH}_3\text{CH}_2\text{-S-CH}_2\text{CH}_3$ ), a simulant for mustard chemical warfare agents, was studied in a turbulent flow reactor with extractive gas composition analysis by GC/MS and FT-IR. Experiments were performed at approximately atmospheric pressure for four different temperatures between 630 °C and 740 °C with maximum residence times between 0.06 and 0.08 s. Temperature and species profiles were obtained on the centerline of the reactor. The mixing characteristics in the reactor were determined by using carbon monoxide as a tracer. 80% destruction of diethyl sulfide was observed for the experiment at the temperature of 740 °C and the residence time of 0.06 second. The following species were quantified: diethyl sulfide, ethylene, methane, ethane, acetylene, carbon disulfide, and thiophene. In addition, ethanethiol, methyl thirane, ethyl methyl disulfide, and diethyl disulfide were identified but not quantified. A light yellow solid containing sulfur condensed in sampling probes. Thermochemical properties for all species and a detailed mechanism were developed for modeling the reaction system. Thermodynamic and kinetic parameters were based on density functional theory and ab initio calculations using isodesmic work reactions for enthalpies. Kinetic parameters for chemical activation and unimolecular dissociation reactions were

determined with multi-frequency quantum RRK analysis for  $k(E)$  and master equation for fall-off. Important reactions were identified by sensitivity analysis and reaction pathway analysis of the mechanism. Model predictions show overall good agreement with experiments.

## 2.1 INTRODUCTION

Bis(2-chloroethyl) sulfide also called HD, or mustard gas, is a vesicant and is the principal component of munitions grade mustard. This material is highly poisonous, and has been manufactured and stored in many locations worldwide as a chemical warfare agent during the cold war [1, 2]. In recent decades, a great deal of effort has been put into the investigation of different disposal methods that include incineration, perhydrolysis [3], hydrolysis by aqueous alkalis, oxidative chlorination, chemical binding [4] and photocatalysis [5-9]. Chemical kinetic mechanisms relating to the incineration are needed to assess the impact of incinerator design and operational changes on destruction efficiency, and on the emission and stability of products of incomplete combustion. Although the chemistry of small hydrogen-sulfur oxide moieties ( $H_xSO_y$ ,  $x \leq 2$ ,  $y \leq 3$ ) has been studied extensively under combustion conditions [10, 11], the initial steps of destruction of HD or other sulfur hydrocarbons have not. Detailed kinetic data on the reactions of species with hydrocarbon C-S bonds is sparse [12-16].

Objectives of the present study were to investigate and construct a model for gas-phase pyrolysis of diethyl sulfide ( $CH_3CH_2-S-CH_2CH_3$ , subsequently abbreviated as CCSCC), as a simulant of mustard gas in a flow reactor. Diethyl sulfide is a good simulant of HD mustard because of its similar molecular structure. If hydrogens are substituted for the two chlorines in HD mustard, diethyl sulfide is produced.



## **2.2 EXPERIMENTAL APPARATUS AND METHODOLOGY**

### **2.2.1 MATERIALS**

The diethyl sulfide used in the experiments was 99% pure from Fluka, with only ethyl bromide and diethyl disulfide identified as impurities by the authors' GC/MS analysis, at about 0.01% levels. Carbon disulfide ( $\text{CS}_2$ ) (Aldrich, 99%), thiophene (cyc- $\text{C}_4\text{H}_4\text{S}$ ) (Aldrich, 99%), ethylene ( $\text{C}_2\text{H}_4$ ) (Airgas, 99%), methane ( $\text{CH}_4$ ) (Airgas, 99%), ethane ( $\text{C}_2\text{H}_6$ ) (GT&S, chemically pure) and acetylene ( $\text{C}_2\text{H}_2$ ) (Smith, 99%) were used for calibration. Nitrogen (Airgas) was the main constituent of the reactor flow. Carbon monoxide, 5% in nitrogen from Airgas, was used as a tracer to determine the flow mixing characteristics of the reactor.

### **2.2.2 FLOW REACTOR**

The flow reactor used for the current diethyl sulfide pyrolysis experiments was validated through acetate pyrolysis experiments, for which kinetics is well established [17]. The flow reactor consisted of a main flow and a secondary flow. The main flow started as liquid nitrogen, which was vaporized by heat transfer from room air, in a heat exchanger. It was then metered and passed through a retort inside a furnace. The main flow went through a stainless steel pipe with 53 mm ID, 60.3 mm OD, and 80 cm length, surrounded by clamshell heaters and ceramic fiber insulation. This flow development section maintained the elevated temperature of the nitrogen flow while achieving fully developed turbulent flow. From there, the gas flowed through a secondary flow injection section, where a nitrogen flow doped with diethyl sulfide was introduced; see Figure A.1 in Appendix A. The reaction section, pictured in Figure A.4 (Appendix A), was a quartz tube with 45 mm ID, 48 mm OD, and 100 cm length. This quartz tube was held inside a larger stainless steel pipe with 53 mm ID and 60.3 mm OD by rings of ceramic fiber insulation near each end. In turn the pipe was

surrounded by a second set of clamshell heaters and ceramic fiber insulation. Four ports on the stainless steel pipe were aligned with the holes in the quartz tube, allowing the insertion of probes for centerline gas sampling.

The secondary flow, as shown in Figure A.3 (Appendix A), making up about approximately 5% mass of the total reactor flow, was routed as follows: downstream of the flow meter it was sent through a liquid injection device consisting of a tee where diethyl sulfide was injected through a septum via a Harvard PHD 2000 syringe pump. The injection device was wrapped with heating tapes to help vaporize the injected diethyl sulfide. In order to reduce oscillations in the loading of the diethyl sulfide, a residence chamber with a volume of 3800 cm<sup>3</sup> was added downstream of the injection tee. The secondary flow was mixed with metered CO/N<sub>2</sub> flow, and then flowed through Sulfinert® (Restek) treated stainless tubing to the flow reactor. The injection of the secondary flow into the main flow occurred through four open-ended 4 mm ID, 6 mm OD quartz tubes inserted into the flow at a 60 ° angle (Figure A.2 in Appendix A). The tips of the tubes were 1 cm from the centerline of the reactor. During the experiments, an exhaust system kept the reactor interior approximately 5 torr below atmospheric pressure to prevent chemicals from leaking out. The exhaust system was equipped with carbon filters to reduce odors from the experiments.

The experiments reported in this study were performed at four different conditions, listed in Table A.1 (Appendix A). All of the reactor flows were turbulent with a Reynolds number of approximately 5000 based on volumetric flow rate and tube diameter. As computed for homogeneous mixing, the initial diethyl sulfide loading in the reactor was 150 ppm with a measurement uncertainty of 3%, while the CO tracer loading remained close to 66 ppm. The residence time in the reaction section was less than 0.1 second. Figure A.9 (Appendix A) shows the gas temperature profiles measured on the centerline by inserting a sheathed K type thermocouple (uncertainty

around 7 °C) with a diameter of 6.2 mm (as shown in Figure A.8 in Appendix A) from the downstream end of the reactor. The numbers in Figure A.9 are the average temperatures (rounded to the nearest 10) in the sampling region of the reaction section and are used to identify each condition.

### 2.2.3 SAMPLING & ANALYSIS

Samples were withdrawn from the reactor via a quartz probe (Figure A.5 in Appendix A). In order to quench reactions, the sample flow was diluted to approximately 50% of its original concentration with a concentric, metered, flow of nitrogen inside the quartz probe. A simple mixing calculation indicates that the dilution should cool the sample flow to be below 400 °C, at which temperature no composition changes in the product stream are predicted to occur during the sampling process. Downstream of the probe, the diluted sample was drawn through 6.35 mm OD Teflon® (Dupont) tubing into either a FT-IR (Nicolet 6700) or a GC/MS (Thermo Ultra Trace GC/DSQ II MS) for sample analysis.

For the GC/MS, as shown in Figure A.7 (Appendix A), the diluted sample was drawn by a vacuum pump through a gas sampling valve with a 500 µl loop from Valco. The valve body, the sample loop, and the transfer line from the valve to the GC/MS injection port were Sulfinert® (Restek) treated stainless steel. This loop with 1.6 mm OD highly restricted the sampling flow rate. A parallel bypass tube was installed between a tee just upstream of the sampling loop and the vacuum pump, to increase sampling rate from about 400 ml/min to 4000 ml/min, in the part of the flow upstream of the tee. The tiny volume of the loop (500 µl) resulted in repeatability problems, because the mixture composition at the sampling location varied over the short timescale corresponding to that sample loop size. A Sulfinert® (Restek) treated residence chamber, approximately 200 cm<sup>3</sup> in volume, was installed upstream of the

tee to average the flow composition over a period of 3 seconds, resulting in improved repeatability. Needle valves were used to adjust pressures at each end of the loop, for repeatable sample injection conditions. Compounds were separated in a J&W GS-Gaspro capillary column (30 m  $\times$  0.32 mm) with a temperature program, which started at 80 °C for 6 minutes, ramped to 260 °C with 15 °C/min, and stayed at 260 °C for 4 minutes. Molecules were electronically ionized for mass spectral analyses. Compounds were identified through comparison of a full scan spectrum to the NIST mass spectral library [18], and quantified through integration of selected ion monitoring chromatogram peaks.

For FT-IR analysis, as shown in Figure A.6 (Appendix A), diluted samples were passed through a 6-m-path cell (Infrared Analysis) with KBr windows, gold-coated mirrors, and a volume of approximately 10 liters. Compounds were identified by comparison with reference spectra created with the same cell, instrument, and pressure. Subtraction factors were obtained by subtracting multiples of reference spectra from unknown spectra in specific regions with significant absorbance features. Quantification was done by using calibration curvefits based on these subtraction factors [19]. Successive subtractions allowed quantification of overlapping spectra.

The sample species concentrations depend on the sample dilution and on the rate of mixing of main and secondary flows, as well as on the rates of chemical reactions occurring in the flow reactor. Corrections to the measured species concentrations were made using the CO tracer to account for mixing and dilution: the measured mole fraction of each compound was multiplied by the ratio of the well-mixed to measured CO mole fraction, to account for mixing and dilution. The measured mole fraction CO versus distance is shown in Figure A.12 (Appendix A) for the different temperature conditions. CO was determined to be inert under the conditions of the experiments via both equilibrium calculations and kinetics calculations which include standard CO

combustion reactions as well as newly estimated reactions  $\text{CO} + \text{SH} \leftrightarrow \text{OCS} + \text{H}$ , and  $\text{CO} + \text{CH}_3\text{S}^* \leftrightarrow \text{OCS} + \text{CH}_3$ . Inertness was also verified experimentally by comparing measured CO levels in the flow reactor in the absence and presence of diethyl sulfide/ethyl methyl sulfide in the 700 °C operating condition, as seen in Figure A.11 (Appendix A).

### 2.3 MECHANISM AND MODEL CALCULATION

An initial reaction mechanism has been developed, along with species thermochemical parameters; these are included as supplemental material (Appendix B). The mechanism is a sulfur-hydrocarbon mechanism of 171 elementary reactions and 78 species that are components of approximately 25 chemical activation or multi-channel dissociation reaction systems. The chemical activation analysis involved QRRK analysis for  $k(E)$  and master equation analysis for the fall-off. Thermochemical parameters,  $\Delta H_{f,298}^\circ$ ,  $S_{298}^\circ$ ,  $C_p^\circ(T)$  ( $300 \leq T/K \leq 1500$ ), for reactants, intermediates and products were evaluated from limited literature data and group additivity; while the primary source is from ab initio (at the CBS-QB3 level) and density functional calculations using isodesmic work reactions [20]. Examples of thermochemical and kinetic parameters are published in Zhu and Bozzelli [21, 22, 23], and Asatryan and Bozzelli [24]. Many of the group additivity parameters for sulfur hydrocarbon radicals had been developed from computational chemistry, due to the near complete lack of thermochemical parameters for this class of compounds. Thermochemical and group additivity parameters will be published separately. Since most rate parameters and thermodynamic properties characterizing the sulfur hydrocarbon and intermediate radical reactions were unknown, the following set of procedures for estimating their values was developed.

Unimolecular dissociation and isomerization reactions of the chemically activated and stabilized adducts resulting from addition or combination reactions were analyzed by first evaluating thermodynamic properties and constructing potential energy diagrams. Saddle points for isomerization and dissociation (elimination) transition states were determined using computational chemistry.

Rate constants for the abstraction of H atoms by hydrogen atom, and methyl and methylthiol radicals were calculated using formula given by Bozzelli and Dean [25] as

$$k = n_H \times A \times T_n \times \exp(-E_a/RT) \text{ cm}^3 \text{ mole}^{-1} \text{ sec}^{-1}$$

where  $n_H$  is the number of equivalent hydrogen atoms that could be abstracted. The value of activation energy  $E_a$  is estimated using the following expression:

$$E_a = E_{\text{ref}} - f \times (\Delta_r H_{\text{ref},298}^\circ - \Delta_r H_{298}^\circ)$$

where  $E_{\text{ref}}$  and  $\Delta_r H_{\text{ref},298}^\circ$  are respectively the activation energy and the enthalpy change of a particular reference reaction, and  $\Delta_r H_{298}^\circ$  is the enthalpy change of the reaction of interest. Values of  $A$ ,  $n$  and  $f$  are given in [25].

The rate constants for simple dissociation reactions utilized the activation energy ( $E_a$ ) equal to the enthalpy change of the reaction, as determined from the thermochemistry developed in this study. The pre-exponential factors ( $A$  factors) for these reactions used generic estimates from similar reactions with known pre-exponential factors.

Association reactions are the reverse of simple dissociation reactions, and the kinetics was determined by two methods, and results were compared. One method was to use microscopic reversibility to estimate the rate from thermochemical parameters and the forward rate constant already estimated for the simple dissociation reaction. The second method was to assign an  $E_a$  of 0.0 (two radicals combine with no barrier) and use a generic pre-exponential factor for the association. The generic  $A$  factor is obtained from the literature, e.g. Allara and Shaw [26]; for example, the  $A$  factor for

hydrogen atom plus a sulfur hydrocarbon radical would have a similar pre-exponential to that of hydrogen atom association with a hydrocarbon radical [27, 28].

Addition reactions comprised the addition of a radical to a sp<sup>2</sup> hybridized carbon or sulfur atom (unsaturated-olefin or carbonyl or corresponding sulfur system), forming a radical adduct. These rate constants were determined via two methods (1) established data were used for the well known hydrocarbon olefins and carbonyl reactions in the literature and (2) computational chemistry was used for addition transition states involving sulfur hydrocarbon and intermediate. Hydrocarbon radicals and hydrogen atoms have small (usually less than 10 kcal/mole) barriers for the addition reaction.

$\beta$ -scission reactions are the reverse of addition reactions. A radical site would form a double bond to an adjacent atom, while simultaneously cleaving a bond on the adjacent atom. The rate constants were estimated from the thermochemistry of the reaction and the rate constant of the addition (reverse reaction) described above. The pre-exponentials were further checked by using a generic estimation method [26, 29]. Activation energies were further checked by comparing them to the sum of the change in enthalpy of the  $\beta$ -scission reaction and the activation energy of the reaction for corresponding addition reaction.

Calculations modeled the flow reactor as a plug flow reactor, using Chemkin [30, 31] with no wall reactions, and with the measured centerline temperatures as inputs. Sensitivity analysis and analysis based on rates of production were performed.

## 2.4 RESULTS AND DISCUSSION

Quantitative results are shown in Figures 2.1A-D. Lines represent calculations while symbols represent experimental results. If a species was detected by both GC/MS and FT-IR, hollow symbols represent FT-IR measurements, and filled

symbols represent GC/MS measurements. Included in these figures are all quantified species above 1 ppm from the experiments and their predictions in the calculations. Experimentally observed but unquantified species, namely ethanethiol, methyl thiirane, ethyl methyl disulfide, and diethyl disulfide, were estimated to be present at levels of 0.1 ppm or lower. Besides the gaseous species detected by the analyzers, a light yellow solid was observed coating the internal surface of the sampling probes during the experiments. This condensate consisted mainly of sulfur, as determined from the x-ray emissions produced by the focused electron beam of a JEOL 8900 EPMA Electron Microprobe.

Each experimental data point was repeated once with good repeatability. Diethyl sulfide, carbon disulfide and thiophene were quantified by both FT-IR and GC/MS, and the two methods yielded consistent results. Destruction of diethyl sulfide is predicted well by the chemical kinetic model. The only major product observed experimentally was ethylene, which appears at roughly the rate that the diethyl sulfide disappears. The calculations underpredict observed ethylene levels by approximately 30% at higher conversions (Figure 2.1D). The calculations predicted three major products that were not observed experimentally: hydrogen ( $H_2$ ), thioacetaldehyde ( $CH_3CH^*S$ ) and thioformaldehyde ( $CH_2^*S$ ).  $H_2$  was not detectable experimentally by FT-IR or by the current GC/MS method. The thioaldehydes, thioacetaldehyde and thioformaldehyde, were unstable species and are readily polymerized [32]. It is hypothesized that these species are lost through polymerization, with the resulting low-volatility polymer responsible for the deposit observed on the surfaces of the sampling system. Among the product species observed and predicted, methane was overpredicted. Carbon disulfide, thiophene, and acetylene were underpredicted. Ethane was underpredicted at the 630 °C and 670 °C operating conditions, and overpredicted as the temperature increased.



Element balances are shown in Figure 2.2. The carbon balance and hydrogen balance decreased from 99% to 80% and 69% respectively, while the sulfur balance decreased from 99% to 27%, as the parent compound was destroyed in the experiments, with almost no sulfur detected in products. These trends are probably due to the increased production of undetectable major species such as  $H_2$  and thioaldehydes. In Figure 2.3, the elemental balance information is presented in a different format and compared to the predicted carbon, hydrogen, and sulfur content of the major undetectable species ( $H_2$  and the thioaldehydes). For example, Figure 2.3 shows the fraction of the initial sulfur that is unaccounted for experimentally (symbols), along with lines representing the fraction of the initial sulfur that is predicted to be in the form of undetected species (thioaldehydes). Figure 2.3 shows that the undetected species ( $H_2$  and thioaldehydes) account well for the missing C, H, and S up to 40% destruction efficiency, supporting the hypothesis that the elemental loss is mainly due to these undetectable species. For higher destruction efficiencies, the sulfur loss continues to be well represented by the sum of predicted contributions from undetected species. The carbon and hydrogen losses, however, begin to be overpredicted by the contributions from the undetected species. This finding suggests that secondary reactions converting carbon and hydrogen in the thioaldehydes into detectable species at higher temperatures may not be adequately represented in the mechanism.

Rate of production analysis for the 740 °C operating condition has identified the reaction pathways responsible for the production and destruction of major species. As shown in Figure 2.4, the pyrolysis of diethyl sulfide involves reactions of diethyl sulfide with hydrogen atom, and methyl radical, and unimolecular dissociation. The most important pathway for diethyl sulfide destruction is abstraction of H atoms by hydrogen atom leading to production of  $H_2$  and the  $CC^*SCC$  radical. Hydrogen

abstraction by other radicals, and at the other site (producing C<sup>•</sup>CSCC), is also important; unimolecular dissociation becomes important at the higher temperatures in the range studied, accounting for 27% of destruction at 740 °C. The CC<sup>•</sup>SCC radical dissociates to thioacetaldehyde and the ethyl radical (C<sub>2</sub>H<sub>5</sub>). C<sub>2</sub>H<sub>5</sub> is the main source for ethylene and hydrogen atom. Thioformaldehyde and methyl radical were mainly generated from the dissociation of the ethylthio radical that is produced by the unimolecular dissociation of diethyl sulfide and by β-scission of the C<sup>•</sup>CSCC radical. Production of ethane is a main sink of the methyl radical. Methane comes primarily from methyl attack on diethyl sulfide.

Sensitivity analysis also provided insight into the mechanism. The ten reactions to which the five most abundant species mole fractions were the most sensitive are presented in Table 2.1, for the 740 °C condition. Interestingly, a single reaction (the unimolecular decomposition of diethyl sulfide to ethyl and ethylthio radicals) has the highest sensitivity coefficient for four of the five major species, and the second highest sensitivity coefficient for the fifth major species (H<sub>2</sub>). This reaction affects the levels of all major species because unimolecular decomposition is the initiation process ultimately responsible for all the radicals appearing in other reaction pathways. The thioaldehydes' sensitivity coefficients reflect the competition between abstractions at the two different sites on the diethyl sulfide molecule, with each site leading to production of a different thioaldehyde. The different rate constants for the two different abstraction sites result from different enthalpies of the abstraction reactions and different numbers of H atoms available for abstraction (degeneracy).

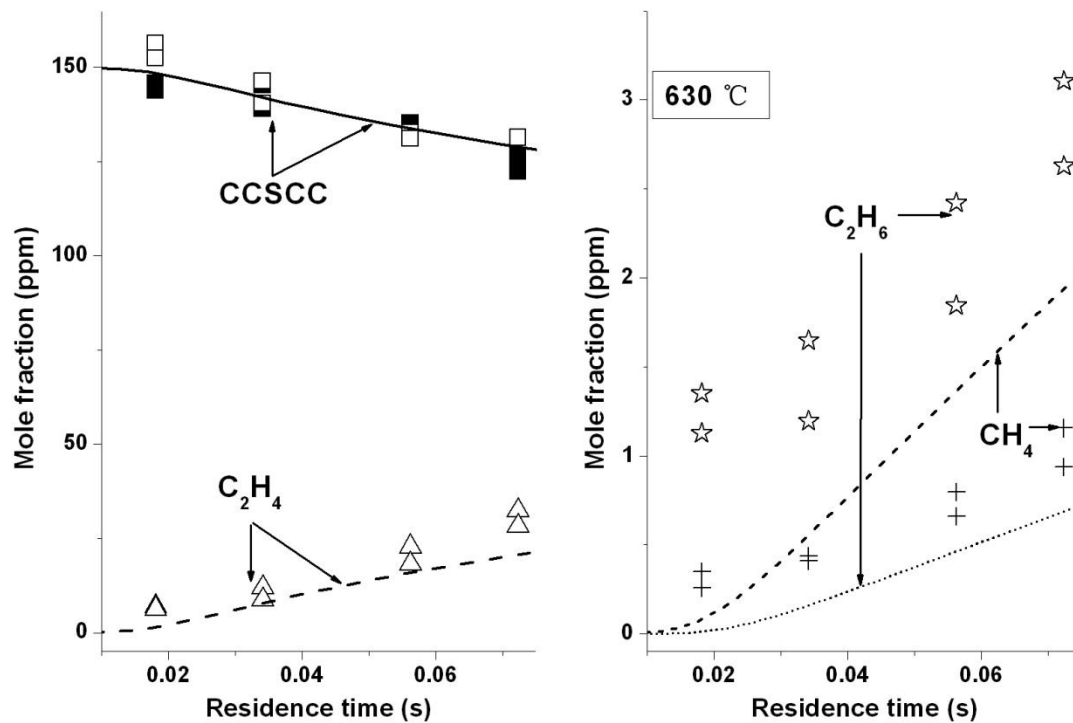


Figure 2.1A Pyrolysis of diethyl sulfide at 630 °C.

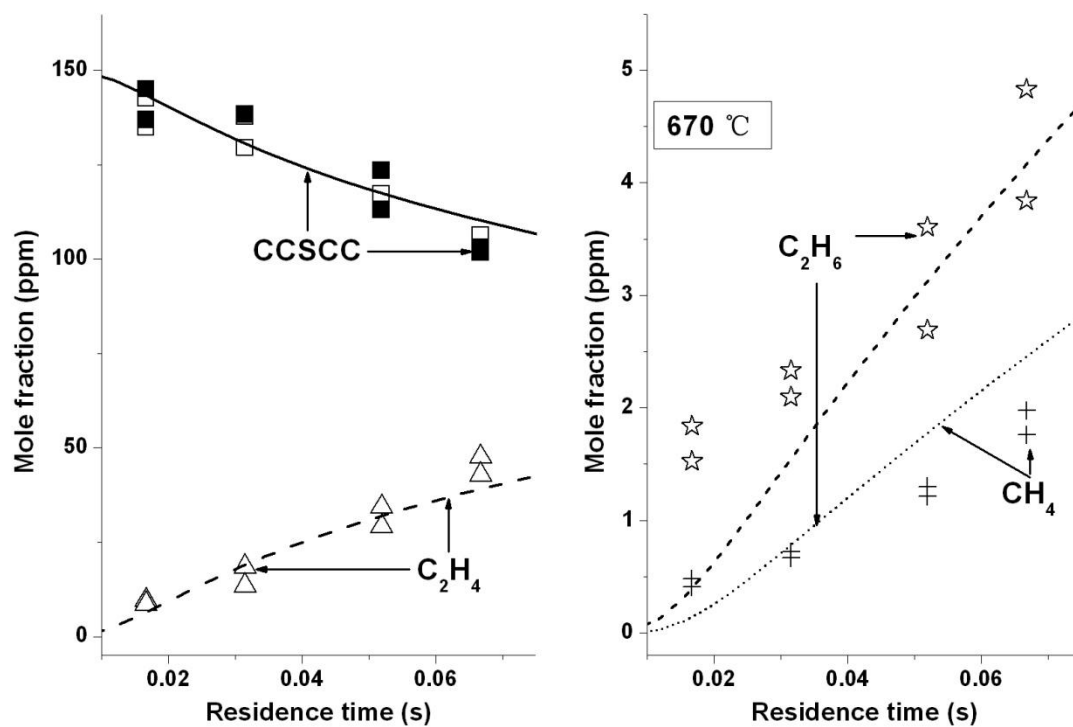


Figure 2.1B Pyrolysis of diethyl sulfide at 670 °C.

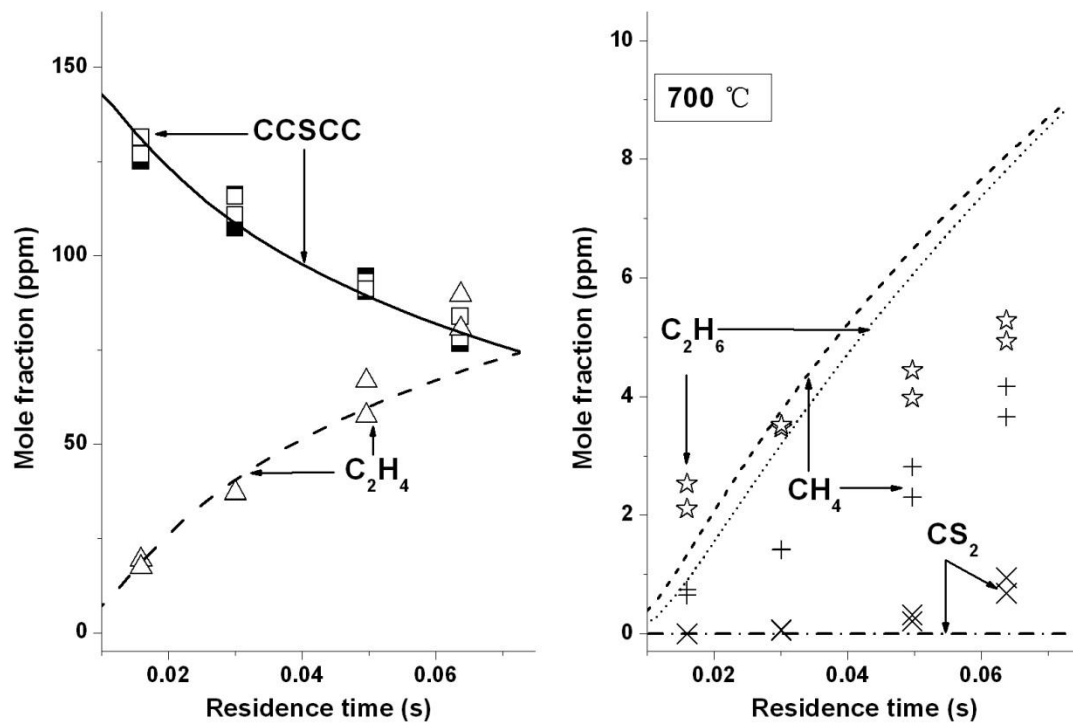


Figure 2.1C Pyrolysis of diethyl sulfide at 700 °C.

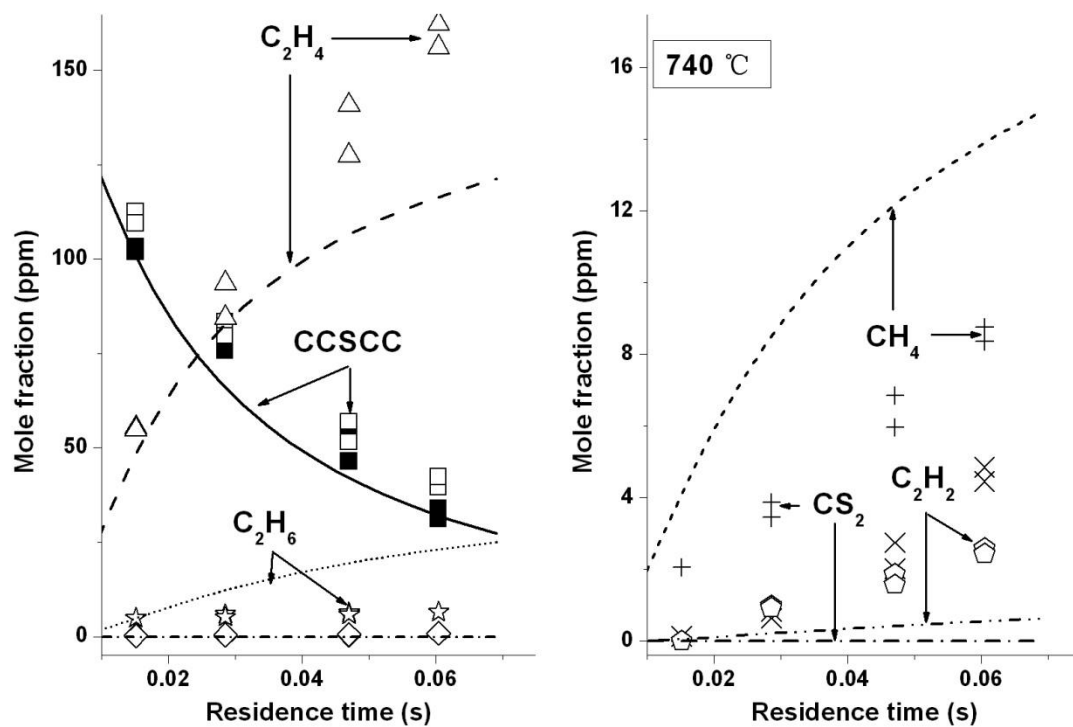


Figure 2.1D Pyrolysis of diethyl sulfide at 740 °C.

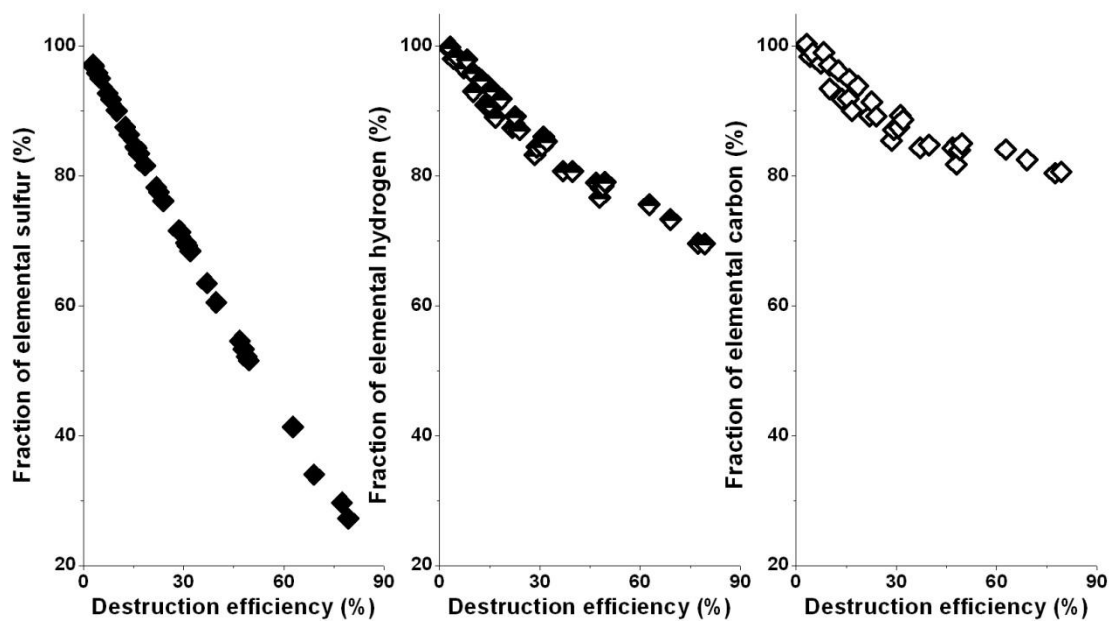


Figure 2.2 Element balances, defined as the mass percent of a given element that is detected in the form of quantified species shown in Figure 2.1 A-D.

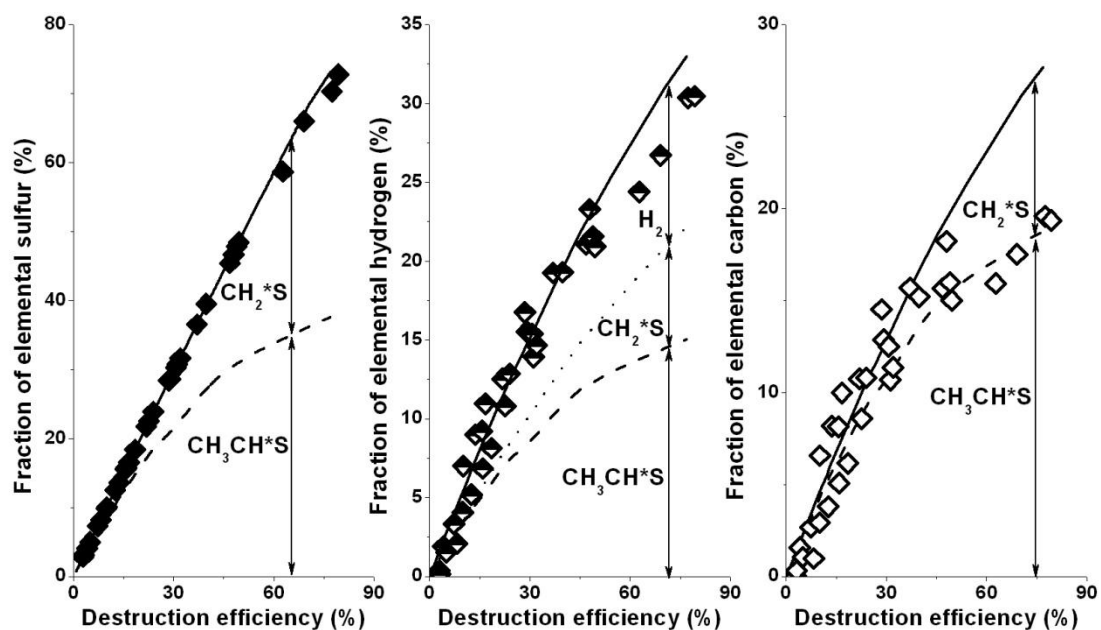


Figure 2.3 Comparison of experimental elemental loss (symbols, defined as 100% - element balance) with predicted contribution of major undetectable species,  $\text{H}_2$ ,  $\text{CH}_3\text{CH}^*\text{S}$  and  $\text{CH}_2^*\text{S}$  (regions between lines). The comparison indicates that predicted undetectable species account well for elemental loss except at high destruction efficiencies.

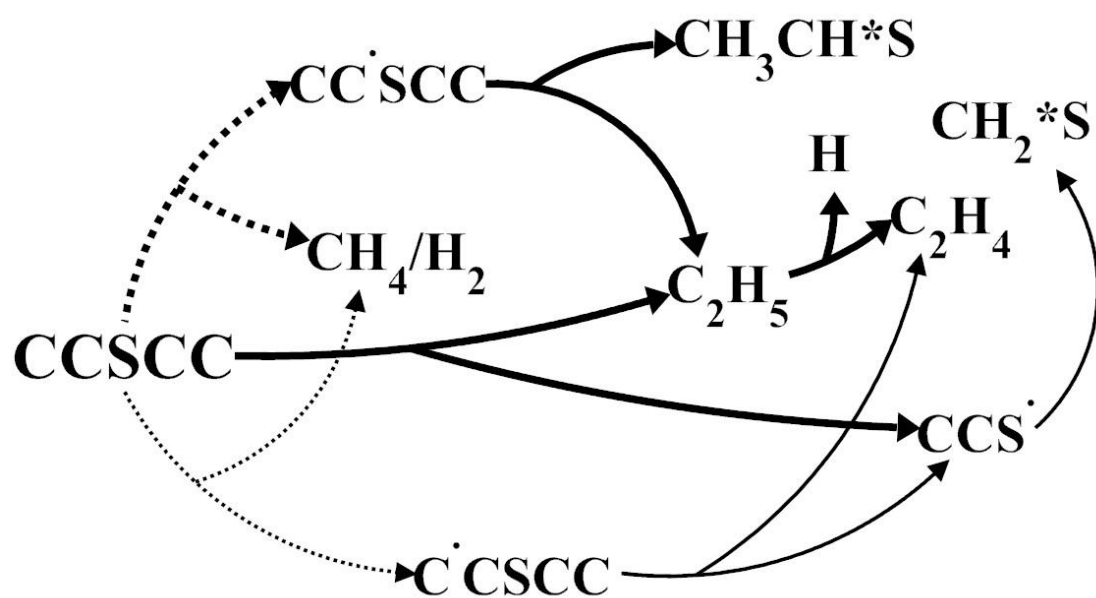


Figure 2.4 Major reaction pathways. Solid lines represent unimolecular reactions, while dash lines indicate radical attack reactions. Thicker lines represent reactions with larger rates.

Table 2.1 Reactions with the highest sensitivity coefficient affecting the concentrations of major species at the 740 °C.

Reactions	Kinetic parameters			Sensitivity coefficient				
	A	N	E <sub>a</sub>	CCSCC	C <sub>2</sub> H <sub>4</sub>	H <sub>2</sub>	CH <sub>3</sub> CH*S	CH <sub>2</sub> *S
CCSCC ↔ CCS*+C <sub>2</sub> H <sub>5</sub>	2.00E+16	0.0	71200.0	-0.770	0.448	0.399	0.988	0.998
CCSCC+H ↔ CC'SCC+H <sub>2</sub>	9.60E+08	1.5	1330.0	-0.361	0.352	0.459	0.700	-0.167
CCSCC+CH <sub>3</sub> ↔ CC'SCC+CH <sub>4</sub>	3.24E+06	1.9	4390.0	-0.156	0.146	0.1279	0.233	0.120
H +C <sub>2</sub> H <sub>4</sub> ↔ C <sub>2</sub> H <sub>5</sub>	5.41E+35	-6.8	11700.0		0.055	0.056	0.447	0.133
CCS* ↔ CH <sub>3</sub> CH*S+H	1.00E+14	0.0	45540.0	0.211	-0.132	-0.188	-0.314	0.184
CCSCC+H ↔ C'CSCC+H <sub>2</sub>	1.44E+09	1.5	6640.0	0.039	0.001	-0.117	-0.404	0.232
CH <sub>2</sub> *S+H ↔ H'CS+H <sub>2</sub>	1.80E+13	0.0	3500.0	0.036				-0.065
CH <sub>3</sub> +CH <sub>3</sub> ↔ C <sub>2</sub> H <sub>6</sub>	2.68E+29	-5.0	6130.0	0.043				
H+CH <sub>3</sub> (+M) ↔ CH <sub>4</sub> (+M)	1.39E+16	-0.5	536.0	0.024	-0.027	-0.035	-0.039	-0.029
H +C <sub>2</sub> H <sub>4</sub> (+M) ↔ C <sub>2</sub> H <sub>5</sub> (+M)	5.40E+11	0.5	1820.0		0.006	0.006	0.054	
2CH <sub>3</sub> (+M) ↔ C <sub>2</sub> H <sub>6</sub> (+M)	6.77E+16	-1.2	654.0	0.022				-0.037
2CH <sub>3</sub> ↔ H+C <sub>2</sub> H <sub>5</sub>	6.84E+12	0.1	10600.0		-0.028	-0.032	-0.057	
CCS* ↔ CH <sub>3</sub> + CH <sub>2</sub> *S	2.00E+14	0.0	41410.0					0.095

A blank cell in the section of sensitivity coefficient indicates that the reaction does not occur among the top 10 reactions with high sensitivity for the species. Kinetic parameters are in modified Arrhenius format,  $k = AT^n \exp(-E_a/RT)$ , where A(mol, cm, s), T(K), E<sub>a</sub>(cal/mol), R = 1.9859 cal/mol K, n is dimensionless.



## **2.5 SUMMARY AND CONCLUSIONS**

Experimental results, a chemical kinetic model, and predictions of the model are reported for the pyrolysis of diethyl sulfide in a flow reactor. Agreement between experiment and prediction is excellent for the disappearance of the parent compound, and reasonably good for the appearance of the major product, ethylene, which is underpredicted at high temperatures. It appears that some of the major products of the destruction process are lost in the sampling system. A number of minor hydrocarbon and sulfur hydrocarbon species are observed and predicted experimentally. According to the mechanism predictions, destruction of diethyl sulfide proceeds mainly through two steps, hydrogen abstraction by the hydrogen atom, and an unimolecular dissociation reaction. Reactions relevant to radical production are the reactions to which major species mole fractions are most sensitive.

## **2.6 ACKNOWLEDGMENTS**

The authors acknowledge the support of the U. S. Army Research Office under contract **W911NF0410120**, and acknowledge Rubik Asatryan for working on reactions of sulfur radicals with carbon monoxide.

## REFERENCES

- [1] Y.C. Yang, Chem. Ind., 1 (1995) 334-337.
- [2] L.R. Ember, Chem. Eng. News, 68 (33) (1990) 9-19.
- [3] Y.C. Yang, F.J. Berg, L.L. Szafraniec, W.T. Beaudry, C.A. Bunton, A. Kumar, J. Chem. Soc. Perkin Trans2 (1997) 607-613.
- [4] Y.C. Yang, J.A. Baker, J. Richard Ward, Chem. Rev. 92 (1992) 1729-1743.
- [5] A.V. Vorontsov, L. Davydov, E.P. Reddy, C.L., E.N. Savinov, P.G. Smirniotis, New J. Chem. 26 (2002) 732-744.
- [6] R.S. Davidson, J.E. Pratt. Tetrahedron Lett. 52 (1983) 5903-5906.
- [7] M.A. Y.S. Kim, A.A. Abdel-Wahab, M. Dulay, Catal. Lett. 5 (1990) 369-376.
- [8] D.V. Kozlov, A.V. Vorontsov, P.G. Smirniotis, E.N. Savinov, Applied Catalysis B: Environmental 42 (2003) 77-87.
- [9] A.V. Vorontsov, C. Lion, E.N. Savinov, P.G. Smirniotis, Journal of Catalysis 220 (2003) 414-423.
- [10] L. Hindyarti, P. Glarborg, P. Marshall, J. Phys. Chem. A 119 (2007) 3984-3991.
- [11] K. Sendt, B. Haynes, Proc. Comb. Inst. 31 (2007) 257-265.
- [12] Lilian G. S. Shum, S.W. Benson, International Journal of Chemical Kinetics 17(1985) 749-76.
- [13] A.H. Sehon and B. Darwent, J. Am. Chem. Soc. 76 (1954) 4806-4810.
- [14] E.H. Braye, A.H. Sehon, B. Darwent, J. Am. Chem. Soc. 77 (1955) 5282-5285.
- [15] C.J. Thompson, R.A. Meyer, J.S. Ball, J. Am. Chem. Soc. 74 (1952) 3284-3287.
- [16] F.C. Thyron, G. Debecker, International Journal of Chemical Kinetics 5 (1973) 583-592.
- [17] E.J. Zegers, Flow Reactor Pyrolysis of Alkyl Phosphates and Phosphonates, Ph.D thesis, Cornell University, Ithaca, NY, USA, 1997.

- [18] NIST/EPA/NIH Mass spectral library, version 2.0d (2005), available at <http://webbook.nist.gov>.
- [19] Thermo Electron, 2004, Nicolet User Guide, available at <http://www.thermo.com>.
- [20] W.J. Hehre, R. Ditchfield, L. Radom, J. A. Pople, J. Am. Chem. Soc. 92(16)(1970) 4796-4801.
- [21] L. Zhu, J.W. Bozzelli, J. Phys. Chem. A 110(21)(2006) 6923-6937.
- [22] L. Zhu, J.W. Bozzelli, "Reaction paths, kinetics, and thermochemical properties on the thioformyl radical ( $\text{S}=\text{C}^*\text{H}$ ) reaction with  $\text{O}_2$ ", Submitted ACS Journal Physical Chemistry.
- [23] L. Zhu, J.W. Bozzelli, Journal of Molecular Structure - Theochem. 728(2005) 147-157.
- [24] R. Asatryan, J.W. Bozzelli, Physical Chemistry Chemical Physics, 10 (2008) 1769-1780.
- [25] A.M. Dean and J.W. Bozzelli In: W.C. Gardiner, Editor, Gas-phase combustion chemistry, Springer, New York (2000), 125.
- [26] D.L. Allara, R. Shaw, J. Phys. Chem. Ref. Data 9 (1980) 523-559.
- [27] L.B. Harding, Y. Georgievskii, S.J. Klippenstein, J. Phys. Chem. A, 109 (2005) 4646-56.
- [28] L.B. Harding, Y. Georgievskii, S.J. Klippenstein, Proc. Combust. Inst. 31 (2007) 221-229.
- [29] A.M. Dean, J. Phys. Chem. 89 (1980) 4600-4608.
- [30] R.J. Kee, J.A. Miller, T. H. Jefferson, "CHEMKIN: A General-Purpose, Problem-Independent, Transportable, Fortran Chemical Kinetics Package", Technical Report SAND80-8003, Sandia National Laboratories, 1980.
- [31] Reaction Design, 2004, Chemkin User Interface 4.0, available at <http://www.reactiondesign.com>.

- [32] W.S. Chin, B.W. Ek, C.Y. Mok, H.H. Huang, J. Chem. Soc., Perkin Trans. 2, (1994) 883-889.

**CHAPTER 3**  
**EXPERIMENTAL AND COMPUTATIONAL STUDY OF OXIDATION OF**  
**DIETHYL SULFIDE IN A FLOW REACTOR**

Xin Zheng<sup>1</sup>, J.W. Bozzelli<sup>2</sup>, E.M. Fisher<sup>1</sup>, F.C. Gouldin<sup>1</sup>

<sup>1</sup>Sibley School of Mechanical and Aerospace Engineering

Cornell University

Ithaca, NY 14853

<sup>2</sup>Department of Chemistry and Environmental Science

New Jersey Institute of Technology

Newark NJ 07101

**ABSTRACT**

The destruction of diethyl sulfide was studied experimentally and computationally at high temperatures under diluted oxidation conditions. The experiments were conducted in an atmospheric, turbulent flow reactor with a Reynolds number of around 5000, at four different operating temperatures between 630 °C and 740 °C. These oxidation experiments, with diethyl sulfide initially at approximately 100 ppm in the reactor, included near-stoichiometric conditions ( $\Phi \sim 1$ ) and fuel-lean conditions with the equivalence ratio ( $\Phi \sim 0.1$ ). On-line, radially extractive sampling in conjunction with fourier transform infra-red and gas chromatography/mass spectroscopy analysis was performed to quantify species at four locations along the centerline of the flow reactor. Species concentrations are presented as functions of residence time in the reactor and are compared to mechanism predictions. A previously published pyrolysis mechanism has been updated and extended to include kinetics of the partially oxidized intermediates. The new mechanism still reproduces the previously reported experimental pyrolysis results satisfactorily and provides reasonable agreement with experimental measurements for the present oxidation

conditions. Important reactions were identified by sensitivity analysis and rate of production analysis by using the mechanism.

### 3.1 INTRODUCTION

Sulfur mustard (bis(2-chloroethyl) sulfide), also known as H/HD (military designation), is a primary component of the U.S. chemical warfare stockpiles [1]. As a lethal vesicant chemical, sulfur mustard is required to be destroyed under the Chemical Weapons Convention [2]. In the U.S., incineration is employed as the baseline disposal technology due to its high destruction efficiencies, applicability to a wide range of chemicals, and good cost effectiveness. However, there has been strong public opposition to chemical weapons incineration because of concerns over trace level emissions from proper operation conditions as well as high level chemical release from off-design incineration modes [3]. In responding to the public concerns, great efforts have been put to investigate the destruction of chemical warfare agents under incineration-relevant conditions [4-6].

Experiments with actual sulfur mustard would provide the most direct insight into the thermochemical destruction of sulfur mustard. But, because of the high toxicity of sulfur mustard, a simulant compound with related chemical structure is used in the current study. The molecular structure of diethyl sulfide ( $\text{CH}_3\text{CH}_2\text{SCH}_2\text{CH}_3$ , abbreviation CCSCC) is similar to that of sulfur mustard but with ethyl rather than chloroethyl bonded to the sulfur atom. Diethyl sulfide has been investigated in several photolysis experiments [7-8], which show that the substitution of ethyl for chloroethyl does not change major reaction pathways under the conditions studied.

The present work continues the previous study on the pyrolysis of diethyl sulfide [9] by exploring the oxidation of diethyl sulfide. The experimental conditions were chosen to investigate the destruction of diethyl sulfide under incineration-relevant

conditions and to understand the product formations under off-design modes. The experiments were complemented with mechanism development. The experimental data were used to validate and refine the mechanism. The goal of the present research has been to produce a kinetic mechanism of diethyl sulfide, which could be extended in the future to predict the behavior of sulfur mustard in incinerators.

### 3.2 EXPERIMENTAL APPARATUS AND METHODOLOGY

The details of the oxidation experiments are documented in Appendix A and briefly reviewed here. The experiments were conducted in an atmospheric turbulent reactor, consisting of a 4.5 cm ID  $\times$  100 cm long quartz liner inside a stainless steel pipe. The main carrier flow was preheated nitrogen. The secondary flow, diethyl sulfide and oxygen diluted in nitrogen, was injected into the main flow through 4 open-ended quartz tubes and resulted in a chemical loading  $100 \pm 4$  ppm in the reactor. For experiments with approximately stoichiometric conditions ( $\Phi \sim 1$ ), oxygen was provided from a pressurized cylinder ( $21 \pm 0.2\%$  O<sub>2</sub> in N<sub>2</sub>), while for the fuel lean conditions ( $\Phi \sim 0.1$ ), the oxygen was supplied in the form of on-site compressed air, purified by FT-IR purge gas generator (Whatman 75-51) to remove CO<sub>2</sub> and H<sub>2</sub>O. GC/MS analyses of samples taken just upstream of the injectors showed no evidence of reactions between diethyl sulfide and oxygen. Operating parameters are listed in Table A.3 (Appendix A).

Gas samples were extracted through radial sampling probes at four axial positions on the centerline of the reactor. The quartz sampling probes (Figure A.5 in Appendix A) made use of nitrogen dilution to quench reactions. Quenched gas samples were directed to FT-IR or GC/MS for analysis. Instrumental methods as well as species identification and quantification for each technique were the same as those of the pyrolysis study [9]. The uncertainties of species concentration are as follows: CCSCC

(12%), ethylene  $C_2H_4$  (5%), sulfur dioxide  $SO_2$  (5%), carbon monoxide  $CO$  (5%), carbon dioxide  $CO_2$  (5%), methane  $CH_4$  (12%), ethane  $C_2H_6$  (12%) and formaldehyde  $CH_2=O$  (where  $=$  represents a double bond) (15%).

Flow and temperature conditions are essential for interpreting experimental kinetic information. As shown in Table A.3, the reactor flow was turbulent with a Reynolds number of approximately 5000 in all the operating conditions. Figure A.9 (Appendix A) shows gas temperature profiles, consisting of an approximately isothermal region, the mean value of which is used to identify each operating condition, and a mixing region. Mixing conditions were determined in the pyrolysis experiments [9]. The mixing conditions for the present experiments were assumed the same as those of the pyrolysis experiments that had the same flow rates and heater settings. The measured  $CO$  concentrations were used to correct species concentrations: the measured mole fraction of each species was multiplied by the ratio of the well-mixed  $CO$  concentration to the measured  $CO$  concentration at that location [9], to account for the effect of incomplete mixing.

### 3.3 MECHANISM CONSTRUCTION AND COMPUTATIONAL METHOD

The objective of the present work has been to develop thermochemistry of oxygenated sulfur hydrocarbons and a kinetic mechanism that describes the destruction of diethyl sulfide under incineration-relevant conditions. The present chemical mechanism is constructed from the previous diethyl sulfide pyrolysis mechanism [9]; it includes updated thermochemistry and kinetics for a number of the pyrolysis reactions and the addition of new oxidation reactions and thermochemistry for oxygenated sulfur-hydrocarbons and sulfur oxides. The C-H-S-O mechanism used here consists of the following kinetic subsets: (1) reactions of diethyl sulfide and



resulting sulfur intermediates, (2) reactions of small sulfur compounds, (3) hydrocarbon reactions, and (4) interactions between the first three subsets.

Kinetics of diethyl sulfide oxidation is a substantial component in the present work. The destruction of diethyl sulfide, through C-S bond cleavage and hydrogen abstraction by  $\text{CH}_3$  and H, along with subsequent  $\beta$ -scission or isomerization of the resulting ethylthio ( $\text{CCS}^{\bullet}$ , where “ $\bullet$ ” represents a radical site) and ethylthioethyl radicals ( $\text{C}^{\bullet}\text{CSCC}/\text{CC}^{\bullet}\text{SCC}$ ) were published in the pyrolysis study [9]. Mechanism predictions were found to be highly sensitive to the kinetics of these reactions and thus a significant fraction of the kinetics and thermochemical properties have been refined using high accuracy ab initio and density functional theory (DFT) calculations as described in a general review [10] and in [11-14] for similar sulfur containing species. Table 3.1 lists the previous kinetic parameters of these reactions as well as the current rates. In addition to the modifications, two new pyrolysis destruction routes for diethyl sulfide were added with the kinetics evaluated by the methods in [9]. These additional routes are: (1) unimolecular dissociation  $\text{CCSCC} \leftrightarrow \text{C}_2\text{H}_6 + \text{CH}_3\text{CH}^*\text{S}$ , and (2) H addition to sulfur coupled with ethyl elimination  $\text{H} + \text{CCSCC} \leftrightarrow \text{CCSH} + \text{C}_2\text{H}_5$ . The updated mechanism reproduces the experimental pyrolysis results as satisfactorily as the previous mechanism [9] does. As shown in Figure 3.1A-D, the updated mechanism predictions agree well with the experimental pyrolysis results for the concentrations of major species, diethyl sulfide and ethylene, at all temperatures. Predictions are generally good for methane and ethane, detected below 10 ppm with a maximum discrepancy of about 5 ppm at the 740 °C condition. Carbon disulfide ( $\text{CS}_2$ ) and acetylene ( $\text{C}_2\text{H}_2$ ) were the other two species detected, with maximum levels of 4 ppm, and both of them are underpredicted. This level of agreement is comparable to that achieved with the earlier version of the mechanism; see Chapter 2.

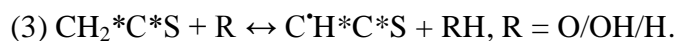
In this work, reactions of the diethyl sulfide and intermediates with O<sub>2</sub>, OH, HO<sub>2</sub> and O were incorporated in the mechanism. These reactions are listed in order of occurrence during the destruction process as follows:

(1) H abstraction from CCSCC by O<sub>2</sub> as one of the initiation reactions.

(2) Destruction routes of CCSCC through (a) H abstraction by OH/HO<sub>2</sub>/O, and (b) addition-elimination reactions via OH/O addition to the sulfur moiety and subsequent elimination of the ethyl group initially bonded to the sulfur. These addition/association reactions were in general exothermic or thermal neutral, as sulfur-oxygen bonds tend to be stronger than sulfur-carbon bonds.

(3) O<sub>2</sub> addition to ethylthio CCS<sup>•</sup> and ethylthioethyl (C<sup>•</sup>CSCC/CC<sup>•</sup>SCC) radicals to form an adduct complex (peroxyl radicals), and subsequent reactions of the peroxyl radicals.

(4) Reactions of thioformaldehyde (CH<sub>2</sub><sup>•</sup>S) and thioacetaldehyde (CH<sub>3</sub>CH<sup>•</sup>S). Three pathways are added for CH<sub>2</sub><sup>•</sup>S, one is H abstraction by OH, O or O<sub>2</sub>, forming thioformyl (HCS) radical. Again OH/O/O<sub>2</sub> can associate at the sulfur moiety and undergo secondary isomerization or elimination resulting in CH<sub>2</sub><sup>•</sup>O along with SH, S and SO respectively, and the third is association reactions between thioaldehydes and their radicals to form sulfur dimer (S<sub>2</sub>) and disulfides. Similar reactions are also included for thioacetaldehyde. As a more complex molecule, thioacetaldehyde can participate in multiple abstraction and β-scission steps as follows:



Subsequent reactions with OH/O/HO<sub>2</sub> form HCO, HCS, CS and OCS. H atom can undergo addition to thioacetaldehyde and subsequent isomerization (intramolecular H transfer) to the carbon bonded to the sulfur forming the CCS<sup>•</sup> radical. Similar addition

routes are ignored for thioformaldehyde in the present mechanism, as the resulting methylthio ( $\text{CH}_3\text{S}^\bullet$ ) is unstable and quickly returns to the reactants  $\text{H} + \text{CH}_2^*\text{S}$ .

The kinetics of the small sulfur containing species derived from the reactions above, include HCS, CS, OCS, SH and S, are described in the small sulfur species subset of the mechanism. The kinetic and thermochemical basis for this subset is primarily the Leeds sulfur mechanism [15]. The reported work here extends it by:

(1) updating the kinetic parameters of H abstraction on HOSHO, as shown in Table 3.2,

(2) extending reaction routes for species SOH/S/S<sub>2</sub>/SO/SO<sub>3</sub>/HOSO<sub>2</sub>,

(3) adding new species HSO<sub>2</sub>, SOOH, CS, HCS, and COS and associated reactions.

The subset consists of 21 species and more than 130 elementary reactions.

In the sub-mechanisms above, the kinetics for H abstraction from parent and intermediates by the radical pool were from the formalism described in [16]. Association was treated as a chemical activation reaction with the kinetics evaluated by the methods in [10][17]. The hydrocarbon reaction subset in the present mechanism is a detailed mechanism for C<sub>1</sub>, C<sub>2</sub> and C<sub>3</sub> hydrocarbons and oxygenated hydrocarbon species. The mechanism subset is constructed from hydrogen-oxygen-carbon monoxide chemistry at the base, with the reactions of larger species including CH<sub>4</sub>, acetylene (C<sub>2</sub>H<sub>2</sub>), C<sub>2</sub>H<sub>4</sub>, C<sub>2</sub>H<sub>6</sub>, propyne (C<sub>3</sub>H<sub>4</sub>), propene (C<sub>3</sub>H<sub>6</sub>), propane (C<sub>3</sub>H<sub>8</sub>), and corresponding C<sub>1</sub>, C<sub>2</sub> and C<sub>3</sub> aldehydes, alcohols and their reaction intermediates. The subset has been published in several parts in [17-27], and provided a basis for the construction of a kinetic mechanism for JP-8 surrogate blends [28]. Validations against experimental data have been reported for opposed flow extinction experiments on ignition delay and flame speed measurements for several gaseous and liquid fuels [28] and for pyrolysis and oxidation of methanol and methanol/methane mixtures at temperatures 873-1073 K over a pressure range of 1-10 atm [29]. The present subset

was adopted from [28]. For simplicity, reactions of nitrogen containing species, which are not likely to be significant under the present conditions, and reactions of  $C_4$  and larger hydrocarbons, which are formed in very minor quantities, are not included. The remaining hydrocarbon subset consists of approximately 450 elementary reactions among 150 species. The pyrolysis mechanism [9] included the hydrocarbon reactions that involved no oxygenated compounds. Three reactions in the hydrocarbon reaction subset, shown in Table 3.3, were updated with recent literature data [16][30][31].

Interactions between the subsets appear in two ways. One way is the coupling effect of major radicals such as H, O and OH between the reactions of the different subsets. For example, small sulfur chemistry may catalyze radical recombination [32] and thus affect the rates of radical attack on diethyl sulfide and other species. This cross-coupling mechanism is indirect, and does not require the addition of further reactions. The second way is through reactions between species in different subsets. The mechanism includes cross reactions between the diethyl sulfide submechanism and the hydrocarbon mechanism, specifically reactions of diethyl sulfide and its derivatives with  $CH_3$  and  $C_2H_5$ . These abstraction reactions were also evaluated by the formalism in [16].

The thermochemical properties come from various sources. For most of the species included here, ab initio estimations at the CBS-QB3 level and DFT calculations [33] were carried out for products and adducts, and group additivity and hydrogen increment methods [34] were employed for radicals, when literature data are not available. Appendix C.1 is a data table for coupling the species with Chemkin codes. And appendix C.2 provides a table of enthalpies of formation, Entropy at 298 K and  $C_p(T)$  from 300 K to 1500 K.

Chemical kinetic modeling was performed with the Chemkin 4 package [35]. The flow reactor was modeled as plug flow with smoothed gas temperature profiles

(Figure A.9 in Appendix A) through curvefits to measured temperatures. Surface reactions were not included in the calculation.

Table 3.1 Modifications of kinetic parameters of the pyrolysis mechanism [9].

Reactions	Old kinetic parameters			New kinetic parameters		
	A	N	E <sub>a</sub>	A	n	E <sub>a</sub>
CCSCC $\leftrightarrow$ CCS <sup>*</sup> +C <sub>2</sub> H <sub>5</sub>	2.00E+16	0.00	71200.0	1.06E+89	-21.7	105718.0
CCSCC+H $\leftrightarrow$ CC <sup>*</sup> SCC+H <sub>2</sub>	9.60E+08	1.50	1330.0	5.99E+08	1.9	5141.0
CCSCC+H $\leftrightarrow$ C <sup>*</sup> CSCC+H <sub>2</sub>	1.44E+09	1.50	6640.0	3.46E+07	2.0	9471.0
CCSCC+CH <sub>3</sub> $\leftrightarrow$ CC <sup>*</sup> SCC+CH <sub>4</sub>	3.24E+06	1.87	4390.0	2.90E+04	2.8	9722.0
CCSCC+CH <sub>3</sub> $\leftrightarrow$ C <sup>*</sup> CSCC+CH <sub>4</sub>	4.86E+06	1.87	9700.0	9.78E+03	3.0	13700.0
CC <sup>*</sup> SCC $\leftrightarrow$ CH <sub>3</sub> CH <sup>*</sup> S+C <sub>2</sub> H <sub>5</sub>	1.20E+14	0.00	30290.0	9.15E+11	0.6	25690.0
C <sup>*</sup> CSCC $\leftrightarrow$ CCS <sup>*</sup> +C <sub>2</sub> H <sub>4</sub>	1.00E+14	0.00	18170.0	2.63E+12	0.1	19000.0
CCS <sup>*</sup> $\leftrightarrow$ CH <sub>2</sub> <sup>*</sup> S+CH <sub>3</sub>	2.00E+14	0.00	41410.0	8.61E+12	0.8	42000.0

Kinetic parameters are in modified Arrhenius format,  $k = AT^n \exp(-E_a/RT)$ , where A(mol, cm, s), T(K), E<sub>a</sub>(cal/mol), R = 1.9859 cal/mol K, n is dimensionless.

Table 3.2 Modifications of kinetic parameters of Leeds sulfur mechanism.

Reactions	Original Leeds mechanism[15]			New kinetic parameters		
	A	n	E <sub>a</sub>	A	n	E <sub>a</sub>
HOSHO+H $\leftrightarrow$ HOSO+H <sub>2</sub>	1.00E+12	0.00	0.00	1.30E+13	0.00	1000.00
HOSHO+OH $\leftrightarrow$ HOSO+H <sub>2</sub>	1.00E+12	0.00	0.00	2.55E+12	0.00	500.00
HOSHO+O $\leftrightarrow$ HOSO+OH	5.00E+12	0.00	0.00	1.50E+13	0.00	700.00

Kinetic parameters are in modified Arrhenius format,  $k = AT^n \exp(-E_a/RT)$ , where A(mol, cm, s), T(K), E<sub>a</sub>(cal/mol), R = 1.9859 cal/mol K, n is dimensionless.

Table 3.3 Modifications of kinetic parameters of Hydrocarbon mechanism.

Reactions	Original Hydrocarbon mechanism[28]			New kinetic parameters		
	A	n	E <sub>a</sub>	A	n	E <sub>a</sub>
1.OH+C <sub>2</sub> H <sub>4</sub> $\leftrightarrow$ C <sub>2</sub> H <sub>3</sub> +H <sub>2</sub> O	3.60E+06	2.00	2500.0	3.60E+06	2.00	6250.0
2.HO <sub>2</sub> +CH <sub>3</sub> $\leftrightarrow$ OH+CH <sub>3</sub> O	1.20E+13	0.00	0.00	9.00E+12	0.00	0.00
3.HO <sub>2</sub> +CO $\leftrightarrow$ OH+CO <sub>2</sub>	8.45E+08	1.21	17267.0	7.14E+07	1.57	17721.0

Kinetic parameters are in modified Arrhenius format,  $k = AT^n \exp(-E_a/RT)$ , where A(mol, cm, s), T(K), E<sub>a</sub>(cal/mol), R = 1.9859 cal/mol K, n is dimensionless. New kinetic parameters of Reactions (1-3) are reported in [16][30][31] respectively.

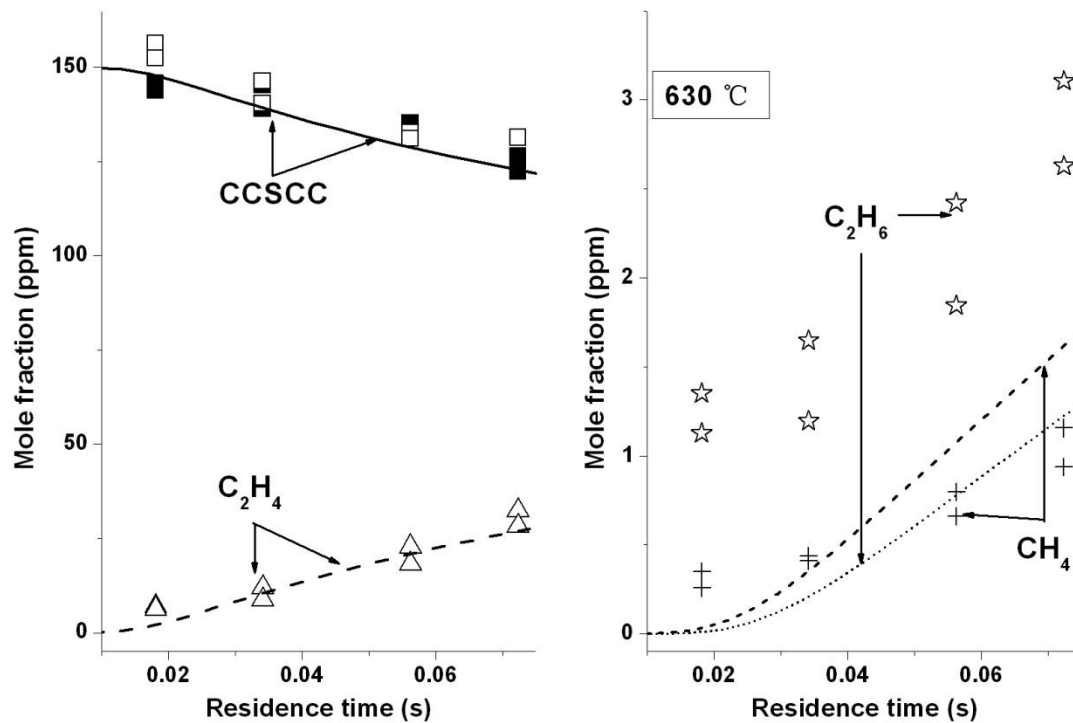


Figure 3.1A Pyrolysis of CCSCC at 630 °C.

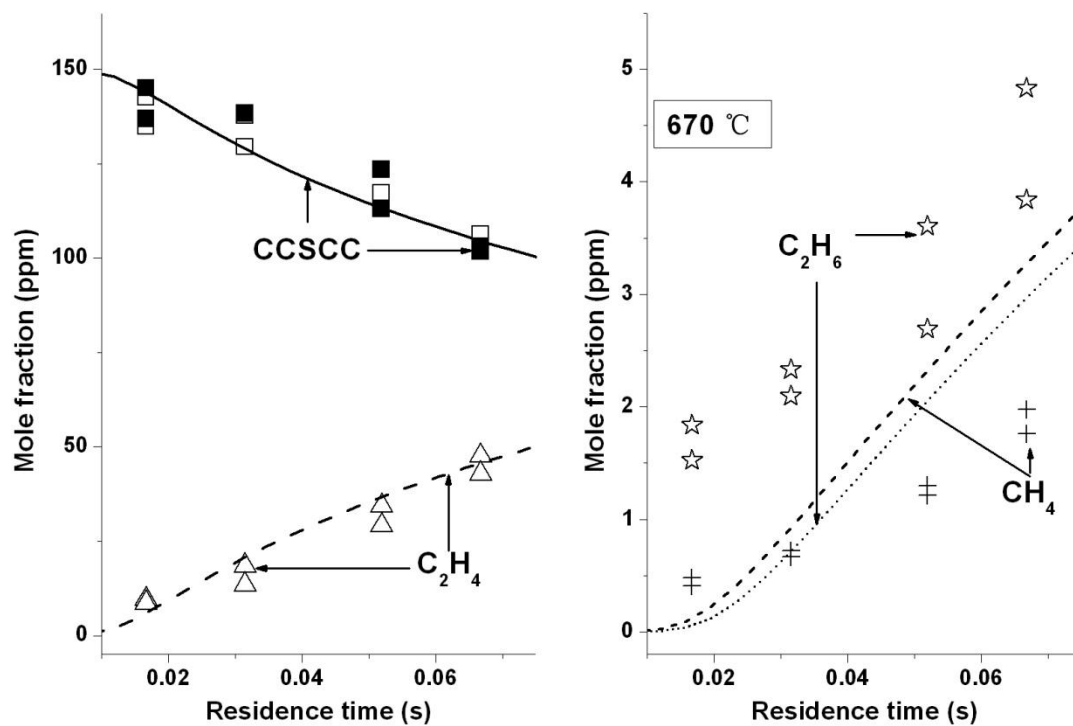


Figure 3.1B Pyrolysis of CCSCC at 670 °C.



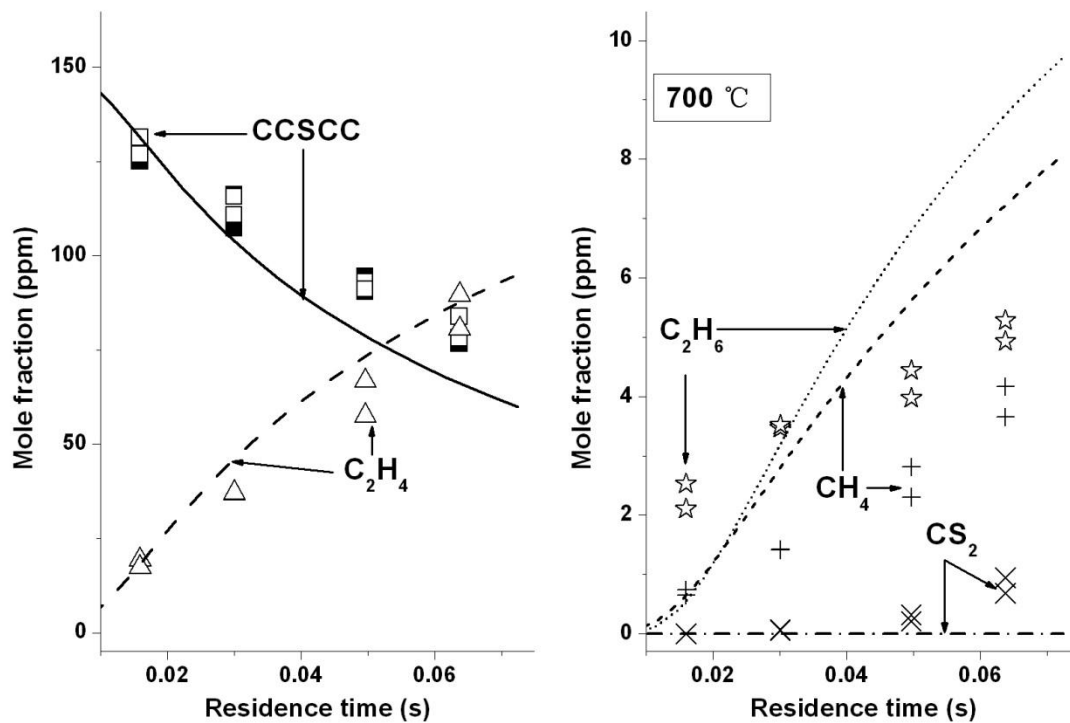


Figure 3.1C Pyrolysis of CCSCC at 700 °C.

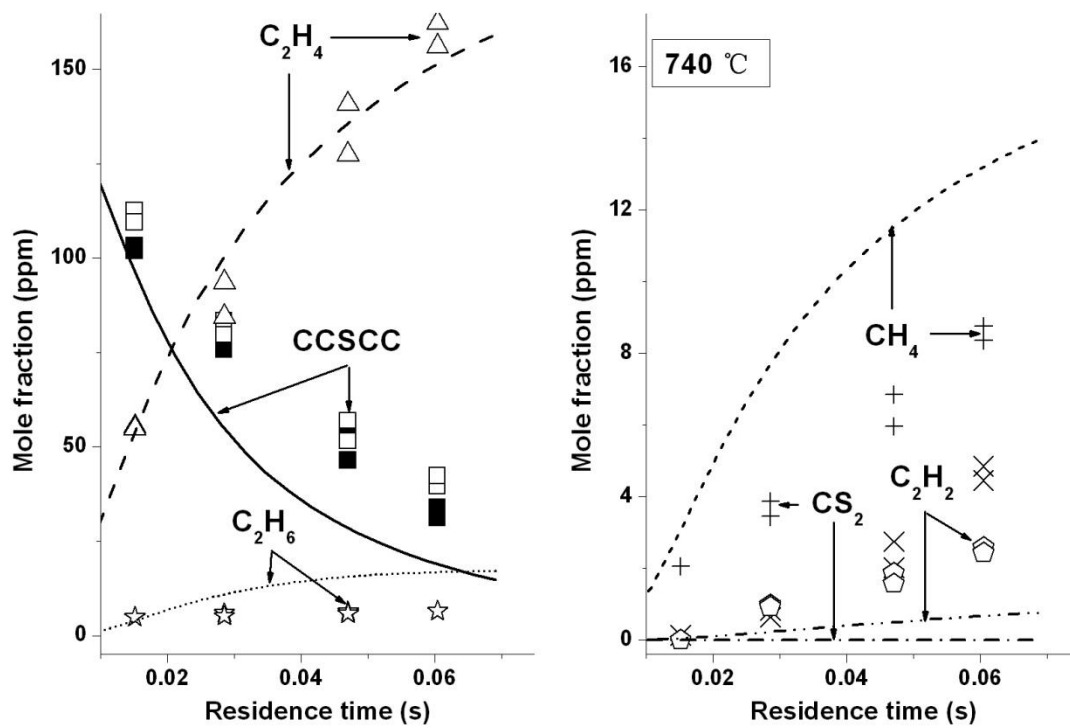


Figure 3.1D Pyrolysis of CCSCC at 740 °C.

### 3.4 RESULTS AND DISCUSSION

Mechanism predictions and experimental measurements of species profiles are shown in Figures 3.2A-D and 3.3A-D. The reported species, including CCSCC,  $C_2H_4$ ,  $C_2H_6$ ,  $CH_4$ ,  $CO$ ,  $CO_2$ ,  $SO_2$  and  $CH_2^*O$ , were detected at levels of 1 ppm or higher in the experiments. Carbon disulfide ( $CS_2$ ), ethyl methyl disulfide ( $CH_3SSCH_2CH_3$ ), and diethyl disulfide ( $CH_3CH_2SSCH_2CH_3$ ) were also detected and estimated to be below 1 ppm. In Figures 3.2A-D and 3.3A-D, experimental data are represented by symbols, while predictions by lines. As mentioned in previous section 3.2, two analytical techniques were employed in the experiments. For species detected by both techniques, hollow symbols are for FT-IR measurements and solid symbols are for GC/MS measurements.

Figures 3.2A-D shows results with approximately stoichiometric compositions at four temperatures, 630 °C, 670 °C, 700 °C and 740 °C, respectively. Repeatability is observed to be under the measurement uncertainties for duplicated measurements, and the results of the two different analytical techniques are in good agreement. Destruction efficiency of diethyl sulfide was experimentally determined to be 29% at 630 °C, 40% at 670 °C, 70% at 700 °C, and 92% at 740 °C (the last sampling port), corresponding to residence times between 0.06 s and 0.072 s. The mechanism prediction shows good agreement with the experiment for diethyl sulfide and  $C_2H_4$  and  $CO$  under all these conditions.  $SO_2$ ,  $CH_2^*O$ ,  $C_2H_6$  and  $CH_4$  are also quantified species, and their maximum concentrations are below 10 ppm. The mechanism overpredicts  $SO_2$  at the 740 °C but underpredicts it at lower temperatures.  $CH_2^*O$  is underpredicted at all four operating temperatures.  $CH_4$  and  $C_2H_6$  are only quantified at the 700 °C and 740 °C temperatures, and are overpredicted at both temperatures.

Figures 3.3A-D presents results of the initial chemical composition with an equivalence ratio of about 0.1 at the 630 °C, 670 °C, 700 °C and 740 °C temperatures.

As shown in Figure 3.3A-D, the destruction efficiency increases with temperature from approximately 34% at the 630 °C, to 60% at the 670 °C, 92% at the 700 °C, and 100% at the 740 °C (the last sampling port). In particular, at the 740 °C, complete destruction of diethyl sulfide is achieved by the second sampling port, corresponding to a residence time of 0.028 s. The destruction of diethyl sulfide is significantly enhanced with excess oxygen compared to the results in Figures 3.2A-D. The experimental profiles of CCSCC are in very good agreement with those of the mechanism prediction. For major species other than CH<sub>2</sub>\*O, the mechanism prediction agrees reasonably well with the measurement. Agreement is good for C<sub>2</sub>H<sub>4</sub> and is fairly good for CO and SO<sub>2</sub> with small overpredictions at high residence times. CH<sub>2</sub>\*O is underpredicted by factors up to 4. However, the use of a formaldehyde solution to calibrate the FT-IR for CH<sub>2</sub>\*O introduces uncertainty regarding quantification of CH<sub>2</sub>\*O. Our measurements of CH<sub>2</sub>\*O are considered upper bounds on mole fractions of the species, as CH<sub>2</sub>\*O may polymerize in calibration gas transfer lines when it leaves the stabilized environment of the methanol solution, producing overestimated concentrations in the calibration curve. Further investigations on CH<sub>2</sub>\*O calibration would be valuable to improve measurement accuracy on the species. C<sub>2</sub>H<sub>6</sub> is only quantified at the 700 °C and 740 °C, and the predictions agree well with the experimental data. Oxidation of CO is not observed to be efficient under the conditions studied as CO<sub>2</sub> is quantified at the 740 °C, and is overpredicted with a maximum discrepancy of 30%.

In general, Figures 3.2A-D and 3.3A-D show that the largest absolute disagreements between the measurements and calculations are in the single digit ppm range for CH<sub>4</sub>, CO<sub>2</sub>, and C<sub>2</sub>H<sub>6</sub>, and in the double digit ppm range for SO<sub>2</sub>, CH<sub>2</sub>\*O, CCSCC, C<sub>2</sub>H<sub>4</sub>, and CO. These maximum discrepancies correspond to factors of ~2 for SO<sub>2</sub>, CO<sub>2</sub>, and CH<sub>2</sub>\*O, 60% for CH<sub>4</sub>, and <40% for all other species. Possible

explanations of the discrepancies observed in our study include: kinetic mechanism error, reactions in sampling lines (either heterogeneous or due to non-instantaneous cooling) and deviation of the experiment from the modeled conditions (plug flow, uniform temperature, no wall reactions). This level of disagreement is very reasonable, given the state of the art of modeling the kinetics of simple systems containing sulfur, see for example [32].

In addition to the species reported above, light yellow condensates were observed on the internal surfaces of the sampling probes. The condensates were dissolved in methylene chloride, and the solution was analyzed by using GC/MS. Cyclooctasulfur ( $S_8$ ) was identified as the major component, and a small unidentified peak was also present in the chromatogram.

As in our previous work [9], element balances (Figures 3.4 and 3.5) show substantial gaps due to the condensates above and to non-detectable species mentioned in the next section. Element balances range approximately from 65 to 90% for C, from 40 to 90% for H, and from 25 to 90% for S.

Rate of production analysis was conducted under several conditions to determine the reactions contributing significantly to the evolution of the parent compound and major species. The results for different temperatures and residence times are similar, and a representative case is shown in Figure 3.6. Initiation of the destruction of diethyl sulfide in the present oxidation conditions is the same as that of our previous pyrolysis study [9], occurring through unimolecular dissociation. Reactions of H abstraction on diethyl sulfide by  $O_2$  are included, but are not found to be a significant initiation source. Once the radical pool is established, abstraction reactions become important as chain propagation steps. The primary difference between oxidation and pyrolysis is the additional contribution of H abstraction by oxygenated reactants  $OH/O/HO_2/O_2$ . These reactions are more important under fuel lean conditions with excess oxygen as

they are more abundant. And among these reactions, abstraction by OH is the more important one as shown in Figure 3.6. Water from the abstraction by OH is predicted to be an important species, but only very small amount was experimentally detected. Attempts to calibrate water have not been successful to date. However, kinetic modeling showed that the predictions were not sensitive to the presence of H<sub>2</sub>O, even at levels well above those believed present. H<sub>2</sub> is an important product from H abstraction but was not detectable by the instrumental methods used here. CH<sub>4</sub> is a minor detected species mainly formed through abstraction by CH<sub>3</sub>.

The radicals derived from CCSCC are ethyl C<sub>2</sub>H<sub>5</sub>•, ethylthio CCS• and primary and secondary ethylthioethyl C•CSCC/CC•SCC. These radicals undergo β-scission to produce C<sub>2</sub>H<sub>4</sub>, CH<sub>2</sub>•S and CH<sub>3</sub>CH•S respectively. C<sub>2</sub>H<sub>4</sub> is the primary hydrocarbon product, as shown in Figures 3.2A-D and 3.3A-D, detected under all the studied conditions. The CH<sub>2</sub>•S and CH<sub>3</sub>CH•S were not experimentally observed, probably because they are too unstable to survive the sampling lines [36]; however, anticipated polymerization products of these compounds were not detected in sampling line and probe rinsate. The primary pathway for thioformaldehyde is hydrogen abstraction to form HCS. In contrast, for thioacetaldehyde, H addition instead of H abstraction and subsequent isomerization to ethylthio CCS• is the most important route under all the conditions, while H abstraction and subsequent β-scission to thioketene CH<sub>2</sub>•C•S become important at high temperatures under fuel-lean conditions. These gas phase reactions involving thioaldehydes, having been discussed so far, are however relatively slow at low temperatures. Thus high levels of thioaldehydes are predicted to persist to the exit of the reactor in the low temperature conditions studied here. The product, HCS radical undergoes the reaction with O<sub>2</sub> to form SOH, subsequent reactions with O and OH to sulfur monoxide (SO) and further oxidation results in SO<sub>2</sub>. The other two detected species, C<sub>2</sub>H<sub>6</sub> and CH<sub>2</sub>•O, are mainly produced through the

recombination of  $\text{CH}_3$  and the reaction of  $\text{CH}_3$  and  $\text{O}_2$  respectively. In Figure 3.6, oxidation of these hydrocarbons, which follows well known steps, is omitted.

Reactions of high importance in determining the mechanism prediction were determined through sensitivity analysis. Table 3.4 lists the ten reactions to which the concentrations of the major species, CCSCC,  $\text{C}_2\text{H}_4$ , CO,  $\text{SO}_2$  and  $\text{CH}_2^*\text{O}$ , are most sensitive for the fuel lean condition at 740 °C.

As seen in Table 3.4, the initiation reaction (simple C-S bond cleavage) has the highest sensitivity for all the listed species as it is the source of H, which in turn affects concentrations of other important radicals, like OH and O, through fast chain propagation reactions. The rate constant for this reaction is obtained from the thermochemistry of the reaction system determined in this study, in combination with the QRRK [10]/master equation analysis [37] for pressure dependence (fall-off). The activation energy was calculated from the dissociation energy of the reaction using enthalpies of reactants and products calculated in this work. The pre-exponential factor was calculated from the reverse association reaction of the two radicals and thermodynamics, which in turn was estimated from our evaluation of the well studied generic reaction: association of methyl radicals, adjusted for steric effects and degeneracy. The accuracy of a similar approach has been shown to be 30-35% for a different chemical system [38].

It is interesting that H abstraction from different carbons of diethyl sulfide and by different radicals shows opposite effects on the formation of products. As shown, the abstraction from the carbon attached to sulfur by OH can promote the formation of  $\text{C}_2\text{H}_4$  as this reaction generates  $\text{CH}_3\text{CH}^*\text{S} + \text{C}_2\text{H}_5$ . In contrast,  $\text{C}_2\text{H}_4$  formation is inhibited by the abstraction by OH on the terminal carbon, as  $\text{C}^*\text{CSCC}$  reacts to  $\text{C}_2\text{H}_4 + \text{CCS}^*$ , and this ethylthio radical reacts with the oxygenated species or undergoes  $\beta$ -scission to  $\text{CH}_3^*\text{S} + \text{CH}_3$ . This difference can be explained by their net effects on the

radical pools as the abstraction on the carbon attached to sulfur initializes a branch sequence to form H, while the abstraction on the terminal carbon converts OH and forms a less reactive CH<sub>3</sub>. For SO<sub>2</sub> formation, two competing reactions involving ethylthio CCS<sup>•</sup> have high sensitivities. The reaction of ethylthio CCS<sup>•</sup> and O<sub>2</sub> is favored to increase SO<sub>2</sub> level as it produces SO<sub>2</sub> directly as well as C<sub>2</sub>H<sub>5</sub>, the dissociation of which increases the reaction rates of the whole system by increasing the level of H. A large part of the reactions with high sensitivities do not involve sulfur compounds, and these reactions are common radical branching, propagation, and termination reactions for hydrocarbon combustion systems.

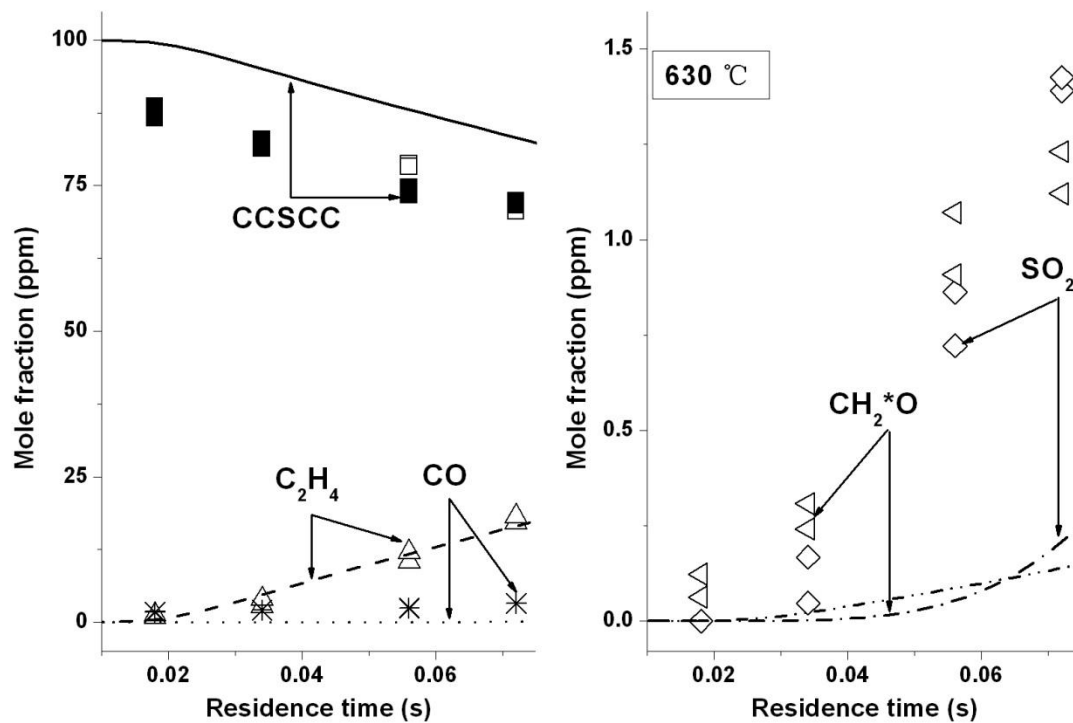


Figure 3.2A Oxidation of CCSCC ( $\Phi \sim 1$ ) at 630 °C.

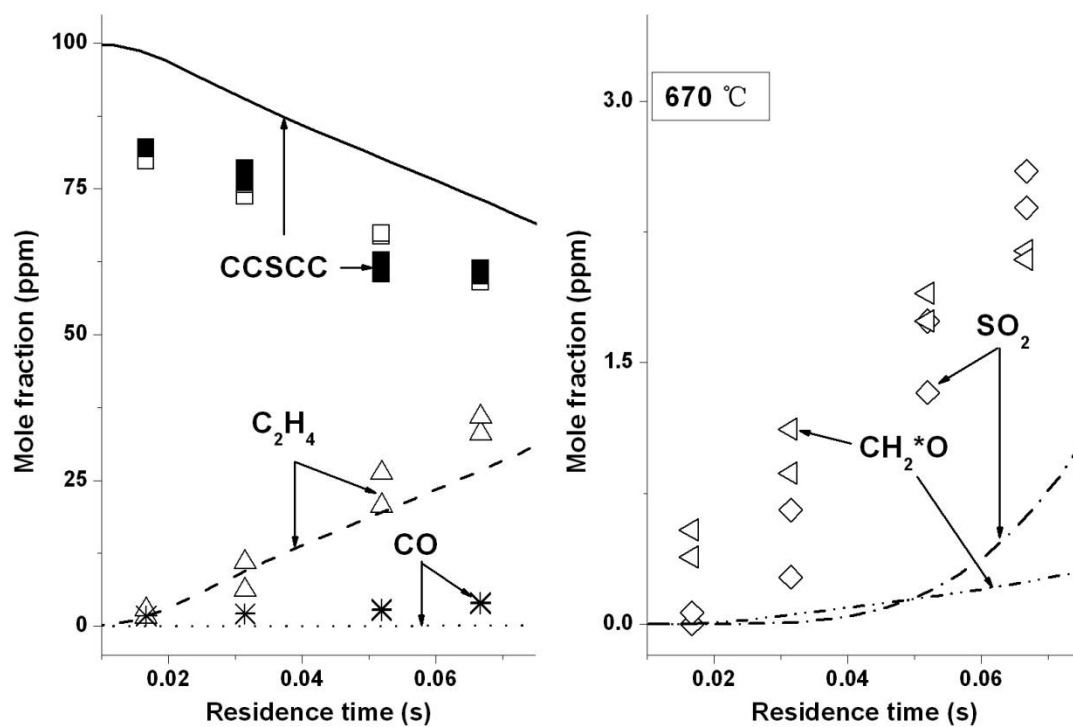


Figure 3.2B Oxidation of CCSCC ( $\Phi \sim 1$ ) at 670 °C.



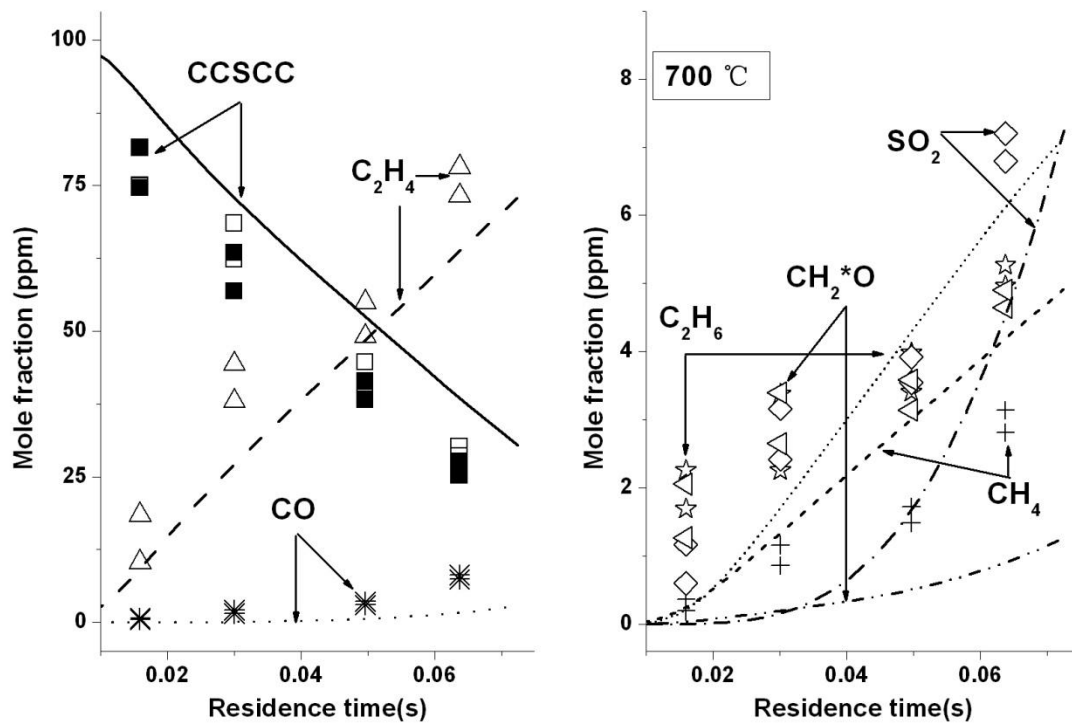


Figure 3.2C Oxidation of CCSCC ( $\Phi \sim 1$ ) at 700 °C.

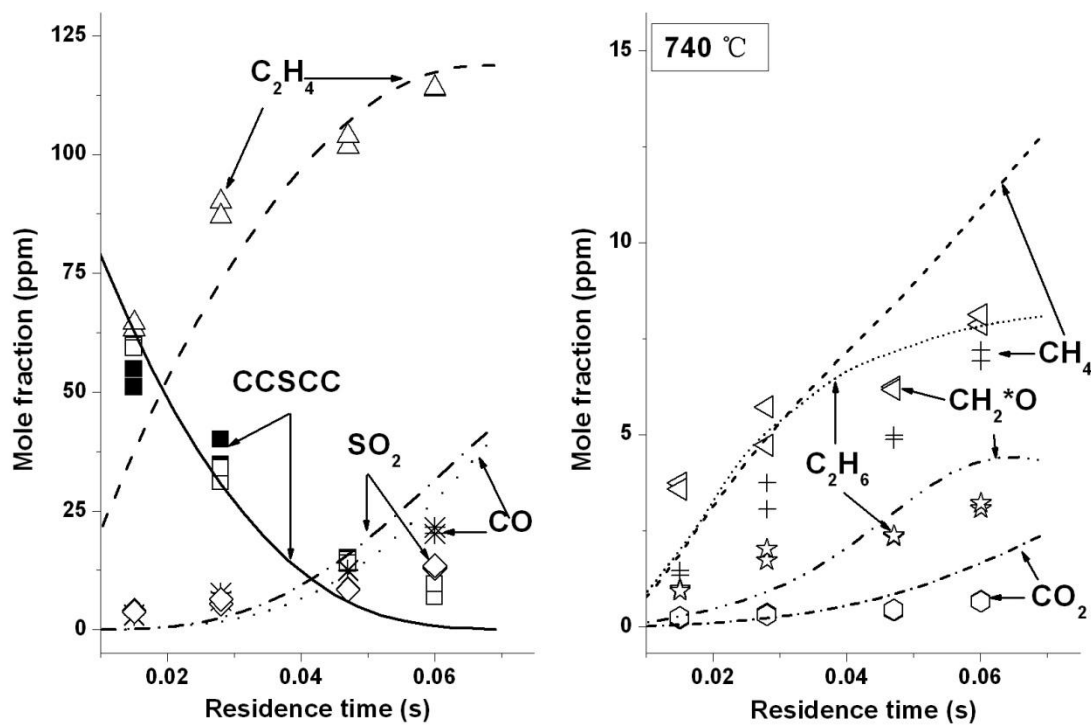


Figure 3.2D Oxidation of CCSCC ( $\Phi \sim 1$ ) at 740 °C.

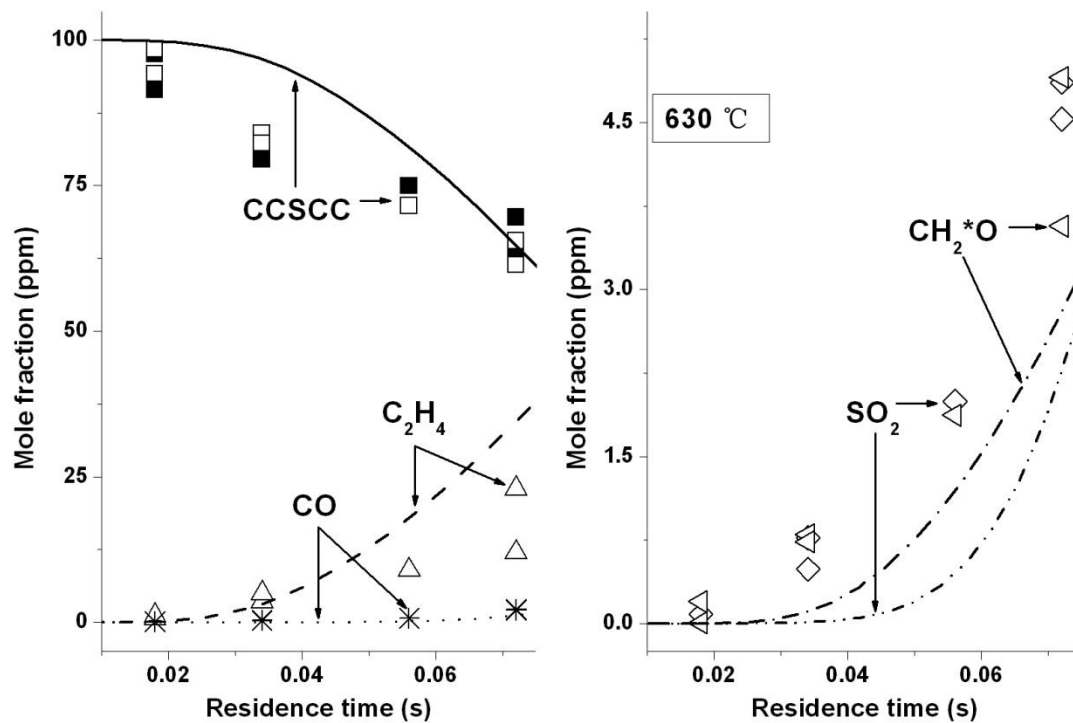


Figure 3.3A Oxidation of CCSCC ( $\Phi \sim 0.1$ ) at 630 °C.

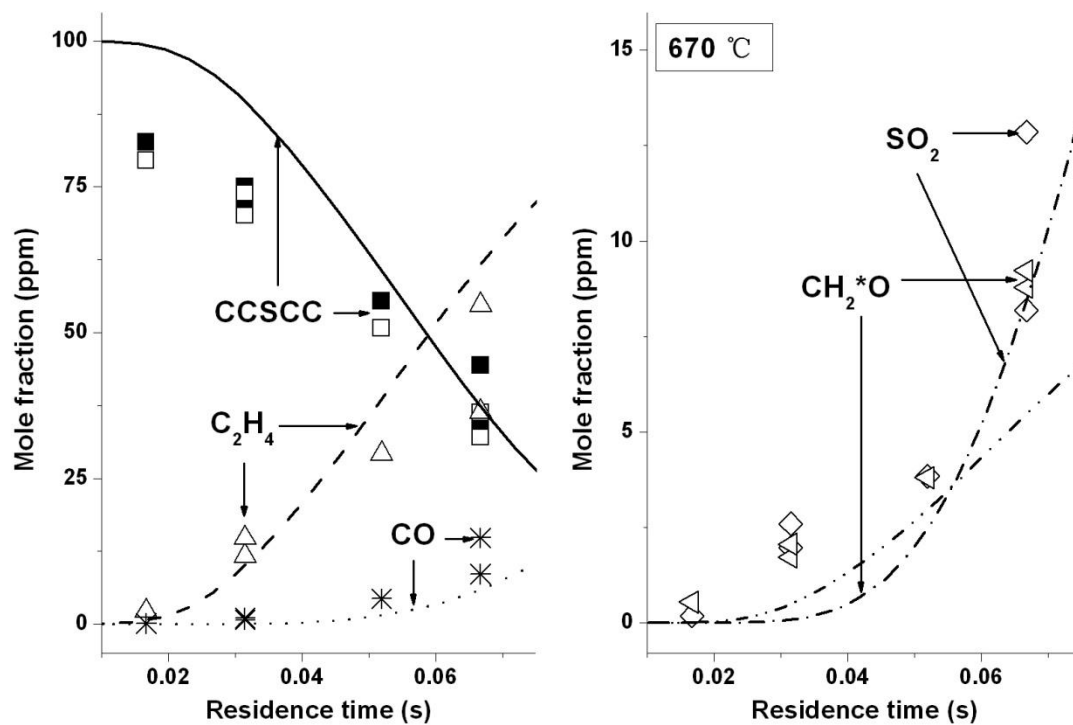


Figure 3.3B Oxidation of CCSCC ( $\Phi \sim 0.1$ ) at 670 °C.

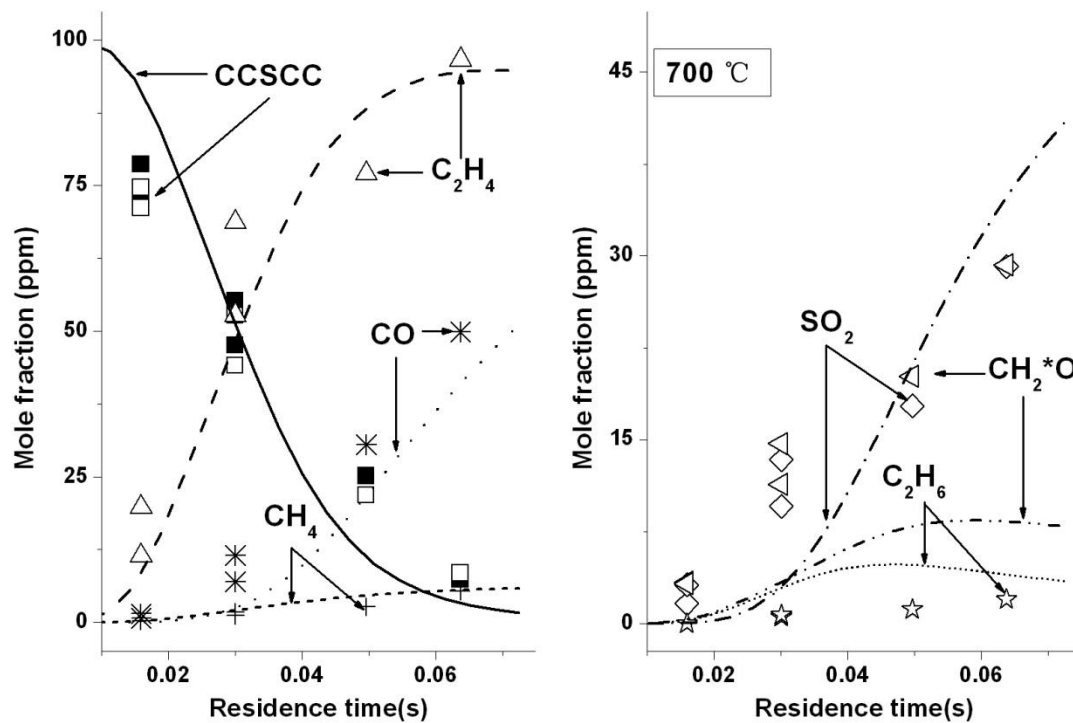


Figure 3.3C Oxidation of CCSCC ( $\Phi \sim 0.1$ ) at 700 °C.

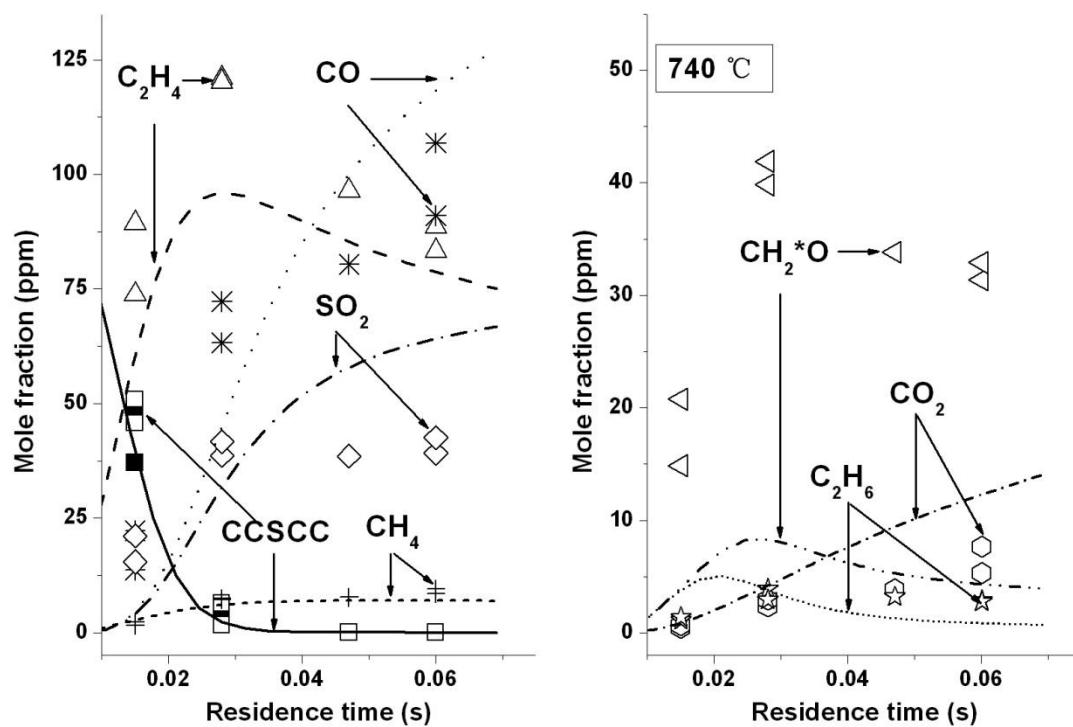


Figure 3.3D Oxidation of CCSCC ( $\Phi \sim 0.1$ ) at 740 °C.

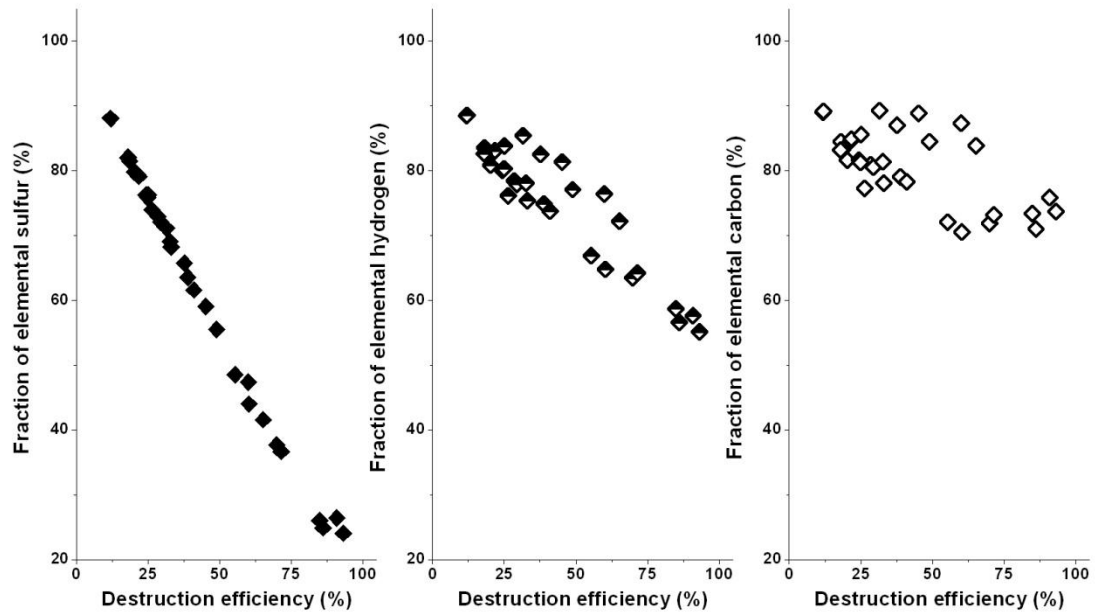


Figure 3.4 Element balances of CCSCC oxidation ( $\Phi \sim 1$ ), defined as the mass percent of a given element that is detected in form of quantified species shown in Figure 3.3.

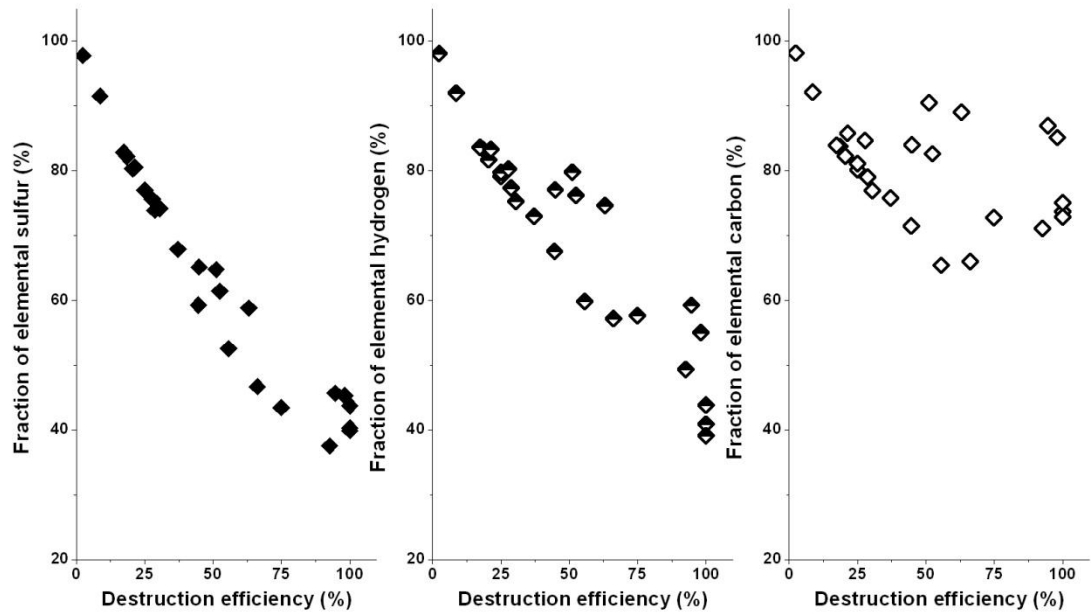


Figure 3.5 Element balances of CCSCC oxidation ( $\Phi \sim 0.1$ ), defined as the mass percent of a given element that is detected in form of quantified species shown in Figure 3.4.

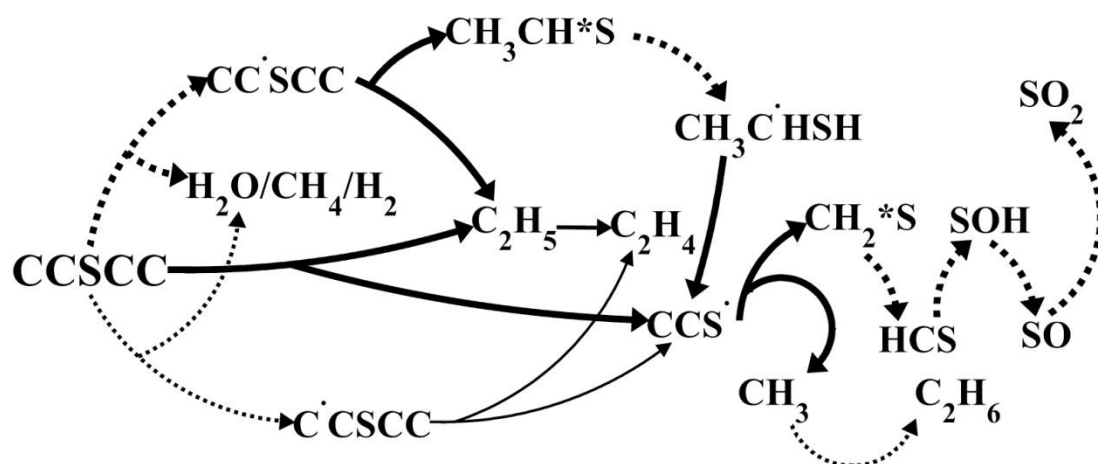


Figure 3.6 Oxidation pathways of 100 ppm diethyl sulfide at the 740 °C with approximately 9000 ppm  $\text{O}_2$  loading and with a residence time of 0.06 second. Solid lines represent unimolecular dissociation, while dashed lines represent reactions involve other reactants.

Table 3.4 Reactions with the highest sensitivity coefficient affecting the concentrations of major species at the 740 °C with approximately 9000 ppm O<sub>2</sub> loading.

Reactions	Kinetic parameters				Sensitivity coefficient			
	A	N	E <sub>a</sub>	CCSCC	C <sub>2</sub> H <sub>4</sub>	CO	SO <sub>2</sub>	CH <sub>2</sub> O
CCSCC ↔ CCS*+C <sub>2</sub> H <sub>5</sub>	1.06E+89	-21.7	105718.0	-9.6	0.95	2.0	1.6	1.7
CCSCC+H ↔ CC*SCC+H <sub>2</sub>	5.99E+08	1.9	5141.0	-2.3	0.26	-0.42		-0.23
CCSCC+HO <sub>2</sub> ↔ CC*SCC+H <sub>2</sub> O <sub>2</sub>	8.80E+13	0.0	11120.0		0.27	0.44	0.48	
CCSCC+OH ↔ C*SCC+H <sub>2</sub> O	7.20E+06	2.0	620.0	-2.0	-0.15	-0.54	-0.44	
CCSCC+OH ↔ CC*SCC+H <sub>2</sub> O	3.80E+06	2.0	300.0		0.19			
CCSCC+O ↔ CC*SCC+OH	6.80E+09	1.5	4000.0	-2.0				
CCS* ↔ CH <sub>3</sub> +CH <sub>2</sub> *S	8.61E+12	0.8	42000.0				-0.82	
CCS*+O <sub>2</sub> ↔ C <sub>2</sub> H <sub>5</sub> +SO <sub>2</sub>	3.00E+12	0.1	10414.0				0.83	
CC*SH ↔ C*CSH	5.10E+12	0.0	40000.0				0.34	
CH <sub>3</sub> CH*S+OH ↔ H <sub>2</sub> C*CHS*+H <sub>2</sub> O	1.08E+07	2.0	700.0			-0.36		
H+O <sub>2</sub> +N <sub>2</sub> ↔ HO <sub>2</sub> +N <sub>2</sub>	2.60E+19	-1.2	0.0	5.2	-0.47	-0.83	-0.80	0.40
H+O <sub>2</sub> ↔ OH+H	2.65E+16	-0.7	17041.0	-6.4	-0.52	1.48	1.2	0.66
OH+HO <sub>2</sub> ↔ O <sub>2</sub> +H <sub>2</sub> O	1.45E+13	0.0	-500.0	2.9				0.44
HO <sub>2</sub> +CH <sub>3</sub> ↔ OH+CH <sub>3</sub> O	1.20E+13	0.0	0.0	-2.3	-0.18	0.52	0.36	0.86
H+C <sub>2</sub> H <sub>4</sub> ↔ C <sub>2</sub> H <sub>5</sub>	5.41E+35	-6.8	11700.0		0.34	0.52	0.48	0.23
OH+CH <sub>2</sub> O ↔ HCO+H <sub>2</sub> O	3.43E+09	1.2	-447.0					-0.93

Table 3.4 (Continued)

$\text{O} + \text{C}_2\text{H}_4 \leftrightarrow \text{H} + \text{H}_2\text{C}^*\text{CHO}$	6.70E+06	1.8	220.0	-0.16	
$\text{OH} + \text{CH}_3 \leftrightarrow \text{CH}_2(\text{S}) + \text{H}_2\text{O}$	6.44E+17	-1.3	1417.0		0.47
$\text{O} + \text{C}_2\text{H}_4 \leftrightarrow \text{CH}_3 + \text{HCO}$	1.25E+07	1.8	220.0	1.6	0.30
$2\text{CH}_3(+\text{M}) \leftrightarrow \text{C}_2\text{H}_6(+\text{M})$	6.77E+16	-1.2	654.0		-0.30
$\text{HCO}(+\text{M}) \leftrightarrow \text{H} + \text{CO}(+\text{M})$	1.87E+17	-1.0	17000.0	-1.8	

A blank cell in the section of sensitivity coefficient indicates that the reaction does not occur among the top 5 reactions with high sensitivity for the species. Kinetic parameters are in modified Arrhenius format,  $k = AT^n \exp(-E_a/RT)$ , where A(mol, cm, s), T(K),  $E_a$ (cal/mol), R = 1.9859 cal/mol K, n is dimensionless.

### 3.5 SUMMARY AND CONCLUSIONS

The oxidation of diethyl sulfide has been studied in an atmospheric, turbulent flow reactor at four temperatures between 630 °C and 740 °C. The initial chemical loadings included near stoichiometric composition and fuel lean composition with an equivalence ratio near 0.1. Complementary development of a chemical kinetic mechanism extended the published pyrolysis mechanism [9] by updating existing reactions and adding oxidation related pathways. Evolution of diethyl sulfide and its derivatives are modeled by more than 1000 reactions among about 300 species.

Experimental measurements and mechanism predictions are reported. The mechanism predictions reproduce the experimental results for CCSCC and C<sub>2</sub>H<sub>4</sub> under all the studied conditions. For SO<sub>2</sub>, CO and C<sub>2</sub>H<sub>6</sub>, the predictions are accurate under the fuel lean conditions where these species were detected at high levels. Mechanism predictions have discrepancies with experimental data on minor species detected at low levels (<10 ppm) but reproduce the correct trends. Mechanism analysis shows that oxidation of CCSCC is initiated through unimolecular dissociation. Once the radical pool is well established, H abstraction from CCSCC becomes an important destruction route. The resulting radicals undergo  $\beta$ -scission and subsequent oxidation steps to form C<sub>2</sub>H<sub>4</sub>, CO and SO<sub>2</sub>. The radical branching, propagation, and termination reactions, involving H, O and OH, are the reactions to which species concentrations are most sensitive.

The study shows that the presence of O<sub>2</sub> accelerates the destruction of CCSCC, which is fully expected. Significant intermediate products remain at the conditions studied, even with large excess O<sub>2</sub>. The kinetics of major reaction intermediates, such as CH<sub>2</sub>\*S and CH<sub>3</sub>CH\*S, are determined to be important. Further investigations involving direct measurements of these species would be highly desirable to provide a data set for improving the mechanism.



### **3.6 ACKNOWLEDGMENTS**

The authors acknowledge the support of the U.S. Army Research Office under contract W911NF0410120.

## REFERENCES

- [1] S.A. Carnes, A.P. Watson, the Journal of the American Medical Association, 262-5 (1989) 653-659.
- [2] Text of Chemical Weapons Convention, <http://www.opcw.org/chemical-weapons-convention/>.
- [3] M.R. Green, American Journal of Public Health, 93-8 (2003) 1222-1226.
- [4] P.A. Glaude, C. Melius, W.J. Pitz, C.K. Westbrook, Proceedings of the Combustion institute, 29 (2002) 2469-2476.
- [5] J.H. Werner, T.A. Cool, Combustion and Flame, 117 (1999) 78-98.
- [6] P.H. Taylor, B. Dellinger, C.C. Lee, Environ. Sci. Technol., 24 (1990) 316-328.
- [7] D.V. Kozlov, A.V. Vorontsov, P.G. Smirniotis, E.N. Savinov, Applied Catalysis B: Enviromental, 42-1 (2003) 77-87.
- [8] A.V. Vorontsov, C. Lion, E.N. Savinov, P.G. Smirniotis, Journal of Catalysis, 220-2 (2003) 414-423.
- [9] X. Zheng, E.M. Fisher, F.C. Gouldin, L. Zhu, and J.W. Bozzelli, Proc. Combust. Inst. 32(2009) 469-476.
- [10] A.Y. Chang, J.W. Bozzelli, A.M. Dean, Zeit. Phys. Ch., 214 (2000) 1533-1568.
- [11] L. Zhu, J.W. Bozzelli, Journal of Physical Chemistry A, 110-21 (2006) 6923-6937.
- [12] L. Zhu, J.W. Bozzelli, in: The 5<sup>th</sup> U.S. National Combustion Meeting, Combustion Institute, San Diego, CA, 2007.
- [13] L. Zhu, J.W. Bozzelli, Journal of Molecular Structure-THEOCHEM, 728 (2005) 147-157.
- [14] R. Asatryan, J.W. Bozzelli, Phys. Chem. Chem. Phys., 10 (2008) 1769-1780.
- [15] Sulfur mechanism, v5 2002, Available at:  
<http://www.chem.leeds.ac.uk/Combustion/sox.html>.
- [16] A.M. Dean, J.W. Bozzelli, Gas Phase Combustion Chemistry, Springer, New York, 1992,

138.

- [17] C.Y. Sheng, J.W. Bozzelli, A.M. Dean, A.Y. Chang, *Journal of Physical Chemistry A*, 106-32 (2002) 7276-7263.
- [18] C.J. Chen, J.W. Bozzelli, *Journal of Physical Chemistry A*, 104-21 (2000) 4997-5012.
- [19] J. Lee, J.W. Bozzelli, *Journal of Physical Chemistry A*, 107-19 (2003) 3778-3791.
- [20] C. Sheng, Elementary, Pressure Dependence Model for Combustion of C1, C2 and Nitrogen Containing hydrocarbons: Operation of A Pilot Scale Incinerator and Model Comparison, Ph.D. Thesis, New Jersey Institute of Technology, Newark, NJ, USA, 2001.
- [21] X. Zhong, J.W. Bozzelli, *Journal of Physical Chemistry A*, 102-20 (1998) 3537-3555.
- [22] C.J. Chen, J.W. Bozzelli, *Journal of Physical Chemistry A*, 103-48 (1999) 9731-9769.
- [23] W.C. Ing, Reaction Kinetics on Methanol and MTBE Oxidation and Pyrolysis, Ph.D. Thesis, New Jersey Institute of Technology, Newark, NJ, USA 1996.
- [24] N. Sebbar, H. Bockhorn, J.W. Bozzelli, *Phys. Chem. Chem. Phys.*, 4 (2002) 3691-3703.
- [25] J.W. Bozzelli, C.Y. Sheng, *Journal of Physical Chemistry A*, 106-7 (2002) 1113-1121.
- [26] T. Yamada, The Oxidation of Dimethyl-Ether and ethylene in the atmosphere and Combustion Environment and Thermodynamic Studies on Hydrofluorocarbons Using Ab Initio Calculation Methods, Ph.D. Thesis, New Jersey Institute of Technology, Newark, NJ, USA, 1999.
- [27] T. Yamada, J.W. Bozzelli, T.H. Lay, *Int. J. Chem. Kinet.* 32-7 (2000) 435-452.
- [28] C.J. Montgomery, Q. Tang, A.F. Sarofim, M.J. Bockelie, J.K. Gritton, J.W. Bozzelli, F.C. Gouldin, E.M. Fisher, S. Chakravarthy, Improved Kinetic Models for High-Speed Combustion Simulation, Report No. AFRL-RZ-WP-TR-2008-2197, Air Force Research Laboratory, 2008.
- [29] W.C. Ing, C.Y. Sheng, J.W. Bozzelli, *Fuel Processing Technology*, 83-1-3 (2003) 111-145.

- [30] G.D. Silva, M.R. Hamdan, J.W. Bozzelli, *J. Chem. Theory and Computation*, 5(12) (2009) 3185-3194.
- [31] J.W. Bozzelli, R. Asatryan, C.J. Montgomery, in: *The 5<sup>th</sup> U.S. National Combustion Meeting*, Combustion Institute, San Diego, CA, 2007.
- [32] M.U. Alzueta, R. Bilbao, P. Glarborg, *Combustion and Flame*, 127-4 (2001) 2234-2251.
- [33] W.J. Hehre, R. Ditchfield, L. Radom, J.A. Pople, *J. Am. Chem. Soc.* 92-16 (1970) 4796-4870.
- [34] T.H. Lay, J.W. Bozzelli, A.M. Dean, E.R. Ritter, *Journal of Physical Chemistry*, 99 (1995) 14514-14527.
- [35] Reaction Design, 2004, Chemkin User Interface 4.0, <http://www.reactiondesign.com>.
- [36] W.S. Chin, B.W. Ek, C.Y. Mok, H.H. Huang, *J. Chem. Soc. Perkin, Trans. 2* (1994) 883-839.
- [37] M.J. Pilling, S.H. Robertson, *Annu. Rev. Phys. Chem.* 54 (2003) 245-2275.
- [38] I.A. Awan, D.R. Burgess, W. Tsang, J.A. Manion, *Standard Reactions for Comparative Rate Studies: Experiments and Computations on the Dehydrochlorination Reactions of 2-Chloropropane, Chlorocyclopentane and Chlorocyclohexane*, *International Journal of Chemical Kinetics*, in Press.

**CHAPTER 4**  
**PYROLYSIS AND OXIDATION OF ETHYL METHYL SULFIDE IN A FLOW**  
**REACTOR**

Xin Zheng<sup>1</sup>, E.M. Fisher<sup>1</sup>, F.C. Gouldin<sup>1</sup>, J.W. Bozzelli<sup>2</sup>

<sup>1</sup>Sibley School of Mechanical and Aerospace Engineering

Cornell University

Ithaca NY 14853

<sup>2</sup>Department of Chemistry and Environmental Science

New Jersey Institute of Technology

Newark NJ 07101

**ABSTRACT**

The reactions and kinetics of ethyl methyl sulfide ( $\text{CH}_3\text{CH}_2\text{SCH}_3$ ), a simulant for the chemical warfare agent sulfur mustard, were studied at temperatures of 630 to 740 °C, under highly diluted pyrolysis and oxidation conditions at one atmosphere in a turbulent flow reactor. The loss of the ethyl methyl sulfide and the formation of intermediates and products were correlated with time and temperature. Destruction efficiencies of 50 % and 99 % were observed for pyrolysis and oxidation, respectively, at 740 °C with a residence time of 0.06 second. For pyrolysis, ethylene, ethane, and methane were detected at significant levels. In addition to these species, carbon monoxide, carbon dioxide, sulfur dioxide, and formaldehyde were detected for oxidation. Conversions of ethyl methyl sulfide were observed to be significantly slower than observed previously for diethyl sulfide; explanations for this observation are postulated, based on (1) lower hydrogen abstraction rates or on (2) lower hydrogen atom production as a result of thermal decomposition pathways. Initial decomposition reactions and production pathways for important species observed in the experiments are discussed on a basis of thermochemistry.

## 4.1 INTRODUCTION

Sulfur mustard, Bis(2-chloroethyl) sulfide ( $\text{ClCH}_2\text{CH}_2\text{-S-CH}_2\text{CH}_2\text{Cl}$ ), known as a cytotoxic chemical with the ability to form blisters on exposed bodies, is a principal component of the stockpile inventory of chemical warfare agents (CWA) in the United States and other major countries [1-2]. As part of the 1993 Chemical Weapons Convention (CWC) [3], sulfur mustard stockpiles must be destroyed by April 29, 2012. Over the past 15 years, significant effort has been put to explore environmentally acceptable destruction methods with a focus on efficiency, completeness and minimal production of by-products [4-10]. In the United States, incineration has been applied as the baseline method due to its high destruction efficiency, high throughput, and high cost effectiveness [11]. Nonetheless, there have been strong oppositions to chemical weapon incineration over the potential formation of toxic emissions. In responding to the public concerns, the U.S. army has sponsored studies to monitor incinerator effluent and to build detailed kinetic mechanisms to model the incineration of mustard agent and to predict the safety of their incinerators [12, 13]. Now, as 60% of chemical stockpiles in the United States have been disposed [14], including complete elimination of the stockpiles of nerves agents, sulfur mustard is the primary component still waiting for destruction. The situations are such that particular interest has been attracted to investigate chemistry of sulfur mustard at incineration relevant conditions.

Although experiments on actual chemical warfare agents are not practical in university laboratories because of safety considerations, studies with simulants provide added validation, and this serves to improve confidence in model predictions and thus alleviate some public concerns over the incineration process. The present work extended the previous study [15] by adding experimental data on pyrolysis and oxidation of ethyl methyl sulfide. The study allows us to compare the effect of methyl

group on the destruction efficiency and product distribution with that of ethyl group from the study on diethyl sulfide [15]. In addition, the data will be used to validate the methyl sulfur reactions under development.

In the forthcoming sections of this paper, we qualitatively discuss product formation and destruction efficiency for ethyl methyl sulfide in light of the kinetic mechanism previously developed for diethyl sulfide and the available thermochemistry [15].

## **4.2 EXPERIMENTAL APPARATUS AND METHODOLOGY**

The present work was performed in a 4.5-cm-ID tubular flow reactor (Figure A.4 in Appendix A), which is fully documented in a previous study [15] and Appendix A, and is briefly described here. Two flow streams were mixed in the reactor: a main flow and a secondary simulant carrier flow. The main flow was approximately 95% by mass of the total reactor flow; it was a turbulent preheated nitrogen flow which became fully developed as it flowed through a 1 m long development section. The secondary carrier flow varied with experimental conditions as follows. In the pyrolysis experiments, the secondary flow was nitrogen, while in the oxidation experiments, it was laboratory compressed air purified by using a Whatman Model 75-52 purge gas generator to remove carbon dioxide and moisture. Ethyl methyl sulfide was injected into the secondary flow through an injection port via a syringe pump (Harvard Apparatus model PHD2000 with 1% uncertainty). Carbon monoxide (CO) was also added to the secondary flow as an inert tracer [15] to determine mixing completeness in the reactor and dilution in the sampling system during the pyrolysis experiments. No tracer was used in the oxidation experiments, in which mixing conditions were assumed to be the same as those in the pyrolysis experiments having the same heater settings and flow rates. The secondary flow was injected into the main carrier flow

through four open-ended quartz tube injectors. GC/MS analysis of gas samples withdrawn from the secondary flow showed no evidence of chemical reactions upstream of the injection point. The main and secondary flows subsequently mixed, and reactions occurred along the length of a tubular quartz reaction section. This reaction section, 4.5 cm in diameter and 1 m long, was sitting inside a stainless steel pipe which was covered by electric resistance heaters and insulation material to effectively maintain the gas temperature at a fixed value.

The experiments were performed at conditions very similar to those used in a previous study of diethyl sulfide [15], at four different operating temperatures between 630 °C and 740 °C and at 1 atm pressure. The detailed experimental flow parameters and chemical loadings for each operating temperature are shown in Tables A.2 (Appendix A) and A.4 (Appendix A), and the uncertainties of the CCSC and O<sub>2</sub> loadings are provided in the table note. As shown in the tables, the flow of the reaction section was turbulent with a Reynolds number of around 5000. The initial loading of ethyl methyl sulfide in the reaction section was 150 ppm for all operating conditions. In this document, ppm refers to parts per million on a volume (or molar) basis. In the oxidation experiments, the initial loading of oxygen (O<sub>2</sub>) was approximately 9000 ppm in the reaction section, which produced a fuel-lean condition with an equivalence ratio of approximately 0.1 based on sulfur dioxide (SO<sub>2</sub>), water (H<sub>2</sub>O), and carbon dioxide (CO<sub>2</sub>) as final products. Gas temperature profiles were adopted from the previous study [15] as the heater settings and flow rates were the same as those of the current experiments. The temperature measurements were performed without the injection of the carbon monoxide (CO) tracer and sulfur compound flows. However, any error in temperature readings due to enthalpies of reaction was negligible under the highly dilute conditions of the experiments. Each experiment is identified with a “nominal temperature”, the average centerline temperature in the sampling region



rounded to the nearest 10 °C. In this region, temperatures vary by approximately  $\pm 10$  °C. Upstream of the first sampling port, there is a region of low temperature (typically reaching 80 °C below the nominal temperature) where the cold secondary flow mixes into the preheated main flow. Temperature profiles are given in Figure A.9 (Appendix A), and were repeatable. Repeated measurements were performed several months after those reported, at two temperature conditions; temperatures were within the measurement uncertainty (1%) of the original ones.

The intent of choosing such experimental conditions was twofold, (1) understanding the initiation of the destruction of sulfur mustard simulants and (2) exploring routes relevant to emissions under off-design incineration modes, such as low temperature quenching, and fuel rich conditions due to inhomogeneous mixing.

In the experiments, all of the independent flow parameters described above, including main flow rate, secondary flow rate, wall temperatures of the reaction section, tracer flow rate, infusion rate of liquid ethyl methyl sulfide, as well as the sample dilution flow rate and sampling pressure, were electronically monitored and independently controlled. The flow reactor system was given sufficient time to reach steady conditions prior to sampling.

Gas samples were extracted at four different positions on the centerline of the reaction section and analyzed by GC/MS and FT-IR. Each sampling probe (Figure A.5) consisted of two radially oriented concentric quartz tubes with respective 4 and 1 mm ID. A nitrogen flow with approximately the same flow rate as the gas sample flow was introduced through the inner tube, to quench reactions. Gas sampled from the flow reactor mixed with the quenching nitrogen flow and was drawn out of the flow reactor through the annular region in the probe. The probe design and testing are described in [16] as well as in Appendix A. The diluted sample flow passed through Teflon® transfer lines to a Nicolet Model 6300 FT-IR or an Ultra Trace GC/DSQ II

MS for analysis. Details regarding analytical methods are available in Appendix A. Detection limits were 0.3 ppm for ethylene, 0.26 ppm for methane, 0.25 ppm for ethane, 0.23 ppm for carbon dioxide, 0.20 ppm for carbon monoxide, 0.25 ppm for formaldehyde, 0.6 ppm for sulfur dioxide and 1.3 ppm for ethyl methyl sulfide.

Species concentrations in the gas samples were affected by the mixing of the secondary flow into the main flow and by dilution in the sampling system, as well as by the chemical reactions in the reaction section. Measurements of tracer concentrations made it possible to account for the mixing and dilution effects [15].

### 4.3 RESULTS

Destruction efficiencies at the last sampling port for the pyrolysis and oxidation of ethyl methyl sulfide are presented in Figure 4.1, along with those reported previously for pyrolysis of diethyl sulfide [15]. Destruction efficiency is defined as the fraction of the parent compound destroyed at a given position. Species concentration profiles from both the pyrolysis and oxidation experiments of ethyl methyl sulfide are reported in Figures 4.2-4.9, for all species detected at levels of 1 ppm or higher. Figures 4.2 and 4.8 show the profiles of the species that were detected by both FT-IR and GC/MS. In these figures, hollow symbols represent FT-IR data, while filled symbols represent GC/MS data.

As shown in Figure 4.1, for the pyrolysis of ethyl methyl sulfide, destruction efficiency at the last sampling port of the reaction section (residence times between 0.06 s and 0.072 s) increased with the operating temperature, from approximately 11% at the 630 °C operating temperature, to 16% at 670 °C, 25% at 700 °C, and 50% at 740 °C. Compared to the pyrolysis of ethyl methyl sulfide, destruction efficiency was enhanced by more than a factor of two in the oxidation of ethyl methyl sulfide, shown in Figure 4.1. Destruction efficiency was approximately 25% at the 630 °C operating

temperature, 41% at 670 °C, and 67% at 700 °C. Nearly complete destruction was observed at the 740 °C operating temperature.

The primary products observed in both pyrolysis and oxidation experiments of ethyl methyl sulfide were ethylene ( $C_2H_4$ ) (Figure 4.3), ethane ( $C_2H_6$ ) (Figure 4.4), and methane ( $CH_4$ ) (Figure 4.5). Carbon monoxide (CO) (Figure 4.6), carbon dioxide ( $CO_2$ ) (Figure 4.7), sulfur dioxide ( $SO_2$ ) (Figure 4.8), and formaldehyde ( $CH_2O$ ) (Figure 4.9) were detected in the oxidation experiments only. The following species: acetylene ( $C_2H_2$ ), carbon disulfide ( $CS_2$ ), thiophene (cyc- $C_4H_4S$ ), dimethyl disulfide ( $CH_3SSCH_3$ ) and ethyl methyl disulfide ( $C_2H_5SSCH_3$ ), were detected but at levels below 1 ppm.  $H_2O$  was detected, but was difficult to quantify because of fluctuating background levels in the FT-IR instrument. In addition, condensates were observed on the internal surface of the sampling probes during both the pyrolysis and oxidation experiments. A condensate sample was obtained by flushing the sampling probes with methylene chloride after the experiments. Cyclooctasulfur ( $S_8$ ) was identified by GC/MS with a DB5 column, and a small unidentified peak was also present. Thioformaldehyde trimers (CAS No. 291-21-4), an anticipated component of the condensates [17], were detectable by this GC/MS method, but not observed in the solution. Elemental balances were calculated based on the species concentrations as present in Figures 4.2-4.9. For the pyrolysis conditions shown in Figure 4.10, the sulfur balances decreased linearly with the destruction efficiency down to 50%, as no sulfur containing products were detected. Carbon and hydrogen balances were approximately 80% at the maximum destruction efficiency of 50%. In contrast, lower elemental balances, 35% for sulfur, 70% for carbon and 40% for hydrogen were found at the maximum destruction efficiency of 100% for the oxidation conditions, as shown in Figure 4.11. Poor elemental balances are probably due to a few undetectable species, as discussed in the following section.

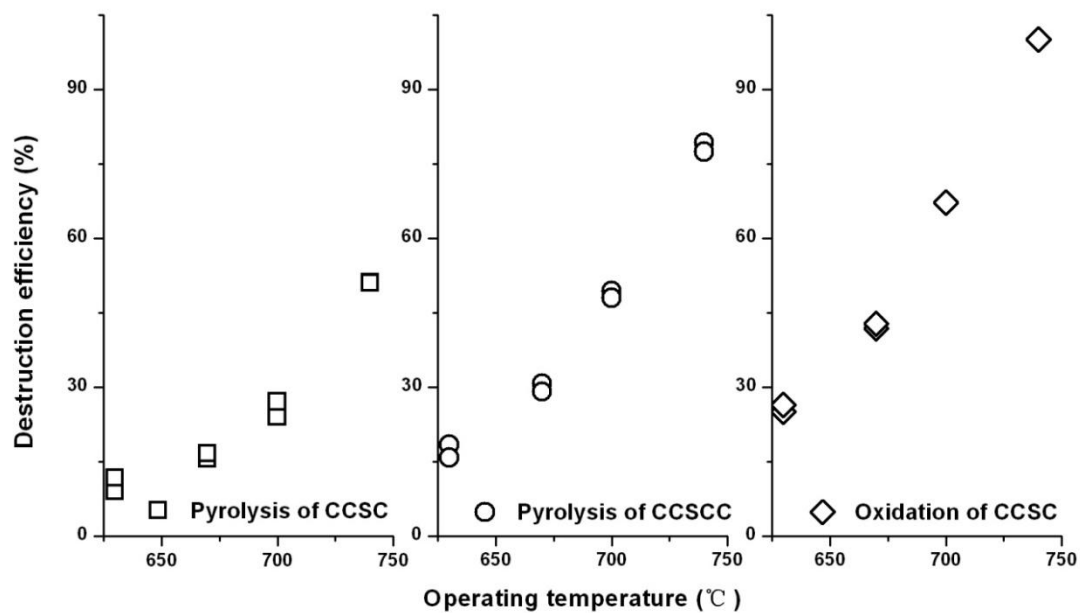


Figure 4.1 Destruction efficiencies of ethyl methyl sulfide by pyrolysis and oxidation, and destruction efficiencies of diethyl sulfide by pyrolysis, measured at the last sampling port of the flow reactor.

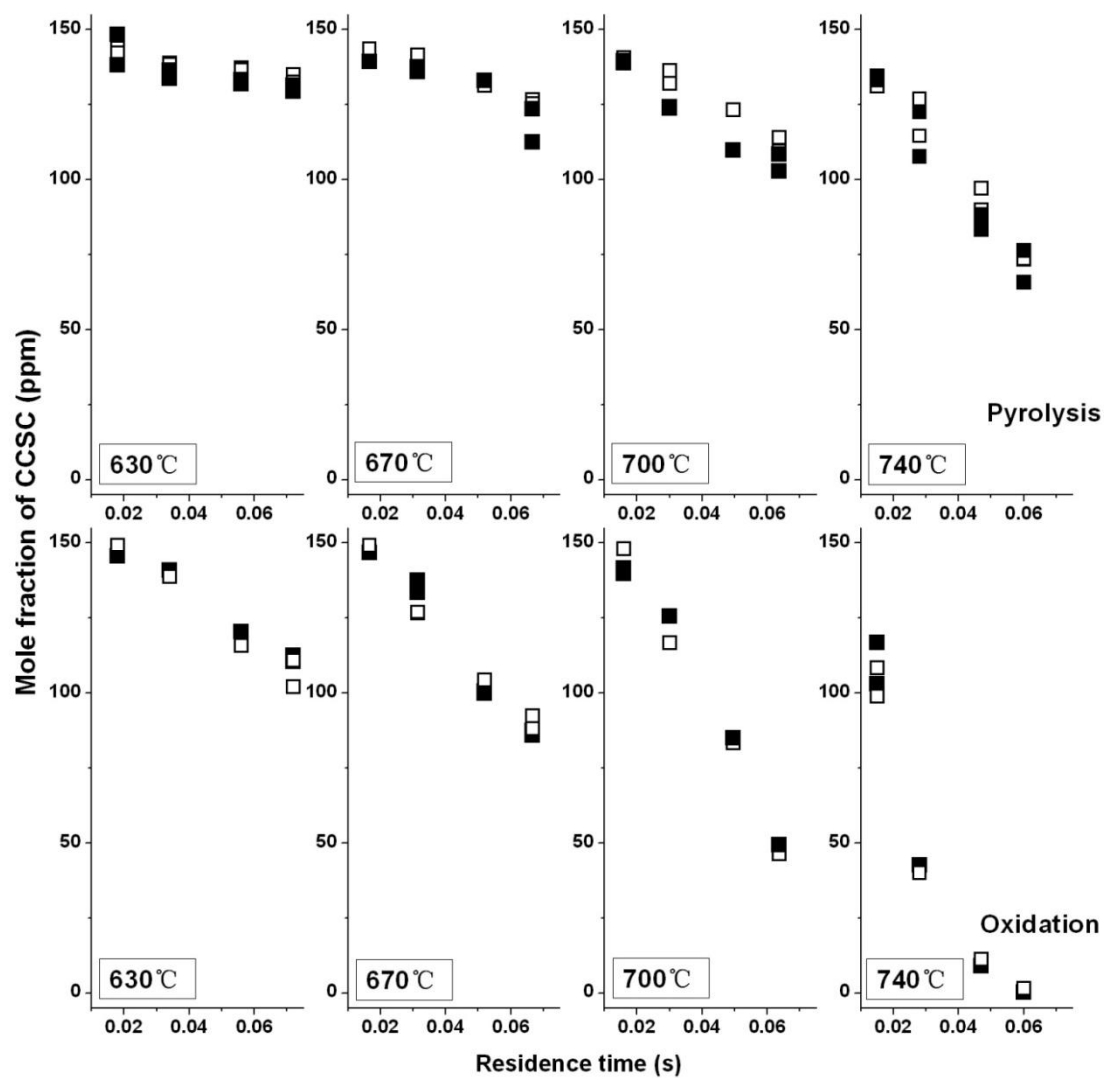


Figure 4.2 Mole fraction of ethyl methyl sulfide in the pyrolysis and oxidation experiments. Hollow symbols represent FT-IR data while filled symbols represent GC/MS data.

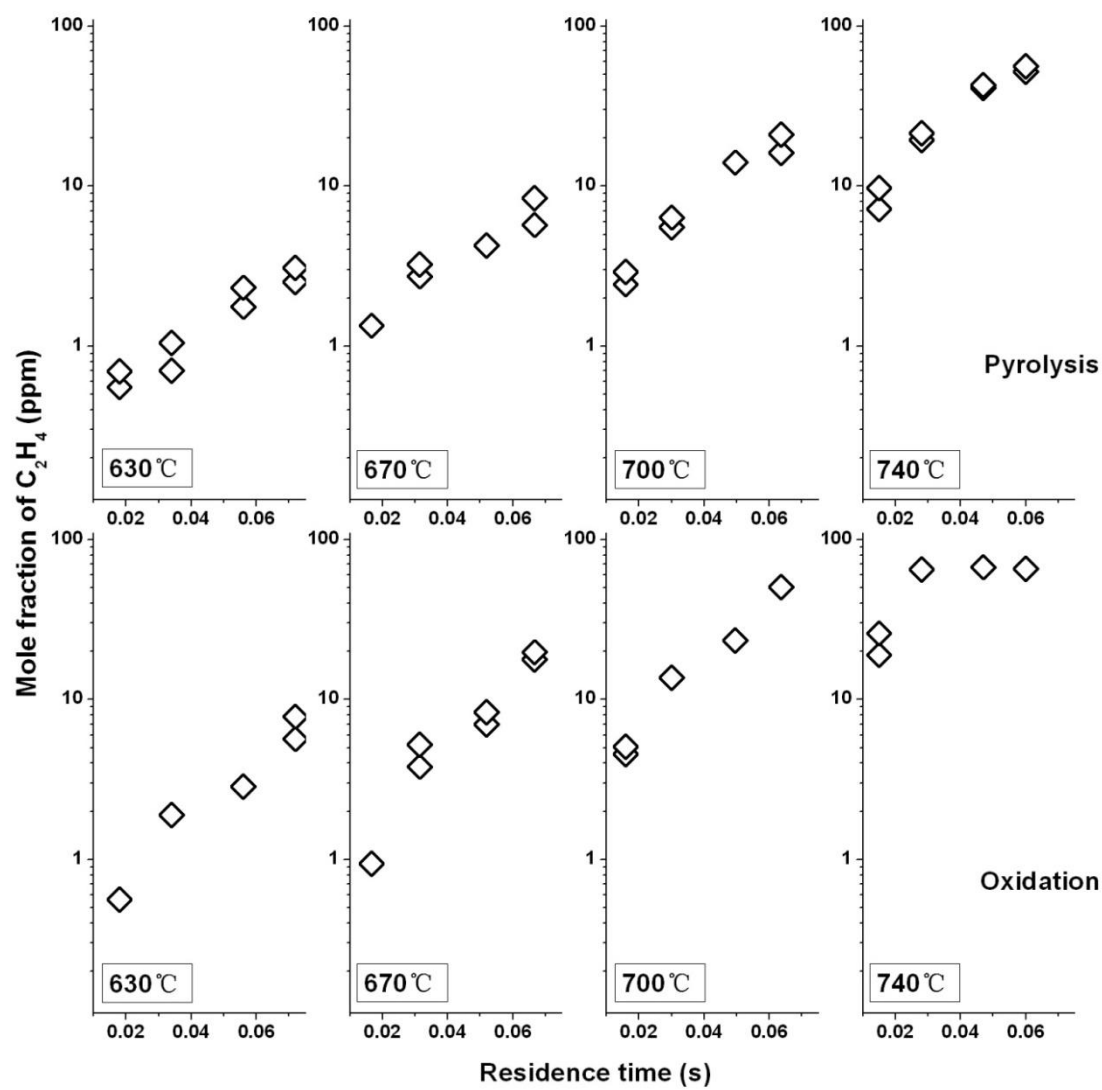


Figure 4.3 Mole fraction of ethylene in the pyrolysis and oxidation experiments.

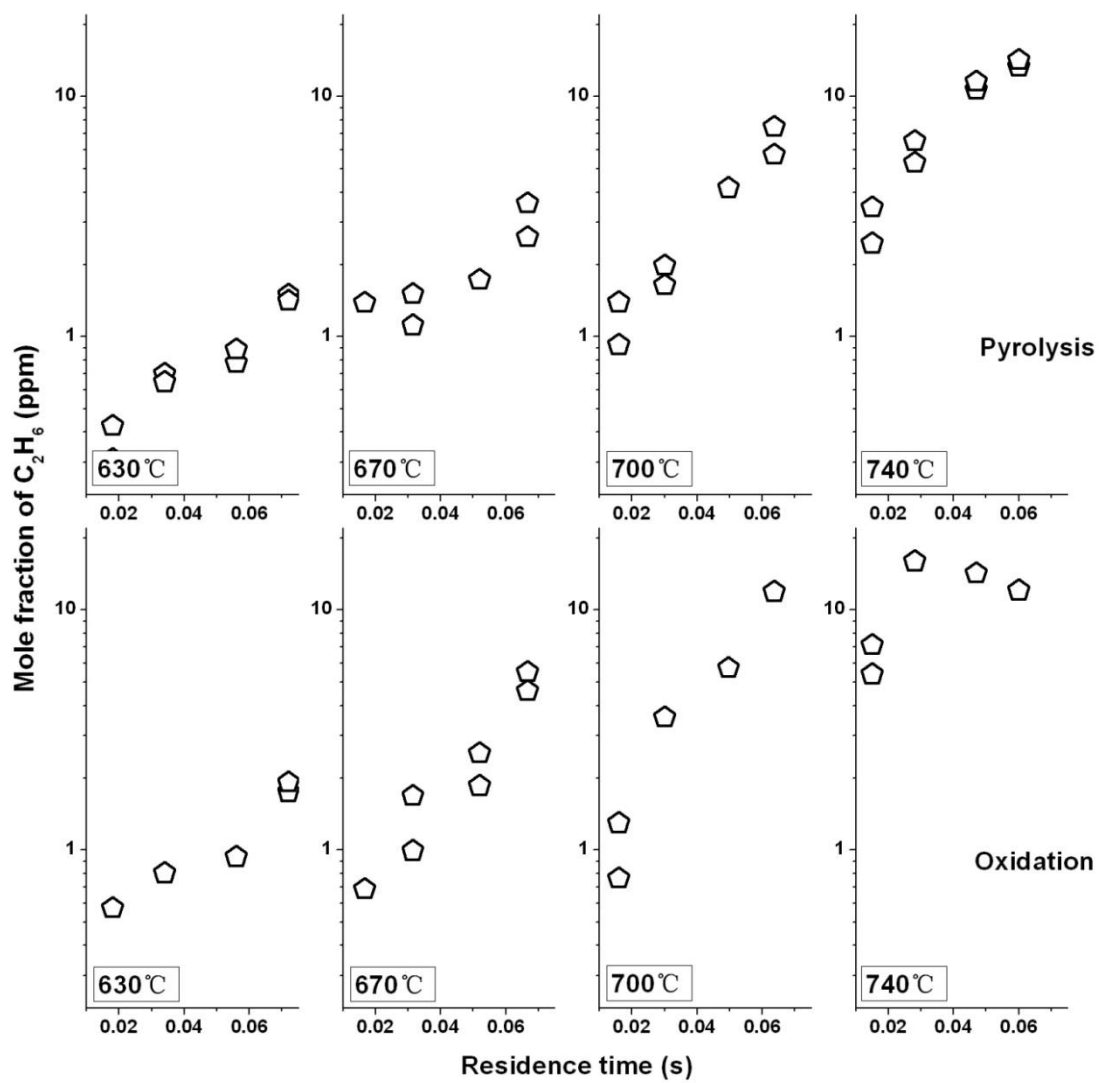


Figure 4.4 Mole fraction of ethane in the pyrolysis and oxidation experiments.

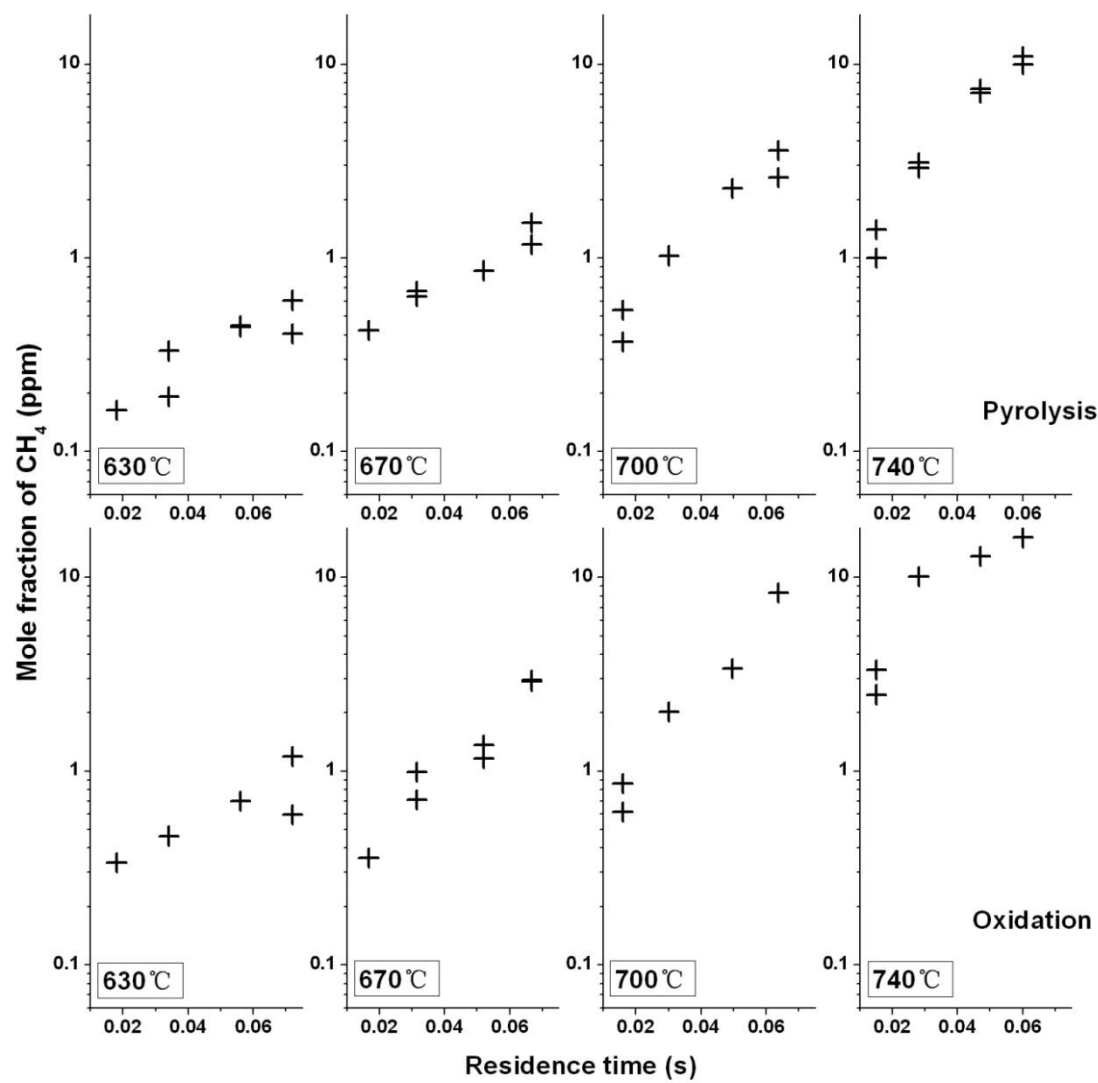


Figure 4.5 Mole fraction of methane in the pyrolysis and oxidation experiments.



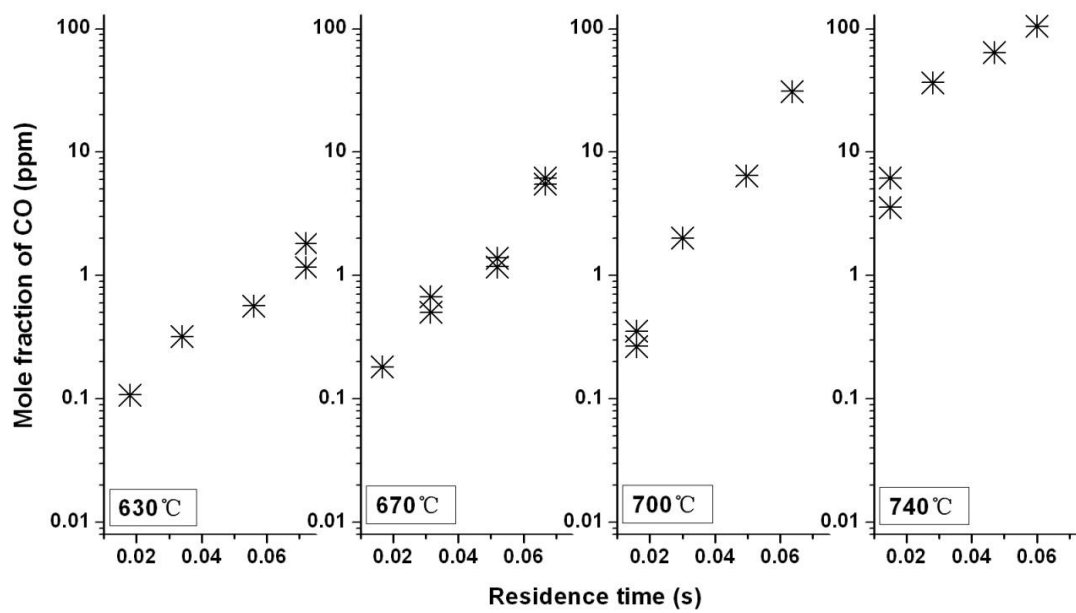


Figure 4.6 Mole fraction of carbon monoxide in the oxidation experiments.

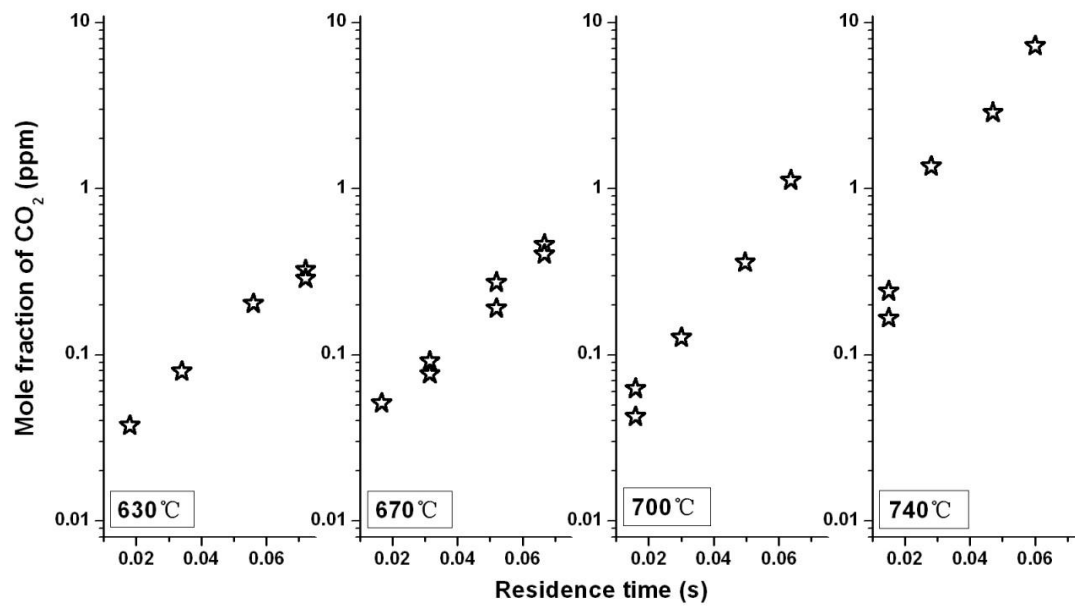


Figure 4.7 Mole fraction of carbon dioxide in the oxidation experiments.

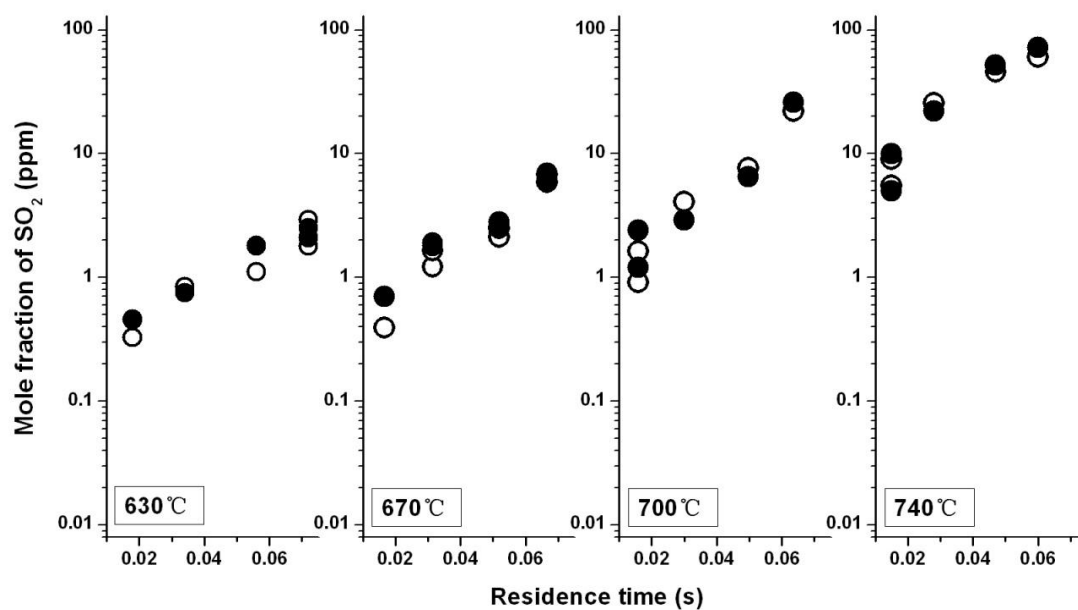


Figure 4.8 Mole fraction of sulfur dioxide in the oxidation experiments. Hollow symbols represent FT-IR data while filled symbols represent GC/MS data.

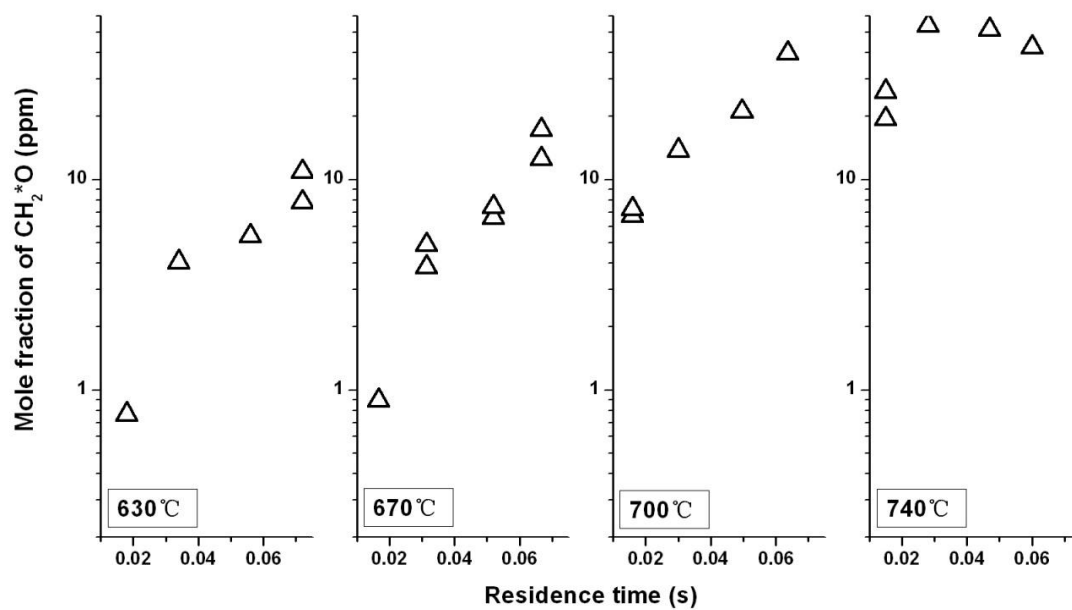


Figure 4.9 Mole fraction of formaldehyde in the oxidation experiments.

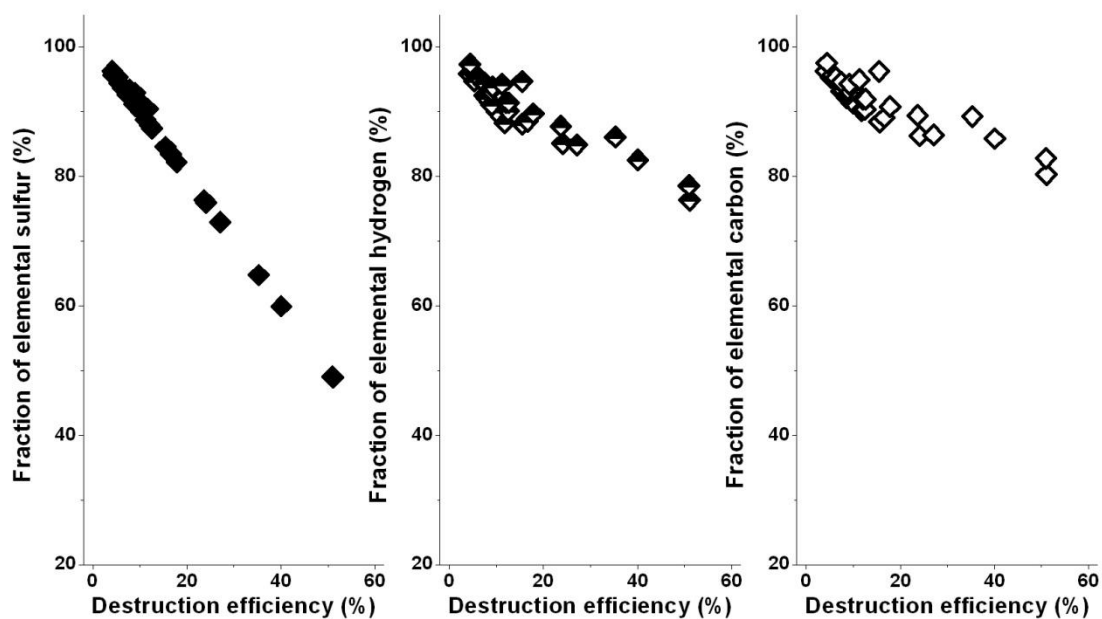


Figure 4.10 Element balances of CCSC pyrolysis, defined as the mass percent of a given element that is detected in the form of quantified species shown in Figures 4.2-4.5.

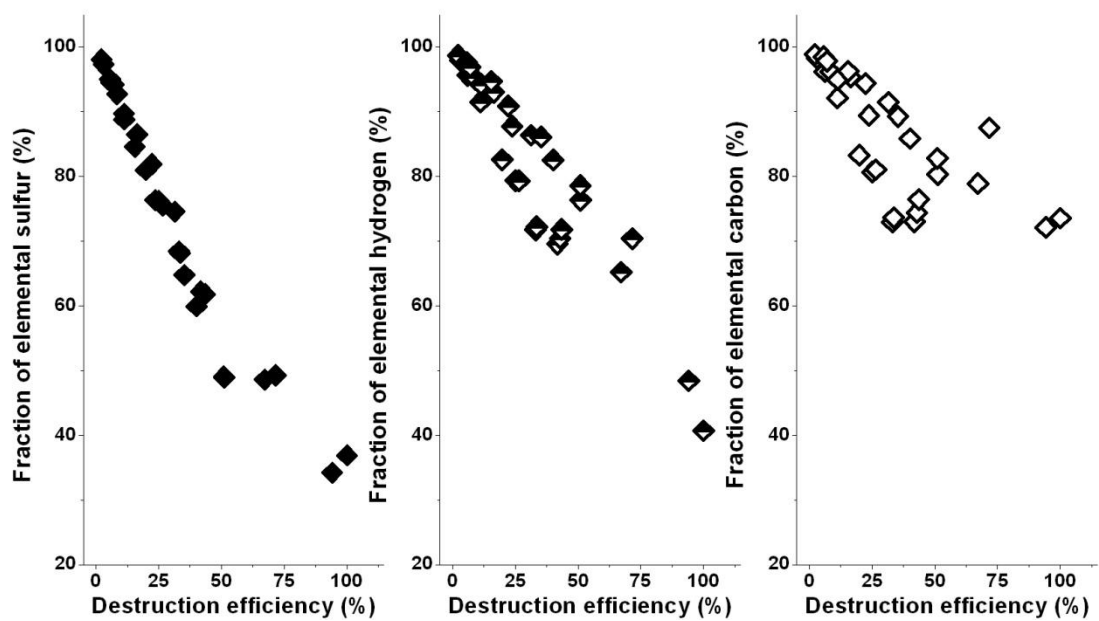


Figure 4.11 Element balances of CCSC oxidation, defined as the mass percent of a given element that is detected in the form of quantified species shown in Figures 4.2-4.9.

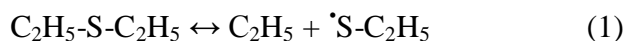
## 4.4 DISCUSSION

### 4.4.1 MECHANISM OF PYROLYSIS OF ETHYL METHYL SULFIDE

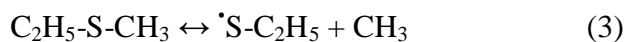
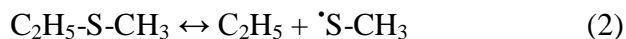
Because the molecular structure and bond dissociation energies (BDEs) of ethyl methyl sulfide (shown in Figure 4.12) resemble those of diethyl sulfide ( $\text{CH}_3\text{CH}_2\text{-S-CH}_2\text{CH}_3$ , abbreviated CCSCC), it is not surprising that during the pyrolysis experiments the same products were observed for these two chemicals [15]. First we qualitatively explain the formation of products from ethyl methyl sulfide with the reaction scheme discussed below, developed by analogy to the detailed mechanism for pyrolysis of diethyl sulfide [15]. Then later in this section, we focus on the destruction efficiency of CCSC. We compare it to the destruction efficiency of CCSCC, and use the reaction scheme to provide possible explanations for the differences.

#### Decomposition Pathways

Initial decomposition of either CCSCC or CCSC occurs via C-S bond cleavage. According to our previous study [15], CCSCC pyrolysis is initiated through C-S bond cleavage.



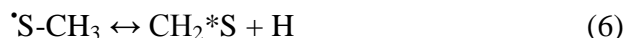
It is important to note that Reaction (1) has two identical paths or a reaction degeneracy of two. In contrast, due to the asymmetric structure of ethyl methyl sulfide, C-S bond cleavage can occur through the two different unimolecular decomposition steps shown below.



As shown in Figure 4.12, BDEs for the C-S bonds broken in Reactions (1) through (3) are the same within uncertainty: The BDEs are  $72.4 \pm 0.1$  and  $73.4 \pm 1.5$  kcal/mol for the bonds broken in Reactions (2) and (3), compared to a BDE of  $72.5 \pm 1.5$  cal/mol for the bond broken in Reaction (1). In addition, initiation can also occur via C-C or

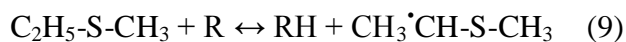
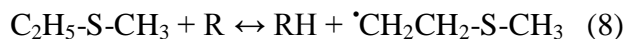
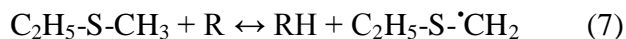
C-H bond cleavage. However these reactions are relatively unimportant as the C-C bond energies are  $\sim 82.0 \pm 2.0$  kcal/mol and the C-H bond energies are  $\sim 100$  kcal/mol, considerably higher than those of the C-S bonds.

The ethyl ( $\text{C}_2\text{H}_5$ ), ethylthio ( $^*\text{S}-\text{C}_2\text{H}_5$ ), and methylthio ( $^*\text{S}-\text{CH}_3$ ) radicals formed in these initiation steps (Reactions (2) and (3)) can undergo  $\beta$ -scission to produce ethylene and thioformaldehyde ( $\text{CH}_2^*\text{S}$ ) along with the methyl radical and H atom respectively. See Reactions (4), (5) and (6).



The resulting ethylene was a major product observed in the experiments (Figure 4.3). The thioformaldehyde product was not detected in the experiments, and its fate is discussed below.

As the radical pool becomes more established from the initiation and initial  $\beta$ -scission reactions, H abstraction (Reactions (7-9)) is expected to become an important route for the destruction of ethyl methyl sulfide.

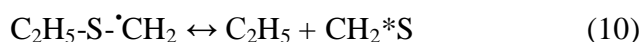


R is H atom or  $\text{CH}_3$  radical in Reactions (7-9). In addition, we expect H abstraction from the  $\alpha$  carbon (carbon bonded to sulfur atom) to be the fastest abstraction reaction. This expectation is based on the thermochemistry of CCSCC developed in our previous study [15] which gives a lower BDE of C-H on the  $\alpha$  carbon than that on the  $\beta$  carbon, in agreement with hydrocarbon thermochemistry [18]. However, no kinetic data are currently available for Reactions (7-9). Two stable products,  $\text{H}_2$  and  $\text{CH}_4$ , are predicted.  $\text{CH}_4$  is detected at levels up to 10 ppm (Figure 4.5). Simulations of diethyl



sulfide pyrolysis [15] indicate that hydrogen (H<sub>2</sub>) yield from the reactions above should be higher than methane yield, because abstraction rates by hydrogen atoms are approximately one order of magnitude higher than those by methyl radicals. However, H<sub>2</sub> is not detectable by our experimental techniques.

The radicals produced by these reactions undergo  $\beta$ -scission, producing ethyl, methyl, and methylthio radicals along with thioformaldehyde, thioacetaldehyde (CH<sub>3</sub>CH\*S), and ethylene:



Further  $\beta$ -scission of the methylthio and ethyl radicals yields additional thioformaldehyde and ethylene. Recombination of CH<sub>3</sub> radicals can form ethane [19], a species observed during the experiments at levels up to 10 ppm.

Two thioaldehydes, thioformaldehyde and thioacetaldehyde, are expected to be major products on the basis of the reactions listed above and subsequent  $\beta$ -scission. Because thioaldehydes were not detected, it appears that their destruction reactions are important. Possible routes for thioaldehyde destruction are speculative. Under pyrolytic conditions, these routes include heterogeneous reactions, either in the flow reactor or in the sampling system, hydrogen abstraction or addition reactions, and disproportionation reactions. With a dearth of detected sulfur-containing products, little evidence exists to distinguish between the importance of these routes. The importance of disproportionation reactions, for instance Reaction (13):



is supported by the fact that S<sub>2</sub> is a precursor [20] for the solid cyclooctasulfur observed in the probe rinsate. However, kinetic simulations in our previous study of CCSCC pyrolysis [15] indicate that disproportionation reactions do not contribute

significantly to thioaldehyde destruction under the conditions studied.

#### 4.4.2 DESTRUCTION EFFICIENCY

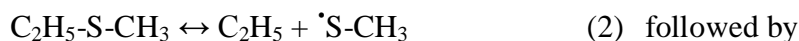
The destruction efficiency of ethyl methyl sulfide depends on the rates of the reactions above and the reactivity of their products. Of particular importance are the reactions resulting in branching, (net positive production of radicals), e.g. unimolecular decomposition. Since the BDE of the initiation steps of ethyl methyl sulfide decomposition are almost the same as that of diethyl sulfide (Reactions (1), (2), and (3); Figure 4.12), destruction efficiencies of diethyl sulfide are expected to be similar to those of ethyl methyl sulfide. In contrast to this expectation, the destruction efficiency of diethyl sulfide was significantly higher than that of ethyl methyl sulfide except at the 630 °C condition, as can be seen in Figure 4.1. Destruction efficiencies at the last sampling port were 15% at the 630 °C condition, 30% at 670 °C, 50% at 700 °C, and 80% at 740 °C for diethyl sulfide, and 11%, 16%, 25% and 50% for ethyl methyl sulfide at the corresponding temperature and residence time conditions.

In the absence of a detailed mechanism for ethyl methyl sulfide, we can propose two possible explanations for the relatively slow thermal destruction of ethyl methyl sulfide, one involving hydrogen abstraction and one involving initial unimolecular dissociation reactions.

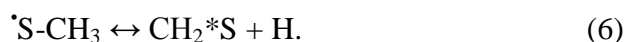
CCSCC and CCSC's hydrogen abstraction rates are expected to differ as that CCSCC has a larger number of weaker C-H bonds as well as a larger total number of hydrogen atoms available to abstract. Thus, at higher temperatures, once the radical pool is established, the observed higher destruction efficiencies for CCSCC are supported by the expected higher hydrogen abstraction rates.

The effect of differences in initial unimolecular decomposition steps is more complex and depends on the relative importance of the two different initiation steps

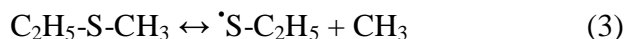
for CCSC, as described below. Differences in the number of relatively reactive hydrogen atoms vs relatively nonreactive methyl radicals ultimately produced through the different initiation steps should influence destruction efficiencies. The first path (Reactions (2), (4) and (6)) is



and by



This path produces two H atoms and no  $\text{CH}_3$  radical per CCSC destroyed. The second path (Reactions (3) and (5)) is

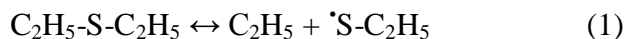


followed by



This path produces no H atoms and two  $\text{CH}_3$  radicals per CCSC destroyed.

In contrast, CCSCC has two degenerate paths, i.e. two identical C-S cleavage reactions:



and each path ultimately produces one H atom and one  $\text{CH}_3$  radical per CCSCC destroyed.



Overall the two identical paths produce two H atoms and two  $\text{CH}_3$  radicals. Thus, the observed lower destruction efficiency for CCSC relative to CCSCC could be explained if Reaction (3), ultimately producing  $\text{CH}_3$  radicals, is faster than Reaction (2), ultimately producing H atoms. Kinetic mechanism development is under way to estimate the rates of these reactions, and currently available data does not clearly

indicate which rate is higher. Figure 4.12 shows that the CH<sub>3</sub>-S bond is ~ 1 kcal mole stronger than the C<sub>2</sub>H<sub>5</sub>-S bond, thus the activation energy term, in the dissociation rate constants, would actually be higher for Reaction (2), which would not explain the different destruction efficiencies observed. However, the CH<sub>3</sub>-S bond energy has a relatively large reported uncertainty as shown in Figure 4.12. Also, it is established that dissociation reactions producing a methyl radical (e.g. Reaction (3)) have about a two to three times higher pre-exponential factor than those producing larger hydrocarbon fragments (e.g. Reaction (2)) [21].

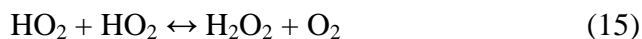
#### 4.4.3 MECHANISM OF OXIDATION OF ETHYL METHYL SULFIDE

Initiation of the destruction of ethyl methyl sulfide in the oxidation experiments includes C-S bond cleavage (Reactions (2) and (3)), as in the pyrolysis regime. An additional path occurs in the presence of O<sub>2</sub>, which is the abstraction of a H atom from the hydrocarbon backbone:



which, on the basis of hydrocarbon kinetics [22], is approximately 50 kcal/mol endothermic, with only a 1 kcal/mol barrier over the endothermicity of the reaction.

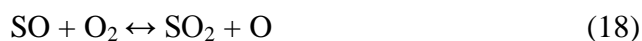
Once the radical pool is established, abstraction becomes as important as these initiation steps. The main difference between oxidation and pyrolysis, in the abstraction reactions, is the additional contribution to hydrogen abstraction by hydroxyl (OH) radicals and oxygen (O) atoms. Other differences involve termination reactions:



Under fuel-lean conditions, the abstraction reactions become especially important as there are high concentrations of hydroxyl radicals and oxygen atoms. Among these reactions, abstraction by hydroxyl radical is more important because of its known

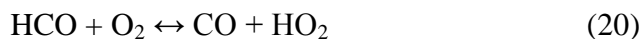
higher reactivity. Formation of H<sub>2</sub>O from the abstraction by OH radicals is expected, but attempts to quantify H<sub>2</sub>O in the gas samples have not been successful to date.  $\beta$ -scission of the radicals resulting from the initiation and abstraction reactions produces thioacetaldehyde, thioformaldehyde and ethylene (Reactions (10-12)). Alternatively, in the oxidative environment, the radicals can combine with O<sub>2</sub> to produce alkylthioperoxy, alkylperoxy or alkylthioalkylperoxy radicals, which can isomerize to form new products. Some of these new products can lead to chain branching. However, data from studies of the oxidation of a similar molecule, dimethyl ether, in a flow reactor [23] suggests that this route is not important in the temperature range studied here.

As in the pyrolytic case, the fate of the thioaldehydes involves a number of possible reactions. Under oxidative conditions, there is evidence of the importance of H abstraction: We can postulate a series of reactions, starting with H abstraction, that explain the approximately equal quantities of SO<sub>2</sub> and CO observed experimentally in all but the highest-temperature oxidative experiments. Specifically, as shown in Reaction (16) below [24] for thioformaldehyde, H abstraction forms the thioformyl radical (HCS). The subsequent reaction of the resulting thioformyl radical with molecular oxygen produces the formyl radical (HCO) along with sulfur monoxide (SO) (Reaction (17)), and rapid oxidation of unstable SO forms sulfur dioxide (SO<sub>2</sub>). SO<sub>2</sub> is observed experimentally (Figure 4.8).



The formyl radical is an unstable species. It undergoes unimolecular dissociation (Reaction (19)) and bimolecular reactions (Reactions (20-22)) [22].





Carbon monoxide was an important species observed at high levels during the oxidation experiments (Figure 4.6).

From the reaction routes above (Reactions (16-22)), approximately equal yields of carbon monoxide and sulfur dioxide are expected, which is consistent with experimental observations except at the highest temperature, as shown in Figures 4.6 and 4.8. At the highest temperature studied, CO is more abundant than SO<sub>2</sub>, probably because the creation of CO by other routes, for example from C<sub>2</sub>H<sub>4</sub>, C<sub>2</sub>H<sub>6</sub>, and CH<sub>2</sub>\*O, becomes important. Some oxidation of CO to form CO<sub>2</sub> is observed, but this process is slow under the present conditions, as can be seen from the low levels of CO<sub>2</sub> profiles in Figure 4.7.

Ethylene is the most abundant product observed in the oxidation experiments at the 630 °C, 670 °C and 700 °C operating temperatures, where ethylene concentration increased approximately linearly with the destruction efficiency. As shown in Figure 4.3, the presence of oxygen doubled ethylene levels from the values in the pyrolysis experiments at those temperatures, just as it doubled the destruction efficiency for ethyl methyl sulfide. In contrast, due to ethylene destruction reactions that become important at the 740 °C condition, ethylene levels no longer increase with the destruction of ethyl methyl sulfide at that temperature (Figure 4.3).

Destruction of ethylene and subsequent oxidation reactions follow well established pathways found in the hydrocarbon combustion kinetic literatures. An important reaction route for ethylene is the conversion to carbon monoxide via the reactions below [25]





Another destruction route for ethylene is H abstraction leading to vinyl radical, and subsequent  $\beta$ -scission producing acetylene [24], which was a minor species observed in both oxidative and pyrolytic experiments.



The last important species observed during the oxidation experiments is formaldehyde ( $\text{CH}_2^*\text{O}$ ), Figure 4.9. Like ethylene, its level increases with CCSC destruction efficiency at all but the highest temperature, where its profile exhibits a maximum. Well known combustion reactions [26] can explain  $\text{CH}_2^*\text{O}$  formation from  $\text{CH}_3$ , via  $\text{CH}_3\text{O}^*$ , as well as the destruction of  $\text{CH}_2^*\text{O}$  to form CO.

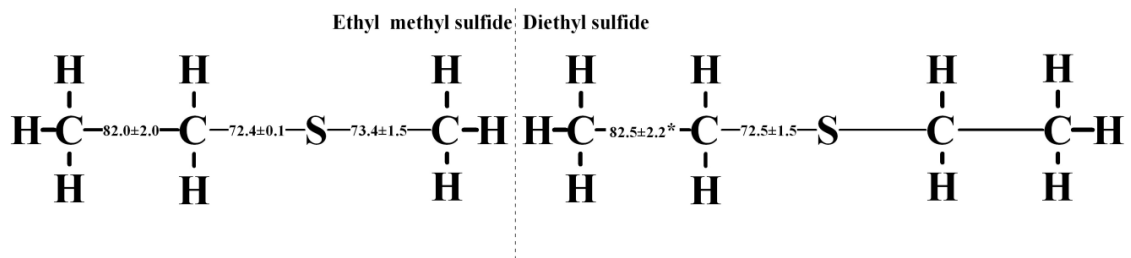


Figure 4.12 Bond dissociation energies (BDEs) (cal/mole) of C-S and C-C bonds in ethyl methyl sulfide and diethyl sulfide, the BDE of C-C bond of diethyl sulfide, which is marked with \*, is not available and adopted from ethylthiol ( $\text{CH}_3\text{-CH}_2\text{SH}$ ), all values are from Y.R. Luo, Handbook of bond dissociation energies in organic compounds, Boca Raton, Fla., CRC Press, c2003 [18].



## 4.5 CONCLUSIONS

The pyrolysis and oxidation of ethyl methyl sulfide were studied in a turbulent flow reactor under diluted conditions at four different operating temperatures. The primary stable products observed during both pyrolysis and oxidation experiments were ethylene, methane, and ethane. In addition to these species, carbon monoxide, carbon dioxide, sulfur dioxide, and formaldehyde were detected in the oxidation experiments. By analogy to pyrolysis of diethyl sulfide, initiation of destruction of ethyl methyl sulfide occurs via C-S cleavage, and abstraction reactions become important once the radical pool is established.  $\beta$ -scission of the resulting radicals forms ethylene, thioformaldehyde and thioacetaldehyde. Subsequent abstraction and  $\beta$ -scission reactions convert these species to formaldehyde, sulfur dioxide, carbon monoxide and carbon dioxide. Significantly slower rates of pyrolysis of ethyl methyl sulfide were observed than previously observed for diethyl sulfide; possible explanations for the different destruction efficiencies include lower hydrogen abstraction rates, and lower hydrogen atom production as a result of thermal decomposition pathways. Further investigations are needed to build kinetic data for the reactions, in particular the initiation and abstraction steps associated with the destruction of ethyl methyl sulfide, and the fate of thioaldehyde intermediates.

## 4.6 ACKNOWLEDGEMENT

The authors acknowledge the support of the U.S. Army Research Office under contract W911NF0410120 and through instrument grant DURIP W911NF0610142.

## REFERENCES

- [1] Y.C. Yang, Chem. Ind. 1 (1995) 334-337.
- [2] L.R. Ember, Chem. Eng. News 68 (33) (1990) 9-19.
- [3] Text of Chemical Weapons Convention, available at  
<http://www.opcw.org/chemical-weapons-convention/>.
- [4] Y.C. Yang, F.J. Berg, L.L. Szafraniec, W.T. Beaudry, C.A. Bunton, A. Kumar, J. Chem. Soc. Perkin Trans. 2 (1997) 607-613.
- [5] Y.C. Yang, J. A. Baker, J. Richard Ward, Chem. Rev. 92 (1992) 1729-1743.
- [6] A.V. Vorontsov, L. Davydov, E.P. Reddy, C. Lion, E.N. Savinov, P.G. Smirniotis, New J. Chem. 26 (2002) 732-744.
- [7] R.S. Davidson, J.E. Pratt, Tetrahedron Lett. 52 (1983) 5903-5906.
- [8] M.A. Y.S. Kim, A.A. Abdel-Wahab, M. Dulay, Catal. Lett. 5 (1990) 369-376.
- [9] D.V. Kozlov, A.V. Voronsov, P.G. Smirniotis, E.N. Savinov, Appl. Catal. B: Environ. 42 (2003) 77-87.
- [10] A.V. Vorontsov, C. Lion, E.N., P.G. Smirniotis, J. Catal. 220 (2003) 414-423.
- [11] J.F. Bunnett, Pure&Appl. Chem. 67(1995) 841-858.
- [12] J. Siegel, Bulletin of the Atomic Scientist 62 (2006) 24-25.
- [13] M.J. Bockelie, M.K. Denison, Engineering Design Software for Military Incinerators, Report No. DAAD19-01-C0050, U.S. Army Research Office.
- [14] C.J. Montgomery, M.J. Bockelie, A.F. Sarofim, J. Lee, J.W. Bozzelli, "Thermochemical Properties, Reaction Paths and Kinetic Mechanism for Sulfur-Chloro Hydrocarbon Combustion: Part I: Thermochemistry and Pyrolysis of Chlorosulfides," American Flame Research Committee International Symposium on Combustion, Livermore, CA, Oct. 16-17, 2003.
- [15] X. Zheng, E.M. Fisher, F.C. Gouldin, L. Zhu, and J.W. Bozzelli, Proc. Combust. Inst. 32(2009) 469-476.

- [16] E.J.P. Zegers, Flow Reactor Pyrolysis of Alkyl Phosphates and Phosphonates, Ph.D. Thesis, Cornell University, 1997.
- [17] W.S. Chin, B.W. Ek, C.Y. Mok, H.H. Huang, J. Chem. Soc. Perkin Trans. 2(1994) 883-889.
- [18] Y.R. Luo, Handbook of Bond Dissociation Energies in Organic Compounds, CRC Press, Boca Raton, Florida, USA, c2003.
- [19] B.S. Wang, H. Hou, L.M. Yoder, J.T. Muckerman, C. Fockenberg, J. Phys. Chem. A, 107 (2003) 11414-11426.
- [20] I.I. Zakharov, A.N. Startcov, O.V. Vorochina, A.V. Pachigreva, N.A. Chashkova, V.N. Parmon, Russian Journal of Physical Chemistry 80(2006) 1403-1410.
- [21] A.M. Dean, J. Phys. Chem. 89(1985)4600-4608.
- [22] D.L. Baulch, C.J. Cobos, R.A Cox, C. Esser, P. Frank, Th. Just, J.A. Kerr, M.J. Pilling, J. Troe, R.W. Walker, J. Warnatz, J. Phys. Chem. Ref. Data, 21 (1992) 411-429.
- [23] S.L. Fischer, F.L. Dryer, H.J. Curran, International Journal of Chemical Kinetics, 32(2000) 713-740.
- [24] I. Barnes, K. H. Becker, I. Patroescu, Atmospheric Environment, 30 (1996), 1805-1814.
- [25] Y. Hidaka, T. Nishimori, K. Sato, Y. Henmi, R. Okuda, K. Inami, T. Higashihara, Combustion and Flame 117(1999) 755-776.
- [26] W. Tsang, R.F. Hampson, J. Phys. Chem. Ref. Data, 15 (1986) 1087-1279.

## **APPENDIX A**

### **EXPERIMENTAL APPARATUS AND METHODOLOGY**

#### **A.1 OVERVIEW**

The reaction kinetics of sulfur mustard simulants, diethyl sulfide ( $\text{CH}_3\text{CH}_2\text{-S-CH}_2\text{CH}_3$ , abbreviation CCSCC) and ethyl methyl sulfide ( $\text{CH}_3\text{CH}_2\text{-S-CH}_3$ , abbreviation CCSC), were experimentally studied at high temperatures under highly diluted conditions. The experiments were conducted in an atmospheric pressure, turbulent flow reactor with a Reynolds number of approximately 5000, at four different operating temperatures between 630 °C and 740 °C. These experiments, with an initial loading of sulfur mustard simulants of 150 or 100 ppm, involved either a nitrogen carrier gas for pyrolysis experiments or a nitrogen-oxygen carrier gas (with composition producing an equivalence ratio of approximate 0.1 or 1) for oxidation experiments. On-line, extractive sampling in conjunction with analysis by fourier transform infra-red (FT-IR) spectroscopy and gas chromatography/mass spectrometry (GC/MS) was performed to quantify species composition in the turbulent flow reactor. Details of the flow reactor, gas sampling system, experimental conditions, and analytical methods are documented in the following sections.

#### **A.2 FLOW REACTOR**

The flow reactor used to conduct experimental studies is shown in Figure A.1. This flow reactor has been used to perform the experimental pyrolysis of the organophosphorus compounds [1]. Its ability to produce chemical data was previously validated by performing experiments with two compounds for which the thermal decomposition kinetics are well established: isopropyl acetate and t-butyl acetate [1]. As shown in Figure A.1, the main carrier gas was a turbulent flow of preheated nitrogen

into which a secondary flow doped with sulfur mustard simulants was injected. The two flows mixed and reacted along the length of a constant-diameter reaction section. Samples were extracted at four specific positions along the centerline of the reaction section. After the reaction section, the bulk of the reactor flow was diluted by cool air, purified by carbon filters to remove odor, and vented to the atmosphere. In the following sections, the flow feed system and reaction section are described in great detail.

### **A.2.1 FLOW FEED SYSTEM**

Two vacuum flasks, each with 350 psi relief pressure and 180 L in volume, were used to provide liquid nitrogen for a typical 8-hour experiment. Liquid nitrogen left the flasks, through two parallel flexible, 4 ft long, stainless steel cryogenics hoses (MVE Cryogenics), flowed to a Swagelok® cross incorporating a relief valve (350 psi). After the cross, the vaporizing liquid nitrogen was led by a 3 ft long, 1/2" OD stainless steel line to a free standing vaporizer (MVE Cryogenics). The gaseous nitrogen exited the vaporizer and flowed through a heating line, 32" long and 1/2" OD stainless steel tubing wrapped with heating tapes. Through the heating line, the gas temperature was raised to a level compatible with proper operation of mass flow controllers or meters. The flow then passed a pressure regulator (Matheson Tri-Gas model 3476) set to provide nitrogen at a pressure of about 80 psi. For the pyrolysis experiments and the oxidation experiments with approximate stoichiometric composition, the nitrogen flow was split to two sub flows, a main flow and a secondary flow. For the oxidation experiments with an equivalence ratio of 0.1, the whole nitrogen flow was supplied as the main flow. Under these fuel lean conditions, the secondary flow was supplied by on-site compressed air in the laboratory. The main flow rate was manually controlled by using a valve and monitored with a flow meter (Porter model 114AFASVEAA) with a range of 0-1000 slpm. The secondary flow was metered by a mass flow controller (Sierra model

840D-M-1-V1) with a range of 0-20 slpm. The volumetric rates of these two flows (at standard conditions of 1 atm, 21 °C) are listed in Tables A.1-4, for each operating condition. Downstream of its flow meter, the main flow was directed to a preheater. Downstream of its flow controller, the secondary flow was led to a section of liquid injection. More details on the main flow and secondary flow are described in the following.

#### **A.2.1.1 MAIN FLOW**

The main flow, carrying approximate 95% mass of the reactor flow, went into a, 45” long and 4.5” OD, stainless steel retort (Mellen model ROHE-421-COE), which was sitting inside a split tubular furnace (Mellen model 2-621-HP). The furnace was controlled by an electric controller (Mellen model PS305-240-70-E94) gaining feedback from an Omega® K type thermocouple installed on the outer wall of the retort in the furnace.

Leaving the retort, the preheated main flow proceeded through an elbow. The flow structure was unknown at the outlet of the elbow. In order to obtain a well defined flow, a development section, 1 m long and 52.5 mm ID stainless steel pipe, was installed at the downstream of the elbow. This 1 m long development section allowed the velocity profile of the main flow to attain its fully developed shape. Two pairs of clam shell heaters (Watlow Electric) surrounded the development section to maintain the gas temperature.

Downstream of the development section, the injection of the secondary flow into the main flow occurred through four open-ended 4 mm ID and 6 mm OD quartz tubes, held in place by Cajon® fittings with Viton® O-rings (Figure A.2). These fittings were welded to four pieces of small flanges which were aligned with counterparts on the ends of equally spaced wells mounted on the injectors. Copper gaskets were employed to seal

connections. The secondary flow was a mixture. Its composition varied with experimental conditions. The details are described in the next section.

#### **A.2.1.2 SECONDARY FLOW**

As mentioned in the previous section, the secondary flow (Figure A.3) was split from the nitrogen flow out of the vaporizer or was on-site compressed air. When compressed air was used, it was purified by a FT-IR purge gas generator (Whatman model 75-51) to remove CO<sub>2</sub> and moisture. After being metered by the mass flow controller, the secondary flow passed through a polyethylene line (1/4" OD) to reach a heating section, a 50 cm long and 1/4" OD stainless steel line wrapped with heating tapes. Through the heating section, the gas temperature of the secondary flow was increased to 100-130 °C before reaching an injection port, where sulfur mustard simulants were injected into the secondary flow. The heated secondary flow helped with vaporizing the injected simulants, which are liquid at room temperature. The power of the heating tapes was controlled by a variac. The flow temperature was measured by using an Omega® K type thermocouple at a position of about 2 cm upstream of the injection port.

The injection port consisted of a 1/4" OD Swagelok® stainless steel tee and a 1/4" OD stainless steel adapter (Swagelok® to Cajon®). The liquid was injected through a septum by using a syringe pump (Harvard Apparatus variable speed model PHD2000 with 1% uncertainty) along with a 100 ml syringe (Hamilton Gastight® model 1100). The injection rates were such as to yield the loadings either 150 ppm or 100 ppm (Tables A.1-4) in the reaction section. The low loadings have the benefit of minimizing the occurrence of high order reactions as well as reducing product emission, which was critical for the experiments of sulfur containing compounds with a strong irritative odor.

After the injection port, the secondary flow was directed to a Swagelok® tee where

it mixed with another flow in the pyrolysis experiments and in the oxidation experiments with approximate stoichiometric composition. For the pyrolysis experiments, this additional flow was  $5 \pm 0.25$  % CO diluted in  $N_2$ . CO was included in the mixture because it was used as a tracer to determine mixing conditions in the reaction section as well as dilution in the sampling system. For the oxidation experiments with approximate stoichiometric composition, the flow was  $21 \pm 0.2$  %  $O_2$  balanced by  $N_2$ . No tracer was used in the oxidation experiments, in which the mixing conditions were assumed to be the same as those in the pyrolysis experiments having the same flow rates and heater settings. Both  $CO/N_2$  and  $O_2/N_2$  mixtures were provided in pressurized cylinders, certified products from Airgas East. The additional flow passed a pressure regulator and then metered by a rotameter (Matheson Tri-gas model 608) incorporating a pressure gauge. For safety issues, a solenoid valve (Omega® model SV3309) was installed to shut off CO flow automatically in the case of accidental power outages. In general, the rate of the additional flow was such as to yield approximately 67 ppm CO loading (Tables A.1-2) for the pyrolysis experiments or approximately 750 ppm  $O_2$  loading (Table A.3) for the oxidation experiments with approximately stoichiometric composition in the reaction section. For the oxidation experiments with an equivalence ratio of approximately 0.1, no additional flow was added to the secondary flow after the injection port, and the corresponding well-mixed  $O_2$  loading was approximately 9000 ppm in the reaction section (Tables A.3 and 4).

Leaving the tee, the secondary flow passed through a length of 1/8" ID Sulfinert® tubing, specially coated to minimize the loss of sulfur containing compounds, and into a residence chamber, 1 gallon in volume (Micro Filtration Systems). The residence chamber was installed in order to damp out oscillations in the chemical loadings [1]. Out of the chamber, the secondary flow was guided to the injectors (Figure A.2) through 4 m of Sulfinert® tubing. In order to confirm the chemical stabilities of the simulants in



the secondary flow, a few samples were taken at the inlet of the injectors, and no reaction was found by capillary GC/MS analysis.

#### **A.2.1.3 REACTION SECTION**

The two flows, main flow and secondary flow, mixed and flowed along the length of a 1 m long, 45 mm ID and 48 mm OD quartz liner (Technical Glass Products), sitting inside a 1 m long and 52.5 mm ID and 60.3 mm OD, stainless steel pipe, shown in Figure A.4. The quartz liner was held at the radial position by two rings made of porous, flexible ceramic insulation. On the downstream end, a stainless steel collar prevented the quartz liner from slipping past the stainless steel pipe. The ceramic rings and collar minimized flow through the gap between the quartz liner and stainless steel pipe. The stainless steel pipe was surrounded by five pairs of ceramic clamshell heaters (Watlow model VS103J07XC) to maintain the gas temperature at a fixed value. The quartz liner had four holes aligned with the sampling ports. These sampling ports were made of 3/8" ID stainless steel tubing with 1/4" Cajon fitting welded to the end, and were positioned on the bottom of the stainless steel pipe. Sampling probes were inserted through the ports to extract gas samples on the centerline of the reaction section.

After the reaction section, the effluent flow passed a cross tee to a dilution section. A 1/2" ID port on one end of the tee allowed thermocouples to be inserted axially into the reaction section to measure gas temperatures on the centerline of the reaction section. The effluent was diluted with cool air, purified by carbon filters and then drawn out of the building by a fan on the building roof. The ventilation rates were such as to keep the pressure inside the reactor approximately 5 torr below the ambient pressure. Subatmospheric pressures would prevent harmful organic sulfur containing compounds from leaking out of the reactor if leaks occurred.

The 4.5 cm diameter of the reaction section along with the total flow rates of around

370 slpm (Tables A.1-4) were significantly higher, when compared to those of the reactors usually used in laboratories. Smaller diameters of the reaction section would lessen the amount of reactants required to perform the experiments. However, for studies in destruction of the sulfur mustard simulants in gas phase, using the reaction section of large diameter, corresponding to a low surface to volume ratio, has the benefit of minimizing the significance of surface reactions.

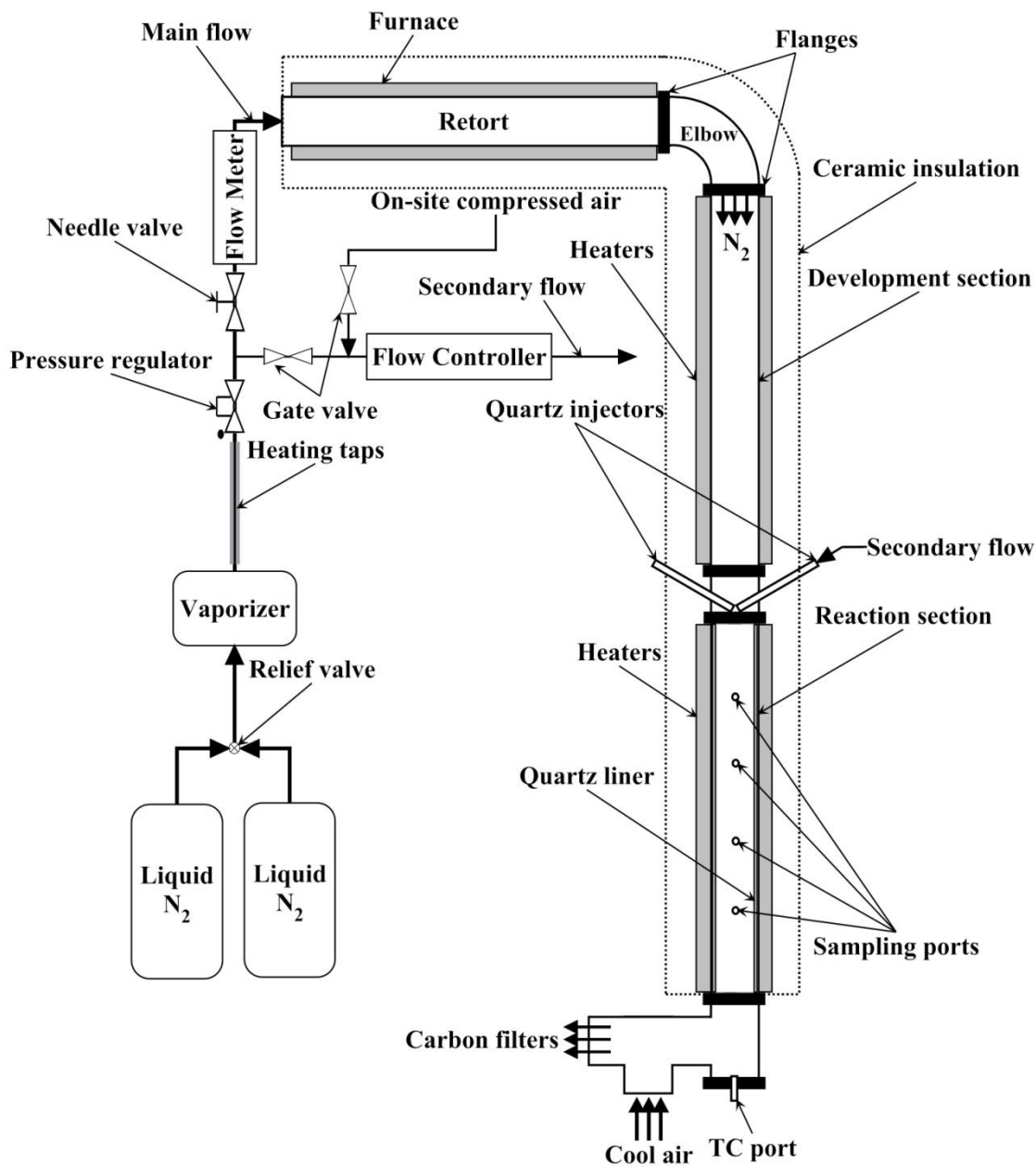


Figure A.1 Flow reactor, flow feed system and main flow.

Table A.1 Flow parameters of pyrolysis experiments of diethyl sulfide.

Nominal T ( $^{\circ}\text{C}$ )	Main flow (slpm)	Secondary flow (slpm)	Velocity (m/s)	$\text{Re}_D$	CO loading (ppm)	CCSCC loading (ppm)
630	330	14.1	11.12	5020	68.6	150
670	341	15.3	12.02	5060	66.3	150
700	347	16.0	12.64	5060	65.1	150
740	350	16.8	13.30	4990	64.4	150

Table A.2 Flow parameters of pyrolysis experiments of ethyl methyl sulfide.

Nominal T ( $^{\circ}\text{C}$ )	Main flow (slpm)	Secondary flow (slpm)	Velocity (m/s)	$\text{Re}_D$	CO loading (ppm)	CCSC loading (ppm)
630	330	14.1	11.12	5020	68.6	150
670	341	15.3	12.02	5060	66.3	150
700	347	16.0	12.64	5060	65.1	150
740	350	16.8	13.30	4990	64.4	150

Table A.3 Flow parameters of oxidation experiments of diethyl sulfide.

Nominal T ( °C)	Main flow (slpm)	Secondary flow (slpm)	Velocity (m/s)	Re <sub>D</sub>	O <sub>2</sub> loading (ppm)	CCSCC loading (ppm)
630	330	14.1	11.12	5020	730	100
630	330	14.1	11.12	5020	9321	100
670	341	15.3	12.02	5060	704	100
670	341	15.3	12.02	5060	9270	100
700	347	16.0	12.64	5060	720	100
700	347	16.0	12.64	5060	9366	100
740	350	16.8	13.30	4990	710	100
740	350	16.8	13.30	4990	9472	100

Table A.4 Flow parameters of oxidation experiments of ethyl methyl sulfide

Nominal T ( °C)	Main flow (slpm)	Secondary flow (slpm)	Velocity (m/s)	Re <sub>D</sub>	O <sub>2</sub> loading (ppm)	CCSC loading (ppm)
630	330	14.1	11.12	5020	9321	150
670	341	15.3	12.02	5060	9270	150
700	347	16.0	12.64	5060	9366	150
740	350	16.8	13.30	4990	9472	150

Note: The loading uncertainties are approximately 4% and 3.3% for the CCSC and O<sub>2</sub> respectively.

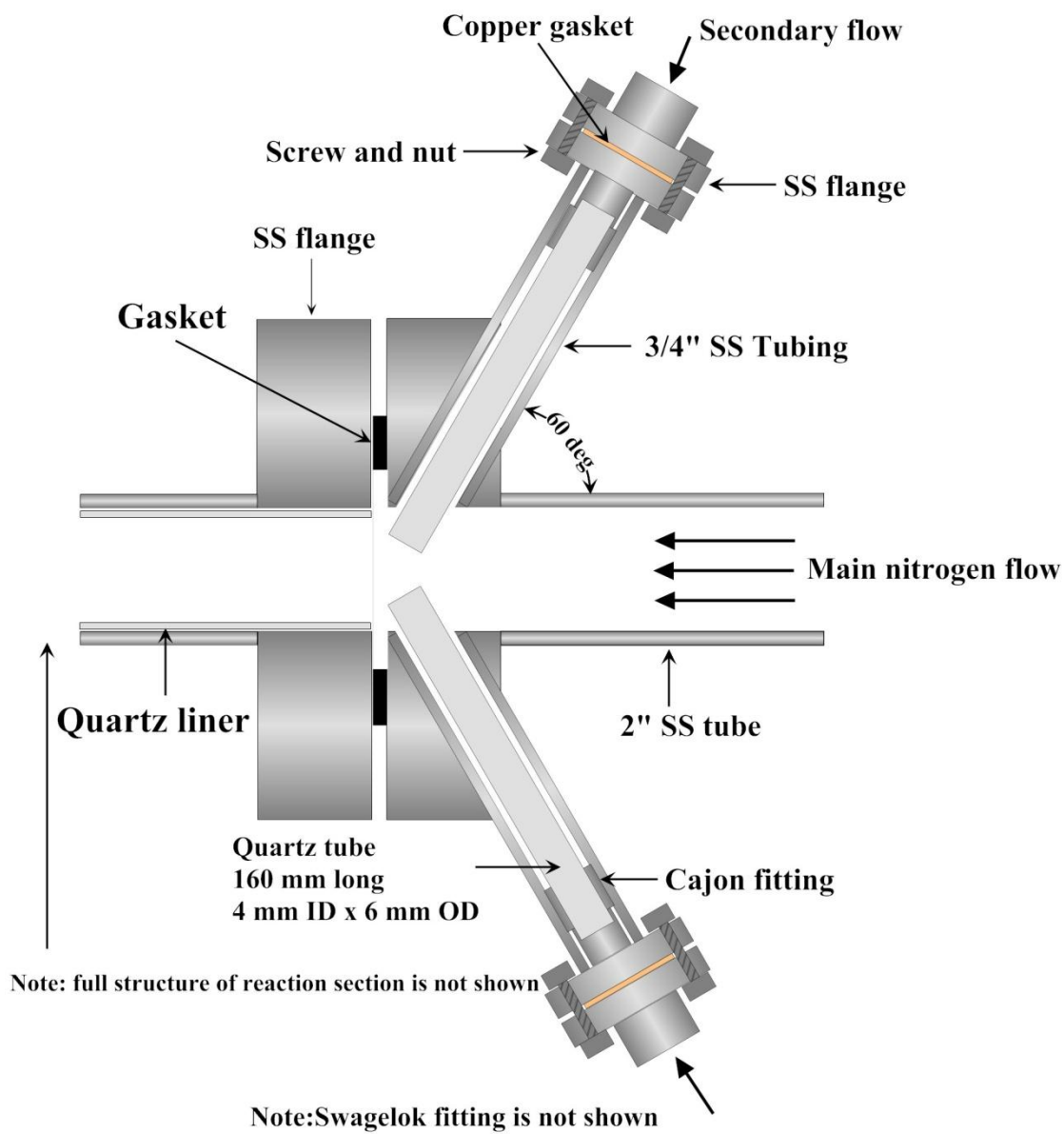


Figure A.2 Injectors.

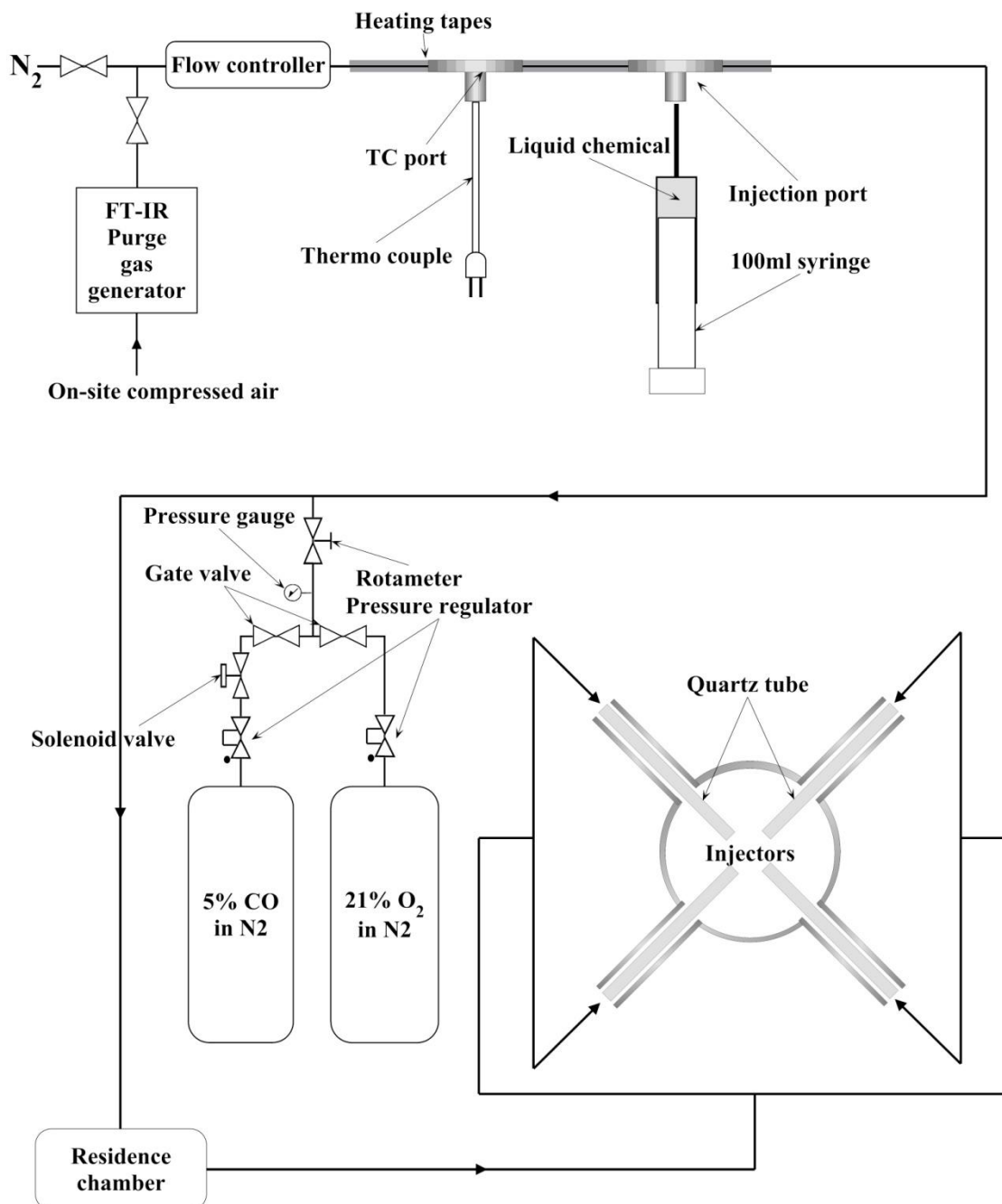
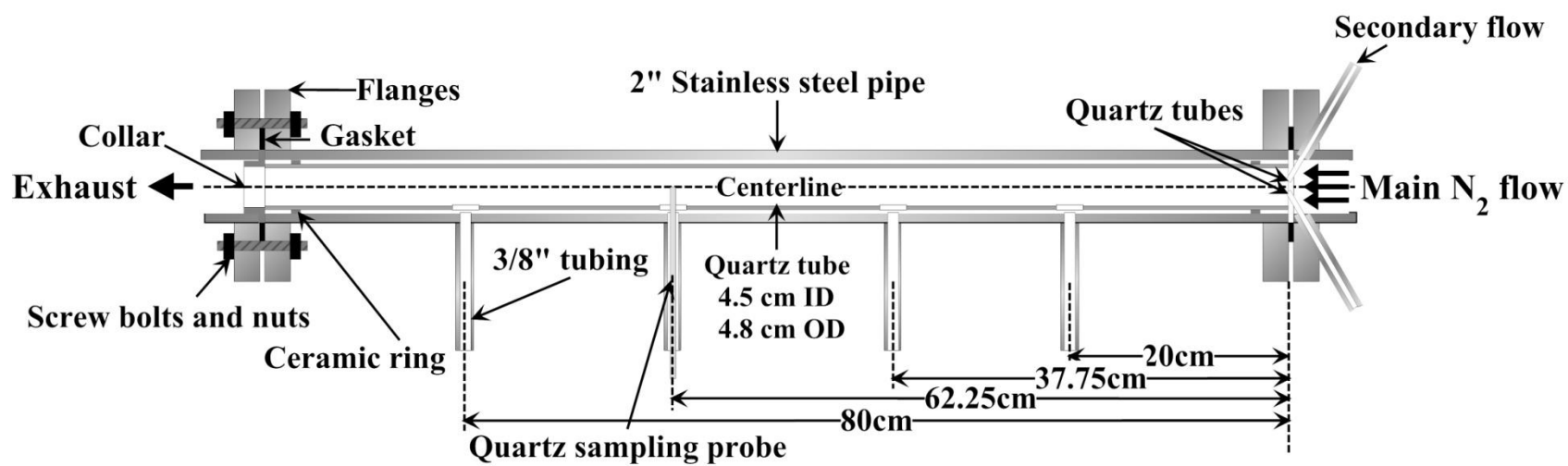


Figure A.3 Secondary flow.



Note: full structures of sampling ports and sampling probes are not shown.

Figure A.4 Reaction section.



### A.2.2 SAMPLING SYSTEM

As shown in Figure A.4, gas samples were extracted at four specific positions along the center line of the reaction section, by using open-ended quartz probes inserted through the sampling ports on the bottom of the reaction section. The quartz probe (Figure A.5) was a piece of “T” shape junction, fabricated by the Cornell Glass Shop, consisting of two concentric quartz tubes. In order to quench reactions in gas samples, cool nitrogen, with the flowrate approximately equal to the sample flowrate, was injected at a position of 15 mm below the sample intake. Injection closer to the probe opening would be desirable to quench reactions more quickly, but the loss of the dilution nitrogen to the reaction section would reduce the quenching performances if the dilution injection was too close to the sample intake. The injection position of 15 mm from the probe opening was determined on the basis of Zegers’ investigations [1]; it was the shortest distance without loss of the dilution nitrogen. Duplicated experiments were conducted and the results were consistent with the previous data. The resulting temperatures of the diluted gas samples were calculated to be below 370 °C, at which no reaction was predicted by the kinetic modeling. In addition, dilution of the gas samples prevented Viton® O-rings, inside the Cajon® fitting of the sampling ports, from melting. Deterioration of seal function of the Viton® O-rings was observed when no dilution was employed. However, one drawback of the sample dilution was the decrease of the species concentrations in the gas samples, approximately half of those in the reaction section, resulting in reduced measurement signals. To compensate, some experiments were attempted with higher simulant loadings than reported here, but those experiments had to be discontinued because the higher simulant levels produced complaints about the unpleasant odor of the product emissions from the building ventilation exhaust.

Out of the sampling probes, diluted samples flowed through Teflon® transfer lines

to instruments for composition analysis. Two analytical techniques, FT-IR and GC/MS, were used in the experiments. For the FT-IR, the gas samples entered a 10 L gas cell (Figure A.6). During the sampling period, the cell pressure was set at  $700 \pm 1$  torr, corresponding to a sampling rate of about 4.3 slpm, to keep the gas samples continuously flushing the cell for 7 minutes, which displaced gas contents of the cell about 3 times in term of volume. However, the continuous flush was found to be not very effective in removing the residue of the previous samples from Zegers' experiments [1]. An emptying-filling action, venting the cell to 50 torr and consequently filling it with pure nitrogen to approximately 900 torr, was performed three times, through which the residue was left no more than 0.017% in terms of volume, before the continuous sample flush started. For the GC/MS, the diluted sample entered a gas sampling valve with a 500  $\mu$ l loop made of stainless steel from Valco (Figure A.7). The valve body, the sample loop, and the transfer line from the valve to the GC/MS injection port were Sulfinert® treated. The 500- $\mu$ l sampling loop, which had an outer diameter of 1/16", greatly restricted the sample flowrate. In order to obtain a reasonable sample flowrate through the probes, a bypass tee was installed upstream of the loop. In addition, the tiny volume of the loop (500  $\mu$ l) posed repeatability problems, because the mixture composition at the sampling position varied over the short timescale corresponding to that sample loop size. A Sulfinert® treated residence chamber, approximately 200 cm<sup>3</sup> in volume, was installed upstream of the bypass tee, allowing the sample composition to be averaged over a longer time period. This resulted in improved measurement repeatability. Needle valves were used to maintain gas pressures at the outlets of both the loop and residence chamber at fixed values ( $675 \pm 1$  Torr and  $400 \pm 1$  Torr at upstream and downstream of the loop respectively), leading to a constant sampling flow rate and an equal amount of sample for each injection. The pressures were selected so as to obtain a sampling rate same as that of the FT-IR. Having the same sampling rates

resulted in the same dilution ratio and mixing conditions between the FT-IR and GC/MS. And thus the mixing data from the FT-IR measurements could be used to correct the GC/MS measurements, as the CO tracer was not detectable by the GC/MS analysis method implemented in the experiments. The valve body and loop were maintained at 100 °C to minimize condensation of the gas samples. The sample loop was conditioned by continuously flushing with gas samples for 4 minutes before each injection.

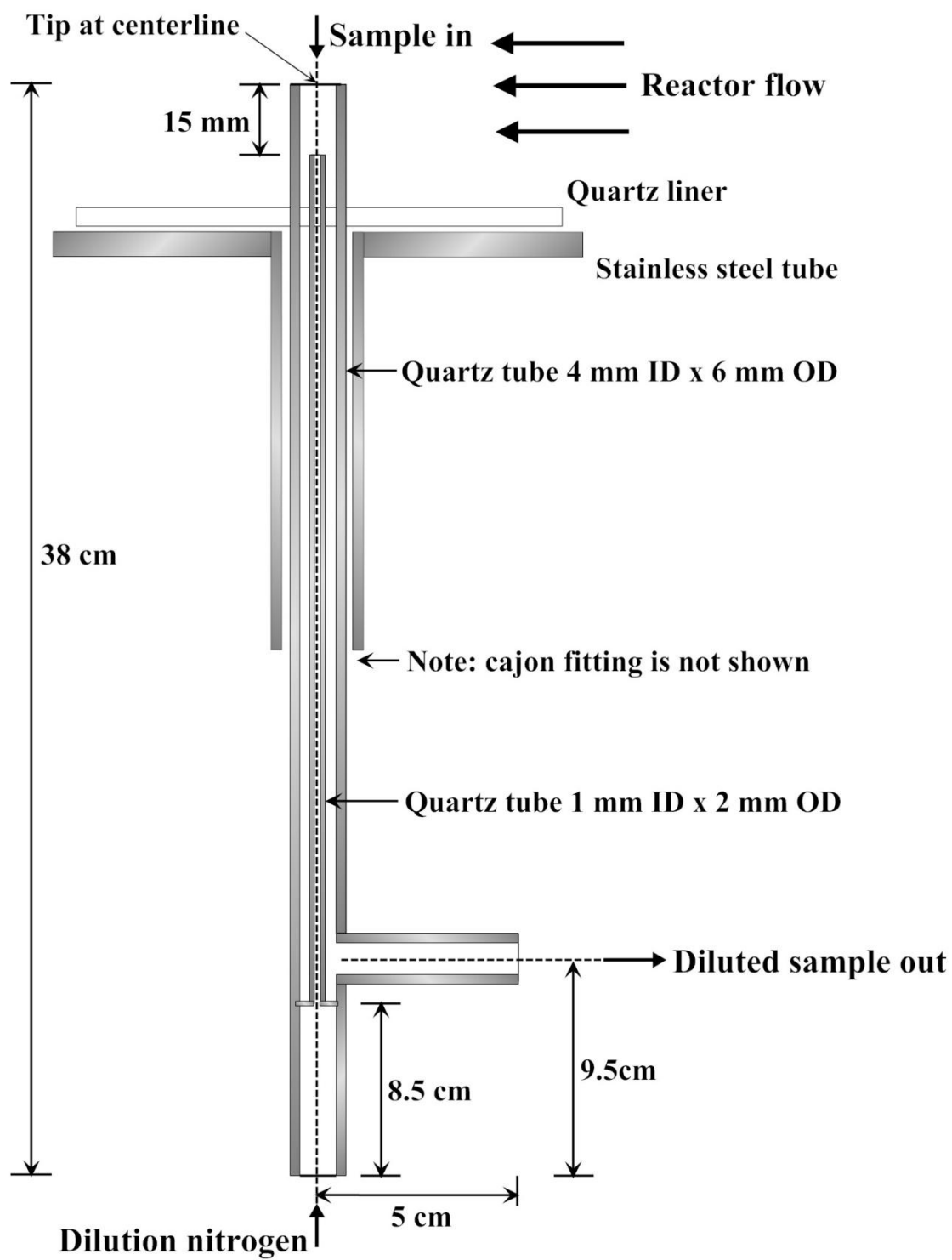


Figure A.5 Sampling probe.

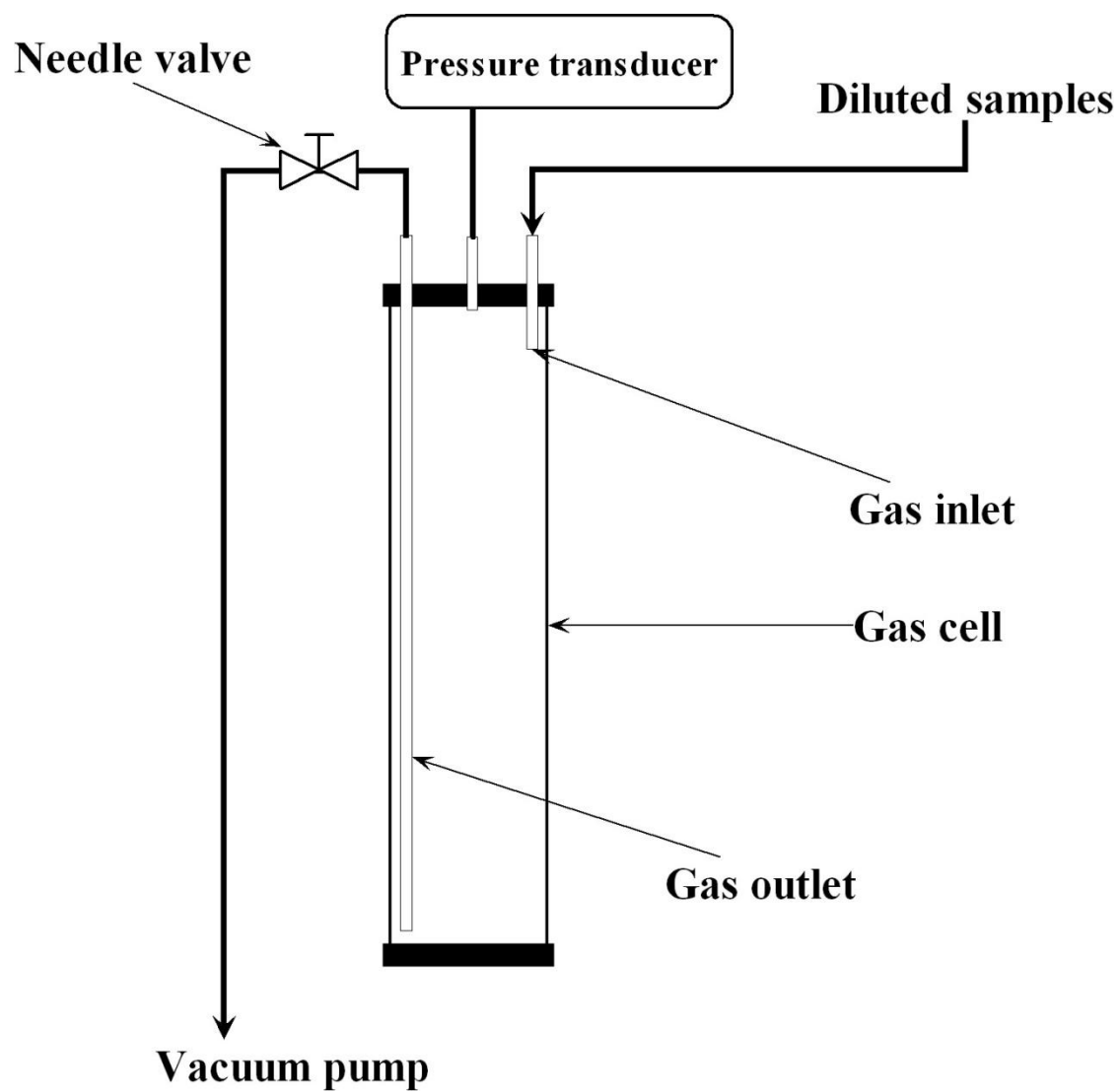


Figure A.6 Sampling system for FT-IR.

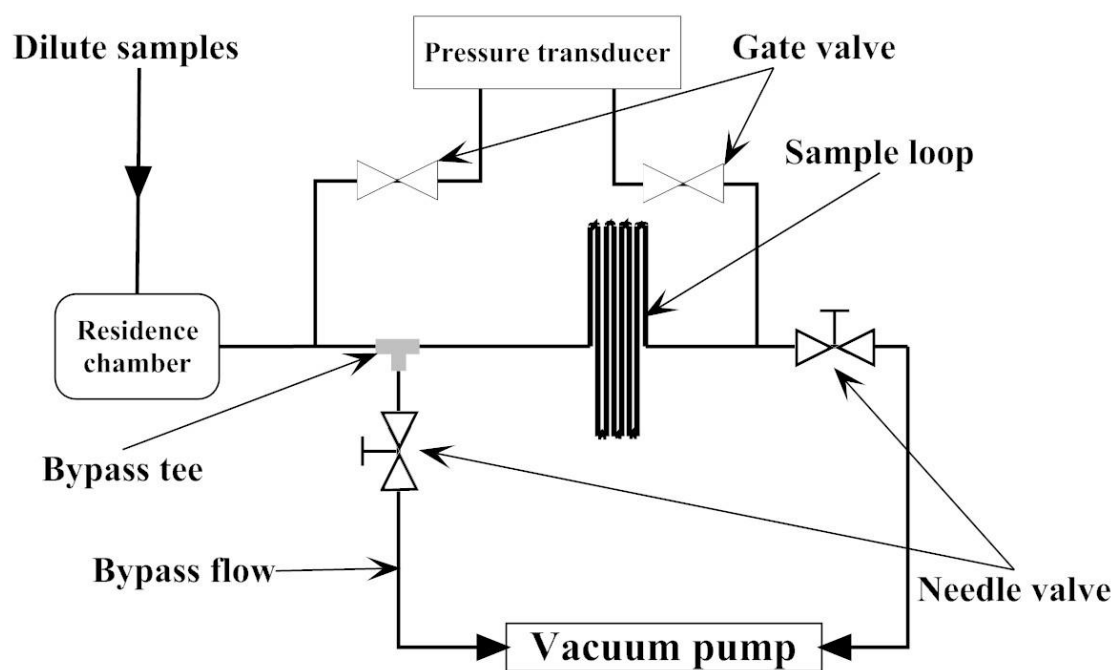


Figure A.7 Sampling system for GC/MS.

### **A.3 FLOW CONDITIONS IN THE REACTION SECTION**

Understanding flow conditions is essential for the interpretation of the resulting data from the flow reactor experiments. From the previous sections, it is known that experiments were conducted at four different operating temperatures involving a nitrogen carrier flow and a nitrogen-oxygen carrier flow corresponding to pyrolysis and oxidation respectively, and detailed flow rates and chemical loadings are shown in Tables A.1-4 at each operating temperature. As shown in the tables, the operating temperature is designated by a temperature value, e.g. 630 °C, 670 °C, 700 °C and 740 °C, which is the mean temperature in the sampling region, rounded to the nearest 10 °C. In these tables, chemical loadings are calculated by assuming radial homogeneity in the reaction section. The actual mixing conditions at the sampling location were determined by using CO as a tracer. Measured CO concentrations normalized by CO loadings were used for the correction on the species concentrations to account the mixing effects. In the following sections, measurements of the gas temperature and mixing condition in the reaction section as well as air leak rates into the reactor will be described.

#### **A.3.1 GAS TEMPERATURES**

Gas temperatures were measured with operating conditions the same as in the actual pyrolysis and oxidation experiments, but without injection of sulfur mustard simulants. However, under the highly diluted conditions reported here, temperature changes due to reactions can be neglected.

The centerline gas temperatures were measured at 18 positions at 5 cm intervals by using an Omega K type 1/4" stainless steel sheathed thermocouple. An alignment device (Figure A.8) was installed to keep the thermocouple on the centerline. As shown in Figure A.9, in the sampling region, from the first sampling port to the fourth sampling

port corresponding to the region of 20-80 cm downstream of the injectors, gas temperatures vary by approximately  $\pm 10$  °C around a mean value, which is the value rounded to the nearest 10 to designate the operating temperature. The gas temperature at the positions of the sampling ports is typically low, as shown in Figure A.9, because there is no heater covering in those regions. Upstream of the first sampling port, there is a region of low temperature (typically reaching 80 °C below the mean temperature) where the cold secondary flow mixes into the preheated main flow. Repeated measurements were performed several months after the measurements of the temperature profiles reported here at two operating temperatures; the results were within the measurement uncertainty (1%) of the original ones.

A radial temperature profile was measured at the position of the second sampling port at the 700 °C operating temperature by using an Omega® type K 1/8" thermocouple inserted through the sampling port. As shown in Figure A.10, the gas temperatures were very similar at 11 radial positions, which indicate radial homogeneity in temperature by the second sampling port.

### **A.3.2 MIXING CONDITIONS**

In the pyrolysis experiments, CO was added to the secondary flow as a tracer to determine the mixing conditions in the reaction section as well as in the sampling system. CO's inertness was investigated experimentally at the operating temperature 700 °C. As shown in Figure A.11, where measured CO concentrations normalized by CO loadings and dilution ratio are plotted, CO concentrations were not affected by the presence of either CCSCC or CCSC. Both kinetic and equilibrium calculations also showed that CO reactions could be neglected in the studied experimental conditions.

The flow was turbulent with a Reynolds number of approximately 5000 as shown in Tables A.1-4. These Reynolds numbers were calculated on basis of the volumetric flow



rates and mean centerline gas temperatures. Under such turbulent conditions, the secondary flow was expected to quickly mix the main flow, to obtain radial homogeneity in gas composition in the reaction section. Figure A.12 shows normalized CO concentrations for the pyrolysis experiments. At the position of the second sampling port, 37.75 cm downstream of the injectors, normalized CO concentrations reach a value close to one, indicating radial homogeneity by the second sampling port. Upstream of the second sampling port, there is an induction region, where the mixing process was under way to form the radial homogeneity. Increasing the flow rates, resulting increased turbulent levels based on the Reynolds number, may help with reducing the length of the induction region. However, increasing flow rates significantly was not practical, both because of the large quantities of reactants required and because, with a fixed flow reactor length, they would have reduced flow reactor residence times below the values desired for destruction of the sulfur mustard simulants at the studied operating temperatures.

### **A.3.3 LEAK TEST ON THE FLOW REACTOR**

The flow reactor was assembled from parts connected by flanges (schedule 40, nominal 2”), welded to the ends of the parts, and standard stainless steel hex-nuts and bolts. Graphite 304 stainless steel gaskets for standard 2” pipe flanges were used to seal connections between the flanges. The whole flow reactor, which had clamshell heaters except at the flange and sampling port locations, was supported at the flanges by steel cradles and wrapped by fiber ceramic insulation to reduce the heat loss to the environment.

A leak test was made to check the sealing performance of the assembly. During the test, the flow reactor was disconnected from the flow feed system and ventilation system. The flow reactor was sealed at the both ends by using caps and valves. Only two

sampling ports on the reaction section were left open, one was connected to a pressure transducer (MKS Baratron model 122AA-01000AB) and the other was to a vacuum pump (Edwards Model 3). The connection between the flow reactor and the pump was controlled by a gate valve. At the beginning of the test, the gate valve was open to evacuate the flow reactor to a low pressure, and then was closed.

The reactor pressure was recorded as a function of time in Figure A.13. The ambient atmosphere was recorded as 728 torr and the ambient temperature was 16 °C when this leak test was conducted. Since the pressure inside the flow reactor was maintained at approximately 5 torr lower than the ambient atmosphere when the reactor was hooked to the ventilation system under the actual experimental conditions, the slope of the pressure vs time curve at  $p = 723$  torr, where the test condition was similar as the actual condition, was used to estimate the leak rate into the reactor.

The internal volume of the flow reactor was estimated to 7.7 liters, which was the total volume of the parts involved in the leak test, e.g. retort, elbow, development section, injectors and reaction section. The 7.7 liters was slightly higher than the actual volume as volumes of items such as the quartz liner were not considered in the calculation. The rate of pressure increase was about 0.5 torr/min, was got from the data on right end of the plot and thus the leak rate was calculated to be 0.0048 l/min based on the idea gas law. Therefore the oxygen background due to leaks, 2.8 ppm, was estimated in the typically 370 slpm reacting flow. Kinetic calculations showed that such low levels of O<sub>2</sub> present had no effect on the destruction of the studied sulfides.

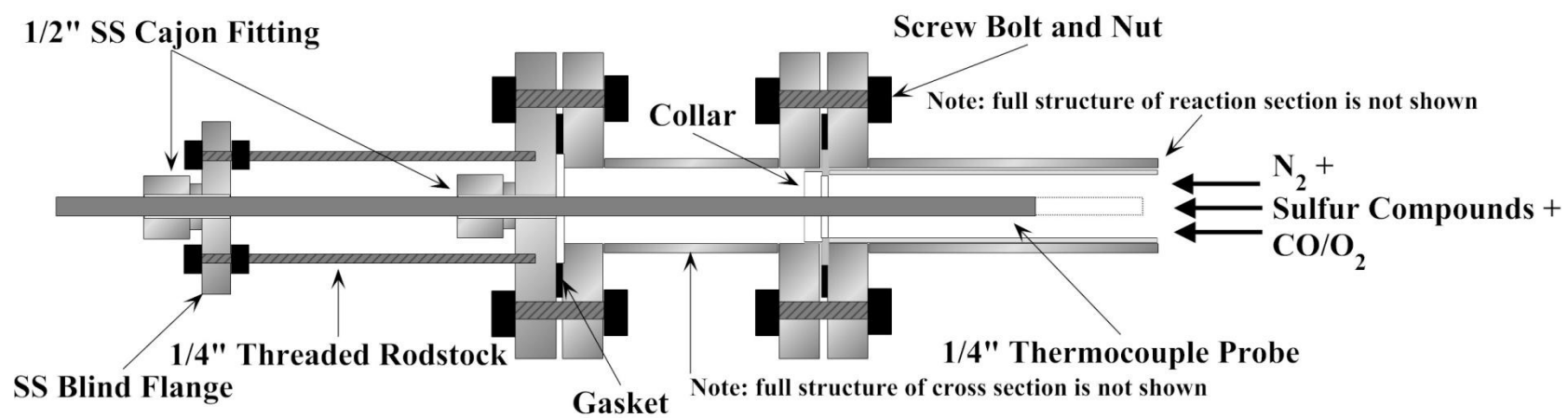


Figure A.8 Axial alignment device.

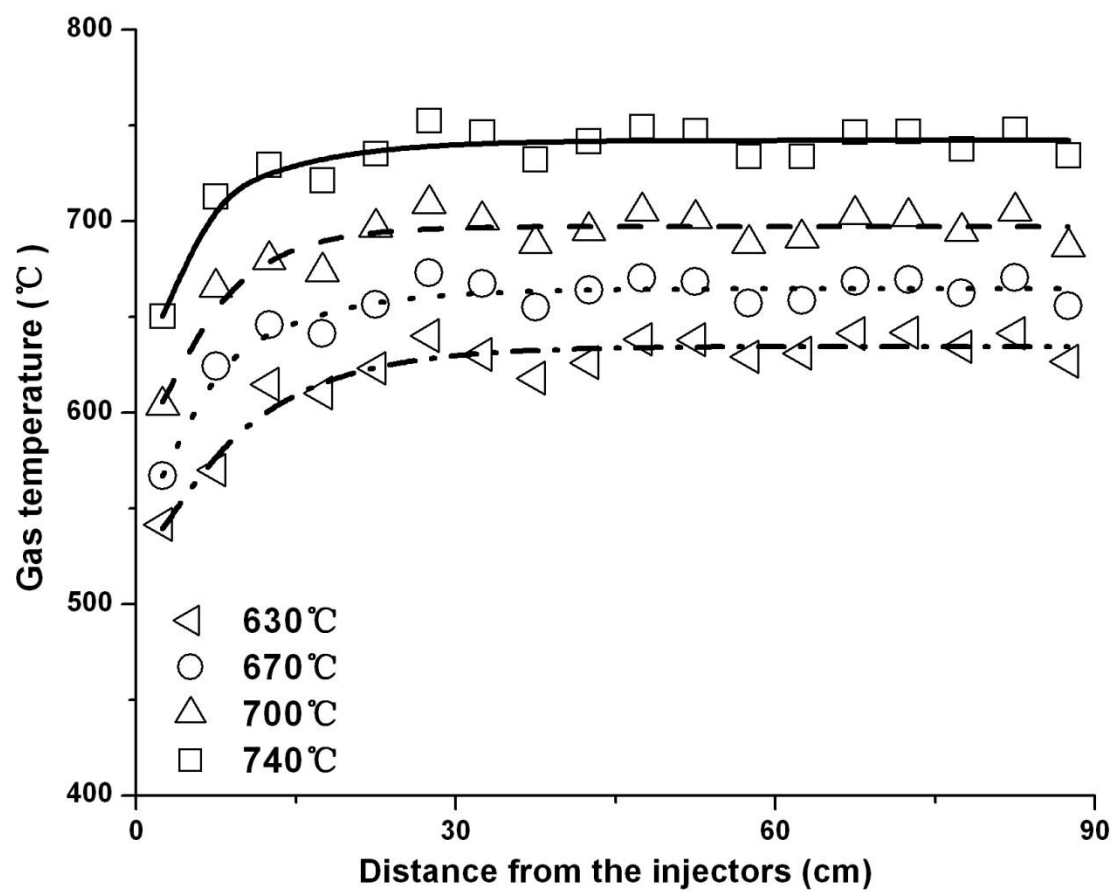


Figure A.9 Gas temperatures on the centerline of the reaction section, symbols represent the experimental measurements and lines are polynomial fits to the measurements.

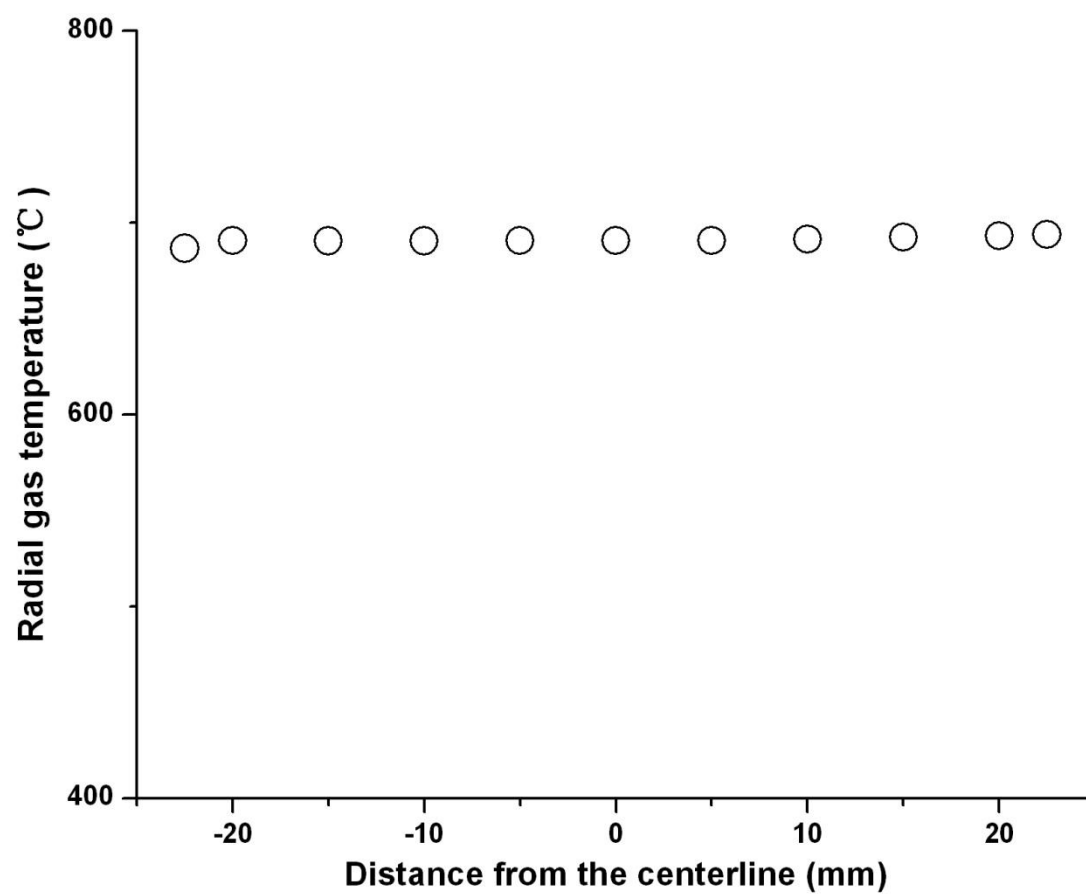


Figure A.10 Gas temperatures at the position of the second sampling port in the reaction section at the 700 °C operating temperature.

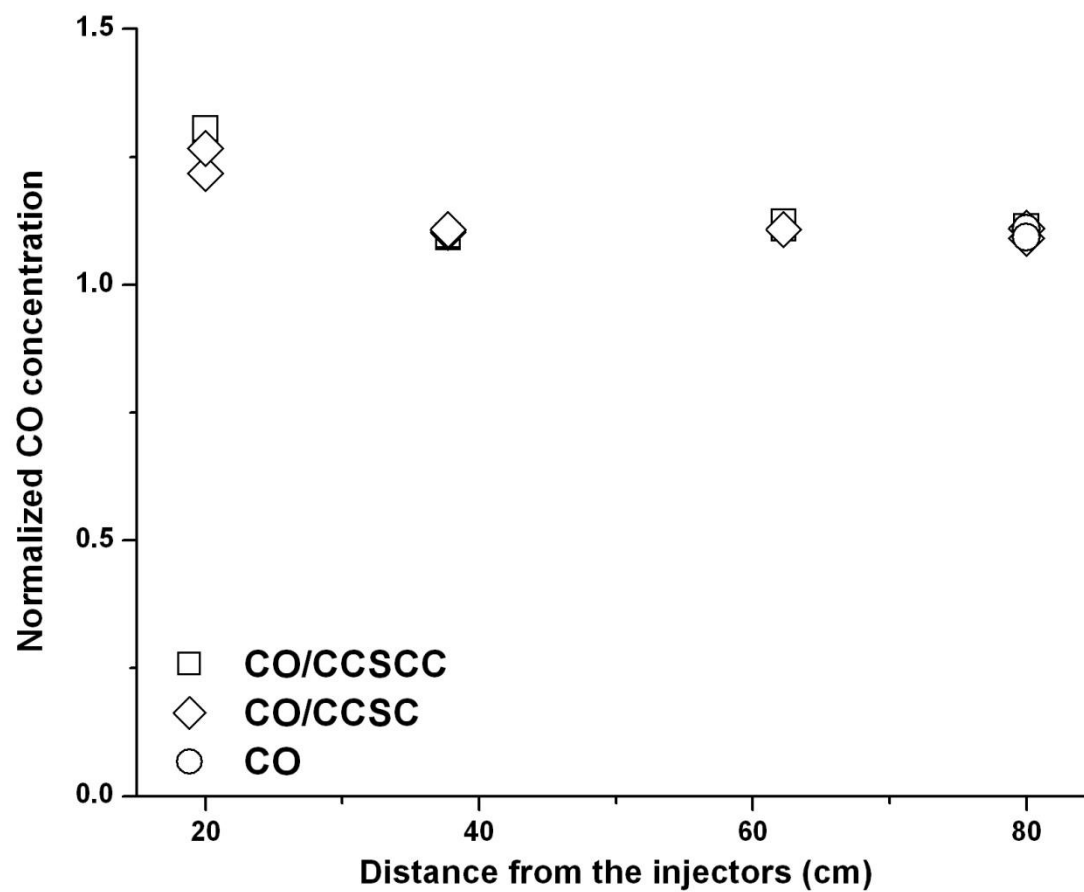


Figure A.11 Normalized CO concentrations with or without presence of CCSCC/CCSC.

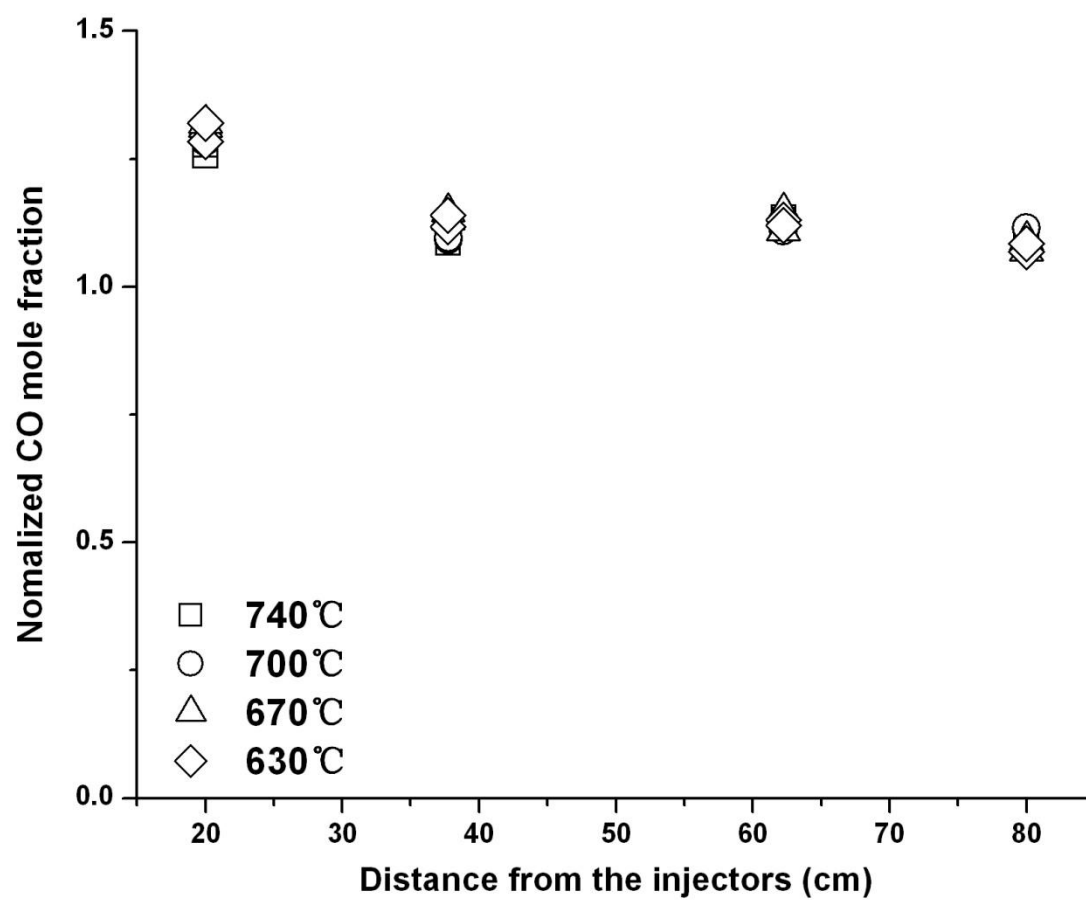


Figure A.12 Normalized CO concentrations.

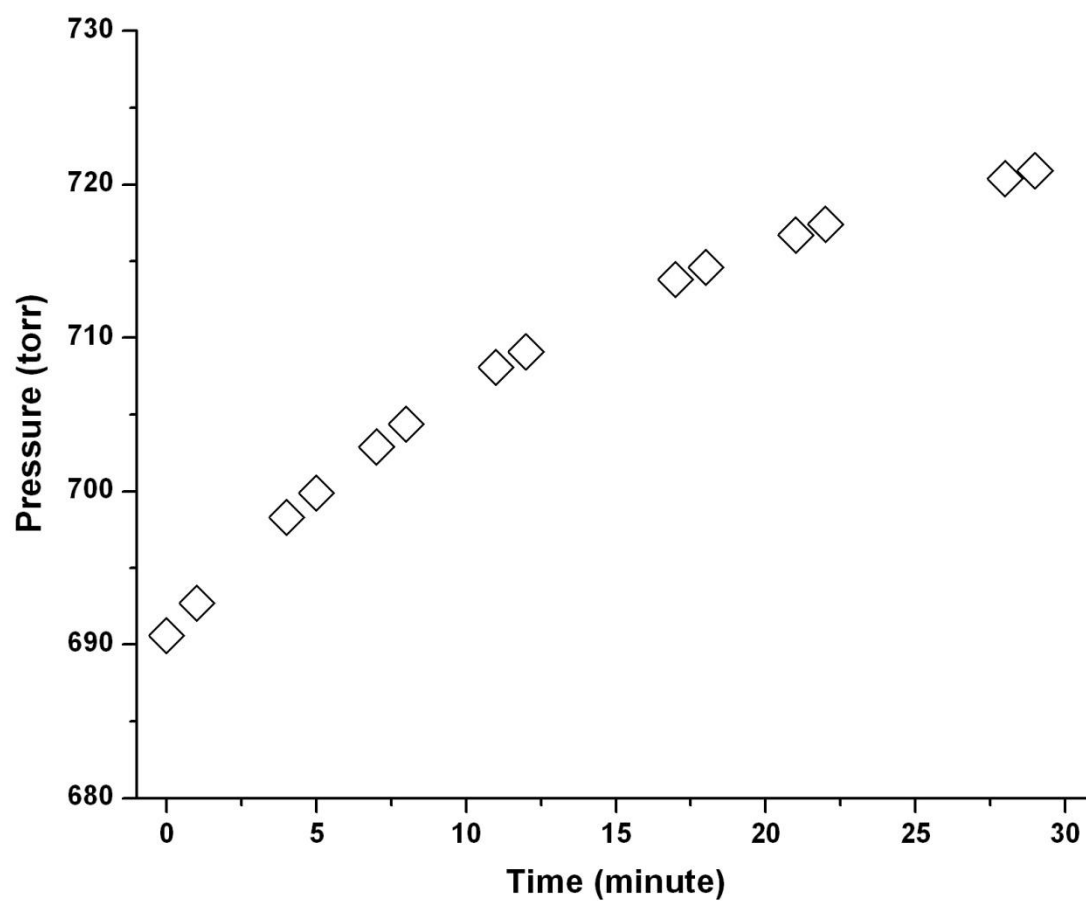


Figure A.13 Reactor pressure in the leak test.



## **A.4 ANALYSIS METHODS**

Fourier transform infra-red spectroscopy (FT-IR) and gas chromatography/mass spectrometry (GC/MS) were the principal techniques employed for composition analysis.

### **A.4.1 Fourier-transform infrared spectroscopy**

A Nicolet 6700 single beam spectrometer from Thermo Scientific was employed, in conjunction with a MCT-B detector. The analysis of the gas samples were conducted at room temperature in a gas cell with a volume of 10 liters and an optical path length of 6 m (Infrared Analysis). The gas cell was equipped with KBr windows (25 mm diameter and 4 mm thick) and glass mirrors with antireflection coating. The whole spectrometer was purged by using purified air to reduce background moisture and carbon dioxide. The purified air was supplied by an on-site compressor incorporating with the FT-IR purge gas generator (Whatman 75-51). For a few runs, nitrogen was used to purge the spectrometer, and no reduction on the background species were observed when compared to the purified air.

The spectrometer settings were such that 196 scans were averaged in a time of 13 minutes. The obtained single beam spectra were at a resolution of  $1/4\text{ cm}^{-1}$  with a scan range of  $400\text{--}4000\text{ cm}^{-1}$ . For composition identification and quantification, the spectra were ratioed against a background spectrum to produce absorbance spectra. The background spectrum was collected with the gas cell filled with nitrogen from the vacuum flasks. The background spectrum was obtained at the beginning of each experiment as well as about every two hours during the experimental run. Each sample single beam spectrum was converted to absorbance spectrum using the background spectrum obtained closest in time.

Species identification was conducted by comparing the sample spectra with the

reference spectra of interest. The reference spectra were produced by using the same instrument, same scan method, and in the same condition. In general, only the species, of which the absorption features in the whole scan range were coincident with those of the reference spectra, were considered to be positively identified. However, this standard was not practical for the identification of the species at trace levels or for species whose absorption features overlapped with those of the major species. Interactive subtractions between the sample spectra and the reference spectra of the major species were performed to help with finding the absorption features of these minor species. Noise in the subtracted spectra results in a deterioration in the quality of the residual spectra. Therefore, these minor species, even though their features in the sample spectra were not exactly the same as those of the reference spectra, were considered to be identified through personal judgment.

The amount of an identified species present in gas samples was determined by computerized spectral subtraction. First, for the species of interest, a set of spectra, usually 3-5 spectra, with known concentrations were collected. Among the spectra, one was chosen as the standard reference spectrum, which was used to subtract other spectra in the data set to calculate subtraction factors. The resulting subtraction factors were correlated with the known species concentrations. Application of simple linear regression on the data generated calibration curves. Figures A.14-22 show the calibration data as well as the curves for the species detected at high levels in the experiments; see Chapters 2-4. The species concentrations in the gas samples were calibrated through curve fitting. It has to be mentioned that, unlike the identification, the subtractions were not operated over the whole region of the spectra, only the region where the absorption features were significant as well as non/little overlap was included in the subtractions. Table A.5 lists the chemicals used for calibration samples, along with purity of each.

For the liquid chemicals at room temperature, e.g. CCSCC, CCSC and CH<sub>2</sub>\*O, calibration samples were made by using the secondary flow system (Figure A.3). The injection rate of the chemicals was varied to make the calibration samples at different concentrations. The flow rate was 16 slpm, which was similar to the flow rates of the secondary flow in the experiments. The flow was split through a tee before flowing into the reactor. About 25% of the sample flow was led to the gas cell. The flushing and filling procedure is the same as for the pyrolysis and oxidation experiments already reported.

For the species which are gaseous at room temperature, they were extracted by using a syringe through a gas release line from the pressurized cylinders. The syringe gas was given one minute to reach equilibrium with the ambient atmosphere. The ambient pressure and temperature were measured for the calculation of the species mass in the syringe. The gas cell was pumped down to a low pressure. The calibration gas was injected through a port equipped on the top of the gas cell. After the injection, nitrogen was added to the cell to bring the pressure back to 700 torr. Before the spectrum collection, 5-7 minutes were given for the species gas to mix the dilution nitrogen to produce a homogeneous composition in the cell.

#### **A.4.2 GAS CHROMATOGRAPHY-MASS SPECTROMETRY**

As described in the section of sampling system, gas injection into the GC/MS was through a pressure actuated 6-port valve with a 500 µl sample loop. A Thermo Scientific Ultra Trace GC/DSQ II MSD was used for the analysis, with ionization achieved by electron impact. The capillary column used was a J&W Scientific Gaspro® column (30 m long and 0.32 mm ID). The operating conditions were: injection port temperature 200 °C; interface temperature 260 °C; column oven temperature, 80 °C for 6 minutes, ramped at 15 °C/min to 260 °C with a 4 minute hold at 260 °C; helium carrier gas 1.9

ml/min. The injector was operated in the splitless mode for 3 minutes after the injection of the gas samples. It is known that the experiments were conducted under highly diluted conditions and thus approximately 99% of the sample was nitrogen. In order to avoid nitrogen saturation, the mass detector was operated in the off mode for 4 minutes after the injection. Therefore, species eluting in this period could not be detected by the mass detector.

In the experiments, the first sample was extracted from the last sampling port, where species abundances were the highest in the four sampling ports. This first sample was analyzed in full scan mode of the mass spectrometer. The resulting data was used to determine the products formed and the corresponding elution time. Species identification was conducted by searching the NIST mass spectral database. From the second sample, the analysis was performed in a mixed mode, in which the parent compounds were still analyzed in full scan mode, while the products were analyzed in SIM mode with three characteristic ions for each product. Analysis in SIM mode enhanced the signal/noise ratio and thus helped with detecting the products at trace levels, but was not desirable for the more abundant parent compound.

The species amount present in the gas samples was determined on basis of the molecule ion abundance. For the species detected, calibration data were collected. The technique of calibration sample preparation for the GC/MS was the same as that for the FT-IR. The details were documented in the previous section and thus are not repeated here. The measured ion abundances were correlated with the known species concentrations. Application of simple linear regression on the data generated calibration curves. The species concentrations in the gas samples were also calibrated through curve fitting. Figures A.23-24 shows the calibration data and corresponding calibration curves for the detected species. Due to early elution of hydrocarbons and other light molecules, only a few sulfur containing compounds were detected by the GC/MS when

compared to those detected by the FT-IR.

The measured ion abundance for a given amount of compound was affected by the status of the mass spectrometer, e.g. ionization efficiency and detector sensitivity. In order to determine the spectrometer status, a certain amount of acetone was injected into the GC/MS for analysis before other analyses were conducted. The acetone ion abundance before each experimental runs was compared to that measured on the day of the calibration data collection. A maximum variation was observed at about 20%. The resulting ratio was used to correct the calibrated species concentrations to account for the effects of the spectrometer operation.

Table A.5 Chemicals for calibration data collection

Chemical name	Formula	Purity	Manufacturer
Diethyl sulfide	$\text{CH}_3\text{CH}_2\text{SCH}_2\text{CH}_3$	99%	Fluka
Ethyl methyl sulfide	$\text{CH}_3\text{CH}_2\text{SCH}_3$	99%	Fluka
Carbon disulfide	$\text{CS}_2$	99%	Aldrich
Thiophene	Cyc- $\text{C}_4\text{H}_4\text{S}$	99%	Aldrich
Carbon monoxide	$\text{CO}$	5%	Airgas
Carbon dioxide	$\text{CO}_2$	5%	Airgas
Formaldehyde	$\text{CH}_2\text{O}$	97%	Aldrich
Sulfur dioxide	$\text{SO}_2$	1%	Airgas
Ethylene	$\text{C}_2\text{H}_4$	99%	Airgas
Methane	$\text{CH}_4$	99%	Airgas
Ethane	$\text{C}_2\text{H}_6$	Chemically pure	GT&S
Acetylene	$\text{C}_2\text{H}_2$	99%	Smith

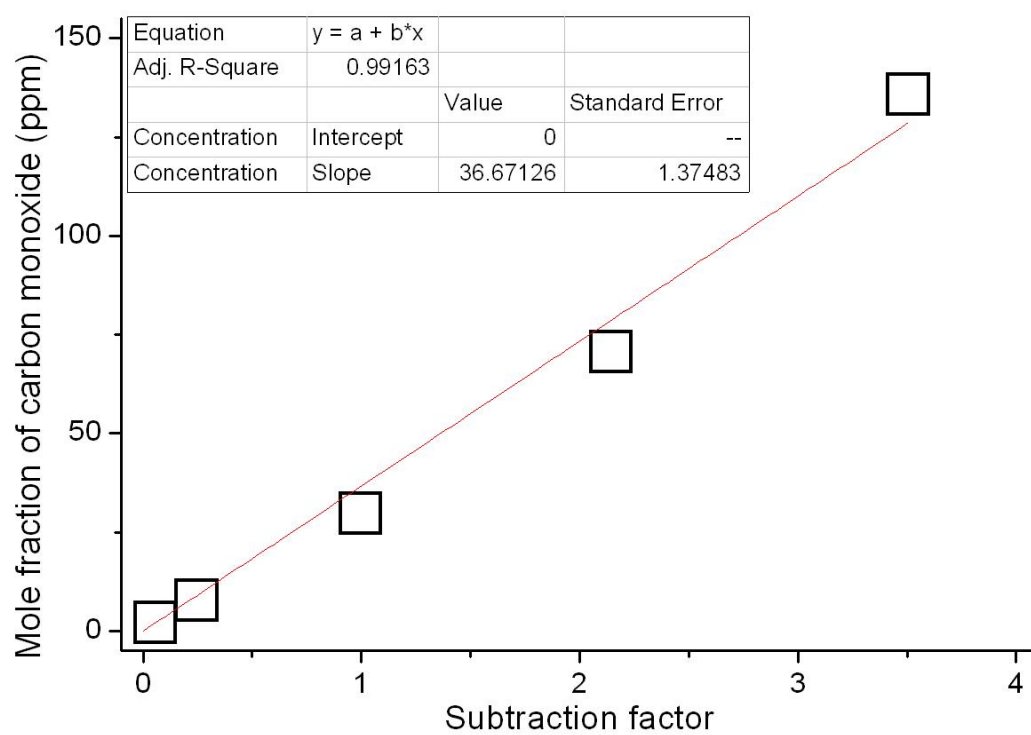


Figure A.14 Carbon monoxide calibration data and curve (FT-IR)  
(Wavenumber 2250-2040  $\text{cm}^{-1}$ )

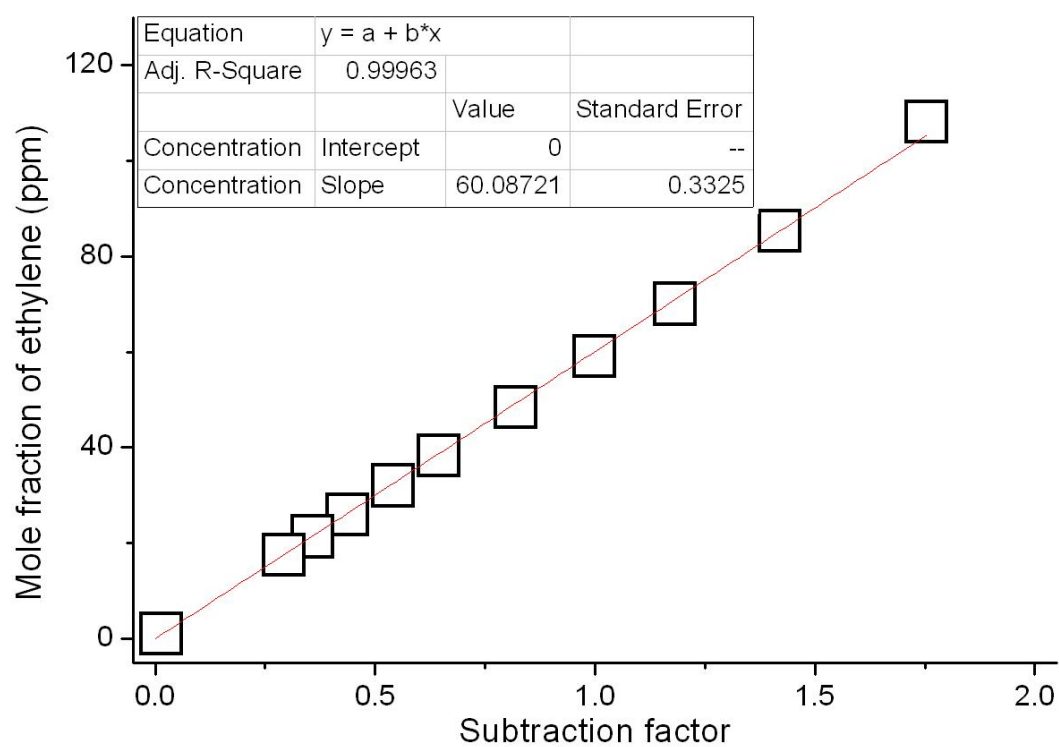


Figure A.15 Ethylene calibration data and curve (FT-IR)  
(Wavenumber 1030-870  $\text{cm}^{-1}$ )



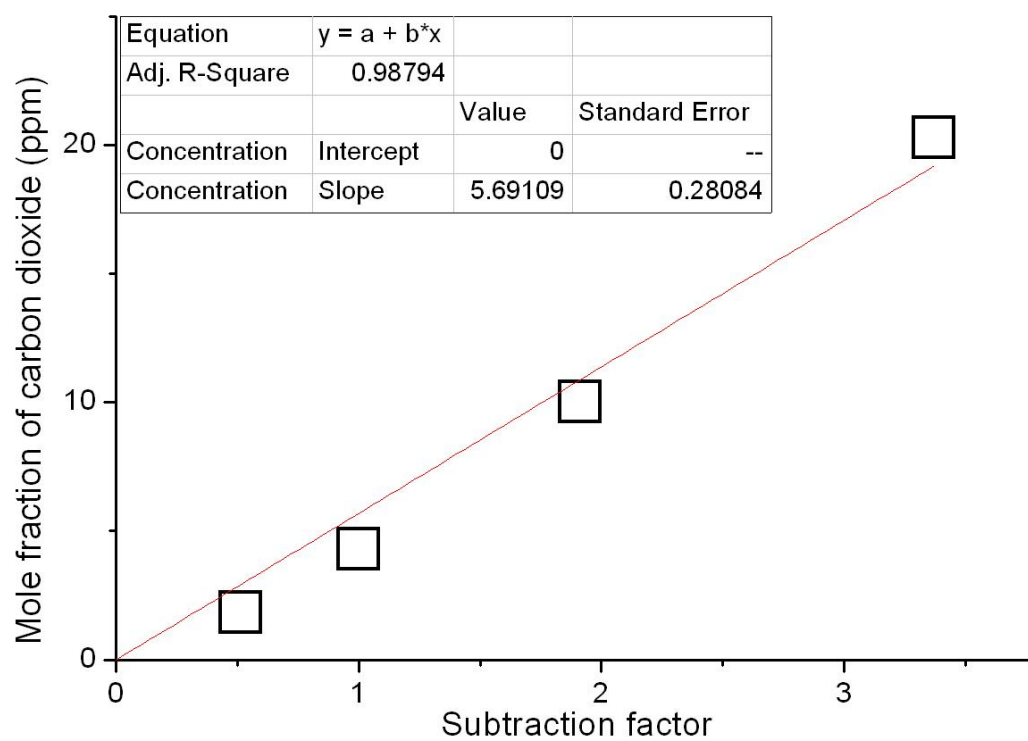


Figure A.16 Carbon dioxide calibration data and curve (FT-IR)  
(Wavenumber 2390-2290  $\text{cm}^{-1}$ )

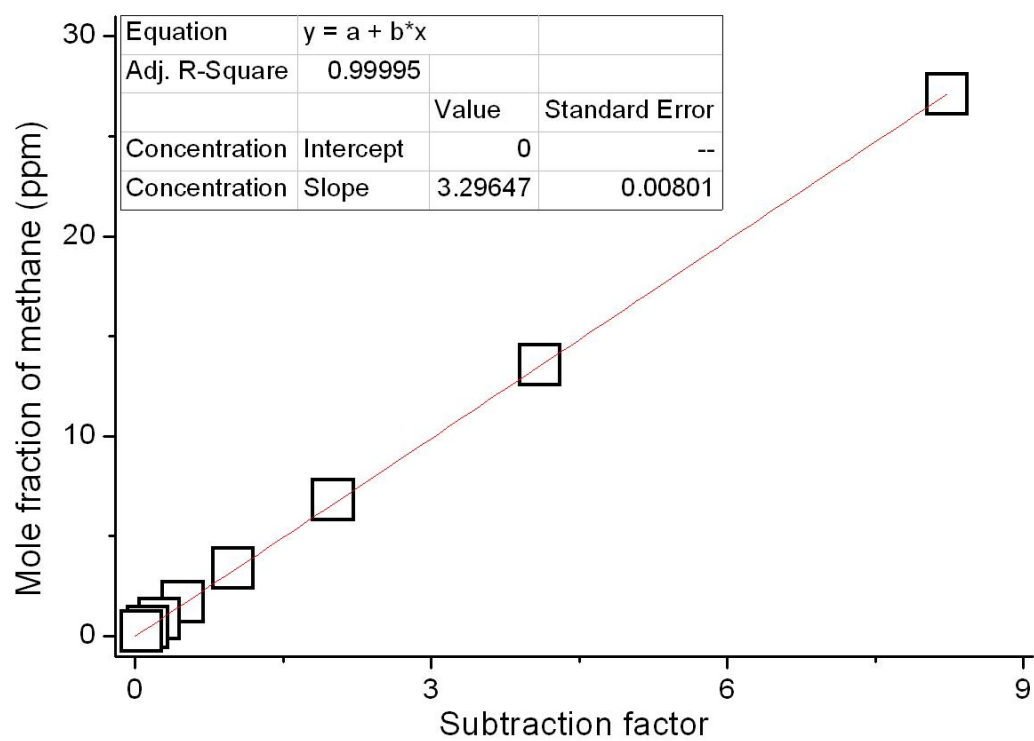


Figure A.17 Methane calibration data and curve (FT-IR)  
(Wavenumber 3190-2850  $\text{cm}^{-1}$ )

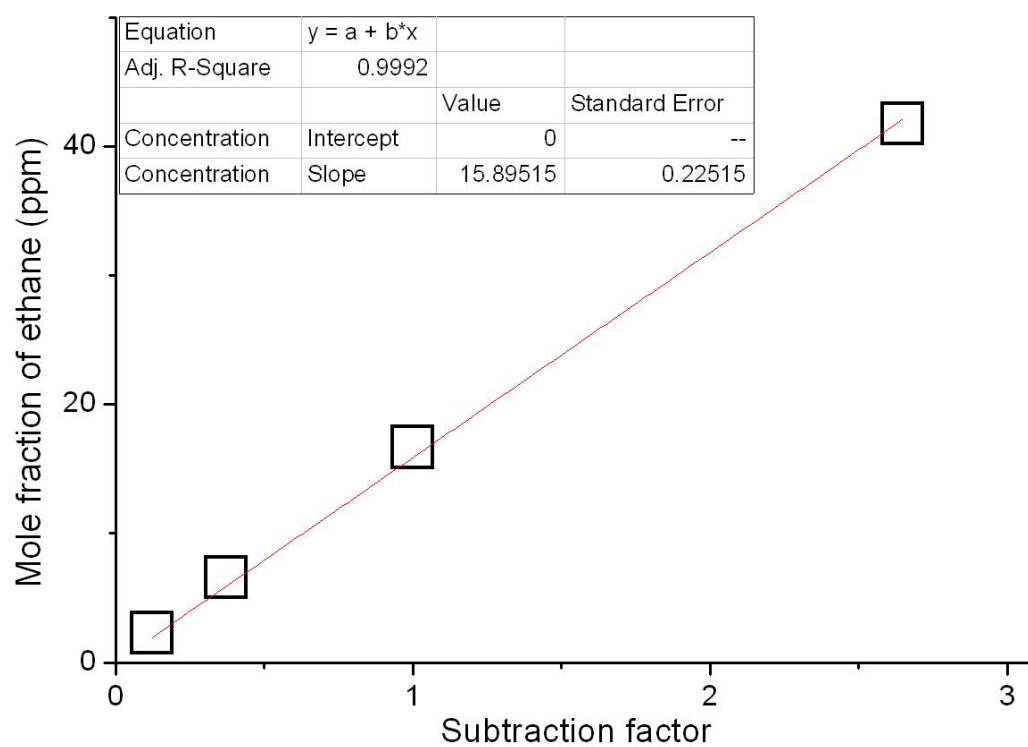


Figure A.18 Ethane calibration data and curve (FT-IR)  
(Wavenumber 3020-2950  $\text{cm}^{-1}$ )

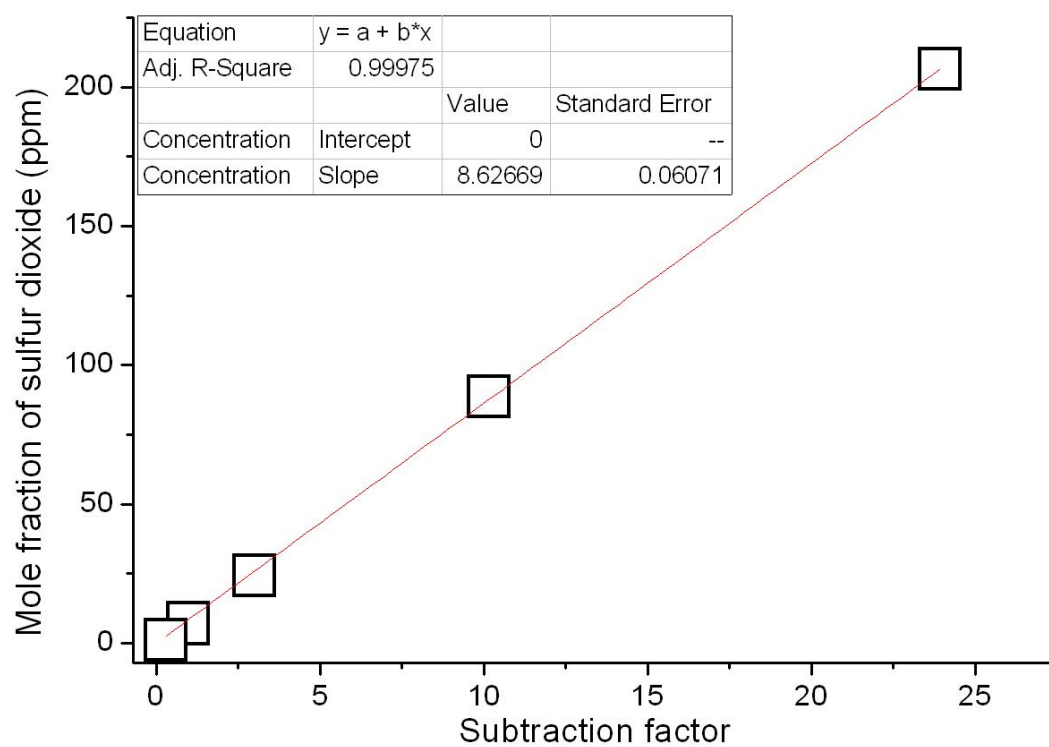


Figure A.19 Sulfur dioxide calibration data and curve (FT-IR)  
(Wavenumber 1390-1330  $\text{cm}^{-1}$ )

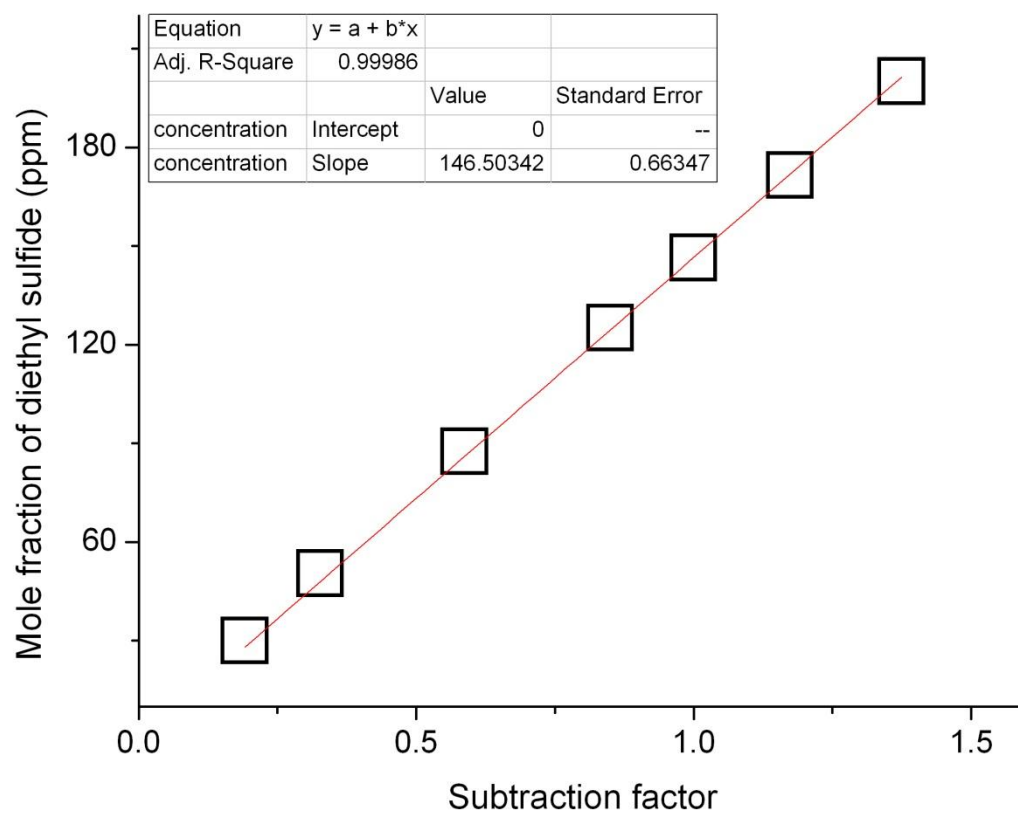


Figure A.20 Diethyl sulfide calibration data and curve (FT-IR)

(Wavenumber 1320-1220  $\text{cm}^{-1}$ )

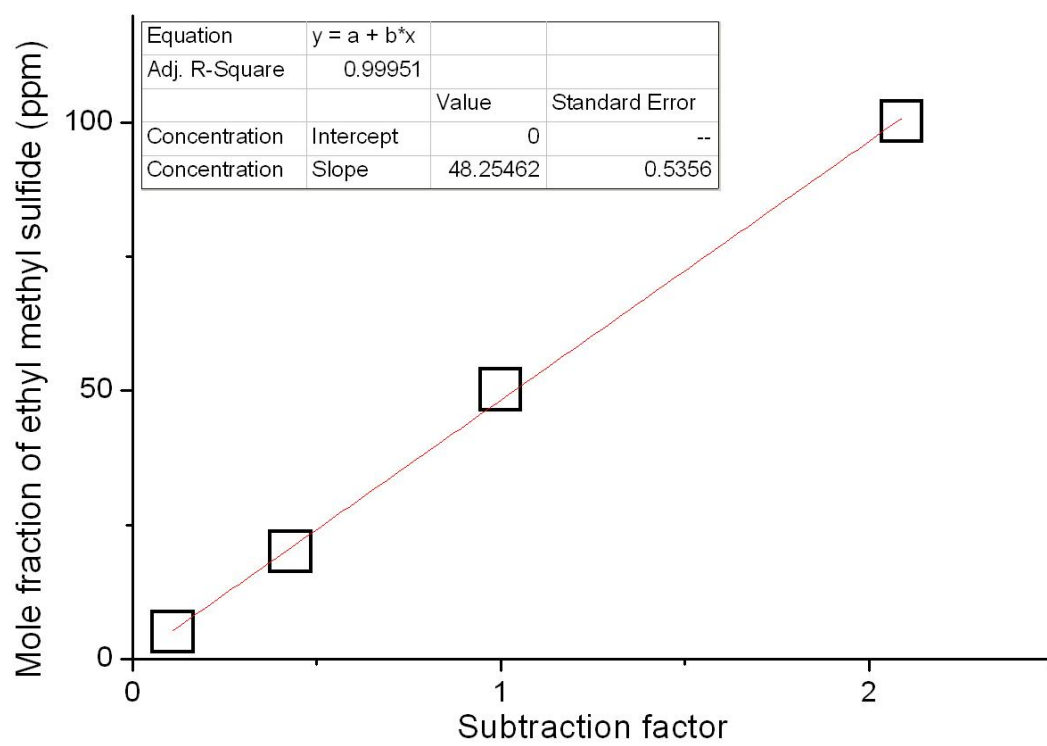


Figure A.21 Ethyl methyl sulfide calibration data and curve (FT-IR)  
(Wavenumber 1320-1220  $\text{cm}^{-1}$ )

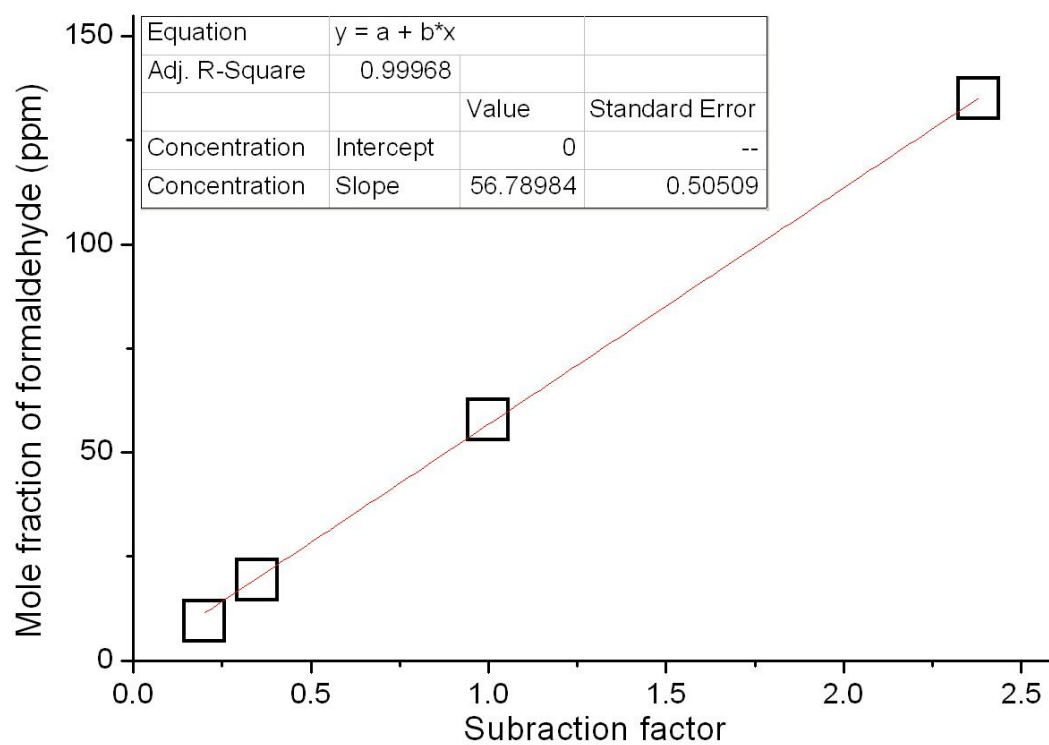


Figure A.22 Formaldehyde calibration data and curve (FT-IR)  
(Wavenumber 1800-1680  $\text{cm}^{-1}$ )

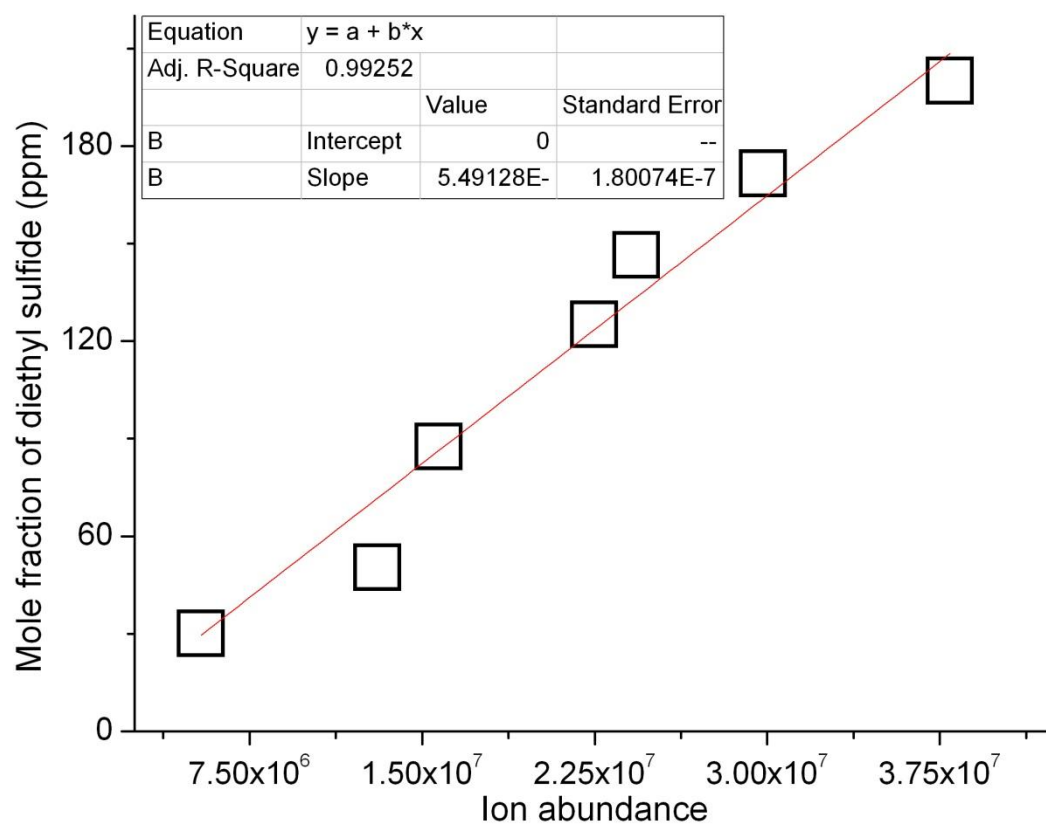


Figure A.23 Diethyl sulfide calibration data and curve (GC/MS)



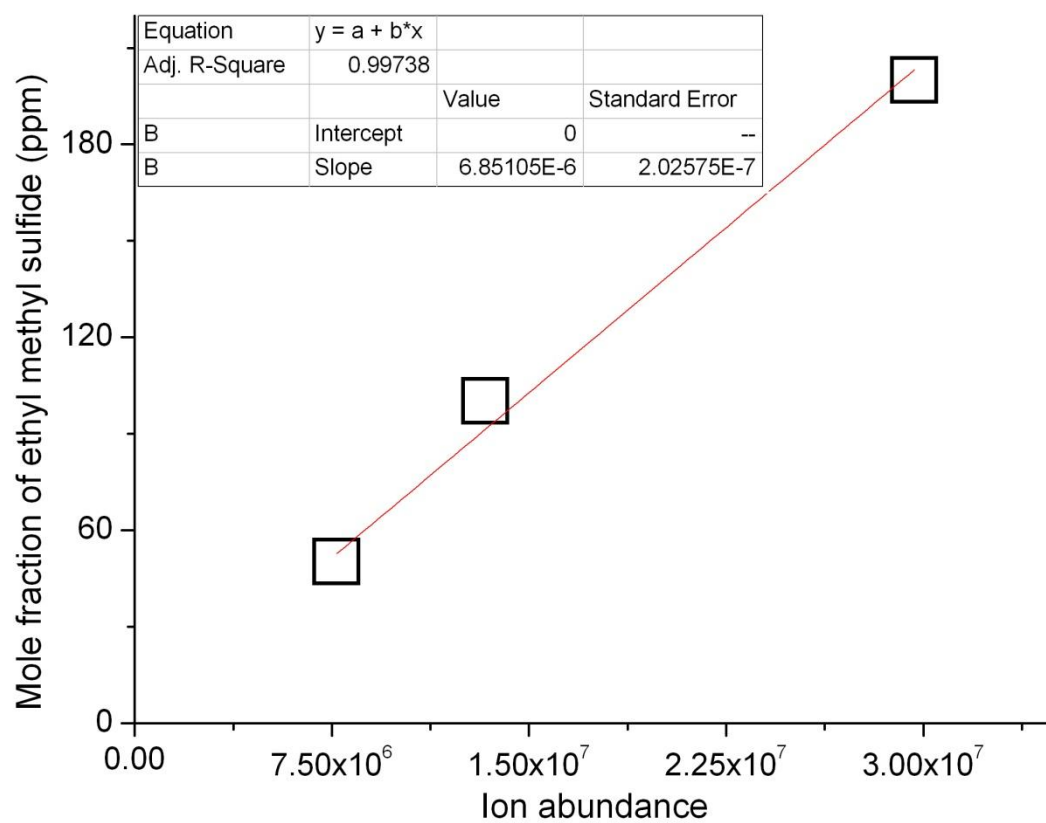


Figure A.24 Ethyl methyl sulfide calibration data and curve (GC/MS)

## **REFERENCES**

- [1] E.J. Zegers, Flow Reactor Pyrolysis of Alkyl Phosphates and Phosphonates, Ph.D. Thesis, Cornell University, Ithaca, NY 14853, 1997.

## APPENDIX B

### KINETIC MECHANISM OF PYROLYSIS OF DIETHYL SULFIDE

#### B.1 KINETIC MECHANISM USED FOR CALCULATIONS IN CHAPTER 2

REACTIONS CONSIDERED		$k = AT^n \exp(-E_a/RT)$		
		A	n	$E_a$
1	$C^*CSCJ=C_2H_3+CH_2S$	3.30E+10	1	40500
2	$C^*CCJ=C_2H_2+CH_3$	2.40E+48	-9.9	82080
	Reverse Arrhenius coefficients:	2.61E+46	-9.8	36950
3	$YCCSCCS=CH_3CH^*S+C^*CSH$	4.50E+12	0	60600
4	$YCCSCCS+H=YCJCSCCS+H_2$	3.00E+13	0	8500
5	$YCJCSCCS=C^*CSCCSJ$	4.30E+10	1	22500
6	$C^*CSCCSJ=C^*CSCJ+CH_2S$	2.30E+10	1	41500
7	$C^*CSSC^*C=C^*CSJ+C^*CSJ$	4.80E+15	0	25000
8	$C^*CSSCC^*C=C^*CSJ+C^*CCSJ$	8.30E+15	0	55000
9	$C^*CCSJ=C_2H_3+CH_2S$	5.50E+13	0	46500
10	$C^*CSC^*C+H=C_2H_4+C^*CSJ$	1.30E+13	0	2500
11	$CH_3CH^*S+H=C^*CSJ+H_2$	4.50E+13	0	12000
12	$C^*CSH+H=H_2+C^*CSJ$	1.30E+13	0	4300
13	$C^*CSJ+H=S+C_2H_4$	1.20E+13	0	3400
14	$C^*CSH+H=C_2H_4+SH$	9.50E+12	-1.1	0
15	$CH_2S+H=HCS+H_2$	1.80E+13	0	3500
16	$CH_3+CH_3=C_2H_6$	2.68E+29	-5	6130
17	$CH_3+H=CH_4$	7.09E+31	-5.8	5890
18	$CH+C_2H_2=C_3H_2+H$	1.00E+14	0	0
19	$H+C_2H_4=C_2H_5$	5.41E+35	-6.8	11700
20	$C_2H_5+H=C_2H_6$	5.18E+35	-6.8	6810
21	$C_2H_3=C_2H_2+H$	5.62E+31	-6.1	51720
22	$C_2H_3+CH_2=C_2H_2+CH_3$	3.00E+13	0	0
23	$C_2H_3+C_2H=2C_2H_2$	3.00E+13	0	0
24	$C_2H_3+CH=CH_2+C_2H_2$	5.00E+13	0	0
25	$C_2H+C_2H_2=C_4H_2+H$	3.00E+13	0	0
26	$CH_2(S)+M=CH_2+M$	1.00E+13	0	0
	H Enhanced by 0.00E+00			
27	$CH_2(S)+H=CH_2+H$	2.00E+14	0	0
28	$CH_2+C_2H_2=C_3H_3+H$	1.20E+13	0	6600
29	$2C_2H_2=C_4H_3+H$	2.00E+12	0	45900
30	$C_4H_3+M=C_4H_2+H+M$	1.00E+16	0	59700
31	$CH_2(S)+C_2H_2=C_3H_3+H$	3.00E+13	0	0
32	$H+C_2H(+M)=C_2H_2(+M)$	1.00E+17	-1	0
	Low pressure limit:	3.75E+33	-4.80E+00	1.90E+03
	TROE centering:	6.46E-01	1.32E+02	1.32E+03 5.57E+03
	H2	Enhanced by 2.00E+00		
	CH4	Enhanced by 2.00E+00		
	CO	Enhanced by 1.50E+00		

	C2H6	Enhanced by 3.00E+00			
33	H+C2H3(+M)=C2H4(+M)	6.08E+12	0.3	280	
	Low pressure limit:	1.40E+30 -3.86E+00 3.32E+03			
	TROE centering:	7.82E-01 2.08E+02 2.66E+03 6.10E+03			
	H2	Enhanced by 2.00E+00			
	CH4	Enhanced by 2.00E+00			
	CO	Enhanced by 1.50E+00			
	C2H6	Enhanced by 3.00E+00			
34	H2S+M=S+H2+M	1.60E+24	-2.6	89027	
	N2	Enhanced by 1.50E+00			
35	H2S+H=SH+H2	1.20E+07	2.1	696	
36	2SH=S2+H2	1.00E+12	0	0	
37	S2+M=2S+M	4.80E+13	0	77104	
38	S2+H+M=HS2+M	1.00E+16	0	0	
	N2	Enhanced by 1.50E+00			
39	HS2+H=S2+H2	1.20E+07	2.1	700	
40	HS2+H+M=H2S2+M	1.00E+16	0	0	
	N2	Enhanced by 1.50E+00			
41	H2S2+H=HS2+H2	1.20E+07	2.1	715	
42	H2S2+S=HS2+SH	8.30E+13	0	7353	
43	S+CH4=SH+CH3	6.00E+14	0	24000	
44	H2S+CH3=CH4+SH	1.80E+11	0	2340	
45	2H+M=H2+M	1.00E+18	-1	0	
	H2	Enhanced by 2.00E+00			
	CH4	Enhanced by 2.00E+00			
	CO	Enhanced by 1.50E+00			
	C2H6	Enhanced by 3.00E+00			
46	2H+H2=2H2	9.00E+16	-0.6	0	
47	H+CH=C+H2	1.65E+14	0	0	
48	H+CH2(+M)=CH3(+M)	6.00E+14	0	0	
	Low pressure limit:	1.04E+26 -2.76E+00 1.60E+03			
	TROE centering:	5.62E-01 9.10E+01 5.84E+03 8.55E+03			
	H2	Enhanced by 2.00E+00			
	CH4	Enhanced by 2.00E+00			
	CO	Enhanced by 1.50E+00			
	C2H6	Enhanced by 3.00E+00			
49	H+CH2(S)=CH+H2	3.00E+13	0	0	
50	H+CH3(+M)=CH4(+M)	1.39E+16	-0.5	536	
	Low pressure limit:	2.62E+33 -4.76E+00 2.44E+03			
	TROE centering:	7.83E-01 7.40E+01 2.94E+03 6.96E+03			
	H2	Enhanced by 2.00E+00			
	CH4	Enhanced by 2.00E+00			
	CO	Enhanced by 1.50E+00			
	C2H6	Enhanced by 3.00E+00			
51	H+CH4=CH3+H2	6.60E+08	1.6	10840	
52	H+C2H2(+M)=C2H3(+M)	5.60E+12	0	2400	
	Low pressure limit:	3.80E+40 -7.27E+00 7.22E+03			
	TROE centering:	7.51E-01 9.85E+01 1.30E+03 4.17E+03			

	H2	Enhanced by 2.00E+00		
	CH4	Enhanced by 2.00E+00		
	CO	Enhanced by 1.50E+00		
	C2H6	Enhanced by 3.00E+00		
53	H+C2H3=H2+C2H2	3.00E+13	0	0
54	H+C2H4(+M)=C2H5(+M)	5.40E+11	0.5	1820
	Low pressure limit: 6.00E+41 -7.62E+00 6.97E+03			
	TROE centering: 9.75E-01 2.10E+02 9.84E+02 4.37E+03			
	H2	Enhanced by 2.00E+00		
	CH4	Enhanced by 2.00E+00		
	CO	Enhanced by 1.50E+00		
	C2H6	Enhanced by 3.00E+00		
55	H+C2H4=C2H3+H2	1.32E+06	2.5	12240
56	H+C2H5(+M)=C2H6(+M)	5.21E+17	-1	1580
	Low pressure limit: 1.99E+41 -7.08E+00 6.69E+03			
	TROE centering: 8.42E-01 1.25E+02 2.22E+03 6.88E+03			
	H2	Enhanced by 2.00E+00		
	CH4	Enhanced by 2.00E+00		
	CO	Enhanced by 1.50E+00		
	C2H6	Enhanced by 3.00E+00		
57	H+C2H5=H2+C2H4	2.00E+12	0	0
58	H+C2H6=C2H5+H2	1.15E+08	1.9	7530
59	C+CH2=H+C2H	5.00E+13	0	0
60	C+CH3=H+C2H2	5.00E+13	0	0
61	CH+H2=H+CH2	1.08E+14	0	3110
62	CH+CH2=H+C2H2	4.00E+13	0	0
63	CH+CH3=H+C2H3	3.00E+13	0	0
64	CH+CH4=H+C2H4	6.00E+13	0	0
65	CH2+H2=H+CH3	5.00E+05	2	7230
66	2CH2=H2+C2H2	1.60E+15	0	11944
67	CH2+CH3=H+C2H4	4.00E+13	0	0
68	CH2+CH4=2CH3	2.46E+06	2	8270
69	CH2(S)+N2=CH2+N2	1.50E+13	0	600
70	CH2(S)+H2=CH3+H	7.00E+13	0	0
71	CH2(S)+CH3=H+C2H4	1.20E+13	0	-570
72	CH2(S)+CH4=2CH3	1.60E+13	0	-570
73	CH2(S)+CO=CH2+CO	9.00E+12	0	0
74	CH2(S)+C2H6=CH3+C2H5	4.00E+13	0	-550
75	2CH3(+M)=C2H6(+M)	6.77E+16	-1.2	654
	Low pressure limit: 3.40E+41 -7.03E+00 2.76E+03			
	TROE centering: 6.19E-01 7.32E+01 1.18E+03 1.00E+04			
	H2	Enhanced by 2.00E+00		
	CH4	Enhanced by 2.00E+00		
	CO	Enhanced by 1.50E+00		
	C2H6	Enhanced by 3.00E+00		
76	2CH3=H+C2H5	6.84E+12	0.1	10600
77	CH3+C2H4=C2H3+CH4	2.27E+05	2	9200
78	CH3+C2H6=C2H5+CH4	6.14E+06	1.7	10450

79	C2H+H2=H+C2H2	5.68E+10	0.9	1993
80	C2H4(+M)=H2+C2H2(+M)	8.00E+12	0.4	86770
	Low pressure limit:	1.58E+51 -9.30E+00 9.78E+04		
	TROE centering:	7.35E-01 1.80E+02 1.04E+03 5.42E+03		
	H2	Enhanced by 2.00E+00		
	CH4	Enhanced by 2.00E+00		
	CO	Enhanced by 1.50E+00		
	C2H6	Enhanced by 3.00E+00		
81	CH+H2(+M)=CH3(+M)	1.97E+12	0.4	-370
	Low pressure limit:	4.82E+25 -2.80E+00 5.90E+02		
	TROE centering:	5.78E-01 1.22E+02 2.54E+03 9.37E+03		
	H2	Enhanced by 2.00E+00		
	CH4	Enhanced by 2.00E+00		
	CO	Enhanced by 1.50E+00		
	C2H6	Enhanced by 3.00E+00		
82	CH2+CH2=2H+C2H2	2.00E+14	0	10989
83	CH3+C2H5(+M)=CCC(+M)	9.43E+12	0	0
	Low pressure limit:	2.71E+74 -1.68E+01 1.31E+04		
	TROE centering:	1.53E-01 2.91E+02 2.74E+03 7.75E+03		
	H2	Enhanced by 2.00E+00		
	CH4	Enhanced by 2.00E+00		
	CO	Enhanced by 1.50E+00		
	C2H6	Enhanced by 3.00E+00		
84	CH3+C2H4(+M)=CCC.(+M)	2.55E+06	1.6	5700
	Low pressure limit:	3.00E+63 -1.46E+01 1.82E+04		
	TROE centering:	1.89E-01 2.77E+02 8.75E+03 7.89E+03		
	H2	Enhanced by 2.00E+00		
	CH4	Enhanced by 2.00E+00		
	CO	Enhanced by 1.50E+00		
	C2H6	Enhanced by 3.00E+00		
85	H+CCC.(+M)=CCC(+M)	3.61E+13	0	0
	Low pressure limit:	4.42E+61 -1.35E+01 1.14E+04		
	TROE centering:	3.15E-01 3.69E+02 3.29E+03 6.67E+03		
	H2	Enhanced by 2.00E+00		
	CH4	Enhanced by 2.00E+00		
	CO	Enhanced by 1.50E+00		
	C2H6	Enhanced by 3.00E+00		
86	CH3+CCC.=2C2H5	1.93E+13	-0.3	0
87	CCC+H=CC.C+H2	4.80E+08	1.5	5690
88	CCC+H=CCC.+H2	1.44E+09	1.5	7412
89	CCC+CH3=CC.C+CH4	1.63E+06	1.9	8908
90	CCC+CH3=CCC.+CH4	4.89E+06	1.9	10630
91	CCC+CCC.=CC.C+CCC	1.31E+04	2.5	9990
92	CCC=CCC.+H	3.79E+71	-17	123908
93	CCC=H+CC.C	2.61E+74	-17.8	123075
94	CCC=CH3+C2H5	4.07E+82	-19.5	118513
95	CCC.+H=H+CC.C	6.32E+07	1.4	5679
96	CCC.+H=CH3+C2H5	5.74E+19	-1.6	5229

97	H+CC.C=CH3+C2H5	5.58E+21	-2.1	7201
98	CH3+C2H4=CCC.	3.02E+31	-6.5	11926
99	CCC.=C*CC+H	1.57E+28	-5.2	36039
100	CC.C=H+C*CC	1.61E+47	-10.4	50324
101	CH3+C2H4=C*CC+H	2.64E+20	-2.4	21368
102	CCC.=CC.C	5.80E+33	-6.5	45457
103	H+CCC.=C*CC+H2	1.80E+12	0	0
104	CH3+CCC.=C*CC+CH4	1.10E+13	0	0
105	C2H5+CCC.=C*CC+C2H6	1.00E+13	0	0
106	CCC.+C2H5=C2H4+CCC	1.00E+13	0	0
107	2CCC.=C*CC+CCC	1.00E+13	0	0
108	H+CC.C=C*CC+H2	3.20E+12	0	0
109	CH3+CC.C=C*CC+CH4	2.20E+14	-0.7	0
110	C2H5+CC.C=C*CC+C2H6	1.00E+13	0	0
111	CC.C+C2H5=C2H4+CCC	1.00E+13	0	0
112	2CC.C=C*CC+CCC	1.00E+13	0	0
113	CCC.+CC.C=C*CC+CCC	1.00E+13	0	0
114	CCSCC+H=CJCSCC+H2	1.44E+09	1.5	6640
115	CCSCC+CH3=CJCSCC+CH4	4.86E+06	1.9	9700
116	CCSCC=CCSJ+C2H5	2.00E+16	0	71200
117	CCSCC=CCSH+C2H4	5.70E+07	1.6	64060
118	CJCSCC=C2H4+CCSJ	1.00E+14	0	18170
119	CJCSCC=C*CSCC+H	3.00E+13	0	34080
120	CCSCC+H=CCJSCC+H2	9.60E+08	1.5	1330
121	CCSCC+CH3=CCJSCC+CH4	3.24E+06	1.9	4390
122	CCJSCC=C*CSCC+H	3.00E+13	0	41400
123	CCJSCC=CH3CH*S+C2H5	1.20E+14	0	30290
124	C*CSCC+H=C*CSCJC+H2	4.80E+08	1.5	2220
125	C*CSCC+CH3=C*CSCJC+CH4	1.62E+06	1.9	5280
126	C*CSCC+CCSJ=C*CSCJC+CCSH	1.62E+06	1.9	16580
127	C*CSCJC=C*CSC*C+H	3.00E+13	0	41980
128	C*CSCJC=CH3CH*S+C2H3	2.00E+14	0	42500
129	C*CSCC+H=C*CSCCJ+H2	7.20E+08	1.5	7300
130	C*CSCC+CH3=C*CSCCJ+CH4	2.43E+06	1.9	10350
131	C*CSCC+CCSJ=C*CSCCJ+CCSH	2.43E+06	1.9	21660
132	C*CSCCJ=C*CSJ+C2H4	1.50E+14	0	20550
133	C*CSCCJ=C*CSC*C+H	3.00E+13	0	34170
134	C*CSCC=C*CSJ+C2H5	2.00E+16	0	74440
135	CCSCC+SH=CJCSCC+H2S	7.29E+06	1.9	13120
136	CCSCC+SH=CCJSCC+H2S	4.86E+06	1.9	18430
137	CCSJ+H=SH+C2H5	1.00E+13	0	500
138	C*CSC*CJ=YC4H5S	1.00E+12	0	7200
139	C*CSC*CJ=THIOPHENE+H	1.00E+14	0	27400
140	C*CSJ+C2H4=YC4H7S	2.00E+09	0	9500
141	YC4H7S=YC4H6S+H	1.00E+14	0	41820
142	YC4H6S=YC4H5S+H	3.00E+13	0	88320
143	YC4H5S=THIOPHENE+H	1.00E+14	0	23970
144	CH3CH*S+C2H5=CCCICSJ	3.00E+13	0	8000

145	CCCICSJ=CCCIC*S+H	1.00E+14	0	42200
146	CCCICSJ=CCC*S+CH3	2.00E+14	0	39900
147	CCCICSH+CH3=CCCICSJ+CH4	8.10E+05	1.9	32800
148	H+OCS=SH+CO	1.72E+09	1.7	3484
149	CH3+OCS=CH3S+CO	1.88E+08	0.5	10806
150	SH+CS=H+CS2	8.70E+14	-0.8	775
151	CH3S+CS=CH3+CS2	5.90E+04	1.7	1080
152	S2+CS=S+CS2	8.70E+14	-0.8	775
153	HCS+S2=CS2+SH	3.00E+11	0	4000
154	HCS+S=H+CS2	2.00E+13	0	0
155	CCSH=CCSJ+H	1.15E+29	-4.7	89964
156	CCSH=CH3+CH2SH	5.94E+27	-4.2	86073
157	CCSH=CH3CH*S+H2	5.39E+25	-4.1	84940
158	CCSH=C2H4+H2S	1.46E+20	-2.4	68189
159	CCSH+H=CCSJ+H2	2.40E+08	1.5	500
160	CCSH+CH3=CCSJ+CH4	8.10E+05	1.9	1700
161	CCSJ=CH3CH*S+H	1.00E+14	0	45540
162	CCSJ=CH3+CH2S	2.00E+14	0	41410
163	CCSH+H=CCJSH+H2	4.80E+08	1.5	2810
164	CCSH+CH3=CCJSH+CH4	1.60E+06	1.9	5870
165	CCJSH=CH3+CH2S	1.38E+12	0	37880
166	2CCSJ=CCSSCC	2.00E+13	0	0
167	2SH=HSSH	2.50E+13	0	0
168	SH+CCSJ=CCSSH	2.00E+13	0	0

NOTE: A units mole-cm-sec-K, T(K), n dimensionless, E<sub>a</sub> units cal/mole



## B.2 THERMOCHEMICAL PROPERTIES FOR DIETHYLSULFIDE PYROLYSIS (CHAPTER 2)

SPECIES	H <sub>F</sub> (298)	S(298)	C <sub>P</sub> (300)	C <sub>P</sub> (400)	C <sub>P</sub> (500)	C <sub>P</sub> (600)	C <sub>P</sub> (800)	C <sub>P</sub> (1000)	C <sub>P</sub> (1500)
C2H	135.33	50.99	10.52	10.58	10.82	11.2	12.12	13.03	14.14
N2	0	45.77	6.9	7	7.12	7.24	7.51	7.78	8.33
AR	0	36.98	4.97	4.97	4.97	4.97	4.97	4.97	4.97
CCC.	23.67	70.69	17.09	21.37	25.15	28.48	33.97	38.15	44.58
C*CC	4.65	63.83	15.45	19.34	22.77	25.79	30.74	34.5	40.33
C*CCJ	40.06	62.96	14.93	18.63	21.78	24.45	28.65	31.7	36.34
CC.C	21.02	70.33	16.22	20.42	24.19	27.56	33.19	37.53	44.14
CCC	-25.33	64.52	17.87	22.76	27.08	30.88	37.14	41.9	49.24
C.*CC	63.77	65.22	15.24	18.5	21.36	23.86	27.93	31	35.78
C*C.C	61.57	65.64	15.06	18.1	20.83	23.27	27.38	30.58	35.57
C#CC	44.28	59.3	13.98	16.66	19.11	21.32	25.03	27.87	31.89
C*CCCC*C	20.18	88.6	28.58	36.62	43.46	49.26	58.31	64.82	74.67
H	52.1	27.39	4.97	4.97	4.97	4.97	4.97	4.97	4.97
H2	0	31.21	6.94	6.94	6.96	6.99	7.1	7.25	7.72
CO	-26.42	47.21	6.9	7.03	7.17	7.32	7.61	7.89	8.42
C	171.32	37.76	4.97	4.97	4.97	4.97	4.97	4.97	4.97
CH	142.01	43.72	7.1	6.94	6.92	7.01	7.4	7.89	8.71
CH2	92.36	46.32	8.37	8.65	8.99	9.36	10.14	10.88	12.14
CH2(S)	102.76	45.22	8.1	8.33	8.64	9	9.77	10.53	11.87
CH3	35.09	46.46	9.23	10.05	10.82	11.55	12.86	14.02	16.24
CH4	-17.83	44.54	8.54	9.8	11.14	12.51	15.16	17.49	21.17
C2H	133.01	49.58	10.51	10.58	10.83	11.2	12.13	13.03	14.14
C2H2	54.19	48	10.38	11.45	12.42	13.29	14.75	15.9	17.66
C2H3	71.63	55.24	10.09	11.98	13.61	15.02	17.3	19.03	21.82
C2H4	12.55	52.41	10.3	12.72	14.88	16.81	20.01	22.46	26.22
C2H5	28.4	58.87	12.46	15.08	17.44	19.57	23.14	25.93	30.32
C2H6	-20	54.87	12.41	15.79	18.82	21.53	26.07	29.59	35.08
C3H2	119.23	58.93	13.11	14.86	16.38	17.69	19.79	21.32	23.43

C3H3	80.42	57.53	14.04	16.61	18.81	20.68	23.59	25.59	28.11
C4H2	105.75	59.51	17.68	19.97	21.81	23.28	25.42	26.88	29.13
C4H3	117.9	67.49	17.61	20.66	23.21	25.34	28.59	30.83	33.97
S	66.69	40.09	5.34	5.34	5.34	5.34	5.34	5.34	5.34
S2	30.84	54.51	7.69	8.16	8.48	8.69	8.88	8.92	9.05
SH	34.6	46.73	7.69	7.6	7.54	7.53	7.61	7.79	8.38
H2S	-4.88	49.15	8.35	8.66	9.02	9.42	10.24	11	12.28
HS2	26.05	60.92	9.56	10.22	10.75	11.18	11.82	12.27	12.98
H2S2	3.98	60.01	11.71	12.89	13.86	14.65	15.85	16.69	17.99
HCS	69.37	52.38	7.89	8.5	9.03	9.47	10.17	10.69	11.5
CS	66.88	50.28	7.04	7.4	7.68	7.91	8.23	8.44	8.7
C*CSC*C	35.72	87.71	23.17	27.93	32.4	36.51	43.47	48.59	54.62
C*CSC*CJ	96.01	85.21	25.22	29.27	32.55	35.21	39.17	41.96	46.62
C*CSJ	54.65	64.46	13.08	15.67	17.82	19.61	22.33	24.27	27.31
CH3CH*S	17.05	64.42	13.6	16.38	18.83	20.96	24.43	27.04	31.03
CH2S	28.3	55.15	9.11	10.36	11.45	12.41	13.98	15.18	17.07
CH3S	29.9	57.62	10.73	12.49	14.01	15.34	17.5	19.15	21.83
C*CSH	17.73	67.44	15.53	18.15	20.42	22.4	25.57	27.92	31.45
CCSH	-11.03	70.66	17.46	20.96	24.04	26.74	31.17	34.56	39.88
C*CSSCC*C	34.97	102.79	36.11	42.55	47.84	52.18	58.73	63.41	71.07
C*CSSC*C	42.3	96.41	28.38	33.6	37.9	41.43	46.77	50.55	56.6
VSCCSV	34.92	114.5	40.05	48.19	54.98	60.63	69.3	75.49	85.2
C*CSCJ	55.2	77.99	20.75	24.57	27.71	30.27	34.12	36.82	41.13
YCCSCCS	1.04	78.17	26.21	33.74	40.04	45.29	53.34	59.02	67.54
YCJCSCCS	43.14	82.47	26.89	33.65	39.24	43.87	50.86	55.75	63.14
C*CSCCSJ	50.9	93.96	29.67	35.39	40.17	44.17	50.31	54.71	61.57
C*CCSJ	48.47	73.15	18.68	22.71	26.09	28.92	33.3	36.47	41.43
CS2	27.95	56.82	10.43	12.04	13.14	13.83	14.4	14.42	16.13
CCSCC	-20	89.15	27.48	33.99	39.65	44.56	52.51	58.48	67.83
CJCSCC	27.83	92.95	29.02	34.55	39.34	43.48	50.17	55.24	63.38
CCJSCC	19.66	92.28	28.37	33.87	38.69	42.92	49.83	55.09	63.37
CCSJ	24.5	67.31	15.67	18.97	21.82	24.28	28.23	31.2	35.89

[illegible]

CH	142.01	43.72	7.1	6.94	6.92	7.01	7.4	7.89	8.71
CH2	92.36	46.32	8.37	8.65	8.99	9.36	10.14	10.88	12.14
CH2(S)	102.76	45.22	8.1	8.33	8.64	9	9.77	10.53	11.87
CH3	35.09	46.46	9.23	10.05	10.82	11.55	12.86	14.02	16.24
CH4	-17.83	44.54	8.54	9.8	11.14	12.51	15.16	17.49	21.17
C2H	133.01	49.58	10.51	10.58	10.83	11.2	12.13	13.03	14.14
C2H2	54.19	48	10.38	11.45	12.42	13.29	14.75	15.9	17.66
C2H3	71.63	55.24	10.09	11.98	13.61	15.02	17.3	19.03	21.82
C2H4	12.55	52.41	10.3	12.72	14.88	16.81	20.01	22.46	26.22
C2H5	28.4	58.87	12.46	15.08	17.44	19.57	23.14	25.93	30.32
C2H6	-20	54.87	12.41	15.79	18.82	21.53	26.07	29.59	35.08
C3H2	119.23	58.93	13.11	14.86	16.38	17.69	19.79	21.32	23.43
C3H3	80.42	57.53	14.04	16.61	18.81	20.68	23.59	25.59	28.11
C4H2	105.75	59.51	17.68	19.97	21.81	23.28	25.42	26.88	29.13
C4H3	117.9	67.49	17.61	20.66	23.21	25.34	28.59	30.83	33.97
*S	66.69	40.09	5.34	5.34	5.34	5.34	5.34	5.34	5.34
S2	30.84	54.51	7.69	8.16	8.48	8.69	8.88	8.92	9.05
SH	34.6	46.73	7.69	7.6	7.54	7.53	7.61	7.79	8.38
H2S	-4.88	49.15	8.35	8.66	9.02	9.42	10.24	11	12.28
OCS	-34.21	55.32	10.06	10.94	11.63	12.14	12.81	13.16	13.55
HS2	26.05	60.92	9.56	10.22	10.75	11.18	11.82	12.27	12.98
H2S2	3.98	60.01	11.71	12.89	13.86	14.65	15.85	16.69	17.99
HCS	69.37	52.38	7.89	8.5	9.03	9.47	10.17	10.69	11.5
CS	66.88	50.28	7.04	7.4	7.68	7.91	8.23	8.44	8.7
C*CSC*C	35.72	87.71	23.17	27.93	32.4	36.51	43.47	48.59	54.62
C*CSC*CJ	96.01	85.21	25.22	29.27	32.55	35.21	39.17	41.96	46.62
C*CSJ	54.65	64.46	13.08	15.67	17.82	19.61	22.33	24.27	27.31
CH3CH*S	17.05	64.42	13.6	16.38	18.83	20.96	24.43	27.04	31.03
CH2S	28.3	55.15	9.11	10.36	11.45	12.41	13.98	15.18	17.07
CH3S	29.9	57.62	10.73	12.49	14.01	15.34	17.5	19.15	21.83
C*CSH	17.73	67.44	15.53	18.15	20.42	22.4	25.57	27.92	31.45
CCSH	-11.03	70.66	17.46	20.96	24.04	26.74	31.17	34.56	39.88

C*CSSCC*C	34.97	102.79	36.11	42.55	47.84	52.18	58.73	63.41	71.07
C*CSSC*C	42.3	96.41	28.38	33.6	37.9	41.43	46.77	50.55	56.6
C*CSCJ	55.2	77.99	20.75	24.57	27.71	30.27	34.12	36.82	41.13
YCCSCCS	1.04	78.17	26.21	33.74	40.04	45.29	53.34	59.02	67.54
YCJCSCCS	43.14	82.47	26.89	33.65	39.24	43.87	50.86	55.75	63.14
C*CSCCSJ	50.9	93.96	29.67	35.39	40.17	44.17	50.31	54.71	61.57
C*CCSJ	48.47	73.15	18.68	22.71	26.09	28.92	33.3	36.47	41.43
CS2	27.95	56.82	10.43	12.04	13.14	13.83	14.4	14.42	16.13
CCSCC	-20	89.15	27.48	33.99	39.65	44.56	52.51	58.48	67.83
CJCSCC	27.83	92.95	29.02	34.55	39.34	43.48	50.17	55.24	63.38
CCJSCC	19.66	92.28	28.37	33.87	38.69	42.92	49.83	55.09	63.37
CCSJ	24.5	67.31	15.67	18.97	21.82	24.28	28.23	31.2	35.89
C*CSCC	6.81	86.66	25.93	31.53	36.31	40.4	46.88	51.69	59.3
C*CSCJC	47.84	88.82	25.78	31.02	35.37	38.98	44.52	48.51	54.92
C*CSCCJ	55.66	89.98	27.05	31.72	35.69	39.06	44.38	48.35	54.82
THIOPHENE	26.3	66.49	17.39	22.69	26.94	30.32	35.15	38.32	43.03
YC4H5S	55.84	65.31	19.24	24.66	29.08	32.67	37.96	41.55	47.04
YC4H6S	19.35	62.72	18.65	24.75	29.81	33.99	40.31	44.7	51.34
YC4H7S	30.63	66.62	20.54	26.99	32.39	36.92	43.85	48.76	56.21
CCCICSH	-23.75	75.5	27.07	33.65	39.38	44.36	52.43	58.49	67.92
CCCICSJ	12.42	83.72	26.96	33.58	39.2	43.96	51.37	56.68	64.7
CCCIC*S	0.21	75.52	22.99	28.52	33.39	37.67	44.66	49.94	58.07
CCC*S	11.21	73.51	18.76	23.01	26.72	29.93	35.14	39.04	45.05
CH2SH	36.65	62.56	11.2	12.56	13.73	14.75	16.39	17.64	19.69
CCJSH	30.91	73.53	16.72	19.54	21.97	24.06	27.39	29.88	33.87
HSSH	3.98	63.07	11.67	12.85	13.81	14.59	15.76	16.59	17.98
CCSSH	-7.78	82.61	22.38	26.42	29.83	32.71	37.22	40.54	45.92
CCSSCC	-18.07	101.97	32.91	39.72	45.57	50.57	58.56	64.48	73.81

Note: S (cal/mol K), H<sub>F</sub> (kcal/mol) and C<sub>P</sub> (cal/mol K)

## APPENDIX C

### KINETIC MECHANISM OF OXIDATION OF DIETHYL SULFIDE

#### C.1 KINETIC MECHANISM USE FOR CALCULATIONS IN CHAPTER 3

REACTIONS CONSIDERED		$k = AT^n \exp(-E_a/RT)$		
		A	n	$E_a$
1	$VSEOSV = C*CSH + C_2H_4 + C*CSCC*O$	2.30E+11	0	55000
2	$C*CSCC*O = C*CSJ + C.CHO$	6.50E+15	0	48000
3	$HOCCSJ = CH_2S + C.H_2OH$	4.70E+13	0	36300
4	$SJCC*O = CH_2S + HCO$	2.50E+13	0	19000
5	$C*CSCJ = C_2H_3 + CH_2S$	3.30E+10	1	45500
6	$C*CCJ = C_2H_2 + CH_3$	2.40E+48	-9.9	82080
	Reverse Arrhenius coefficients:	2.61E+46	-9.8	36950
7	$C*CCJ + O_2 = CH_3C.*O + CH_2O$	7.14E+15	-1.2	21050
	Reverse Arrhenius coefficients:	4.94E+16	-1.4	88620
8	$YCCSCCS = CH_3CH*S + C*CSH$	4.50E+12	0	60600
9	$YCCSCCS + OH = YCJCSCCS + H_2O$	5.60E+12	0	3500
10	$YCCSCCS + O = YCJCSCCS + OH$	3.20E+13	0	6100
11	$YCCSCCS + H = YCJCSCCS + H_2$	3.00E+13	0	8500
12	$YCCSCCS + O_2 = YCJCSCCS + HO_2$	3.30E+13	0	46500
13	$YCJCSCCS = C*CSCCSJ$	4.30E+10	1	22500
14	$C*CSCCSJ = C*CSJ + CH_2S$	2.30E+10	1	35000
15	$C*CSSC*C = C*CSJ + C*CSJ$	4.80E+15	0	25000
16	$VSCCSV + OH \Rightarrow C*CSC*C + C*CSJ + H_2O$	1.70E+13	0	6500
17	$VSCCSV + O \Rightarrow C*CSC*C + C*CSJ + OH$	7.20E+13	0	9100
18	$VSCCSV + H \Rightarrow C*CSC*C + C*CSJ + H_2$	9.00E+13	0	11500
19	$C*CSSCC*C = C*CSJ + C*CCSJ$	8.30E+15	0	55000
20	$C*CCSJ = C_2H_3 + CH_2S$	5.50E+13	0	51500
21	$C*CSC*C + OH = C*COH + C*CSJ$	3.30E+12	0	1000
22	$C*CSC*C + O = C.CHO + C*CSJ$	8.50E+12	0	4400
23	$C*CSC*C + H = C_2H_4 + C*CSJ$	1.30E+13	0	2500
24	$CH_3CH*S + OH = CH_3CHO + SH$	2.10E+11	0	1500
25	$CH_3CH*S + O = CH_3CHO + S$	8.50E+11	0	4500
26	$C*CSH + OH = H_2O + C*CSJ$	2.40E+12	0	1500
27	$C*CSH + O = OH + C*CSJ$	1.50E+13	0	3800
28	$C*CSH + H = H_2 + C*CSJ$	1.30E+13	0	4300
29	$C*CSJ + OH = S + C*COH$	2.40E+12	0	3400
30	$C*CSJ + O = C.CHO + S$	2.10E+13	0	6000
31	$C*CSJ + H = S + C_2H_4$	1.20E+13	0	3400
32	$C*CSH + H = C_2H_4 + SH$	9.50E+12	-1.1	0
33	$C*CSH + O = C.CHO + SH$	1.10E+13	0	5500
34	$C*COH + OH = C.CHO + H_2O$	5.50E+12	0	400
35	$C*COH + CH_3 = C.CHO + CH_4$	9.20E+11	0	2000
36	$C*COH + O = C.CHO + OH$	5.50E+13	0	400
37	$C*COH + H = C.CHO + H_2$	2.20E+13	0	400

38	H+CH2O(+M)=CH3O(+M)	5.40E+11	0.5	2600
	Low pressure limit:	0.22000E+31	-0.48000E+01	0.55600E+4
	TROE centering:	0.75800E+00	0.94000E+02	0.15550E+04 0.42000E+00
	H2	Enhanced by	2.000E+00	
	H2O	Enhanced by	6.000E+00	
	CH4	Enhanced by	2.000E+00	
	CO	Enhanced by	1.500E+00	
	CO2	Enhanced by	2.000E+00	
	C2H6	Enhanced by	3.000E+00	
39	H+CH2O(+M)=C.H2OH(+M)	5.40E+11	0.5	3600
	Low pressure limit:	0.12700E+33	-0.48200E+01	0.65300E+4
	TROE centering:	0.71870E+00	0.10300E+03	0.12910E+04 0.41600E+06
	H2	Enhanced by	2.000E+00	
	H2O	Enhanced by	6.000E+00	
	CH4	Enhanced by	2.000E+00	
	CO	Enhanced by	1.500E+00	
	CO2	Enhanced by	2.000E+00	
	C2H6	Enhanced by	3.000E+00	
40	CH+C2H2=C3H2+H	1.00E+14	0	0
41	CH2+CO2=CH2O+CO	1.10E+11	0	1000
42	CH2+O=CO+2H	5.00E+13	0	0
43	CH2+O=CO+H2	3.00E+13	0	0
44	CH2+O2=CO2+H2	6.90E+11	0	500
45	CH2+O2=CO+H2O	1.90E+10	0	-1000
46	CH2+O2=HCO+OH	4.30E+10	0	-500
47	H+HCO(+M)=CH2O(+M)	1.09E+12	0.5	-260
	Low pressure limit:	0.24700E+25	-0.25700E+01	0.42500E+3
	TROE centering:	0.78240E+00	0.27100E+03	0.27550E+04 0.65700E+06
	H2	Enhanced by	2.000E+00	
	H2O	Enhanced by	6.000E+00	
	CH4	Enhanced by	2.000E+00	
	CO	Enhanced by	1.500E+00	
	CO2	Enhanced by	2.000E+00	
	C2H6	Enhanced by	3.000E+00	
	AR	Enhanced by	7.000E-01	
48	O+CO(+M)=CO2(+M)	1.80E+10	0	2385
	Low pressure limit:	0.60200E+15	0.00000E+00	0.30000E+4
	H2	Enhanced by	2.000E+00	
	O2	Enhanced by	6.000E+00	
	H2O	Enhanced by	6.000E+00	
	CH4	Enhanced by	2.000E+00	
	CO	Enhanced by	1.500E+00	
	CO2	Enhanced by	3.500E+00	
	C2H6	Enhanced by	3.000E+00	
	AR	Enhanced by	5.000E-01	
49	H+C2H4=C2H5	5.41E+35	-6.8	11700
50	C2H5+H=C2H6	5.18E+35	-6.8	6810
51	C2H3=C2H2+H	5.62E+31	-6.1	51720

52	C2H3+CH2=C2H2+CH3	3.00E+13	0	0
53	C2H3+C2H=2C2H2	3.00E+13	0	0
54	C2H3+CH=CH2+C2H2	5.00E+13	0	0
55	OH+C2H2=HCCOH+H	5.04E+05	2.3	13500
56	HCCOH+H=CH2CO+H	1.00E+13	0	0
57	CH2CO=CH2+CO	2.01E+35	-6.7	82990
58	C2H+O2=2CO+H	5.00E+13	0	1500
59	C2H+C2H2=C4H2+H	3.00E+13	0	0
60	CH2(S)+M=CH2+M	1.00E+13	0	0
	H Enhanced by 0.000E+00			
61	CH2(S)+H=CH2+H	2.00E+14	0	0
62	CH2+C2H2=C3H3+H	1.20E+13	0	6600
63	C4H2+OH=C3H2+HCO	6.66E+12	0	-410
64	C3H2+O2=HCO+HCCO	1.00E+13	0	0
65	C3H3+O2=CH2CO+HCO	3.00E+10	0	2868
66	C3H3+O=CH2O+C2H	2.00E+13	0	0
67	C3H3+OH=C3H2+H2O	2.00E+12	0	0
68	2C2H2=C4H3+H	2.00E+12	0	45900
69	C4H3+M=C4H2+H+M	1.00E+16	0	59700
70	CH2(S)+C2H2=C3H3+H	3.00E+13	0	0
71	C4H2+O=C3H2+CO	1.20E+12	0	0
72	C2H2+O2=HCCO+OH	2.00E+08	1.5	30100
73	H+C2H(+M)=C2H2(+M)	1.00E+17	-1	0
	Low pressure limit: 0.37500E+34 -0.48000E+01 0.19000E+4			
	TROE centering: 0.64640E+00 0.13200E+03 0.13150E+04 0.55660E+06			
	H2 Enhanced by 2.000E+00			
	H2O Enhanced by 6.000E+00			
	CH4 Enhanced by 2.000E+00			
	CO Enhanced by 1.500E+00			
	CO2 Enhanced by 2.000E+00			
	C2H6 Enhanced by 3.000E+00			
	AR Enhanced by 7.000E-01			
74	H+C2H3(+M)=C2H4(+M)	6.08E+12	0.3	280
	Low pressure limit: 0.14000E+31 -0.38600E+01 0.33200E+4			
	TROE centering: 0.78200E+00 0.20750E+03 0.26630E+04 0.60950E+06			
	H2 Enhanced by 2.000E+00			
	H2O Enhanced by 6.000E+00			
	CH4 Enhanced by 2.000E+00			
	CO Enhanced by 1.500E+00			
	CO2 Enhanced by 2.000E+00			
	C2H6 Enhanced by 3.000E+00			
	AR Enhanced by 7.000E-01			
75	H2+O2=2OH	1.70E+13	0	47780
76	CH3CHO=CH3+HCO	1.21E+35	-6.2	87118
77	CH3CHO=CH3C.*O+H	1.47E+39	-8.1	93791
78	CH3CHO+O2=CH3C.*O+HO2	3.01E+13	0	39143
79	CH3CHO+OH=CH3C.*O+H2O	3.37E+12	0	-536
80	CH3CHO+H=CH3C.*O+H2	4.00E+13	0	4206



81	CH3CHO+HO2=CH3C.*O+H2O2	3.01E+12	0	8000
82	CH3CHO+CH3=CH3C.*O+CH4	1.86E+08	0	2464
83	CH3CHO+OH=C.CHO+H2O	4.31E+11	0	1000
84	CH3CHO+HO2=C.CHO+H2O2	1.40E+04	2.7	14068
85	CH3CHO+CH3=C.CHO+CH4	8.10E+05	1.9	5251
86	CH3C.*O+O2=CH2CO+HO2	4.13E+20	-2.4	5400
	Declared duplicate reaction...			
87	CH3C.*O+O2=CH2CO+HO2	4.87E+08	0.1	8373
	Declared duplicate reaction...			
88	C.CHO+O2=CH2CO+HO2	4.76E+05	2.5	23909
	Declared duplicate reaction...			
89	C.CHO+O2=CH2CO+HO2	9.00E+03	0.3	10490
	Declared duplicate reaction...			
90	CQJCHO=CQCJO	1.63E+20	-3	22214
	Declared duplicate reaction...			
91	CQCJO=CQJCHO	5.86E+07	-2.8	13687
	Declared duplicate reaction...			
92	CH3C.*O+O2=CCOQJ	1.40E+65	-17.3	13857
	Declared duplicate reaction...			
93	CCOQJ=CH3C.*O+O2	6.81E+51	-12.4	41514
	Declared duplicate reaction...			
94	CCOQJ=CJCOQ	2.06E+31	-6.2	31423
	Declared duplicate reaction...			
95	CJCOQ=CCOQJ	1.38E+10	0	17801
	Declared duplicate reaction...			
96	C.CHO=CH3C.*O	4.48E+35	-7.3	45939
	Declared duplicate reaction...			
97	CH3C.*O=C.CHO	4.03E-48	13.4	26679
	Declared duplicate reaction...			
98	C.CHO+O2=CQJCHO	5.18E+58	-14.9	18340
	Declared duplicate reaction...			
99	CQJCHO=C.CHO+O2	1.10E+41	-9	34788
	Declared duplicate reaction...			
100	CH3C.*O+O2=CC*OOJ+O	6.62E+13	-0.3	21647
101	CH3C.*O+O2=CJCOQ	1.48E+60	-16.1	15312
102	CH3C.*O+O2=OCYCO+OH	1.73E+26	-5.1	7430
103	CH3C.*O+O2=CJCO2+OH	2.98E+21	-2.9	6642
104	CCOQJ=CH2CO+HO2	2.23E+39	-8.4	35083
105	CCOQJ=CC*OOJ+O	2.94E+58	-17.3	59752
106	CJCOQ=CH2CO+HO2	2.30E-24	9.2	14948
107	CJCOQ=OCYCO+OH	6.24E+13	-1	18103
108	CJCOQ=CJCO2+OH	3.67E+08	1.1	18277
109	CC*OOJ=CH3+CO2	3.41E+15	-0.5	17466
110	CJCO2=CH2(S)+CO2	6.44E+02	2.4	3419
111	OCYCO=CO+CH2O	3.00E+11	1.1	27500
112	C.CHO+O2=CQCJO	4.11E+47	-15.1	18200
113	CQJCHO=CH2CO+HO2	8.48E+55	-15.6	53744
114	CQCJO=CH2CO+HO2	7.02E+08	-3.8	21147

115	CQCJO=CO+CH2O+OH	2.78E+19	-3	8137
116	CH3C.*O=CH2CO+H	5.19E-47	13.5	25699
117	CH3C.*O=CH3+CO	2.11E-06	5.1	8292
118	C.CHO=CH2CO+H	4.04E+37	-7.7	47770
119	2CCOQJ=2CC*OOJ+O2	8.51E+10	0	248
120	CH3CHO+CCOQJ=CCOQ+CH3C.*O	2.40E+08	1.5	3643
121	CH3CHO+CCOQJ=CCOQ+C.CHO	2.40E+08	1.5	7933
122	O*CCOJ=CH2O+HCO	3.59E+23	-4.8	91861
123	CJCOQ+O2=CQJCOQ	1.10E+11	0	0
124	COJCOQ=CJOQ+CH2O	1.35E+12	0	20800
125	CJOQ=CO+HO2	1.73E+10	0	16550
126	CJOQ=CO2+OH	3.34E+12	0	24290
127	H2S+M=S+H2+M	1.60E+24	-2.6	89027
	N2	Enhanced by	1.500E+00	
	SO2	Enhanced by	1.000E+01	
	H2O	Enhanced by	1.000E+01	
128	H2S+H=SH+H2	1.20E+07	2.1	696
129	H2S+O=SH+OH	7.50E+07	1.8	2901
130	H2S+OH=SH+H2O	2.70E+12	0	0
131	SH+O=H+SO	1.00E+14	0	0
132	SH+OH=S+H2O	1.00E+13	0	0
133	SH+HO2=HSO+OH	1.00E+12	0	0
134	S+OH=H+SO	4.00E+13	0	0
135	2SH=S2+H2	1.00E+12	0	0
136	S2+M=2S+M	4.80E+13	0	77104
137	S2+H+M=HS2+M	1.00E+16	0	0
	N2	Enhanced by	1.500E+00	
	SO2	Enhanced by	1.000E+01	
	H2O	Enhanced by	1.000E+01	
138	S2+O=SO+S	1.00E+13	0	0
139	HS2+H=S2+H2	1.20E+07	2.1	700
140	HS2+O=S2+OH	7.50E+07	1.8	2901
141	HS2+OH=S2+H2O	2.70E+12	0	0
142	HS2+H+M=H2S2+M	1.00E+16	0	0
	N2	Enhanced by	1.500E+00	
	SO2	Enhanced by	1.000E+01	
	H2O	Enhanced by	1.000E+01	
143	H2S2+H=HS2+H2	1.20E+07	2.1	715
144	H2S2+O=HS2+OH	7.50E+07	1.8	2901
145	H2S2+OH=HS2+H2O	2.70E+12	0	0
146	H2S2+S=HS2+SH	8.30E+13	0	7353
147	SO3+H=HOSO+O	2.50E+05	2.9	50277
148	SO3+O=SO2+O2	2.00E+12	0	19872
149	SO3+SO=2SO2	1.00E+12	0	9936
150	SO+O(+M)=SO2(+M)	3.20E+13	0	0
	N2	Enhanced by	1.500E+00	
	SO2	Enhanced by	1.000E+01	
	H2O	Enhanced by	1.000E+01	

	Low pressure limit:	0.12000E+22	-0.15400E+01	0.00000E+0	
	TROE centering:	0.55000E+00	0.10000E-29	0.10000E+31	
151	SO2+O(+M)=SO3(+M)	9.20E+10	0		2385
	Low pressure limit:	0.24000E+29	-0.40000E+01	0.26400E+4	
152	SO2+OH(+M)=HOSO2(+M)	5.06E+12	-0.2		0
	Low pressure limit:	0.16880E+28	-0.40900E+01	0.00000E+0	
	TROE centering:	0.10000E+01	0.10000E+31	0.41200E+3	
153	SO2+OH=HOSO+O	3.90E+08	1.9		75912
154	SO2+OH=SO3+H	4.90E+02	2.7		23847
155	SO2+CO=SO+CO2	2.70E+12	0		48289
156	SO+M=S+O+M	4.00E+14	0		107310
	N2	Enhanced by	1.500E+00		
	SO2	Enhanced by	1.000E+01		
	H2O	Enhanced by	1.000E+01		
157	SO+H+M=HSO+M	5.00E+15	0		0
	N2	Enhanced by	1.500E+00		
	SO2	Enhanced by	1.000E+01		
	H2O	Enhanced by	1.000E+01		
158	HOSO(+M)=SO+OH(+M)	9.94E+21	-2.5		75892
	Low pressure limit:	0.11560E+47	-0.90200E+01	0.26647E+5	
	TROE centering:	0.95000E+00	0.29890E+04	0.11000E+1	
159	SO+O2=SO2+O	7.60E+03	2.4		2981
160	2SO=SO2+S	2.00E+12	0		3974
161	HSO+H=HSOH	2.50E+20	-3.1		914
162	HSO+H=SH+OH	4.90E+19	-1.9		1560
163	HSO+H=S+H2O	1.60E+09	1.4		-338
164	HSO+H=H2SO	1.80E+17	-2.5		50
165	HSO+H=H2S+O	1.10E+06	1		10393
166	HSO+H=SO+H2	1.00E+13	0		0
167	HSO+O+M=HSO2+M	1.10E+19	-1.7		-50
168	HSO+O=SO2+H	4.50E+14	-0.4		0
169	SOH+O+M=HOSO+M	6.90E+19	-1.6		1590
170	HSO+O=O+SOH	4.80E+08	1		5365
171	HSO+O=OH+SO	1.40E+13	0.1		298
172	HSO+OH=HOSHO	5.20E+28	-5.4		3180
173	HSO+OH=HOSO+H	5.30E+07	1.6		3776
174	HSO+OH=SO+H2O	1.70E+09	1		467
175	HSO+O2=SO2+OH	1.00E+12	0		9936
176	HSOH=SH+OH	2.80E+39	-8.8		75117
177	HSOH=S+H2O	5.80E+29	-5.6		54450
178	HSOH=H2S+O	9.80E+16	-3.4		86444
179	H2SO=H2S+O	4.90E+28	-6.7		71540
180	H+SO2(+M)=HOSO(+M)	3.12E+08	1.6		7166
	Low pressure limit:	0.26620E+39	-0.64300E+01	0.55770E+4	
	TROE centering:	0.82000E+00	0.13088E+06	0.26600E+3	
181	HOSO+H=SO2+H2	3.00E+13	0		0
182	HOSO+H=SO+H2O	6.30E-10	6.3		-1908
183	HOSO+OH=SO2+H2O	1.00E+12	0		0

184	HSO2+H=SO2+H2	3.00E+13	0	0
185	HSO2+OH=SO2+H2O	1.00E+13	0	0
186	HSO2+O2=HO2+SO2	1.00E+13	0	0
187	H+SO2(+M)=HSO2(+M)	1.06E+09	1.5	1182
	Low pressure limit: 0.12510E+32 -0.51700E+01 0.15630E+4			
	TROE centering: 0.45000E+00 0.93550E+03 0.42700E+2			
188	HOSO2=HOSO+O	5.40E+18	-2.3	106316
189	HOSO2=SO3+H	1.40E+18	-2.9	54847
190	HOSO2+H=SO2+H2O	1.00E+12	0	0
191	HOSO2+O=SO3+OH	5.00E+12	0	0
192	HOSO2+OH=SO3+H2O	1.00E+12	0	0
193	HOSO2+O2=HO2+SO3	7.80E+11	0	656
194	HOSHO=HOSO+H	6.40E+30	-5.9	73726
195	HOSHO=SO+H2O	1.20E+24	-3.6	59616
196	HOSHO+H=HOSO+H2	1.30E+13	0	1000
197	HOSHO+O=HOSO+OH	1.50E+13	0	700
198	HOSHO+OH=HOSO+H2O	2.55E+12	0	500
199	SOH+OH=H2O+SO	2.40E+12	0	1500
200	SOH+O=HSO2	1.50E+16	-2.5	0
201	SOH+OH=HOSHO	1.50E+15	-2	0
202	C+SO2=CO+SO	4.16E+13	0	0
203	HOSO2+H=SO3+H2	1.00E+12	0	0
204	S+CH4=SH+CH3	6.00E+14	0	24000
205	H2S+CH3=CH4+SH	1.80E+11	0	2340
206	S+OH=SH+O	6.30E+11	0.5	8010
207	OCS+M=CO+S+M	1.43E+14	0	61000
208	O+OCS=CO+SO	1.93E+13	0	4627
209	O+OCS=CO2+S	5.00E+13	0	10990
210	CH+SO=CO+SH	1.00E+13	0	0
211	SO3+S=SO+SO2	5.12E+11	0	0
212	2O+M=O2+M	1.20E+17	-1	0
	H2	Enhanced by 2.400E+00		
	H2O	Enhanced by 1.540E+01		
	CH4	Enhanced by 2.000E+00		
	CO	Enhanced by 1.750E+00		
	CO2	Enhanced by 3.600E+00		
	C2H6	Enhanced by 3.000E+00		
	AR	Enhanced by 8.300E-01		
213	O+H+M=OH+M	5.00E+17	-1	0
	H2	Enhanced by 2.000E+00		
	H2O	Enhanced by 6.000E+00		
	CH4	Enhanced by 2.000E+00		
	CO	Enhanced by 1.500E+00		
	CO2	Enhanced by 2.000E+00		
	C2H6	Enhanced by 3.000E+00		
	AR	Enhanced by 7.000E-01		
214	O+H2=H+OH	3.87E+04	2.7	6260
215	O+HO2=OH+O2	2.00E+13	0	0

216	O+H2O2=OH+HO2	9.63E+06	2	4000
217	O+CH=H+CO	5.70E+13	0	0
218	O+CH2=H+HCO	8.00E+13	0	0
219	O+CH2(S)=H2+CO	1.50E+13	0	0
220	O+CH2(S)=H+HCO	1.50E+13	0	0
221	O+CH3=H+CH2O	5.06E+13	0	0
222	O+CH4=OH+CH3	1.02E+09	1.5	8600
223	O+HCO=OH+CO	3.00E+13	0	0
224	O+HCO=H+CO2	3.00E+13	0	0
225	O+CH2O=OH+HCO	3.90E+13	0	3540
226	O+C.H2OH=OH+CH2O	1.00E+13	0	0
227	O+CH3O=OH+CH2O	1.00E+13	0	0
228	O+CH3OH=OH+C.H2OH	3.88E+05	2.5	3100
229	O+CH3OH=OH+CH3O	1.30E+05	2.5	5000
230	O+C2H=CH+CO	5.00E+13	0	0
231	O+C2H2=H+HCCO	1.35E+07	2	1900
232	O+C2H2=OH+C2H	4.60E+19	-1.4	28950
233	O+C2H2=CO+CH2	6.94E+06	2	1900
234	O+C2H3=H+CH2CO	3.00E+13	0	0
235	O+C2H4=CH3+HCO	1.25E+07	1.8	220
236	O+C2H5=CH3+CH2O	2.24E+13	0	0
237	O+C2H6=OH+C2H5	8.98E+07	1.9	5690
238	O+HCCO=H+2CO	1.00E+14	0	0
239	O+CH2CO=OH+HCCO	1.00E+13	0	8000
240	O+CH2CO=CH2+CO2	1.75E+12	0	1350
241	O2+CO=O+CO2	2.50E+12	0	47800
242	O2+CH2O=HO2+HCO	1.00E+14	0	40000
243	H+O2+M=HO2+M	2.80E+18	-0.9	0
	O2 Enhanced by	0.000E+00		
	H2O Enhanced by	0.000E+00		
	CO Enhanced by	7.500E-01		
	CO2 Enhanced by	1.500E+00		
	C2H6 Enhanced by	1.500E+00		
	N2 Enhanced by	0.000E+00		
	AR Enhanced by	0.000E+00		
244	H+2O2=HO2+O2	2.08E+19	-1.2	0
245	H+O2+H2O=HO2+H2O	1.13E+19	-0.8	0
246	H+O2+N2=HO2+N2	2.60E+19	-1.2	0
247	H+O2+AR=HO2+AR	7.00E+17	-0.8	0
248	H+O2=O+OH	2.65E+16	-0.7	17041
249	2H+M=H2+M	1.00E+18	-1	0
	H2 Enhanced by	0.000E+00		
	H2O Enhanced by	0.000E+00		
	CH4 Enhanced by	2.000E+00		
	CO2 Enhanced by	0.000E+00		
	C2H6 Enhanced by	3.000E+00		
	AR Enhanced by	6.300E-01		
250	2H+H2=2H2	9.00E+16	-0.6	0

251	2H+H2O=H2+H2O	6.00E+19	-1.2	0
252	2H+CO2=H2+CO2	5.50E+20	-2	0
253	H+OH+M=H2O+M	2.20E+22	-2	0
	H2 Enhanced by	7.300E-01		
	H2O Enhanced by	3.650E+00		
	CH4 Enhanced by	2.000E+00		
	C2H6 Enhanced by	3.000E+00		
	AR Enhanced by	3.800E-01		
254	H+HO2=O+H2O	3.97E+12	0	671
255	H+HO2=O2+H2	4.48E+13	0	1068
256	H+HO2=2OH	8.40E+13	0	635
257	H+H2O2=HO2+H2	1.21E+07	2	5200
258	H+H2O2=OH+H2O	1.00E+13	0	3600
259	H+CH=C+H2	1.65E+14	0	0
260	H+CH2(+M)=CH3(+M)	6.00E+14	0	0
	Low pressure limit: 0.10400E+27 -0.27600E+01 0.16000E+4			
	TROE centering: 0.56200E+00 0.91000E+02 0.58360E+04 0.85520E+06			
	H2 Enhanced by	2.000E+00		
	H2O Enhanced by	6.000E+00		
	CH4 Enhanced by	2.000E+00		
	CO Enhanced by	1.500E+00		
	CO2 Enhanced by	2.000E+00		
	C2H6 Enhanced by	3.000E+00		
	AR Enhanced by	7.000E-01		
261	H+CH2(S)=CH+H2	3.00E+13	0	0
262	H+CH3(+M)=CH4(+M)	1.39E+16	-0.5	536
	Low pressure limit: 0.26200E+34 -0.47600E+01 0.24400E+4			
	TROE centering: 0.78300E+00 0.74000E+02 0.29410E+04 0.69640E+06			
	H2 Enhanced by	2.000E+00		
	H2O Enhanced by	6.000E+00		
	CH4 Enhanced by	3.000E+00		
	CO Enhanced by	1.500E+00		
	CO2 Enhanced by	2.000E+00		
	C2H6 Enhanced by	3.000E+00		
	AR Enhanced by	7.000E-01		
263	H+CH4=CH3+H2	6.60E+08	1.6	10840
264	H+HCO=H2+CO	7.34E+13	0	0
265	H+CH2O=HCO+H2	5.74E+07	1.9	2742
266	H+C.H2OH(+M)=CH3OH(+M)	1.06E+12	0.5	86
	Low pressure limit: 0.43600E+32 -0.46500E+01 0.50800E+4			
	TROE centering: 0.60000E+00 0.10000E+03 0.90000E+05 0.10000E+05			
	H2 Enhanced by	2.000E+00		
	H2O Enhanced by	6.000E+00		
	CH4 Enhanced by	2.000E+00		
	CO Enhanced by	1.500E+00		
	CO2 Enhanced by	2.000E+00		
	C2H6 Enhanced by	3.000E+00		
267	H+C.H2OH=H2+CH2O	2.00E+13	0	0

268	H+C.H2OH=OH+CH3	1.65E+11	0.7	-284
269	H+C.H2OH=CH2(S)+H2O	3.28E+13	-0.1	610
270	H+CH3O(+M)=CH3OH(+M)	2.43E+12	0.5	50
	Low pressure limit: 0.46600E+42 -0.74400E+01 0.14080E+5			
	TROE centering: 0.70000E+00 0.10000E+03 0.90000E+05 0.10000E+05			
	H2	Enhanced by	2.000E+00	
	H2O	Enhanced by	6.000E+00	
	CH4	Enhanced by	2.000E+00	
	CO	Enhanced by	1.500E+00	
	CO2	Enhanced by	2.000E+00	
	C2H6	Enhanced by	3.000E+00	
271	H+CH3O=H+C.H2OH	4.15E+07	1.6	1924
272	H+CH3O=H2+CH2O	2.00E+13	0	0
273	H+CH3O=OH+CH3	1.50E+12	0.5	-110
274	H+CH3O=CH2(S)+H2O	2.62E+14	-0.2	1070
275	H+CH3OH=C.H2OH+H2	1.70E+07	2.1	4870
276	H+CH3OH=CH3O+H2	4.20E+06	2.1	4870
277	H+C2H2(+M)=C2H3(+M)	5.60E+12	0	2400
	Low pressure limit: 0.38000E+41 -0.72700E+01 0.72200E+4			
	TROE centering: 0.75070E+00 0.98500E+02 0.13020E+04 0.41670E+06			
	H2	Enhanced by	2.000E+00	
	H2O	Enhanced by	6.000E+00	
	CH4	Enhanced by	2.000E+00	
	CO	Enhanced by	1.500E+00	
	CO2	Enhanced by	2.000E+00	
	C2H6	Enhanced by	3.000E+00	
	AR	Enhanced by	7.000E-01	
278	H+C2H3=H2+C2H2	3.00E+13	0	0
279	H+C2H4(+M)=C2H5(+M)	5.40E+11	0.5	1820
	Low pressure limit: 0.60000E+42 -0.76200E+01 0.69700E+4			
	TROE centering: 0.97530E+00 0.21000E+03 0.98400E+03 0.43740E+6			
	H2	Enhanced by	2.000E+00	
	H2O	Enhanced by	6.000E+00	
	CH4	Enhanced by	2.000E+00	
	CO	Enhanced by	1.500E+00	
	CO2	Enhanced by	2.000E+00	
	C2H6	Enhanced by	3.000E+00	
	AR	Enhanced by	7.000E-01	
280	H+C2H4=C2H3+H2	1.32E+06	2.5	12240
281	H+C2H5(+M)=C2H6(+M)	5.21E+17	-1	1580
	Low pressure limit: 0.19900E+42 -0.70800E+01 0.66850E+4			
	TROE centering: 0.84220E+00 0.12500E+03 0.22190E+04 0.68820E+06			
	H2	Enhanced by	2.000E+00	
	H2O	Enhanced by	6.000E+00	
	CH4	Enhanced by	2.000E+00	
	CO	Enhanced by	1.500E+00	
	CO2	Enhanced by	2.000E+00	
	C2H6	Enhanced by	3.000E+00	

	AR	Enhanced by	7.000E-01		
282	H+C2H5=H2+C2H4		2.00E+12	0	0
283	H+HCCO=CH2(S)+CO		1.00E+14	0	0
284	H+CH2CO=HCCO+H2		5.00E+13	0	8000
285	H+CH2CO=CH3+CO		1.13E+13	0	3428
286	H+HC#COH=H+CH2CO		1.00E+13	0	0
287	H2+CO(+M)=CH2O(+M)		4.30E+07	1.5	79600
Low pressure limit: 0.50700E+28 -0.34200E+01 0.84350E+5					
TROE centering: 0.93200E+00 0.19700E+03 0.15400E+04 0.10300E+07					
	H2	Enhanced by	2.000E+00		
	H2O	Enhanced by	6.000E+00		
	CH4	Enhanced by	2.000E+00		
	CO	Enhanced by	1.500E+00		
	CO2	Enhanced by	2.000E+00		
	C2H6	Enhanced by	3.000E+00		
	AR	Enhanced by	7.000E-01		
288	OH+H2=H+H2O		2.16E+08	1.5	3430
289	2OH=O+H2O		3.57E+04	2.4	-2110
290	OH+HO2=O2+H2O		1.45E+13	0	-500
Declared duplicate reaction...					
291	OH+H2O2=HO2+H2O		2.00E+12	0	427
Declared duplicate reaction...					
292	OH+H2O2=HO2+H2O		1.70E+18	0	29410
Declared duplicate reaction...					
293	OH+C=H+CO		5.00E+13	0	0
294	OH+CH=H+HCO		3.00E+13	0	0
295	OH+CH2=H+CH2O		2.00E+13	0	0
296	OH+CH2=CH+H2O		1.13E+07	2	3000
297	OH+CH2(S)=H+CH2O		3.00E+13	0	0
298	OH+CH3(+M)=CH3OH(+M)		2.79E+18	-1.4	1330
Low pressure limit: 0.40000E+37 -0.59200E+01 0.31400E+4					
TROE centering: 0.41200E+00 0.19500E+03 0.59000E+04 0.63940E+06					
	H2	Enhanced by	2.000E+00		
	H2O	Enhanced by	6.000E+00		
	CH4	Enhanced by	2.000E+00		
	CO	Enhanced by	1.500E+00		
	CO2	Enhanced by	2.000E+00		
	C2H6	Enhanced by	3.000E+00		
299	OH+CH3=CH2+H2O		5.60E+07	1.6	5420
300	OH+CH3=CH2(S)+H2O		6.44E+17	-1.3	1417
301	OH+CH4=CH3+H2O		1.00E+08	1.6	3120
302	OH+CO=H+CO2		4.76E+07	1.2	70
303	OH+HCO=H2O+CO		5.00E+13	0	0
304	OH+CH2O=HCO+H2O		3.43E+09	1.2	-447
305	OH+C.H2OH=H2O+CH2O		5.00E+12	0	0
306	OH+CH3O=H2O+CH2O		5.00E+12	0	0
307	OH+CH3OH=C.H2OH+H2O		1.44E+06	2	-840
308	OH+CH3OH=CH3O+H2O		6.30E+06	2	1500



309	OH+C2H=H+HCCO	2.00E+13	0	0
310	OH+C2H2=H+CH2CO	2.18E-04	4.5	-1000
311	OH+C2H2=H+HC#COH	5.04E+05	2.3	13500
312	OH+C2H2=C2H+H2O	3.37E+07	2	14000
313	OH+C2H2=CH3+CO	4.83E-04	4	-2000
314	OH+C2H3=H2O+C2H2	5.00E+12	0	0
315	OH+C2H4=C2H3+H2O	3.60E+06	2	6250
316	OH+C2H6=C2H5+H2O	3.54E+06	2.1	870
317	OH+CH2CO=HCCO+H2O	7.50E+12	0	2000
318	2HO2=O2+H2O2	4.20E+14	0	12000
	Declared duplicate reaction...			
319	HO2+CH2=OH+CH2O	2.00E+13	0	0
320	HO2+CH3=O2+CH4	1.00E+12	0	0
321	HO2+CO=OH+CO2	7.14E+07	1.57	17721
322	HO2+CH2O=HCO+H2O2	5.60E+06	2	12000
323	C+O2=O+CO	5.80E+13	0	576
324	C+CH2=H+C2H	5.00E+13	0	0
325	C+CH3=H+C2H2	5.00E+13	0	0
326	CH+O2=O+HCO	6.71E+13	0	0
327	CH+H2=H+CH2	1.08E+14	0	3110
328	CH+H2O=H+CH2O	5.71E+12	0	-755
329	CH+CH2=H+C2H2	4.00E+13	0	0
330	CH+CH3=H+C2H3	3.00E+13	0	0
331	CH+CH4=H+C2H4	6.00E+13	0	0
332	CH+CO(+M)=HCCO(+M)	5.00E+13	0	0
	Low pressure limit: 0.26900E+29 -0.37400E+01 0.19360E+4			
	TROE centering: 0.57570E+00 0.23700E+03 0.16520E+04			
	H2 Enhanced by 2.000E+00			
	H2O Enhanced by 6.000E+00			
	CH4 Enhanced by 2.000E+00			
	CO Enhanced by 1.500E+00			
	CO2 Enhanced by 2.000E+00			
	C2H6 Enhanced by 3.000E+00			
	AR Enhanced by 7.000E-01			
333	CH+CO2=HCO+CO	1.90E+14	0	15792
334	CH+CH2O=H+CH2CO	9.46E+13	0	-515
335	CH+HCCO=CO+C2H2	5.00E+13	0	0
336	CH2+O2=>OH+H+CO	5.00E+12	0	1500
337	CH2+H2=H+CH3	5.00E+05	2	7230
338	2CH2=H2+C2H2	1.60E+15	0	11944
339	CH2+CH3=H+C2H4	4.00E+13	0	0
340	CH2+CH4=2CH3	2.46E+06	2	8270
341	CH2+CO(+M)=CH2CO(+M)	8.10E+11	0.5	4510
	Low pressure limit: 0.26900E+34 -0.51100E+01 0.70950E+4			
	TROE centering: 0.59070E+00 0.27500E+03 0.12260E+04 0.51850E+06			
	H2 Enhanced by 2.000E+00			
	H2O Enhanced by 6.000E+00			
	CH4 Enhanced by 2.000E+00			

	CO	Enhanced by	1.500E+00			
	CO2	Enhanced by	2.000E+00			
	C2H6	Enhanced by	3.000E+00			
	AR	Enhanced by	7.000E-01			
342	CH2+HCCO=C2H3+CO		3.00E+13	0	0	
343	CH2(S)+N2=CH2+N2		1.50E+13	0	600	
344	CH2(S)+AR=CH2+AR		9.00E+12	0	600	
345	CH2(S)+O2=H+OH+CO		2.80E+13	0	0	
346	CH2(S)+O2=CO+H2O		1.20E+13	0	0	
347	CH2(S)+H2=CH3+H		7.00E+13	0	0	
348	CH2(S)+H2O(+M)=CH3OH(+M)		4.82E+17	-1.2	1145	
Low pressure limit: 0.18800E+39 -0.63600E+01 0.50400E+4						
TROE centering: 0.60270E+00 0.20800E+03 0.39220E+04 0.10180E+07						
	H2	Enhanced by	2.000E+00			
	H2O	Enhanced by	6.000E+00			
	CH4	Enhanced by	2.000E+00			
	CO	Enhanced by	1.500E+00			
	CO2	Enhanced by	2.000E+00			
	C2H6	Enhanced by	3.000E+00			
349	CH2(S)+H2O=CH2+H2O		3.00E+13	0	0	
350	CH2(S)+CH3=H+C2H4		1.20E+13	0	-570	
351	CH2(S)+CH4=2CH3		1.60E+13	0	-570	
352	CH2(S)+CO=CH2+CO		9.00E+12	0	0	
353	CH2(S)+CO2=CH2+CO2		7.00E+12	0	0	
354	CH2(S)+CO2=CO+CH2O		1.40E+13	0	0	
355	CH2(S)+C2H6=CH3+C2H5		4.00E+13	0	-550	
356	CH3+O2=O+CH3O		3.56E+13	0	30480	
357	CH3+O2=OH+CH2O		2.31E+12	0	20315	
358	CH3+H2O2=HO2+CH4		2.45E+04	2.5	5180	
359	2CH3=H+C2H5		6.84E+12	0.1	10600	
360	CH3+HCO=CH4+CO		2.65E+13	0	0	
361	CH3+CH2O=HCO+CH4		3.32E+03	2.8	5860	
362	CH3+CH3OH=C.H2OH+CH4		3.00E+07	1.5	9940	
363	CH3+CH3OH=CH3O+CH4		1.00E+07	1.5	9940	
364	CH3+C2H4=C2H3+CH4		2.27E+05	2	9200	
365	CH3+C2H6=C2H5+CH4		6.14E+06	1.7	10450	
366	HCO+H2O=H+CO+H2O		1.50E+18	-1	17000	
367	HCO+M=H+CO+M		1.87E+17	-1	17000	
	H2	Enhanced by	2.000E+00			
	H2O	Enhanced by	0.000E+00			
	CH4	Enhanced by	2.000E+00			
	CO	Enhanced by	1.500E+00			
	CO2	Enhanced by	2.000E+00			
	C2H6	Enhanced by	3.000E+00			
368	HCO+O2=HO2+CO		1.34E+13	0	400	
369	C.H2OH+O2=HO2+CH2O		1.80E+13	0	900	
370	CH3O+O2=HO2+CH2O		4.28E-13	7.6	-3530	
371	C2H+O2=HCO+CO		1.00E+13	0	-755	

372	C2H+H2=H+C2H2	5.68E+10	0.9	1993
373	C2H3+O2=HCO+CH2O	4.58E+16	-1.4	1015
374	C2H4(+M)=H2+C2H2(+M)	8.00E+12	0.4	86770
	Low pressure limit: 0.15800E+52 -0.93000E+01 0.97800E+5			
	TROE centering: 0.73450E+00 0.18000E+03 0.10350E+04 0.54170E+06			
	H2	Enhanced by	2.000E+00	
	H2O	Enhanced by	6.000E+00	
	CH4	Enhanced by	2.000E+00	
	CO	Enhanced by	1.500E+00	
	CO2	Enhanced by	2.000E+00	
	C2H6	Enhanced by	3.000E+00	
	AR	Enhanced by	7.000E-01	
375	HCCO+O2=OH+2CO	3.20E+12	0	854
376	2HCCO=2CO+C2H2	1.00E+13	0	0
377	O+CH3=H+H2+CO	3.37E+13	0	0
378	O+C2H4=H+C.CHO	6.70E+06	1.8	220
379	O+C2H5=H+CH3CHO	1.10E+14	0	0
380	OH+HO2=O2+H2O	5.00E+15	0	17330
	Declared duplicate reaction...			
381	OH+CH3=H2+CH2O	8.00E+09	0.5	-1755
382	CH+H2(+M)=CH3(+M)	1.97E+12	0.4	-370
	Low pressure limit: 0.48200E+26 -0.28000E+01 0.59000E+3			
	TROE centering: 0.57800E+00 0.12200E+03 0.25350E+04 0.93650E+06			
	H2	Enhanced by	2.000E+00	
	H2O	Enhanced by	6.000E+00	
	CH4	Enhanced by	2.000E+00	
	CO	Enhanced by	1.500E+00	
	CO2	Enhanced by	2.000E+00	
	C2H6	Enhanced by	3.000E+00	
	AR	Enhanced by	7.000E-01	
383	CH2+O2=2H+CO2	5.80E+12	0	1500
384	CH2+O2=O+CH2O	2.40E+12	0	1500
385	CH2+CH2=2H+C2H2	2.00E+14	0	10989
386	CH2(S)+H2O=H2+CH2O	6.82E+10	0.2	-935
387	C2H3+O2=O+C.CHO	3.03E+11	0.3	11
388	C2H3+O2=HO2+C2H2	1.34E+06	1.6	-384
389	O+CH3CHO=OH+C.CHO	2.92E+12	0	1808
390	O+CH3CHO=OH+CH3+CO	2.92E+12	0	1808
391	O2+CH3CHO=HO2+CH3+CO	3.01E+13	0	39150
392	H+CH3CHO=C.CHO+H2	2.05E+09	1.2	2405
393	H+CH3CHO=CH3+H2+CO	2.05E+09	1.2	2405
394	OH+CH3CHO=CH3+H2O+CO	2.34E+10	0.7	-1113
395	HO2+CH3CHO=CH3+H2O2+CO	3.01E+12	0	11923
396	CH3+CH3CHO=CH3+CH4+CO	2.72E+06	1.8	5920
397	H+CH2CO(+M)=C.CHO(+M)	4.86E+11	0.4	-1755
	Low pressure limit: 0.10120E+43 -0.76300E+01 0.38540E+4			
	TROE centering: 0.46500E+00 0.20100E+03 0.17730E+04 0.53330E+06			
	H2	Enhanced by	2.000E+00	

	H2O	Enhanced by	6.000E+00		
	CH4	Enhanced by	2.000E+00		
	CO	Enhanced by	1.500E+00		
	CO2	Enhanced by	2.000E+00		
	C2H6	Enhanced by	3.000E+00		
	AR	Enhanced by	7.000E-01		
398	O+C.CHO=H+CH2+CO2		1.50E+14	0	0
399	H+C.CHO=CH3+HCO		2.20E+13	0	0
400	H+C.CHO=CH2CO+H2		1.10E+13	0	0
401	OH+C.CHO=H2O+CH2CO		1.20E+13	0	0
402	OH+C.CHO=HCO+C.H2OH		3.01E+13	0	0
403	CH3+C2H5(+M)=CCC(+M)		9.43E+12	0	0
Low pressure limit: 0.27100E+75 -0.16820E+02 0.13065E+5					
TROE centering: 0.15270E+00 0.29100E+03 0.27420E+04 0.77480E+06					
	H2	Enhanced by	2.000E+00		
	H2O	Enhanced by	6.000E+00		
	CH4	Enhanced by	2.000E+00		
	CO	Enhanced by	1.500E+00		
	CO2	Enhanced by	2.000E+00		
	C2H6	Enhanced by	3.000E+00		
	AR	Enhanced by	7.000E-01		
404	CH3+C2H4(+M)=CCC(+M)		2.55E+06	1.6	5700
Low pressure limit: 0.30000E+64 -0.14600E+02 0.18170E+5					
TROE centering: 0.18940E+00 0.27700E+03 0.87480E+04 0.78910E+06					
	H2	Enhanced by	2.000E+00		
	H2O	Enhanced by	6.000E+00		
	CH4	Enhanced by	2.000E+00		
	CO	Enhanced by	1.500E+00		
	CO2	Enhanced by	2.000E+00		
	C2H6	Enhanced by	3.000E+00		
	AR	Enhanced by	7.000E-01		
405	O+CCC.=C2H5+CH2O		9.64E+13	0	0
406	H+CCC.(+M)=CCC(+M)		3.61E+13	0	0
Low pressure limit: 0.44200E+62 -0.13545E+02 0.11357E+5					
TROE centering: 0.31500E+00 0.36900E+03 0.32850E+04 0.66670E+6					
	H2	Enhanced by	2.000E+00		
	H2O	Enhanced by	6.000E+00		
	CH4	Enhanced by	2.000E+00		
	CO	Enhanced by	1.500E+00		
	CO2	Enhanced by	2.000E+00		
	C2H6	Enhanced by	3.000E+00		
	AR	Enhanced by	7.000E-01		
407	OH+CCC.=C2H5+C.H2OH		2.41E+13	0	0
408	HO2+CCC.=OH+C2H5+CH2O		2.41E+13	0	0
409	CH3+CCC.=2C2H5		1.93E+13	-0.3	0
410	C2H5+O2=CCOO.		2.34E+55	-14	12838
411	C2H5+O2=CH3CHO+OH		1.28E+05	1.7	6717
412	C2H5+O2=CCO.+O		1.29E+11	0.4	26534

413	$C_2H_5 + O_2 = C.COOH$	1.09E+59	-16	18879
414	$C_2H_5 + O_2 = CY(CCO) + OH$	1.83E+13	-1	7344
415	$CCOO. = CH_3CHO + OH$	2.23E+46	-11.3	51649
416	$CCOO. = C_2H_4 + HO_2$	2.68E+38	-8.1	40474
417	$CCOO. = CCO. + O$	2.10E+43	-12.8	71158
418	$CCOO. = C.COOH$	3.08E+43	-10.2	46455
419	$C.COOH = C_2H_4 + HO_2$	4.10E+50	-12.1	33779
420	$C.COOH = CY(CCO) + OH$	6.43E+49	-11.9	33773
421	$C.COOH + O_2 = HOCCOO.$	1.03E+69	-18.2	18040
422	$C.COOH + O_2 = HOOCCHO + OH$	1.73E+00	3.3	7339
	Declared duplicate reaction...			
423	$C.COOH + O_2 = HOOCCHO + OH$	4.74E+16	-1.6	8338
	Declared duplicate reaction...			
424	$C.COOH + O_2 = C*COOH + HO_2$	1.65E+15	-1	8148
425	$C.COOH + O_2 = OH + JOCCOOJ$	3.84E+08	1.2	9589
426	$HOCCOO. = HOOCCHO + OH$	9.97E+44	-10.5	50776
	Declared duplicate reaction...			
427	$HOCCOO. = HOOCCHO + OH$	7.83E+35	-7.4	39264
	Declared duplicate reaction...			
428	$HOCCOO. = C*COOH + HO_2$	3.24E+36	-7.4	40191
429	$HOCCOO. = OH + JOCCOOJ$	5.85E+57	-14.2	54871
430	$C.CHO + O_2 = HC(*O)COO$	2.93E+59	-15.4	15629
431	$C.CHO + O_2 = CH_2CO + HO_2$	1.20E+07	1.7	22617
	Declared duplicate reaction...			
432	$C.CHO + O_2 = C.*OCOOH$	4.66E+48	-16.5	15011
433	$C.CHO + O_2 = CH_2CO + HO_2$	6.17E+03	0	6389
	Declared duplicate reaction...			
434	$C.CHO + O_2 = CO + CH_2O + OH$	4.89E+23	-4	8759
435	$HC(*O)COO = CH_2CO + HO_2$	3.28E+46	-13	50526
436	$HC(*O)COO = C.*OCOOH$	5.73E+35	-7.8	27822
437	$C.*OCOOH = CH_2CO + HO_2$	9.81E+50	-15.6	46037
438	$C.*OCOOH = CO + CH_2O + OH$	2.82E+61	-14.8	31304
439	$CH_3C.*O + O_2 = O*COO.C$	1.66E+66	-17.2	17343
440	$CH_3C.*O + O_2 = CH_2CO + HO_2$	8.38E+17	-1.8	7947
	Declared duplicate reaction...			
441	$CH_3C.*O + O_2 = CCO_2 + O$	1.55E+13	-0.3	22547
442	$CH_3C.*O + O_2 = C.CO_3H$	4.23E+57	-15.3	18424
443	$CH_3C.*O + O_2 = CH_2CO + HO_2$	1.66E+12	-1.9	8495
	Declared duplicate reaction...			
444	$CH_3C.*O + O_2 = O*YCOC + OH$	1.30E+29	-5.2	9829
445	$O*COO.C = CH_2CO + HO_2$	2.27E+56	-13.9	48198
446	$O*COO.C = CCO_2 + O$	1.88E+62	-18.3	63972
447	$O*COO.C = C.CO_3H$	3.79E+37	-7.9	35636
448	$C.CO_3H = CH_2CO + HO_2$	7.69E+31	-9.7	34076
449	$C.CO_3H = O*YCOC + OH$	4.53E+42	-9.8	27093
450	$C*CCJ + O_2 = C*CCOO.$	9.26E+69	-18	22771
451	$C*CCJ + O_2 = C*CCHO + OH$	6.83E+06	1.4	19827
452	$C*CCJ + O_2 = C*C*C + HO_2$	4.77E+06	1.5	18806

Declared duplicate reaction...				
453	$C*CCJ+O2=C.*CCOOH$	6.87E+64	-16.8	34978
454	$C*CCJ+O2=C2H2+CH2O+OH$	4.47E+32	-6	33634
455	$C*CCJ+O2=YC*CCO+OH$	3.60E+37	-7.9	31118
456	$C*CCJ+O2=C*C.CO OH$	6.34E+72	-19.5	43199
457	$C*CCJ+O2=C*C*C+HO2$	2.62E+27	-4.7	33576
Declared duplicate reaction...				
458	$C*CCJ+O2=C*YCOC+OH$	5.42E+18	-2.5	32997
459	$C*CCJ+O2=C*YCC.CO O$	6.55E+40	-9.3	23261
460	$C*CCJ+O2=C.CHO+CH2O$	3.75E+12	-0.4	28424
Declared duplicate reaction...				
461	$C*CCJ+O2=C.CYCCOO$	1.46E+83	-23.2	37274
462	$C*CCJ+O2=C.CHO+CH2O$	9.76E+07	0.7	23437
Declared duplicate reaction...				
463	$C*CCJ+O2=C.CHO+CH2O$	9.08E+18	-2.4	22126
Declared duplicate reaction...				
464	$C*CCOO.=C*CCHO+OH$	4.54E+68	-19.1	52413
465	$C*CCOO.=C*C*C+HO2$	3.61E+65	-17.9	50850
466	$C*CCOO.=C.*CCOOH$	2.11E+55	-14.4	42707
467	$C*CCOO.=C*C.CO OH$	3.99E+67	-18.9	52459
468	$C*CCOO.=CYCC.CO O$	1.04E+53	-13.7	38779
469	$C*CCOO.=C.CYCCOO$	8.45E+58	-15.6	44069
470	$C.*CCOOH=C2H2+CH2O+OH$	2.78E+51	-11.6	43478
471	$C.*CCOOH=YC*CCO+OH$	3.95E+32	-6.4	26811
472	$C*C.CO OH=C*C*C+HO2$	3.95E+61	-14.8	41373
473	$C*C.CO OH=C*YCOC+OH$	1.53E+57	-14	41385
474	$CYCC.CO O=C.CHO+CH2O$	1.19E+42	-9.1	51504
475	$C.CYCCOO=C.CHO+CH2O$	2.53E+50	-12.7	32930
Declared duplicate reaction...				
476	$C.CYCCOO=C.CHO+CH2O$	1.98E+51	-12.1	32676
Declared duplicate reaction...				
477	$CC.C+O2=CCQJC$	1.77E+75	-20.4	17652
478	$CC.C+O2=C*CC+HO2$	2.90E+23	-3.5	8978
Declared duplicate reaction...				
479	$CC.C+O2=C2C*O+OH$	9.80E+15	-2	10200
480	$CC.C+O2=CJCQC$	5.35E+82	-24	25205
481	$CC.C+O2=C*YCOC+OH$	1.21E+22	-3.4	13339
482	$CC.C+O2=C*CC+HO2$	6.41E+19	-2.8	13160
Declared duplicate reaction...				
483	$CCQJC=C*CC+HO2$	1.55E+26	-4.4	31437
484	$CCQJC=C2C*O+OH$	9.68E+53	-13.7	51058
485	$CCQJC=CJCQC$	2.22E+22	-3.5	34879
486	$CJCQC=C*YCOC+OH$	5.93E+19	-2.5	18016
487	$CJCQC=C*CC+HO2$	7.93E+16	-1.8	16979
488	$CCC.+O2=CCCQJ$	7.57E+56	-14.4	12849
489	$CCC.+O2=C*CC+HO2$	3.24E+17	-1.6	8225
Declared duplicate reaction...				
490	$CCC.+O2=CCC*O+OH$	1.25E+12	-0.2	12231

491	CCC.+O2=CCJCQ	4.94E+67	-18.5	21895
492	CCC.+O2=CYCOC+OH	1.45E+23	-3.5	14519
493	CCC.+O2=C*CC+HO2	1.50E+23	-3.4	14575
	Declared duplicate reaction...			
494	CCC.+O2=CJCCQ	1.38E+78	-21.8	24422
495	CCC.+O2=YCCCO+OH	2.31E+25	-3.9	24138
496	CCC.+O2=C2H4+CH2O+OH	1.06E+29	-4.4	28941
497	CCCQJ=C*CC+HO2	6.42E+34	-7.1	37621
498	CCCQJ=CCC*O+OH	3.40E+46	-11.1	50588
499	CCCQJ=CCJCQ	1.93E+21	-3.2	32356
500	CCCQJ=CJCCQ	5.75E+13	-0.8	27704
501	CCJCQ=CYCOC+OH	2.95E+41	-9.5	25766
502	CCJCQ=C*CC+HO2	9.21E+41	-9.5	25884
503	CJCCQ=YCCCO+OH	3.34E+45	-11	32452
504	CJCCQ=C2H4+CH2O+OH	5.83E+50	-12.2	37165
505	CC.CO+H+O2=CCQ.CO	1.69+124	-34.7	41355
506	CC.CO+H+O2=CC*CO+HO2	1.25E+43	-9	21090
	Declared duplicate reaction...			
507	CC.CO+H+O2=C*CCO+HO2	1.08E+40	-8.2	20385
	Declared duplicate reaction...			
508	CC.CO+H+O2=CCQCO.	6.74E+82	-23.4	29701
509	CC.CO+H+O2=CH2O+CH3CHO+OH	2.01E+42	-8.8	20733
510	CC.CO+H+O2=CCQC.OH	3.46+138	-39.3	51942
511	CC.CO+H+O2=CC*CO+HO2	1.50E+54	-12.6	24196
	Declared duplicate reaction...			
512	CC.CO+H+O2=C.CQCOH	2.32+152	-43.7	63209
513	CC.CO+H+O2=C*CCO+HO2	1.63E+54	-12.6	33490
	Declared duplicate reaction...			
514	CCQ.CO=CC*CO+HO2	2.05E+25	-4.1	29876
515	CCQ.CO=C*CCO+HO2	7.49E+30	-5.9	34293
516	CCQ.CO=CCQCO.	2.79E+28	-5.1	31899
517	CCQ.CO=CCQC.OH	1.00E+55	-13.3	43012
518	CCQ.CO=C.CQCOH	1.26E+43	-10	44057
519	CCQCO.=CH2O+CH3CHO+OH	4.41E-44	16.8	-7074
520	CCQC.OH=CC*CO+HO2	2.73E+32	-6.6	25773
521	C.CQCOH=C*CCO+HO2	1.11E+60	-14.8	38734
522	C2.CO+H+O2=CCOHCQ.	1.09+109	-30	35777
523	C2.CO+H+O2=C*COHC+HO2	6.63E+35	-6.8	16570
	Declared duplicate reaction...			
524	C2.CO+H+O2=CCO.CQ	3.38E+77	-21.8	31477
525	C2.CO+H+O2=QCC*O+CH3	1.15E+26	-4.7	20734
526	C2.CO+H+O2=CH3CHO+CH2O+OH	1.60E+29	-4.7	15836
527	C2.CO+H+O2=C.COHCQ	1.84E+55	-15.6	11169
528	C2.CO+H+O2=C*CCOOH+OH	5.75E+48	-10.8	29194
529	C2.CO+H+O2=C*CO+CH2O+OH	9.23E+46	-10.5	27167
530	C2.CO+H+O2=CC.OHCQ	5.88+101	-27.7	38783
531	C2.CO+H+O2=C*COHC+HO2	2.49E+51	-11.6	25206
	Declared duplicate reaction...			

532	CCOHCQ.=C*COHC+HO2	4.01E+45	-10.2	40760
533	CCOHCQ.=CCO.CQ	3.31E+23	-3.6	30012
534	CCOHCQ.=C.COHCQ	1.21E+16	-1.7	22366
535	CCOHCQ.=CC.OHCQ	7.22E+50	-12.1	41124
536	CCO.CQ=QCC*O+CH3	1.10E-25	9.7	796
537	CCO.CQ=CH3CHO+CH2O+OH	2.02E-18	9.2	915
538	C.COHCQ=C*CCOOH+OH	6.12E+94	-26.4	49899
539	C.COHCQ=C*COH+CH2O+OH	1.40E+80	-22.2	41919
540	CC.OHCQ=C*COHC+HO2	1.02E+39	-8.6	28338
541	CCJCQ+O2=CCQJCQ	4.40+144	-42.7	37414
542	CCJCQ+O2=CC*OCQ+OH	1.66E+22	-3.8	14971
	Declared duplicate reaction...			
543	CCJCQ+O2=CCQC*O+OH	7.86E+33	-7	12806
	Declared duplicate reaction...			
544	CCJCQ+O2=CC*COOH+HO2	1.31E+28	-4.9	12976
545	CCJCQ+O2=C*CCOOH+HO2	4.51E+25	-4.3	12755
	Declared duplicate reaction...			
546	CCJCQ+O2=CCQJCOJT+OH	7.21E+29	-5.2	16380
547	CCJCQ+O2=CCQJCOJS+OH	9.65E+29	-5.2	16274
548	CCJCQ+O2=CCQCQJ	7.00+145	-42.9	42548
549	CCJCQ+O2=CC*OCQ+OH	1.14E+56	-14.1	23638
	Declared duplicate reaction...			
550	CCJCQ+O2=CCQC*O+OH	6.29E+51	-13	26621
	Declared duplicate reaction...			
551	CCJCQ+O2=C*QC+HO2	2.35E+51	-12.4	23610
552	CCJCQ+O2=CCOJCQJT+OH	5.39E+52	-12.7	26968
553	CCJCQ+O2=CCOJCQJS+OH	1.25E+53	-12.8	26797
554	CCJCQ+O2=CJCQC+O2	2.02E+56	-13.7	24936
555	CCJCQ+O2=CJCQCQ	2.76E+92	-27.9	29049
	Declared duplicate reaction...			
556	CCJCQ+O2=QCYCOC+OH	7.77E+16	-2.6	13049
	Declared duplicate reaction...			
557	CCJCQ+O2=QYCCOC+OH	6.14E+09	-0.8	15104
	Declared duplicate reaction...			
558	CCJCQ+O2=C*CQ+CH2O+OH	4.77E+11	-0.7	18081
	Declared duplicate reaction...			
559	CCJCQ+O2=C*CCOOH+HO2	1.50E+21	-3.4	13359
	Declared duplicate reaction...			
560	CCQJCQ=CC*OCQ+OH	3.24E+53	-13.6	49660
561	CCQJCQ=CCQC*O+OH	4.74E+39	-8.9	34719
562	CCQJCQ=CC*COOH+HO2	4.60E+14	-1.1	23803
563	CCQJCQ=C*CCOOH+HO2	2.99E+19	-2.6	27903
564	CCQJCQ=CCQJCOJT+OH	3.93E+69	-17.6	54722
565	CCQJCQ=CCQJCOJS+OH	1.24E+69	-17.4	54348
566	CCQJCQ=CCQCQJ	3.05E+14	-1.6	13796
567	CCQJCQ=CJCQCQ	2.07E+27	-5.4	35547
568	CCQCQJ=CC*OCQ+OH	7.04E+36	-8.1	33487
569	CCQCQJ=CCQC*O+OH	9.10E+59	-15.1	51906



570	CCQCQJ=C*CQC+HO2	5.89E+31	-6.2	33203
571	CCQCQJ=CCOJCQJT+OH	4.28E+63	-15.7	53553
572	CCQCQJ=CCOJCQJS+OH	4.90E+62	-15.4	52766
573	CCQCQJ=CJCQC+O2	8.35E+50	-11.7	43155
	Declared duplicate reaction...			
574	CJCQCQ=QCYCOC+OH	2.35E-15	8	4787
	Declared duplicate reaction...			
575	CJCQCQ=QYCCOC+OH	1.29E-72	24.9	-8985
	Declared duplicate reaction...			
576	CJCQCQ=C*CQ+CH2O+OH	4.43-112	37.5	-15562
	Declared duplicate reaction...			
577	CJCQCQ=C*CCOOH+HO2	2.23E-26	11.8	-159
	Declared duplicate reaction...			
578	CCJCQ+O2=CJCQCQ	1.81+101	-30.6	31015
	Declared duplicate reaction...			
579	CCJCQ+O2=QCYCOC+OH	6.88E+49	-12.4	24873
	Declared duplicate reaction...			
580	CCJCQ+O2=QYCCOC+OH	3.30E+40	-10.2	25644
	Declared duplicate reaction...			
581	CCJCQ+O2=C*CQ+CH2O+OH	8.60E+42	-10.5	28344
	Declared duplicate reaction...			
582	CCJCQ+O2=C*CCOOH+HO2	3.62E+52	-12.8	24467
	Declared duplicate reaction...			
583	CJCQCQ=QCYCOC+OH	3.90E-27	11.4	-1876
	Declared duplicate reaction...			
584	CJCQCQ=QYCCOC+OH	1.63E-78	26.6	-11032
	Declared duplicate reaction...			
585	CJCQCQ=C*CQ+CH2O+OH	3.43-118	39.3	-17684
	Declared duplicate reaction...			
586	CJCQCQ=C*CCOOH+HO2	4.86E-37	14.9	-5388
	Declared duplicate reaction...			
587	CJCQC+O2=CCQCQJ	2.69+137	-40.4	35136
	Declared duplicate reaction...			
588	CJCQC+O2=CC*OCQ+OH	3.02E+32	-6.5	12712
	Declared duplicate reaction...			
589	CJCQC+O2=CCQC*O+OH	4.32E+28	-5.2	17440
	Declared duplicate reaction...			
590	CJCQC+O2=C*CQC+HO2	6.62E+27	-4.8	12673
591	CJCQC+O2=CCOJCQJT+OH	9.10E+29	-5.1	18087
592	CJCQC+O2=CCOJCQJS+OH	1.38E+30	-5.1	17773
593	CJCQC+O2=CJCQCQ	3.68E+91	-27.7	23006
	Declared duplicate reaction...			
594	CJCQC+O2=QCYCOC+OH	3.44E+29	-6	14132
	Declared duplicate reaction...			
595	CJCQC+O2=QYCCOC+OH	1.72E+19	-3.3	15838
	Declared duplicate reaction...			
596	CJCQC+O2=C*CQ+CH2O+OH	3.44E+22	-3.6	19940
	Declared duplicate reaction...			

597	CJCQC+O2=C*CCOOH+HO2	3.21E+31	-6.1	13835
	Declared duplicate reaction...			
598	CJCQC+O2=CCQJCQ	4.05+141	-41.5	41134
599	CJCQC+O2=CC*OCQ+OH	3.57E+47	-11.9	26666
	Declared duplicate reaction...			
600	CJCQC+O2=CCQC*O+OH	3.65E+55	-13.8	23954
	Declared duplicate reaction...			
601	CJCQC+O2=CC*COOH+HO2	1.54E+46	-10.5	23205
602	CJCQC+O2=C*CCOOH+HO2	1.15E+45	-10.3	23339
	Declared duplicate reaction...			
603	CJCQC+O2=CCQJCOJT+OH	2.79E+55	-13.4	27830
604	CJCQC+O2=CCQJCOJS+OH	3.81E+55	-13.4	27751
605	CJCQC+O2=CJCQCQ	4.77E+91	-27.3	34276
	Declared duplicate reaction...			
606	CJCQC+O2=QCYCOC+OH	2.02E+38	-9.2	24489
	Declared duplicate reaction...			
607	CJCQC+O2=QYCCOC+OH	5.30E+34	-8.7	26940
	Declared duplicate reaction...			
608	CJCQC+O2=C*CQ+CH2O+OH	5.34E+36	-8.8	29255
	Declared duplicate reaction...			
609	CJCQC+O2=C*CCOOH+HO2	1.26E+44	-10.5	25052
	Declared duplicate reaction...			
610	2CCCQJ=2CCCO.+O2	2.60E+11	0	0
611	2CCCQJ=CCCOH+CCCHO+O2	1.60E+11	0	0
612	2CCQJC=2C2CO.+O2	1.39E+12	0	5090
613	2CCQJC=C2COH+C2C*O+O2	2.47E+10	0	2860
614	CCCQJ+CCQJC=CCCO.+C2CO.+O2	2.60E+11	0	0
615	CCCQJ+CCQJC=CCCHO+C2COH+O2	1.60E+11	0	0
616	CCCQJ+CCQJC=CCCOH+C2C*O+O2	1.60E+11	0	0
617	CCC.+CCCQJ=CCCO.+CCCO.	7.93E+13	-0.3	406
618	CC.C+CCCQJ=CCCO.+C2CO.	7.93E+13	-0.3	406
619	CCC.+CCQJC=CCCO.+C2CO.	7.93E+13	-0.3	406
620	CC.C+CCQJC=C2CO.+C2CO.	7.93E+13	-0.3	406
621	CCCO.=CCCHO+H	5.66E+06	0.4	4484
	Declared duplicate reaction...			
622	CCCO.=C2H5+CH2O	3.19E+06	0.3	-236
623	CCCO.=CCC.OH	8.39E+00	0.2	16489
624	CCCO.=CCCHO+H	8.18E+05	0.2	26914
	Declared duplicate reaction...			
625	CCCO.=CH3+C*COH	6.25E+06	0	26927
626	CCCO.=H+CC*COH	5.56E+03	0.9	27103
	Declared duplicate reaction...			
627	CCCO.=CC.COH	8.95E-02	0.5	14110
628	CCCO.=C*CC+OH	2.44E+05	0.1	27917
629	CCCO.=H+CC*COH	3.22E+05	0.2	27930
	Declared duplicate reaction...			
630	CCCO.=H+C*CCOH	1.25E+03	0.8	28423
	Declared duplicate reaction...			

631	CCCO.=C.CCOH	4.09E+56	-15.3	26123
632	CCCO.=C2H4+C.H2OH	1.52E+14	-2.4	7921
633	CCCO.=H+C*CCOH	8.17E+08	-0.8	14941
	Declared duplicate reaction...			
634	C2CO.=C2C*O+H	1.90E+10	-1.3	1607
	Declared duplicate reaction...			
635	C2CO.=CH3CHO+CH3	4.43E+08	-0.1	3929
	Declared duplicate reaction...			
636	C2CO.=C2C.OH	9.46E+02	-0.2	17665
637	C2CO.=C2C*O+H	2.75E+06	0.2	26948
	Declared duplicate reaction...			
638	C2CO.=H+C*C(OH)C	2.14E+07	-0.1	26946
	Declared duplicate reaction...			
639	C2CO.=C2.CO	3.45E+05	-1.3	17472
640	C2CO.=C*CC+OH	4.57E+07	-0.4	28398
641	C2CO.=CH3CHO+CH3	1.11E+05	0.4	29048
	Declared duplicate reaction...			
642	C2CO.=H+C*C(OH)C	1.11E+05	0.4	29048
	Declared duplicate reaction...			
643	CCCQJ+OH=CCCO.+HO2	2.41E+13	0	0
644	CCQJC+OH=C2CO.+HO2	2.41E+13	0	0
645	CCC.+HO2=CCCO.+OH	2.55E+22	-2.9	5062
646	CC.C+HO2=C2CO.+OH	2.55E+22	-2.9	5062
647	CCC+H=CC.C+H2	4.80E+08	1.5	5690
648	CCC+H=CCC.+H2	1.44E+09	1.5	7412
649	CCC+O=CC.C+OH	3.33E+08	1.5	3815
650	CCC+O=CCC.+OH	9.99E+08	1.5	5802
651	CCC+OH=CC.C+H2O	2.41E+06	2	-461
652	CCC+OH=CCC.+H2O	7.22E+06	2	864
653	CCC+HO2=CC.C+H2O2	2.90E+04	2.7	17262
654	CCC+HO2=CCC.+H2O2	8.70E+04	2.7	18852
655	CCC+O2=CC.C+HO2	6.00E+13	0	50150
656	CCC+O2=CCC.+HO2	1.80E+14	0	52800
657	CCC+CH3=CC.C+CH4	1.63E+06	1.9	8908
658	CCC+CH3=CCC.+CH4	4.89E+06	1.9	10630
659	CH3CHO+CCC.=CH3C.*O+CCC	6.55E+03	2.5	6872
660	CH3CHO+CCC.=C.CHO+CCC	1.27E+04	2.5	10363
661	CH3CHO+CC.C=CH3C.*O+CCC	1.38E+02	2.9	7592
662	CH3CHO+CC.C=C.CHO+CCC	2.67E+02	2.9	11083
663	CCC+CCC.=CC.C+CCC	1.31E+04	2.5	9990
664	CCC=CCC.+H	3.79E+71	-17	123908
665	CCC=H+CC.C	2.61E+74	-17.8	123075
666	CCC=CH3+C2H5	4.07E+82	-19.5	118513
667	CCC.+H=H+CC.C	6.32E+07	1.4	5679
668	CCC.+H=CH3+C2H5	5.74E+19	-1.6	5229
669	H+CC.C=CH3+C2H5	5.58E+21	-2.1	7201
670	CH3+C2H4=CCC.	3.02E+31	-6.5	11926
671	CCC.=C*CC+H	1.57E+28	-5.2	36039

672	CC.C=H+C*CC	1.61E+47	-10.4	50324
673	CH3+C2H4=C*CC+H	2.64E+20	-2.4	21368
674	CCC.=CC.C	5.80E+33	-6.5	45457
675	H+CCC.=C*CC+H2	1.80E+12	0	0
676	OH+CCC.=C*CC+H2O	2.40E+13	0	0
677	CH3+CCC.=C*CC+CH4	1.10E+13	0	0
678	C2H5+CCC.=C*CC+C2H6	1.00E+13	0	0
679	CCC.+C2H5=C2H4+CCC	1.00E+13	0	0
680	CCC.+HCO=CO+CCC	6.00E+13	0	0
681	2CCC.=C*CC+CCC	1.00E+13	0	0
682	H+CC.C=C*CC+H2	3.20E+12	0	0
683	OH+CC.C=C*CC+H2O	2.40E+13	0	0
684	CH3+CC.C=C*CC+CH4	2.20E+14	-0.7	0
685	C2H5+CC.C=C*CC+C2H6	1.00E+13	0	0
686	CC.C+C2H5=C2H4+CCC	1.00E+13	0	0
687	CC.C+HCO=CO+CCC	1.20E+14	0	0
688	2CC.C=C*CC+CCC	1.00E+13	0	0
689	CCC.+CC.C=C*CC+CCC	1.00E+13	0	0
690	CCSCC+H=CJCSCC+H2	3.46E+07	2	9471
691	CCSCC+CH3=CJCSCC+CH4	9.78E+03	3	13700
692	CCSCC+O=CJCSCC+OH	1.02E+09	1.5	4500
693	CCJSCC=C*CSCC+H	3.00E+13	0	41670
694	CCJSCC=CH3CH*S+C2H5	9.15E+11	0.6	25690
695	CCJSCC=CJCSCC	2.34E+06	1.2	25850
696	CJCSCC=C2H4+CCSJ	2.63E+12	0.1	19000
697	CJCSCC=C*CSCC+H	1.39E+07	1.6	35500
698	CCSCC=CCSH+C2H4	5.20E+06	1.9	63637
699	CCSCC+SH=CJCSCC+H2S	7.29E+06	1.9	13120
700	CCSCC+SH=CCJSCC+H2S	4.86E+06	1.9	18430
701	CCSJ+H=SH+C2H5	1.00E+13	0	500
702	CCSJ=CH3+CH2S	8.61E+12	0.8	42000
703	CCJSH=CH3+CH2S	1.38E+12	0	35900
704	2CCSJ=CCSSCC	1.00E+13	0	0
705	CCSSCC=CCSSH+C2H4	3.31E+08	1.4	55100
706	2SH=HSSH	2.50E+13	0	0
707	SH+CCSJ=CCSSH	1.50E+13	0	0
708	CCSSH=HSSH+C2H4	1.21E+08	1.4	55520
709	HCS+HCS=S*CC*S	1.00E+13	0	0
710	CCJSCC+O2=CCQJSCC	5.47E+38	-9.2	1293
711	CCJSCC+O2=C*CSCC+HO2	3.07E+14	-1	2981
	Declared duplicate reaction...			
712	CCJSCC+O2=CC*OSCC+OH	4.82E+05	1.1	14389
713	CCJSCC+O2=CJCQSCC	8.98E+07	-0.5	1874
714	CCJSCC+O2=C*CSCC+HO2	1.33E+09	0.2	14361
	Declared duplicate reaction...			
715	CCJSCC+O2=CCSJ+C*CQ	7.25E+18	-2.6	9380
716	CCJSCC+O2=CCQSCJC	1.92E+55	-14	14566
717	CCJSCC+O2=CH3CH*S+CH3CHO+OH	1.49E+27	-4.8	11087

718	CCJSCC+O2=CCQSCCJ	3.04E+44	-11.5	11172
719	CCJSCC+O2=C2H4+CCQSJ	4.02E+23	-4.3	4688
720	CCQJSCC=C*SCC+HO2	1.20E+45	-10.6	35206
	Declared duplicate reaction...			
721	CCQJSCC=CC*OSCC+OH	2.56E+00	1.9	31492
722	CCQJSCC=CJCQSCC	6.98E+32	-8.2	32809
723	CCQJSCC=C*SCC+HO2	1.82E+04	0.8	30500
	Declared duplicate reaction...			
724	CCQJSCC=CCSJ+C*CQ	5.95E+30	-6.8	32649
725	CCQJSCC=CCQSCJC	8.38E+65	-17.3	35851
726	CCQJSCC=CH3CH*S+CH3CHO+OH	3.22E+37	-8.4	33492
727	CCQJSCC=CCQSCCJ	3.38E+70	-19.1	42009
728	CCQJSCC=C2H4+CCQSJ	2.68E+60	-15.5	41066
729	CJCQSCC=C*SCC+HO2	2.55E+10	-0.7	13924
	Declared duplicate reaction...			
730	CJCQSCC=CC*OSCC+OH	4.87E-05	3.1	22789
731	CJCQSCC=C*SCC+HO2	1.37E+07	0.5	15142
	Declared duplicate reaction...			
732	CJCQSCC=CCSJ+C*CQ	2.46E+06	0.5	-1030
733	CJCQSCC=CCQSCJC	1.41E+52	-13.8	27325
734	CJCQSCC=CH3CH*S+CH3CHO+OH	2.99E+17	-2.8	19302
735	CJCQSCC=CCQSCCJ	1.80E+45	-12.4	25907
736	CJCQSCC=C2H4+CCQSJ	6.74E+22	-5	17694
737	CCQSCJC=C*SCC+HO2	9.55E+59	-15.1	36717
	Declared duplicate reaction...			
738	CCQSCJC=CC*OSCC+OH	1.80E+30	-7	39529
739	CCQSCJC=C*SCC+HO2	8.40E+32	-7.7	38398
	Declared duplicate reaction...			
740	CCQSCJC=CCSJ+C*CQ	1.40E+51	-12.9	36847
741	CCQSCJC=CH3CH*S+CH3CHO+OH	4.31E+23	-3.7	24647
742	CCQSCJC=CCQSCCJ	1.04E+90	-25.1	46197
743	CCQSCJC=C2H4+CCQSJ	6.65E+74	-19.9	42117
744	CCQSCCJ=C*SCC+HO2	2.52E+50	-12.9	27130
	Declared duplicate reaction...			
745	CCQSCCJ=CC*OSCC+OH	1.20E+13	-2.5	27216
746	CCQSCCJ=C*SCC+HO2	3.08E+16	-3.4	26150
	Declared duplicate reaction...			
747	CCQSCCJ=CCSJ+C*CQ	1.27E+39	-9.9	26245
748	CCQSCCJ=CH3CH*S+CH3CHO+OH	7.58E+45	-11.6	27012
749	CCQSCCJ=C2H4+CCQSJ	3.09E+15	-1.9	6446
750	CCQSJ=CH3CH*S+HO2	2.00E+14	0	26000
751	CJCSCC+O2=CQJCSCC	5.82E+12	0	0
752	CQJCSCC=C*SCC+HO2	8.80E+05	2.2	29610
753	CQJCSCC=O*CCSCC+OH	6.24E+08	1.2	43000
754	CQJCSCC=CQCJSCC	2.10E+07	1.4	32000
755	CQCJSCC=CQC*S+C2H5	1.20E+14	0	32560
756	CQJCSCC=CQCSCJC	2.22E+04	1.4	21000
757	CQCSCJC=CJCQ+CH3CH*S	1.25E+14	0	32950

758	CQJCSCC=CQCSCCJ	4.60E+03	1.8	22200
759	CQCSCCJ=CQCSJ+C2H4	1.58E+14	0	19020
760	CQCSJ=CH2S+CH2O+OH	2.00E+14	0	24090
761	C*CSCC+OH=C*CSCJC+H2O	2.40E+06	2	300
762	C*CSCC+O=C*CSCJC+OH	3.40E+08	1.5	300
763	C*CSCC+H=C*CSCJC+H2	4.80E+08	1.5	2220
764	C*CSCC+CH3=C*CSCJC+CH4	1.62E+06	1.9	5280
765	C*CSCC+CCSJ=C*CSCJC+CCSH	1.62E+06	1.9	16580
766	C*CSCJC=C*CSC*C+H	3.00E+13	0	41980
767	C*CSCJC=CH3CH*S+C2H3	2.00E+14	0	42500
768	C*CSCC+OH=C*CSCCJ+H2O	3.60E+06	2	1100
769	C*CSCC+O=C*CSCCJ+OH	5.10E+08	1.5	5250
770	C*CSCC+H=C*CSCCJ+H2	7.20E+08	1.5	7300
771	C*CSCC+CH3=C*CSCCJ+CH4	2.43E+06	1.9	10350
772	C*CSCC+CCSJ=C*CSCCJ+CCSH	2.43E+06	1.9	21660
773	C*CSCCJ=C*CSJ+C2H4	1.50E+14	0	20550
774	C*CSCCJ=C*CSC*C+H	3.00E+13	0	34170
775	C*CSCC=C*CSH+C2H4	1.00E+12	0	64150
776	C*CSCC=C*CSJ+C2H5	2.00E+16	0	74440
777	C*CSC*CJ=YC4H5S	1.00E+12	0	7200
778	C*CSC*CJ=THIOPHENE+H	1.00E+14	0	27400
779	C2H2+C*CSJ=YC4H5S	1.00E+12	0	2000
780	C*CSJ+C2H4=YC4H7S	2.00E+09	0	9500
781	YC4H7S=YC4H6S+H	1.00E+14	0	41820
782	YC4H6S=YC4H5S+H	3.00E+13	0	88320
783	YC4H5S=THIOPHENE+H	1.00E+14	0	22970
784	CH3CH*S+C2H5=CCCICSJ	3.00E+13	0	8000
785	CCCICSJ=CCCIC*S+H	1.00E+14	0	42200
786	CCCICSJ=CCC*S+CH3	2.00E+14	0	39900
787	CCCICSH+CH3=CCCICSJ+CH4	8.10E+05	1.9	32800
788	CCCICSH+OH=CCCICSJ+H2O	1.20E+06	2	500
789	H+OCS=HSCO	3.04E+11	-3.2	5187
790	H+OCS=SH+CO	1.72E+09	1.7	3484
791	CH3+OCS=CH3SCO	5.73E+28	-8.7	11025
792	CH3+OCS=CH3S+CO	1.88E+08	0.5	10806
793	SH+CS=H+CS2	8.70E+14	-0.8	775
794	CH3S+CS=CH3+CS2	5.90E+04	1.7	1080
795	S2+CS=S+CS2	8.70E+14	-0.8	775
796	HCS+S2=CS2+SH	3.00E+11	0	4000
797	HCS+S=H+CS2	2.00E+13	0	0
798	CCSJ+CO=C2H5+OCS	3.00E+12	0	7000
799	CCSH=CCSJ+H	1.15E+29	-4.7	89964
800	CCSH=CH3+CH2SH	5.94E+27	-4.2	86073
801	CCSH=CH3CH*S+H2	5.39E+25	-4.1	84940
802	CCSH=C2H4+H2S	1.46E+20	-2.4	68189
803	CCSH+H=CCSJ+H2	2.40E+08	1.5	500
804	CCSH+OH=CCSJ+H2O	1.20E+06	2	500
805	CCSH+O=CCSJ+OH	1.70E+08	1.5	500

806	CCSH+CH3=CCSJ+CH4	8.10E+05	1.9	1700
807	CCSH+HO2=CCSJ+H2O2	2.20E+11	0	9050
808	CCSH+H=CCJSH+H2	4.80E+08	1.5	2810
809	CCSH+OH=CCJSH+H2O	2.40E+06	2	500
810	CCSH+O=CCJSH+OH	3.40E+08	1.5	600
811	CCSH+CH3=CCJSH+CH4	1.60E+06	1.9	5870
812	CCSH+HO2=CCJSH+H2O2	4.40E+11	0	12260
813	CCSJ+O2=CCSQJ	1.32E+23	-4.2	1061
814	CCSJ+O2=CCSO+O	2.60E+10	1	16613
815	CCSJ+O2=CH3CH*S+HO2	4.56E+11	0.2	6594
816	CCSJ+O2=CCSO2	5.61E+08	-0.7	7477
817	CCSJ+O2=CCOSO	1.14E+10	-1.7	9095
818	CCSQJ=CCSO+O	3.12E+11	-0.6	22032
819	CCSQJ=CH3CH*S+HO2	2.00E+15	-2.1	11635
820	CCSQJ=CCSO2	4.76E+10	-2.5	12615
821	CCSQJ=C2H5+SO2	1.04E+14	-1.8	15528
	Declared duplicate reaction...			
822	CCSQJ=CCOSO	6.91E+11	-3.5	14127
823	CCSQJ=C2H5+SO2	1.29E+01	1.2	13706
	Declared duplicate reaction...			
824	CCSO2=CCSO+O	7.62E+46	-14.6	103352
825	CCSO2=CH3CH*S+HO2	4.90E+52	-12.8	93171
826	CCSO2=C2H5+SO2	9.06E+30	-6.5	15424
	Declared duplicate reaction...			
827	CCSO2=CCOSO	3.61E+17	-5.4	9313
828	CCSO2=C2H5+SO2	1.72E-15	6	17979
	Declared duplicate reaction...			
829	CCOSO=CCSO+O	1.70E+51	-17	110706
830	CCOSO=CH3CH*S+HO2	3.55E+46	-14.5	100153
831	CCOSO=C2H5+SO2	3.08E+46	-11.2	35364
	Declared duplicate reaction...			
832	CCOSO=C2H5+SO2	3.40E+45	-10.2	39932
	Declared duplicate reaction...			
833	CH2SH+O2=HSCH2OO	5.68E+37	-8.7	4673
834	CH2SH+O2=CH2S+HO2	3.75E+10	-0.3	4113
	Declared duplicate reaction...			
835	CH2SH+O2=SJCOOH	3.96E+40	-9.8	7931
836	CH2SH+O2=CYCH2SO+OH	7.64E+18	-2.6	5053
837	CH2SH+O2=CH2S+HO2	6.11E+19	-2.8	5124
	Declared duplicate reaction...			
838	HSCH2OO=CH2S+HO2	3.11E+28	-6.6	29072
	Declared duplicate reaction...			
839	HSCH2OO=SJCOOH	9.10E+46	-11.7	29087
840	HSCH2OO=CYCH2SO+OH	5.05E+42	-10.4	31717
841	HSCH2OO=CH2S+HO2	2.14E+43	-10.5	31676
	Declared duplicate reaction...			
842	SJCOOH=CH2S+HO2	7.41E+32	-7.8	33166
	Declared duplicate reaction...			

843	SJCOOH=CYCH2SO+OH	3.33E+38	-8.8	29496
844	SJCOOH=CH2S+HO2	1.46E+39	-8.9	29240
	Declared duplicate reaction...			
845	SH+O2=HSOO	1.53E+13	-1.4	-743
846	SH+O2=HSO+O	8.61E+11	0.5	26845
847	SH+O2=SJOOH	2.38E+13	-1.3	19351
848	SH+O2=SO+OH	1.44E+13	-0.4	19143
849	SH+O2=HSO2	1.19E+20	-4.3	20480
850	SH+O2=H+SO2	3.30E+13	-0.6	19602
	Declared duplicate reaction...			
851	SH+O2=HOSO	2.65E+18	-4.1	20451
852	SH+O2=H+SO2	7.31E+11	-0.6	19275
	Declared duplicate reaction...			
853	HSOO=HSO+O	2.02E+09	0.3	29369
854	HSOO=SJOOH	9.03E+10	-1.5	21885
855	HSOO=SO+OH	5.49E+10	-0.7	21677
856	HSOO=HSO2	4.16E+17	-4.6	23009
857	HSOO=H+SO2	1.22E+11	-0.8	22135
	Declared duplicate reaction...			
858	HSOO=HOSO	9.64E+15	-4.3	22981
859	HSOO=H+SO2	2.87E+09	-0.9	21812
	Declared duplicate reaction...			
860	SJOOH=HSO+O	2.27E+18	-3.3	47376
861	SJOOH=SO+OH	9.43E+12	-1	1179
862	SJOOH=HSO2	5.21E+14	-4	1879
863	SJOOH=H+SO2	2.05E+06	0.2	723
	Declared duplicate reaction...			
864	SJOOH=HOSO	1.88E+14	-4.1	2067
865	SJOOH=H+SO2	4.16E+05	-0.2	603
	Declared duplicate reaction...			
866	HSO2=HSO+O	8.94E-10	4.9	89829
867	HSO2=SO+OH	4.50E+27	-5.8	55533
868	HSO2=H+SO2	2.31E+29	-5.9	28124
	Declared duplicate reaction...			
869	HSO2=HOSO	3.59E-14	4.4	23675
870	HSO2=H+SO2	1.55E-09	4.5	30494
	Declared duplicate reaction...			
871	HOSO=HSO+O	1.69E+22	-5.8	123308
872	HCS+O2=SCHOO	2.81E+35	-9.5	4659
873	HCS+O2=CS+HO2	6.83E+03	2.1	7967
874	HCS+O2=SJCHYOO	1.06E+24	-7.5	4257
875	HCS+O2=SCOHOHB	3.79E-24	4.4	1846
876	HCS+O2=OCS+OH	1.48E+01	3.1	3268
877	HCS+O2=SCHOOSYN	1.13E+34	-8.8	4636
878	HCS+O2=SOCHO	1.94E-27	5.4	-458
879	HCS+O2=HSO+CO	2.29E+02	2.7	2815
880	HCS+O2=OSCHOZ	5.04E-14	1.8	-1575
881	HCS+O2=OSCHO	8.12E-15	1.9	-1140



882	HCS+O2=SO+HCO	2.24E+06	1.4	273
883	HCS+O2=SOHCOHB	3.15E-11	0.6	694
884	HCS+O2=SOH+CO	3.94E+09	0.7	863
885	SJCHYOO=SCHOO	8.22E+36	-7	93897
886	SJCHYOO=SOCHO	5.95E+37	-7	93897
887	SCOHCOHB=OCS+OH	2.90E+22	-3.9	9895
888	SCOHCOHB=SCHOO	5.48E-48	-4	94297
889	SCHOOSYN=SCHOO	9.70E+40	-8.1	81125
890	SCHOOSYN=OSCHOZ	1.66E+38	-7.5	81125
891	SOCHO=HSO+CO	5.08E+30	-6	28061
892	OSCHOZ=OSCHO	4.36E+16	-2.2	5594
893	OSCHO=SO+HCO	2.67E-23	-3.4	62987
894	OSCHO=SOHCOHB	8.11E+06	-3	21200
895	SOHCOHB=SOH+CO	1.17E+15	-1.7	3545
896	HCS+HCS=C2H2+S2	1.00E+12	0	1500
897	HCS+CH3CJ*S=C#CC+S2	1.00E+12	0	1500
898	CH3CJ*S+CH3CJ*S=CC#CC+S2	1.00E+12	0	1500
899	CH2S+CH2S=C2H4+S2	3.50E+11	0	7000
900	CH2S+CH3CH*S=C*CC+S2	3.50E+11	0	7000
901	CH3CH*S+CH3CH*S=CC*CC+S2	3.50E+11	0	7000
902	CCSCC=C2H6+CH3CH*S	2.00E+12	0	65000
903	CCSCC+OH=CCSOH+C2H5	6.60E+11	0	3500
904	CCSCC+O=CCSO+C2H5	7.20E+11	0	820
905	CCSOH+OH=CCSO+H2O	2.45E+12	0	1000
906	CCSOH+HO2=CCSO+H2O2	4.50E+12	0	2000
907	CCSOH+O=C2H5+HOSO	9.50E+11	0	820
908	CCSOH+C2H5=CCSO+C2H6	4.50E+11	0	2100
909	CCSOH+CH3=CCSO+CH4	7.10E+11	0	1800
910	CCSO+OH=CCSO2+H	3.50E+12	0	11500
911	CCSO+OH=C2H5+HOSO	4.10E+12	0	2750
912	CCSO+HO2=CCSO2+OH	5.50E+11	0	1500
913	CH3CH*S+SH=C*CSJ+H2S	9.00E+11	0	9800
914	CH3CH*S+CH3=C*CSJ+CH4	8.10E+11	0	6600
915	CH3CH*S+HO2=C*CSJ+H2O2	7.10E+11	0	11000
916	C*CSJ+H=C*CSH	1.20E+12	0	0
917	C*CSOH+OH=H2O+C*CSO	2.40E+12	0	500
918	C*CSOH+H=H2+C*CSO	1.50E+13	0	1500
919	C*CSOH+HO2=H2O2+C*CSO	3.40E+11	0	11500
920	C*CSOH+CH3=CH4+C*CSO	2.40E+12	0	2300
921	C*CSJ+OH=C*CSOH	1.20E+13	0	0
922	C*CSJ+HO2=C*CSO+OH	1.20E+12	0	500
923	C*CSJ+O=C*CSO	1.30E+13	0	0
924	C*CSO=C2H3+SO	3.30E+13	0	71100
925	C*CSO+OH=HOSO+C2H3	2.40E+12	0	7000
926	C*CSO+O=SO2+C2H3	1.50E+13	0	2000
927	C*CSO+HO2=OH+SO2+C2H3	2.40E+11	0	12500
928	HCS=H+CS	2.46E+23	-4	53002
929	HCO+HCS=C2H2+SO	5.50E+12	0	23000

930	CH2S+O2=HO2+HCS	1.00E+13	0	46001
931	CS+O2=OCS+O	3.00E+12	0	12000
932	HOSO+O2=HO2+SO2	7.70E+11	0	4500
933	SOH+O2=OH+SO2	3.50E+12	0	10000
934	CS+HO2=OCS+OH	8.45E+08	1.2	14367
935	CH3S+O2=CH2S+HO2	3.33E+03	2.9	24600
	Declared duplicate reaction...			
936	CH3S+O2=CH2S+HO2	5.25E+24	-4.7	8300
	Declared duplicate reaction...			
937	CH3S=CH2S+H	2.51E+38	-7.8	62053
938	CS+O2=CO+SO	1.93E+13	0	1291.6
939	HCS+CCSCC=CJCSCC+CH2S	1.20E+12	0	12000
940	HCS+C2H4=C2H3+CH2S	8.40E+11	0	20000
941	SOH+CCSCC=CCJSCC+HSOH	1.40E+12	0	19000
942	SOH+CCSCC=CJCSCC+HSOH	2.10E+12	0	23000
943	SOH+C2H4=C2H3+HSOH	1.40E+12	0	34000
944	HCS+CCSCC=CCJSCC+CH2S	1.00E+12	0	12000
945	CCJSH=CH3CH*S+H	2.00E+13	0	39860
946	CCSCC+H=CCJSCC+H2	5.99E+08	1.9	5141
947	H+C2H6=C2H5+H2	2.00E+09	1.9	7530
948	CCSCC+CH3=CCJSCC+CH4	2.90E+04	2.8	9722
949	2CH3(+M)=C2H6(+M)	6.77E+16	-1.2	654
	Low pressure limit: 0.34000E+42 -0.70300E+01 0.27620E+4			
	TROE centering: 0.61900E+00 0.73200E+02 0.11800E+04 0.99990E+06			
	H2 Enhanced by 2.000E+00			
	H2O Enhanced by 6.000E+00			
	CH4 Enhanced by 2.000E+00			
	CO Enhanced by 1.500E+00			
	CO2 Enhanced by 2.000E+00			
	C2H6 Enhanced by 3.000E+00			
	AR Enhanced by 7.000E-01			
950	CCSCC+H=CCSH+C2H5	1.00E+12	0	2000
951	CCSH+H=H2+CJCSH	4.50E+07	1.9	12000
952	CJCSH=SH+C2H4	1.00E+14	0	19000
953	CCJSH=CJCSH	5.10E+12	0	40000
954	CCSJ=CCJSH	1.58E+12	0.6	44300
955	CCSC=C2H5+CH3S	1.00E+17	0	72000
956	CCSC=CH3+CCSJ	1.00E+17	0	73500
957	CCSCJ=CH2S+C2H5	1.00E+14	0	36000
958	CCJSC=CH3CH*S+CH3	1.00E+14	0	33000
959	CJCSC=C2H4+CH3S	1.00E+14	0	17000
960	CCSC+H=CJCSC+H2	3.46E+07	2	9471
961	CCSC+H=CCJSC+H2	5.99E+07	1.9	5141
962	CCSC+H=CCSCJ+H2	3.46E+07	2	9471
963	CCSC+CH3=CJCSC+CH4	9.78E+03	3	13700
964	CCSC+CH3=CCJSC+CH4	2.90E+04	2.8	9722
965	CCSC+CH3=CCSCJ+CH4	9.78E+03	3	13700
966	CCSC=C2H4+CH3SH	5.20E+06	1.9	63637

967	CH3SH=CH3S+H	1.15E+29	-4.7	89964
968	CH3SH+OH=CH2SH+H2O	7.50E+12	0	700
969	CH3SH+CH3=CH2SH+CH4	1.50E+12	0	6500
970	CH3SH+C2H5=CH2SH+C2H6	7.50E+11	0	7500
971	CH3SH+HO2=CH2SH+H2O2	2.00E+11	0	14500
972	CH3SH+H=CH2SH+H2	8.12E+05	2.3	4720
973	CH3SH+H=CH3S+H2	2.40E+08	1.5	500
974	CH3SH+OH=CH3S+H2O	1.20E+06	2	500
975	CH3SH+O=CH3S+OH	1.70E+08	1.5	500
976	CH3SH+CH3=CH3S+CH4	8.10E+05	1.9	1700
977	CH3SH+HO2=CH3S+H2O2	2.20E+11	0	9050
978	CCSJ+HO2=CCSO+OH	5.00E+12	0	0
979	2OH(+M)=H2O2(+M)	7.40E+13	-0.4	0
Low pressure limit: 0.23000E+19 -0.90000E+00 -0.17000E+4				
TROE centering: 0.73460E+00 0.94000E+02 0.17560E+04 0.51820E+06				
	H2	Enhanced by	2.000E+00	
	H2O	Enhanced by	6.000E+00	
	CH4	Enhanced by	2.000E+00	
	CO	Enhanced by	1.500E+00	
	CO2	Enhanced by	2.000E+00	
	C2H6	Enhanced by	3.000E+00	
	AR	Enhanced by	7.000E-01	
980	CCSCC+HO2=CJCSCC+H2O2	6.32E+12	0	15200
981	2HO2=O2+H2O2	1.30E+11	0	-1630
	Declared duplicate reaction...			
982	C2H5+O2=C2H4+HO2	1.05E+13	-1.5	4996
	Declared duplicate reaction...			
983	C2H5+O2=C2H4+HO2	1.69E+10	-0.7	7052
	Declared duplicate reaction...			
984	C2H5+HO2=CCOJ+OH	7.00E+12	0	0
985	C2H5+HO2=C2H6+O2	3.50E+11	0	4000
986	OH+SO=HOSO	6.11E+20	-6.5	1249
987	OH+SO=OH+SO	2.10E+05	1.9	203
988	OH+SO=H+SO2	1.27E+13	-0.1	124
989	OH+SO=SOH+O	7.76E+10	0.3	48485
990	HOSO=H+SO2	6.15E+31	-6.1	54973
991	HOSO=SOH+O	9.14E-06	-6.3	117347
992	CCSCC+HO2=CCJSCC+H2O2	8.80E+13	0	11120
993	CCSCC+OH=CCJSCC+H2O	3.80E+07	2	300
994	CCSCC+OH=CJCSCC+H2O	7.20E+07	2	620
995	CCSJ+O2=C2H5+SO2	3.00E+12	0.1	10414
	Declared duplicate reaction...			
996	CCSJ+O2=C2H5+SO2	5.50E-01	3	8770
	Declared duplicate reaction...			
997	CCSCC+O=CCJSCC+OH	6.80E+09	1.5	4000
998	HO2+CH3=OH+CH3O	9.00E+12	0	0
999	CCSCC+O2=CJCSCC+HO2	2.00E+11	0	51631
1000	CCSCC+O2=CCJSCC+HO2	2.00E+11	0	43901

1001	CH2S+OH=HCS+H2O	1.20E+13	0	500
1002	CH2S+O=HCS+OH	2.10E+13	0	3000
1003	CH2S+H=HCS+H2	2.84E+07	2	7760
1004	CH2S+CH3=HCS+CH4	2.31E+04	2.4	12280
1005	CH3S+O2=CH3+SO2	2.00E+26	-3.8	12300
1006	S+O2=SO+O	1.40E+07	1.8	-1192
1007	CH3CH*S+H=CH3CJ*S+H2	2.40E+08	1.5	8000
1008	CH3CH*S+OH=CH3CJ*S+H2O	1.20E+06	2	1500
1009	CH3CH*S+O=CH3CJ*S+OH	1.70E+08	1.5	8000
1010	CH3CH*S+O2=CH3CJ*S+HO2	1.00E+13	0	47800
1011	CH3CH*S+HO2=CH3CJ*S+H2O2	1.40E+04	2.7	16800
1012	CH3CH*S=CH3+HCS	1.50E+16	0	85500
1013	CH3CH*S+H=C*CSJ+H2	2.40E+08	1.5	8000
1014	CH3CH*S+OH=C*CSJ+H2O	1.08E+07	2	700
1015	CH3CH*S+O=C*CSJ+OH	5.10E+08	1.5	3000
1016	CH2S+OH=CH2O+SH	1.00E+11	0	13000
1017	CH2S+O=CH2O+S	3.40E+12	0	0
1018	CH2*C*S+H=HCCS+H2	2.40E+08	1.5	1800
1019	CH2*C*S+OH=HCCS+H2O	6.25E+04	2	2930
1020	CH2*C*S+O=HCCS+OH	5.10E+08	1.5	9000
1021	CH2*C*S+O2=HCCS+HO2	5.50E+12	0	28479
1022	HCCS+OH=HCO+HCS	1.50E+10	0	21000
1023	HCCS+O=HCO+CS	9.10E+13	0	2700
1024	HCCS+O2=HCO+OCS	9.50E+10	0	13000
1025	HCCS+OH=CH2O+CS	1.50E+10	0	17500
1026	C*CSJ=CH2*C*S+H	1.30E+14	0	58760
1027	CH3CJ*S=CH2*C*S+H	1.30E+14	0	51000
1028	C*CSJ=CH3CJ*S	5.50E+12	0	41000
1029	C*CSJ=CS+CH3	2.40E+14	0	58300
1030	C*CSJ+O2=CH2*C*S+HO2	2.50E+12	0	17500
1031	CH3CJ*S+O2=CH2*C*S+HO2	2.50E+12	0	12000
1032	CH2+CS(+M)=CH2*C*S(+M)	8.10E+11	0.5	4510
Low pressure limit: 0.26900E+34 -0.51100E+01 0.70950E+4				
TROE centering: 0.59070E+00 0.27500E+03 0.12260E+04 0.51850E+06				
H2	Enhanced by	2.000E+00		
H2O	Enhanced by	6.000E+00		
CH4	Enhanced by	2.000E+00		
CO	Enhanced by	1.500E+00		
CO2	Enhanced by	2.000E+00		
C2H6	Enhanced by	3.000E+00		
AR	Enhanced by	7.000E-01		
1033	S2+O2=SO+SO	1.00E+11	0	7000
1034	C2H3+CH3=C*CC	2.50E+13	0	0
1035	C*CC+O=CH2CO+CH3+H	8.00E+07	1.6	327
1036	C*CC+O=C2H5+HCO	3.50E+07	1.6	-972
1037	CH3CH*S+O2=C*CSJ+HO2	3.00E+13	0	36000
1038	CCSCC=CCSJ+C2H5	1.06E+89	-21.7	105718

NOTE: A units mole-cm-sec-K, T(K), n dimensionless, E<sub>a</sub> units cal/mole

## C.2 THERMOCHEMICAL PROPERTIES FOR DIETHYLSULFIDE OXIDATION (CHAPTER 3).

SPECIES	H <sub>F</sub> (298)	S(298)	C <sub>P</sub> (300)	C <sub>P</sub> (400)	C <sub>P</sub> (500)	C <sub>P</sub> (600)	C <sub>P</sub> (800)	C <sub>P</sub> (1000)	C <sub>P</sub> (1500)
CH3OH	-48.02	57.33	10.51	12.46	14.3	16.02	19.03	21.43	25.18
C2H	135.33	50.99	10.52	10.58	10.82	11.2	12.12	13.03	14.14
HC#COH	18.7	56.27	14	15.62	16.95	18.06	19.77	21.03	23.13
N2	0	45.77	6.9	7	7.12	7.24	7.51	7.78	8.33
AR	0	36.98	4.97	4.97	4.97	4.97	4.97	4.97	4.97
CCC.	23.67	70.69	17.09	21.37	25.15	28.48	33.97	38.15	44.58
C.CHO	6	64.02	13.17	15.21	17.07	18.76	21.64	23.87	27.16
CCO.	-4.24	65.66	14.48	17.95	20.97	23.59	27.82	30.97	35.79
CC.OOH	2.27	79.96	20.4	23.81	26.79	29.38	33.56	36.64	41.11
CY(CCO)	-12.57	59.37	11.43	14.92	17.91	20.47	24.52	27.46	31.78
C.COOH	11.22	81.92	20.24	23.56	26.36	28.72	32.43	35.16	39.63
CCOO.	-6.72	73.84	16.11	19.97	23.35	26.29	31.07	34.63	39.99
HOOCCHO	-57.06	83.26	21.11	25.27	28.65	31.38	35.34	37.93	41.54
C*COOH	-10.87	73.61	17.71	21.65	24.82	27.35	30.98	33.31	36.64
HOCCOO.	-23.89	90.69	25.04	30.47	34.84	38.33	43.32	46.53	51.05
CCOH	-56.2	67.12	15.44	19.23	22.54	25.44	30.17	33.75	39.32
JOCCOOJ	10.26	85.19	20.41	23.94	26.99	29.61	33.8	36.89	41.56
CH3C.*O	-3.08	64.29	12.25	14.41	16.34	18.06	20.93	23.13	26.45
HC(*O)COO	-21.01	80	17.48	21.87	25.37	28.14	32.04	34.49	37.78
C.*OCOOH	-19.64	81.8	20.84	24.2	26.95	29.2	32.5	34.65	37.56
O*COO.C	-38.57	75.58	19.51	23.23	26.29	28.78	32.43	34.83	38
C.CO3H	-32.95	79.27	21.91	25.43	28.21	30.39	33.39	35.22	37.53
CCO2	-41.35	68.44	13.56	16.67	19.29	21.48	24.87	27.28	30.97
O*YCOC	-44.42	62.31	12.02	14.73	17.04	19.01	22.09	24.27	27.26
C*CC	4.65	63.83	15.45	19.34	22.77	25.79	30.74	34.5	40.33
C#CC	44.28	59.29	13.98	16.64	19.07	21.28	25	27.86	31.94
CC*O	-39.18	63.15	13.17	15.84	18.26	20.46	24.16	27.02	31.25
CCCOH	-61.15	76.54	20.93	26.2	30.78	34.77	41.22	46.06	53.54

CC.CO <sub>H</sub>	-14.78	80.98	19.28	23.92	28.03	31.64	37.56	41.99	48.63
CCCO.	-9.17	75.08	19.96	24.9	29.18	32.89	38.85	43.27	49.98
C.CCO <sub>H</sub>	-12.13	81.33	20.15	24.82	28.87	32.39	38.07	42.33	48.92
CH <sub>3</sub> CHO	-39.72	63.15	13.04	15.73	18.16	20.35	24.03	26.88	31.18
C <sub>2</sub> CO <sub>H</sub>	-65.52	74.54	21.54	26.92	31.56	35.54	41.89	46.61	53.96
C <sub>2</sub> .CO <sub>H</sub>	-14.5	79.49	20.84	25.62	29.71	33.21	38.78	42.89	49.32
C <sub>2</sub> CO.	-13.54	73.08	20.56	25.62	29.95	33.66	39.52	43.82	50.37
QCC*O	-55.87	82.83	19.33	24.17	28.04	31.11	35.46	38.23	42.04
QCC*OC	-68.27	91.17	24.02	30.44	35.69	39.96	46.23	50.42	56.33
C*CO <sub>H</sub>	-29.71	59.95	15.31	19.33	22.39	24.71	27.73	29.5	32.23
QCCO <sub>H</sub> *C	-58.67	88.97	28.65	34.3	38.85	42.51	47.79	51.29	56.51
CCO <sub>H</sub> CQ	-85.22	93.86	29.36	35.81	41.22	45.74	52.67	57.58	64.84
CCO.CQ	-33.24	92.4	28.4	34.51	39.6	43.83	50.26	54.74	61.21
CCO <sub>H</sub> CQ.	-51	94.08	27.4	32.93	37.64	41.64	47.95	52.56	59.7
CC.O <sub>H</sub> CQ	-44.5	98.33	28.77	34.06	38.6	42.47	48.61	53.08	59.77
C.CO <sub>H</sub> CQ	-34.2	98.8	28.75	34.51	39.33	43.35	49.48	53.8	60.16
C*CO <sub>H</sub> C	-40.31	69.66	20.51	25.34	29.24	32.38	36.99	40.15	45.23
CCQCO <sub>H</sub>	-85.22	93.86	29.36	35.81	41.22	45.74	52.67	57.58	64.84
CCQCO.	-33.24	92.4	28.4	34.51	39.6	43.83	50.26	54.74	61.21
CCQ.CO <sub>H</sub>	-51	94.08	27.4	32.93	37.64	41.64	47.95	52.56	59.7
CCQC.O <sub>H</sub>	-43.3	94.64	29.94	35.58	40.28	44.17	50.09	54.22	60.37
C.CQCO <sub>H</sub>	-34.2	98.8	28.75	34.51	39.33	43.35	49.48	53.8	60.16
CC*CO <sub>H</sub>	-37.58	68.54	20.83	25.97	30.05	33.29	37.9	40.96	45.87
C*CQ	-11.39	71.61	18.31	21.77	24.58	26.85	30.19	32.47	36.08
C*CCO <sub>H</sub>	-29.81	74.47	18.54	22.86	26.62	29.88	35.1	38.96	44.76
CCOO <sub>H</sub>	-40.1	75.79	20.33	24.69	28.44	31.66	36.77	40.48	45.86
C*CCJ	40.06	62.96	14.93	18.63	21.78	24.45	28.65	31.7	36.34
C*CCOO.	21.02	82.94	20.84	25.05	28.75	31.96	37.12	40.88	46.17
C.*CCOO <sub>H</sub>	46.77	87.17	22.27	26.32	29.81	32.81	37.53	40.9	45.66
C*C.CO <sub>H</sub>	44.58	86.13	25.16	28.91	32.17	34.97	39.39	42.52	46.76
C.CYCCOO	40.18	75.22	20.53	25.5	29.62	33.02	38.16	41.71	47
C*CCHO	-16.08	67.67	16.85	20.4	23.43	25.99	30	32.85	37.03

CYCC.COO	19.18	72.82	19.15	24.49	28.95	32.66	38.3	42.21	47.87
QYCCOOC	-51.25	86.01	27.08	34.55	40.64	45.58	52.77	57.46	63.82
QJYCCOOC	-17.05	86.23	24.96	31.61	37.06	41.52	48.09	52.49	58.7
QYCCJOOC	-7.35	89.83	27.18	33.69	39	43.3	49.57	53.65	59.11
HOCCQCHO	-102.9	100.43	29.93	35.97	40.96	45.07	51.19	55.35	61.22
JOCCQCHO	-50.94	98.97	28.94	34.66	39.35	43.17	48.8	52.52	57.59
O*CC*O	-50.6	65.44	14.9	17.53	19.7	21.49	24.14	25.87	28.1
YC*CCOO	-8.8	66.96	15.19	20.14	24.25	27.65	32.78	36.3	41.44
QC*CCQ	-38.94	99.51	31.69	37.34	41.99	45.83	51.55	55.46	61.09
QJC*CCQ	-4.74	99.73	29.63	34.43	38.44	41.78	46.88	50.5	56
QC*CCHO	-45.55	83.78	25.33	30.07	33.84	36.82	41.01	43.66	47.43
QCCCHO	-64.22	92.06	27.36	32.28	36.53	40.17	45.94	50.12	56.14
QCCJCHO	-22.8	89.69	25.99	30.78	34.81	38.19	43.37	46.94	51.85
QCC*COH	-55.94	87.85	28.86	34.93	39.72	43.47	48.69	51.97	56.79
QCC*COJ	-20.04	86.79	26.62	32.33	36.85	40.39	45.32	48.39	52.78
C*COCHO	-69.72	51.36	15.11	18.04	20.4	22.26	24.78	26.04	25.76
C*COC*O	-56.3	51.1	15.21	17.93	20.16	21.97	24.61	26.38	30.07
QCCOC*O	-112.3	100.66	28.64	34.32	39.21	43.41	50.03	54.74	61.15
QCCJOC*O	-67.41	101.21	30.7	36.15	40.6	44.2	49.44	52.84	57.37
QCCOHC*O	-102.9	100.43	29.93	35.97	40.96	45.07	51.19	55.35	61.22
QCCOJC*O	-50.94	98.97	28.94	34.66	39.35	43.17	48.8	52.52	57.59
QYCCOOC	-56.2	88	27.11	33.78	39.33	43.91	50.8	55.51	62.15
QJYCCOOC	-22	86.14	24.23	30.74	36.14	40.59	47.26	51.78	58.1
QYCCJOOC	-12.3	67.26	31.85	37.87	42.75	46.68	52.33	55.93	60.53
CC.C	21.02	70.33	16.22	20.42	24.19	27.56	33.19	37.53	44.14
C2C*O	-51.56	70.11	17.9	22.15	25.95	29.33	34.92	39.16	45.43
CYCOC	-22.43	66.81	17.4	22.59	26.96	30.63	36.31	40.33	46.29
YCCCO	-15.59	64.89	14.9	20.3	24.95	28.94	35.24	39.78	46.4
CCCQJ	-12.62	85.26	22.93	28.2	32.74	36.65	42.89	47.48	54.47
CJCCQ	4.95	92.2	25.05	29.97	34.2	37.81	43.52	47.71	54.11
CCJCQ	2.46	91.36	24.42	29.09	33.2	36.8	42.66	47.08	53.78
CCQJC	-17.29	83.1	22.62	27.83	32.34	36.25	42.51	47.17	54.27

CJCQC	1.67	87.86	26.63	31.29	35.26	38.64	43.99	47.91	54.08
C*CQC	-22.88	82.86	23.48	28.14	32.11	35.49	40.81	44.64	50.37
CC*OCQ	-71.43	90.6	27.11	31.83	36	39.64	45.55	49.92	56.12
C*CCOOH	-13.56	83.14	23.48	28.29	32.42	35.96	41.54	45.56	51.35
QCYCOC	-40.89	86.12	25.32	31.48	36.56	40.75	47	51.23	57.15
QYCCOC	-41.8	83.59	23.33	29.9	35.34	39.83	46.57	51.15	57.54
CCQC*O	-67.69	89.79	26.83	32.53	37.26	41.19	47.1	51.14	56.75
CC*COOH	-17.49	81.74	23.83	28.84	33	36.45	41.69	45.34	50.79
QCCC*O	-64.51	92.06	27.36	32.28	36.53	40.17	45.94	50.12	56.14
C*CQ	-11.39	71.61	18.31	21.77	24.58	26.85	30.19	32.47	36.08
CCQCQJ	-32.16	96.71	35.86	42.12	47.06	50.93	56.35	59.87	65.57
CCQJCQ	-32.93	97.5	36.84	42.26	46.64	50.19	55.44	59.09	65.17
CJCQCQ	-16.18	98.76	37.22	44.5	50.12	54.41	60.07	63.34	67.82
QCCCQJ	-30.29	99	33.79	41.03	46.77	51.29	57.57	61.42	66.37
QCCJCQ	-18.14	102.2	33.84	41.38	47.52	52.47	59.6	64.11	69.67
CCJCQ	2.46	91.36	24.42	29.09	33.2	36.8	42.66	47.08	53.78
CJCQC	1.67	87.86	26.63	31.29	35.26	38.64	43.99	47.91	54.08
CJCCQ	4.95	92.2	25.05	29.97	34.2	37.81	43.52	47.71	54.11
CCQJCOJS	-1.95	87.53	26.18	31.6	36.13	39.92	45.71	49.8	55.89
CCQJCOJT	-1.71	89.88	26.41	31.77	36.26	40.01	45.76	49.82	55.9
CCOJCQJS	-0.91	86.77	26.12	31.9	36.65	40.54	46.35	50.31	56.17
CCOJCQJT	-0.33	89.19	26.24	31.96	36.68	40.55	46.33	50.3	56.17
OJCCCQJS	1.81	91.8	25.83	31.17	35.67	39.46	45.33	49.51	55.74
OJCCCQJT	1.83	93.92	25.79	31.13	35.64	39.44	45.31	49.5	55.74
OJCCQJS	10.65	81.32	20.23	24.06	27.32	30.08	34.35	37.36	41.57
C*C*C	46.72	58.49	14.12	17.14	19.73	21.95	25.47	28.05	32.01
YC*CCO	13.18	62.91	13.97	18.28	21.87	24.86	29.4	32.55	37.17
C*YCOC	15.16	64.54	15.38	19.37	22.71	25.48	29.72	32.7	37.17
CCC	-25.33	64.52	17.87	22.76	27.08	30.88	37.14	41.9	49.24
CCCHO	-44.5	72.75	19.32	23.36	26.93	30.08	35.25	39.18	45.16
CCC.OH	-19.23	77.32	21.26	25.82	29.76	33.15	38.61	42.7	49.14
C2C.OH	-23.6	73.95	21.88	26.54	30.51	33.89	39.25	43.22	49.49



C*C(OH)C.	-2.71	70.88	18.55	22.58	25.97	28.8	33.15	36.23	40.84
C*C(OH)C	-38.81	72.64	18.99	23.33	27.1	30.37	35.6	39.44	45.17
C.*CC	63.77	65.22	15.24	18.5	21.36	23.86	27.93	31	35.78
C*C.C	61.57	65.64	15.06	18.1	20.83	23.27	27.38	30.58	35.57
C#CC	44.28	59.3	13.98	16.66	19.11	21.32	25.03	27.87	31.89
C*CCCC*C	20.18	88.6	28.58	36.62	43.46	49.26	58.31	64.82	74.67
CCCOOH	-46.56	85.56	25.79	31.66	36.7	41.02	47.85	52.81	60.11
C2COOH	-49.93	82.81	26.3	32.36	37.49	41.81	48.52	53.31	60.34
CH3OO. not	2.15	64.67	13.08	15.2	17.07	18.71	21.39	23.41	26.51
CH3OOH	-31.6	66.34	15.14	18.13	20.66	22.79	26.07	28.36	31.58
CC.OH	-14.3	67.9	15.87	18.89	21.53	23.83	27.57	30.42	34.98
C.CO	-7.2	70.53	14.67	17.85	20.63	23.06	27.02	30.02	34.7
C*CCO.	22.15	73.01	17.55	21.55	25	27.96	32.66	36.07	41.1
O.CYCCO	-4.14	76.18	20.03	24.65	28.67	32.14	37.65	41.6	47.05
YCCO	-12.57	58	11.43	14.92	17.91	20.47	24.52	27.46	31.78
YCC.O	32.33	62.68	10.69	13.56	16.03	18.13	21.44	23.79	27.16
HOYCCOC	-59.41	74.92	18.54	24.47	29.44	33.6	39.96	44.44	51.1
O.YCCOC	-7.45	72.08	17.56	23.16	27.83	31.71	37.58	41.63	47.51
COCC*O	-67.29	82	20.52	25.69	30.08	33.81	39.65	43.88	50.26
C.OCC*O	-22.37	84.73	20.48	25.88	30.15	33.51	38.23	41.28	45.98
CC*OC*O	-64.5	76.25	19.04	22.99	26.42	29.38	34.1	37.49	42.16
CC*OCOH	-84.37	82.5	19.35	25	29.71	33.61	39.56	43.76	50.11
CC*OCO.	-32.39	81.04	18.93	24.09	28.36	31.88	37.18	40.87	46.38
CCOHC*O	-83.22	81.12	22.07	27.1	31.36	34.93	40.48	44.44	50.38
CCO.C*O	-31.24	79.66	21.07	25.78	29.73	33.03	38.09	41.63	46.78
CCC*O	-44.5	72.75	19.32	23.36	26.93	30.08	35.25	39.18	45.16
CC.C*O	-3.1	70.38	18.07	21.89	25.2	28.07	32.66	36.05	41.05
CC*C*O	-19.39	72.75	21.42	24.24	27.41	30.69	36.8	41.44	45.35
C.CO.CQ	15.76	97.19	27.64	33.11	37.65	41.41	47.07	50.96	56.52
CCQJCOJ	-1.95	87.53	26.18	31.6	36.13	39.92	45.71	49.8	55.89
CCOJCQJ	-0.91	86.77	26.12	31.9	36.65	40.54	46.35	50.31	56.17
OJCCCQJ	1.81	91.8	25.83	31.17	35.67	39.46	45.33	49.51	55.74

C.H2OOH	12.71	68.27	16.56	18.41	19.98	21.31	23.39	24.88	27.04
HOCCC*O	-80.32	83.39	22.38	26.81	30.66	34	39.37	43.37	49.47
O.CCC*O	-28.34	81.93	21.41	25.5	29.04	32.1	36.99	40.58	45.94
CYCOC	-21.87	66.81	17.4	22.59	26.96	30.63	36.31	40.33	46.29
CYCOC.	23.03	70.11	16.64	21.22	25.06	28.27	33.19	36.63	41.64
CYC.OC	20.63	70.43	16.49	20.39	23.85	26.9	31.9	35.64	41.16
C.YCOC	27.13	71.6	16.59	21.18	25.02	28.24	33.15	36.59	41.61
C*CC*O	-20.32	67.41	17.05	20.86	24.03	26.66	30.63	33.38	37.39
C2C*O	-51.56	70.11	17.9	22.15	25.95	29.33	34.92	39.16	45.43
C2.C*O	-7.61	72.51	18.28	22.29	25.77	28.76	33.51	36.94	41.76
YC.CCO	25.66	69.57	14.15	18.94	23.06	26.57	32.09	36.03	41.68
YCC.CO	27.11	69.33	13.35	18.09	22.21	25.77	31.45	35.54	41.31
C*COC.	20.06	70.23	20.83	25.47	28.99	31.63	35.1	37.23	40.93
C*COH	-29.71	59.95	15.31	19.33	22.39	24.71	27.73	29.5	32.23
CC*CC	-3.22	72.4	20.67	25.84	30.45	34.53	41.29	46.45	54.32
CC#CC	34.12	71.35	17.82	22.04	25.97	29.61	35.86	40.73	47.43
H	52.1	27.39	4.97	4.97	4.97	4.97	4.97	4.97	4.97
H2	0	31.21	6.94	6.94	6.96	6.99	7.1	7.25	7.72
O	59.57	38.47	5.07	5.07	5.07	5.07	5.07	5.07	5.07
OH	8.89	43.88	7.15	7.09	7.07	7.07	7.15	7.31	7.88
H2O	-57.8	45.11	8.05	8.22	8.44	8.71	9.32	9.97	11.34
O2	0	49	6.98	7.23	7.46	7.67	8.05	8.34	8.73
HO2	3.3	54.38	8.36	8.95	9.48	9.96	10.75	11.37	12.34
CO	-26.42	47.21	6.9	7.03	7.17	7.32	7.61	7.89	8.42
CO2	-94.06	51.07	9.16	9.92	10.64	11.3	12.4	13.19	13.93
C	171.32	37.76	4.97	4.97	4.97	4.97	4.97	4.97	4.97
CH	142.01	43.72	7.1	6.94	6.92	7.01	7.4	7.89	8.71
CH2	92.36	46.32	8.37	8.65	8.99	9.36	10.14	10.88	12.14
CH2(S)	102.76	45.22	8.1	8.33	8.64	9	9.77	10.53	11.87
CH3	35.09	46.46	9.23	10.05	10.82	11.55	12.86	14.02	16.24
CH4	-17.83	44.54	8.54	9.8	11.14	12.51	15.16	17.49	21.17
C2H	133.01	49.58	10.51	10.58	10.83	11.2	12.13	13.03	14.14



S2	30.84	54.51	7.69	8.16	8.48	8.69	8.88	8.92	9.05
SH	34.6	46.73	7.69	7.6	7.54	7.53	7.61	7.79	8.38
H2S	-4.88	49.15	8.35	8.66	9.02	9.42	10.24	11	12.28
SO	1.2	53.02	7.2	7.56	7.85	8.08	8.41	8.61	8.84
SO2	-70.95	59.31	9.4	10.15	10.79	11.31	12.09	12.6	13.24
SO3	-94.6	61.35	12.13	13.79	15.08	16.08	17.42	18.17	19.03
HSO2	-38.36	61.62	10.95	12.57	13.88	14.93	16.43	17.38	18.57
HOSO2	-91.25	70.76	17.31	18.74	19.9	20.81	22.1	22.88	23.84
HOSO	-61.36	67.5	12.4	13.3	14.07	14.71	15.69	16.37	17.37
OCS	-34.21	55.32	10.06	10.94	11.63	12.14	12.81	13.16	13.55
HSO	-7.29	57.75	8.71	9.42	10.04	10.57	11.44	12.06	12.9
HSOH	-27.65	59.65	10.47	11.62	12.6	13.44	14.75	15.71	17.14
H2SO	-11.98	57.28	9.19	10.66	11.95	13.07	14.86	16.16	17.9
HOSHO	-63.54	64.51	13.76	15.96	17.69	19.05	20.91	22.01	23.37
HS2	26.05	60.92	9.56	10.22	10.75	11.18	11.82	12.27	12.98
H2S2	3.98	60.01	11.71	12.89	13.86	14.65	15.85	16.69	17.99
HCS	70.01	56.38	8.77	9.44	9.99	10.46	11.19	11.73	12.6
SCHOO	37.41	69.15	14.37	16.46	18.12	19.43	21.25	22.37	23.9
SCHOOSYN	39.45	69.42	14.24	16.41	18.11	19.44	21.26	22.37	23.89
SCOHOHB	-25.1	80.27	18.59	19.46	20.12	20.64	21.36	21.89	22.97
SOHCOHB	-30.59	79	16.88	17.89	18.72	19.42	20.5	21.3	22.66
SJCHYOO	39.84	68.57	14.1	16.27	17.99	19.33	21.19	22.34	23.89
SOCHO	-30.12	69.5	14.22	16.1	17.64	18.9	20.77	22.02	23.73
OSCHO	-34.09	70.62	15.02	16.8	18.25	19.43	21.15	22.28	23.88
OSCHOZ	-31.84	70.41	14.95	16.78	18.26	19.44	21.17	22.29	23.88
HSCJYOO	49.29	71.6	15.97	17.77	19.13	20.15	21.46	22.23	23.41
HSOCJDO	-13.31	73.49	16.4	17.74	18.83	19.72	21.04	21.94	23.25
HSCO2	-29.72	70.46	15.52	17.5	19.04	20.25	21.88	22.88	24.24
HS	35.19	46.73	7.69	7.6	7.54	7.53	7.61	7.79	8.38
HSCOO	79.53	70.25	16.37	18.38	19.9	21.03	22.47	23.28	24.45
SJCO2H	-51.31	68.59	14.37	16.38	17.97	19.2	20.9	21.96	23.54
HSCO	3.6	64.53	12.65	13.7	14.58	15.3	16.39	17.17	18.36

CHO	10	53.66	8.3	8.78	9.28	9.79	10.72	11.49	12.58
CS	66.88	50.28	7.04	7.4	7.68	7.91	8.23	8.44	8.7
SCHO	8.19	64.16	11.18	12.41	13.46	14.36	15.75	16.74	18.12
C*CSC*C	35.72	87.71	23.17	27.93	32.4	36.51	43.47	48.59	54.62
C*CSC*CJ	96.01	85.21	25.22	29.27	32.55	35.21	39.17	41.96	46.62
CH3CJ*S	58.42	69.25	12.62	14.77	16.68	18.37	21.15	23.24	26.36
CH3CH*S	17.05	64.42	13.6	16.38	18.83	20.96	24.43	27.04	31.03
CH2S	28.3	55.15	9.11	10.36	11.45	12.41	13.98	15.18	17.07
CH3S	29.9	57.62	10.73	12.49	14.01	15.34	17.5	19.15	21.83
C*CSH	17.73	67.44	15.53	18.15	20.42	22.4	25.57	27.92	31.45
CCSH	-11.03	70.66	17.46	20.96	24.04	26.74	31.17	34.56	39.88
C*CSSCC*C	34.97	102.79	36.11	42.55	47.84	52.18	58.73	63.41	71.07
C*CSSC*C	42.3	96.41	28.38	33.6	37.9	41.43	46.77	50.55	56.6
VSCCSV	34.92	114.5	40.05	48.19	54.98	60.63	69.3	75.49	85.2
C*CSCJ	55.2	77.99	20.75	24.57	27.71	30.27	34.12	36.82	41.13
YCCSCCS	1.04	78.17	26.21	33.74	40.04	45.29	53.34	59.02	67.54
YCJCSCCS	43.14	82.47	26.89	33.65	39.24	43.87	50.86	55.75	63.14
C*CSCCSJ	50.9	93.96	29.67	35.39	40.17	44.17	50.31	54.71	61.57
C*CCSJ	48.47	73.15	18.68	22.71	26.09	28.92	33.3	36.47	41.43
HOCCSJ	-13.06	72.21	21.08	25.47	28.81	31.35	34.77	37	41.11
SJCC*O	5.37	71.51	16.44	19.4	21.86	23.9	26.98	29.13	32.34
VSEOESV	28.14	138.71	49.57	61.4	71.97	81.31	96.58	07.73	22.17
C*CSCC*O	-11.94	89.47	28.07	33.17	37.43	40.99	46.49	50.44	56.65
CS2	27.95	56.82	10.43	12.04	13.14	13.83	14.4	14.42	16.13
CCSCC	-20	95.95	27.62	34.08	39.71	44.6	52.53	58.5	67.85
CJCSCC	27.83	97.22	29.14	34.63	39.39	43.51	50.19	55.25	63.39
CCJSCC	20.1	97.34	28.5	33.95	38.74	42.95	49.84	55.09	63.34
CCSJ	24.5	67.31	15.67	18.97	21.82	24.28	28.23	31.2	35.89
C*CSCC	6.81	86.66	25.93	31.53	36.31	40.4	46.88	51.69	59.3
C*CSCJC	47.84	88.82	25.78	31.02	35.37	38.98	44.52	48.51	54.92
C*CSCCJ	55.66	89.98	27.05	31.72	35.69	39.06	44.38	48.35	54.82
CQJSCC	-9.32	105.31	32.98	39.9	45.89	51.05	59.31	65.38	74.51

CQCSCJC	-0.18	105.76	35.51	42.31	48.12	53.08	60.9	66.62	75.44
CQCJSCC	-1.17	105.01	35.41	42.47	48.4	53.39	61.12	66.71	75.47
CQCSCCJ	7.83	104.16	36.15	42.95	48.71	53.58	61.2	66.74	75.44
CQC*S	-1.71	78.55	20.82	25.12	28.66	31.56	35.9	38.88	43.33
CJCQ	11.22	81.92	20.28	23.56	26.33	28.69	32.4	35.15	39.65
CQCSJ	5.3	80.4	24.3	28.47	31.89	34.71	38.93	41.9	46.61
CCQJSCC	-13.99	100.87	34.28	41.38	47.35	52.37	60.18	65.84	74.68
CC*OSCC	-55.29	85.48	28.02	34.41	39.87	44.53	51.89	57.29	65.61
CJCQSCC	4.24	97.04	35.99	43.22	49.21	54.16	61.68	67.05	75.62
CCQSCJC	-3.64	102.51	35.79	42.51	48.24	53.11	60.8	66.45	75.32
CCQSCCJ	2.27	100.65	36.79	43.6	49.31	54.08	61.47	66.84	75.47
CCQSJ	-0.32	81.89	23.5	27.85	31.45	34.43	38.95	42.14	47.17
O*CCSCC	-40.55	85.53	29.65	35.71	40.85	45.2	52.06	57.11	65.09
THIOPHENE	26.3	66.49	17.39	22.69	26.94	30.32	35.15	38.32	43.03
CYCOS	-2.58	62.5	16.23	19.81	22.79	25.27	29.04	31.7	35.86
YC4H5S	55.84	65.31	19.24	24.66	29.08	32.67	37.96	41.55	47.04
YC4H6S	19.35	62.72	18.65	24.75	29.81	33.99	40.31	44.7	51.34
YC4H7S	30.63	66.62	20.54	26.99	32.39	36.92	43.85	48.76	56.21
C2CCSH	-23.41	74.55	27.26	33.84	39.55	44.5	52.5	58.51	67.91
CCCICSH	-23.75	75.5	27.07	33.65	39.38	44.36	52.43	58.49	67.92
TS1X6M	0.9	92.99	32.69	40.27	46.65	52.01	60.29	66.18	75.09
TS2XHO2	14.11	101.06	34.15	42.04	48.49	53.76	61.57	66.89	74.98
TS3XCCQ	17.04	102.5	37.1	43.93	49.46	53.96	60.66	65.41	73.5
TS4X5M	19.96	99.32	33.43	41.68	48.37	53.78	61.7	67.02	75.09
TS5X7M	7.59	90.19	32.47	40.64	47.41	52.99	61.4	67.25	76.13
TS6XCCS	13.29	97.11	31.79	38.83	44.77	49.77	57.55	63.21	72.23
TS7XCJC	10.19	99.05	35.54	42.46	48.17	52.88	60.04	65.17	73.63
TS9XOH	0	101.1	34.26	41.8	47.99	53.06	60.63	65.86	73.93
TS10XHO2	17	98.69	35.62	43.1	49.13	53.99	61.11	66.03	74.16
TCYC4SXH	81.01	71.77	20.45	26.1	30.56	34.08	39.01	42.17	46.98
HSCO	6.4	64.59	12.85	13.9	14.76	15.46	16.53	17.28	18.44
CH3SCO	2.23	66.17	14.39	16.8	18.88	20.67	23.56	25.73	29.3

CCCICSJ	12.42	83.72	26.96	33.58	39.2	43.96	51.37	56.68	64.7
CCCIC*S	0.21	75.52	22.99	28.52	33.39	37.67	44.66	49.94	58.07
CCC*S	11.21	73.51	18.76	23.01	26.72	29.93	35.14	39.04	45.05
CH2SH	36.65	62.56	11.2	12.56	13.73	14.75	16.39	17.64	19.69
CCJSH	30.91	73.53	16.72	19.54	21.97	24.06	27.39	29.88	33.87
CCSQJ	13.33	90.44	25.09	28.47	31.4	33.92	37.97	41.01	45.79
CCSO2	-59.78	84.5	22.93	27	30.45	33.36	37.91	41.22	46.33
CCOSO	-64.15	89.49	21.74	26.16	29.84	32.89	37.53	40.79	45.71
CCSO	-24.29	80.32	19.2	22.71	25.75	28.38	32.6	35.74	40.63
HSCH2OO	9.51	77.44	18.34	21.07	23.28	25.06	27.66	29.4	32.03
TS1	29.41	70.89	15.76	19.11	21.83	24.02	27.19	29.26	32.07
SJCOOH	8.62	72.76	17.54	20.55	23.01	25	27.95	29.97	33.09
CYCH2SO	7.63	60.29	11.22	13.44	15.26	16.76	18.99	20.5	22.71
HOO	28.67	70.31	15.27	15.68	16.04	16.35	16.85	17.24	17.88
SJOH	13.19	67.55	13.2	14.2	14.96	15.52	16.27	16.72	17.49
TS1_HOO	50.4	64.78	10.81	12.36	13.56	14.46	15.66	16.39	17.49
HOO2	-38.36	61.62	10.95	12.57	13.88	14.93	16.43	17.38	18.57
HOSO	-60.74	63.71	11.01	12.25	13.3	14.2	15.57	16.5	17.65
TS3_HOO	50.6	64.43	11.59	12.67	13.53	14.24	15.25	15.91	16.79
HSSH	3.98	63.07	11.67	12.85	13.81	14.59	15.76	16.59	17.98
CCSSH	-7.78	82.61	22.38	26.42	29.83	32.71	37.22	40.54	45.92
CCSSC	-18.07	101.97	32.91	39.72	45.57	50.57	58.56	64.48	73.81
S*CC*S	54.33	71.3	15.47	18.07	20.19	21.92	24.45	26.13	28.54
SOH	-1.14	57.45	8.89	9.56	10.09	10.52	11.15	11.58	12.38
TCCSCC_HS	37.3	99.56	31.1	38.25	44.33	49.49	57.6	63.5	72.58
TCCSCC_HP	41.6	98.98	32.35	39.12	44.92	49.87	57.72	63.5	72.55
TCCSCC_MES	25.4	115.55	37.39	45.22	51.99	57.84	67.26	74.36	85.73
TCCSCC_MEP	29.4	113.97	37.69	45.56	52.32	58.14	67.48	74.49	85.79
TCCSCCXV	44.2	89.97	28.67	35.57	41.47	46.5	54.44	60.27	69.38
TCCJSCCXV	45.6	99.12	27.02	32.62	37.55	41.88	49	54.4	62.82
TCCJSCC_5	46.4	83.09	25.53	32.39	38.18	43.07	50.69	56.17	64.6
TCJCSCCXV	46.4	95.46	26.42	32.25	37.27	41.59	48.53	53.73	62.11

TCJCSCCXH	63.71	90.61	29.4	35.52	40.64	44.92	51.56	56.37	64.16
TCCSJXME	66.11	76.25	18.01	20.57	22.76	24.64	27.69	30.05	34.21
TCCSJXH	71.61	72.68	17.09	20.06	22.63	24.83	28.34	30.92	34.95
TCCSJ_SH	58.51	70.63	15.83	18.82	21.43	23.71	27.41	30.19	34.57
TCDCSCCXV	71.71	83.76	26.13	32.26	37.42	41.76	48.48	53.3	60.78
TCH2S_H	88.41	61.67	12.14	13.98	15.61	17.03	19.28	20.84	22.72
TCH2S_ME	76.11	71.23	16.85	19.88	22.41	24.55	27.88	30.34	34.57
TCCSSCCXV	37.3	99.57	33.43	40.52	46.52	51.6	59.54	65.31	74.37
TCCSSHXV	48	78.07	22.88	27.17	30.73	33.68	38.19	41.38	46.44
CCSOH	-40.08	79.68	21.97	25.87	29.21	32.06	36.59	39.94	45.29
CH3SOO	20.16	78.13	19.25	21.32	23.07	24.55	26.89	28.64	31.54
CH3SO2	-53.65	71.85	17.52	20.27	22.54	24.42	27.25	29.24	32.31
C*CSO	2.23	66.17	14.39	16.8	18.88	20.67	23.56	25.73	29.3
CJCDOH	9.82	67.93	12.36	14.44	16.35	18.08	21.02	23.3	26.67
CCJDO	-2.13	64.28	12.27	14.39	16.3	18.02	20.9	23.12	26.46
CCDOH	-39.18	63.14	13.17	15.83	18.26	20.47	24.19	27.06	31.22
CJC	29	59.66	11.76	14.55	17.06	19.3	23.05	25.95	30.49
CH2*CHSOH	-11.22	74.11	20.58	23.62	26.1	28.13	31.19	33.37	36.97
CH2*CHSO.	-24.29	70.63	16.84	19.97	22.54	24.64	27.77	29.91	33
CH2*CHOSH	-1.78	75.66	19.19	22.51	25.22	27.42	30.68	32.94	36.56
CH2*CHOS.	24.01	70.98	16.46	19.58	22.15	24.28	27.48	29.69	32.87
CH2*CSOH	-11.22	74.11	20.58	23.62	26.1	28.13	31.19	33.37	36.97
CH2*CSO.	-24.29	70.63	16.84	19.97	22.54	24.64	27.77	29.91	33
C*CSOH	-11.22	74.11	20.58	23.62	26.1	28.13	31.19	33.37	36.97
C*CSO.	-24.29	70.63	16.84	19.97	22.54	24.64	27.77	29.91	33
CJCSh	36.56	76.85	18.83	21.55	24.04	26.3	30.1	33.01	37.06
CCSCQ	-34.27	98.81	30.83	36.69	41.92	46.58	54.24	59.97	67.88
CJCSCQ	14.73	103.6	29.69	35.2	40.08	44.36	51.29	56.33	63.07
CCJSCQ	7.59	101.28	30.29	36.04	40.99	45.23	51.92	56.69	63.22
CCSCQJ	-0.07	99.03	28.48	33.77	38.54	42.78	49.82	55.09	62.33
CCQSC	-38.49	96.35	31.45	37.5	42.68	47.09	54.07	59.16	66.77
CCQJSC	-4.29	96.57	29.47	34.56	39	42.87	49.17	53.93	61.23



CCQSCJ	3.37	101.01	31.37	37.06	41.78	45.71	51.69	55.9	62.26
CJCQSC	9.34	102.33	32.86	37.9	42.18	45.82	51.56	55.76	62.21
CQCSC	-34.87	98.81	30.65	36.57	41.86	46.54	54.22	59.89	67.49
CQCJSC	6.99	101.28	30.29	36.04	40.99	45.23	51.92	56.69	63.22
CQCSCJ	6.99	103.46	30.29	36.04	40.99	45.23	51.92	56.69	63.22
CQJCSC	-0.67	99.03	28.48	33.77	38.54	42.78	49.82	55.09	62.33
CCSC	-15.17	79.49	22.58	27.76	32.46	36.69	43.78	49.15	56.56
CCSCJ	26.69	84.15	22.42	27.14	31.35	35.1	41.23	45.75	51.81
CCJSC	26.69	84.15	22.42	27.14	31.35	35.1	41.23	45.75	51.81
CJCSC	32.66	85.47	24.13	28.35	32.19	35.65	41.48	45.92	52.04
CH3SH	-6.19	61	11.98	13.96	15.75	17.36	20.1	22.25	25.7
CCOJ	-4.24	64.68	14.03	17.62	20.74	23.42	27.73	30.9	35.61
C*CSJ	50.65	64.46	13.08	15.67	17.82	19.61	22.33	24.27	27.31
CH2*C*S	49.3	59.95	12.58	14.45	16	17.26	19.18	20.53	22.7
HCCS	79.15	56.46	12.01	13.5	14.66	15.56	16.8	17.61	18.94

Note: S (cal/mol K), H<sub>F</sub> (kcal/mol) and C<sub>P</sub> (cal/mol K).